NAS1.60:1254

JUL 7 1978

NASA Technical Paper 1254

COMPLETED
ORIGINAL

A Flight Investigation of the Stability, Control, and Handling Qualities of an Augmented Jet Flap STOL Airplane

Richard F. Vomaske, Robert C. Innis,
Brian E. Swan, and Seth W. Grossmith

JUNE 1978

NASA

148

[illegible] 830-A-15 [illegible]

NASA Technical Paper 1254

A Flight Investigation of the Stability, Control, and Handling Qualities of an Augmented Jet Flap STOL Airplane

Richard F. Vomaske and Robert C. Innis
Ames Research Center, Moffett Field, California
Brian E. Swan
Canadian Armed Forces, Ottawa, Ontario
Seth W. Grossmith
Canadian Department of Transport, Ottawa, Ontario

NASA
National Aeronautics
and Space Administration

Scientific and Technical
Information Office

1978

SYMBOLS

A_X	acceleration along longitudinal axis, m/sec^2
A_Z	acceleration along vertical axis, m/sec^2
b	wing span, m
$\bar{c}$	reference aerodynamic chord, m
C_D	drag coefficient, $\dfrac{\text{drag}}{\bar{q}S}$
C_{D_A}	drag coefficient excluding hot thrust contribution
C_{D_G}	drag coefficient in ground effect (excluding hot thrust contribution)
C_J	jet momentum coefficient, isentropic, $\dfrac{\text{cold thrust}}{\bar{q}S}$
C_L	lift coefficient, $\dfrac{\text{lift}}{\bar{q}S}$
C_{L_A}	lift coefficient excluding hot thrust contribution
C_{L_G}	lift coefficient in ground effect (excluding hot thrust contribution)
C_{L_T}	total lift coefficient, $\dfrac{Wn_z}{\bar{q}S}$
C_l	rolling-moment coefficient, $\dfrac{\text{rolling moment}}{\bar{q}Sb}$
C_{l_i}	$\dfrac{\partial C_l}{\partial i}$
C_{l_j}	$\dfrac{\partial C_l}{\partial j} \dfrac{2V}{b}$
C_m	pitching-moment coefficient, $\dfrac{\text{pitching moment}}{\bar{q}S\bar{c}}$
C_{m_G}	pitching-moment coefficient in ground effect
C_{m_i}	$\dfrac{\partial C_m}{\partial i}$
C_{m_j}	$\dfrac{\partial C_m}{\partial j} \dfrac{2V}{\bar{c}}$

C_n	yawing-moment coefficient, $\frac{\text{yawing moment}}{\bar{q}Sb}$
C_{n_i}	$\frac{\partial C_n}{\partial i}$
C_{n_j}	$\frac{\partial C_n}{\partial j} \frac{2V}{b}$
C_T	thrust (hot) coefficient, $\frac{\text{thrust}}{\bar{q}S}$
C_X	drag-force coefficient, body longitudinal axis, $\frac{\text{drag force}}{\bar{q}S}$
C_{x_i}	$\frac{\partial C_x}{\partial i}$
C_{x_j}	$\frac{\partial C_x}{\partial j} \frac{2V}{\bar{c}}$
C_y	side-force coefficient, $\frac{\text{side force}}{\bar{q}S}$
C_{y_i}	$\frac{\partial C_y}{\partial i}$
C_{y_j}	$\frac{\partial C_y}{\partial j} \frac{2V}{b}$
C_z	lift-force coefficient, body vertical axis, $\frac{\text{lift force}}{\bar{q}S}$
C_{z_i}	$\frac{\partial C_z}{\partial i}$
C_{z_j}	$\frac{\partial C_z}{\partial j} \frac{2V}{\bar{c}}$
CG	center of gravity, percent $\bar{c}$
F_{COL}	control column (stick) force, N (lb)
F_W	control wheel force, N (lb)
g	acceleration due to gravity, 9.81 m/sec^2 (32.17 ft/sec^2)
h	radio altitude, m (ft)
i	aerodynamic coefficient independent variable supersubscripts C_J, α_F, β, or δ_e
I_x	moment of inertia about the longitudinal axis, kg-m^2

I_y	moment of inertia about the lateral axis, kg-m^2
I_z	moment of inertia about the vertical axis, kg-m^2
j	aerodynamic coefficient independent variable supersubscripts p, q, or r
n_z	vertical load factor
n_{z_α}	load factor per unit angle of attack, g/rad
N_H	high pressure engine rotor *rpm*, percent (100 percent equals 12,135 *rpm*)
p	roll rate, rad/sec
$\dot{p}$	roll acceleration, rad/sec^2
P	period of oscillation, sec
q	pitch rate, rad/sec
$\dot{q}$	pitch acceleration, rad/sec^2
$\bar{q}$	free-stream dynamic pressure, $\frac{\rho V^2}{2}$, N/m^2 (lb/ft^2)
r	yaw rate, rad/sec
$\dot{r}$	yaw acceleration, rad/sec^2
rpm	revolutions per minute
s	Laplace transform variable
S	wing area, m^2 (ft^2)
t	time, sec
$T_{1/2}$	time to 1/2 amplitude, sec
T_2	time to double amplitude, sec
V	velocity, m/sec (ft/sec)
V_E	equivalent airspeed (EAS), knots
V_{MO}	maximum operating airspeed, knots
VFR	visual flight rules

W	weight, N (lb)
α_F	angle of attack of fuselage corrected for upwash, positive nose up, deg
β	angle of sideslip, positive nose left, deg
$\dot{\beta}$	rate of change of sideslip, deg/sec
γ	flight-path angle, positive up, deg
δ_{AIL}	aileron deflection, positive T.E. down, deg
δ_{CH}	choke deflection, positive T.E. up, percent (100% equals 38°)
δ_{COL}	control column deflection in pitch, positive aft, deg
δ_e	elevator deflection, positive T.E. down, deg
δ_f	flap deflection, positive T.E. down relative to the wing chord plane, deg
δ_p	rudder pedal deflection, positive left forward, cm (in.)
δ_r	rudder deflection, positive T.E. left, deg
δ_{sp}	spoiler deflection, positive T.E. up, deg
δ_w	control wheel deflection, positive clockwise, deg
ζ	damping ratio
θ	pitch angle, positive nose up, deg
ν	nozzle deflection, positive down from full aft, relative to fuselage datum line, deg
ρ	ambient air density, kg/m^3 (slugs/ft^3)
τ_A	apparent roll mode time constant, sec
ϕ	roll angle, positive right wing down, deg
ϕ_1	roll angle after 1 sec, deg
ψ	yaw angle, positive nose right, deg
ω_n	undamped natural frequency, rad/sec

A FLIGHT INVESTIGATION OF THE STABILITY, CONTROL, AND HANDLING QUALITIES OF AN AUGMENTED JET FLAP STOL AIRPLANE

Richard F. Vomaske,* Robert C. Innis,* Brian E. Swan,† and Seth W. Grossmith‡

SUMMARY

The stability, control, and handling qualities of an augmented jet flap STOL airplane are described. The airplane is an extensively modified de Havilland C-8A "Buffalo" military transport. The modified airplane has two fan-jet engines which provide vectorable thrust and compressed air for the augmentor flap and for Boundary-Layer Control (BLC). The airplane is equipped with powered flight controls, and stability augmentation is provided on the lateral and directional axes. The test conditions of airplane gross weight varied between 165,000 and 209,000 N (37,000 and 47,000 lb).

Stability, control, and handling qualities are presented for the airspeed range of 40 to 180 knots. With the Stability Augmentation System (SAS) operating, the handling qualities are considered satisfactory for the normal operational envelope (65 to 160 knots airspeed). Without stability augmentation, the lateral-directional handling qualities are considered marginal in the landing approach. Poor turn coordination and spiral instability are the primary deficiencies when operating with the SAS inoperative.

The handling qualities investigation included operation with one engine inoperative (simulated). The cross ducting of augmentor and boundary-layer control (BLC) air, together with adequate control power, provide acceptable handling qualities for the one-engine-inoperative condition. The powered elevator control system, a modification incorporated in the airplane, enhanced controllability in pitch, particularly in the landing flare, and allowed investigation of airplane stall characteristics.

INTRODUCTION

The augmentor jet flap or augmentor wing powered lift concept has been recognized by both government (ref. 1) and industry (refs. 2–4) as one of the promising concepts for research and development. After extensive wind-tunnel studies (ref. 5) and simulation studies (refs. 5–8), a research aircraft program was initiated to provide an aircraft for STOL flight experiments. A de Havilland C-8A Buffalo airplane was modified into an augmentor jet flap research aircraft. A description of the modified airplane and a summarization of the airplane contractors development program is presented in reference 6. Important aerodynamic features of the airplane are presented in reference 9.

---

*Ames Research Center, Moffett Field, Calif. 94035.

†Canadian Armed Forces, Ottawa, Ontario, K1A OK2.

‡Canadian Department of Transportation, Ottawa, Ontario, K1A ON8.

This report presents the results of stability and control, and handling qualities flight testing of the airplane. Test results peculiar to the airplane with the spring-tab elevator system are presented in references 10 and 11 while the present report includes data and information pertinent to the airplane with the powered elevator. Because of the limited elevator control authority usable with the spring-tab elevator system, flight tests with the spring-tab elevator controls did not include flight conditions at angles of attack exceeding 21°.

The stability and control characteristics of the airplane are in some respects unique because of powered lift effects and the slow speed flight capability. The powered lift effects have a primary bearing on the longitudinal stability and control while the slow speed flight capability significantly affects both the longitudinal and lateral-directional stability and control. Piloted simulators (refs. 5–8) were used during the design phase of the airplane development to study the unique stability and control characteristics and the aircraft handling qualities.

The initial airworthiness flight-test program was conducted by the contractor and reported in reference 6. During these tests the airplane was flown within a flight envelope of from 50 to 180 knots and at load factors sufficient to demonstrate that the aircraft flight loads were within design and that the airplane was flutter free. Some preliminary documentation of the stability and control characteristics were obtained and reported in reference 10.

Results of the initial research flight tests to document and evaluate the performance, stability, control, and operational characteristics of the airplane are presented in reference 11. Results presented in reference 11 are for tests performed before the installation of the powered-elevator control system. The airworthiness flight-test results of the powered-elevator control system are presented in reference 12. Aerodynamic and operational performance characteristics are presented in references 10 and 11.

THE RESEARCH AIRCRAFT

The research aircraft is a highly modified de Havilland C-8A Buffalo military turboprop transport. Its high "T" tail made it especially suitable for application of a powered lift system. Photographs of the aircraft in the landing and takeoff configurations are shown in figure 1. Table 1 lists the geometric and mass characteristics of the aircraft. Figure 2 is a three-view drawing of the aircraft. Special features of the aircraft are described briefly below; a more complete description is presented in reference 6. Reference 12 presents details of the powered elevator installation which is not included in the description of the airplane given in reference 6.

Engine

Two Rolls Royce Spey MK 801-SF split flow engines provide thrust for the airplane as well as air for the augmentor flap, body BLC, and aileron BLC. Each engine is fitted with vectorable conical nozzles (fig. 3). The nozzles can vector the thrust between 6° and 104° relative to the fuselage centerline, to provide lift and flight-path control. The nozzle vector angle control handles, one for each engine, are located in the cockpit overhead console adjacent to the engine throttles and within easy reach of the pilot (fig. 4).

Air Distribution System

The air distribution system directs the engine bypass air to the upper and lower augmentor nozzles, to the fuselage boundary-layer blowing nozzles, and to the aileron blowing nozzles (fig. 5). A crossover ducting system is used so that approximately 64% of the bypass mass flow of each engine is ducted to the augmentor and aileron nozzles on the opposite wing and to half of the fuselage boundary-layer blowing nozzles; the remaining 36% of the bypass mass flow is ducted aft to the augmentor nozzles on the same side of the aircraft as the engine. The air distribution systems for each engine are completely separate, but identical. This unique arrangement provides for engine-out operation without large rolling or yawing moments.

Augmented Jet Flap

The flaps are deflected by hydraulic linear actuators mounted external to the wing. The minimum (flaps up) angle is 5.6° and the maximum flap angle is 72°.

The ducts that supply the air to the augmentor flap nozzles are mounted just aft of the rear spars and provide air independently from each engine. The inner duct air is supplied from the engine on the same side of the aircraft as the engine, while the outer duct is supplied from the engine on the opposite side (fig. 5). The arrows shown in the figure indicate air flow from the right-hand engine only.

Fixed leading-edge slats were installed to help maintain airflow over the wing at the high values of circulation obtained during powered-lift operation.

Flight-Control System

Several modifications were made to the basic C-8A Buffalo flight-control system. In the cockpit (fig. 4), the control wheel was replaced with a wheel instrumented to read out lateral and longitudinal control forces. The only other change in the cockpit flight controls was the addition of an electrical lateral and pitch trim switch, which the pilot could control with his left thumb (fig. 4) and the copilot with his right thumb; a manual elevator trim controller is provided for emergency operation. The engine nozzle controls were installed adjacent to the engine throttle controls (fig. 4(a)).

The longitudinal control for the first 78 hr of flight testing consisted of a spring-tab elevator system. A description of the spring-tab system and test results are presented in references 10 and 11. Subsequent flight testing of the airplane was with a powered-elevator system installed. The powered elevator was installed to improve longitudinal pitch control. A detailed description and airworthiness test results of the powered-elevator system are presented in reference 12. Longitudinal pitch control is provided by a single elevator surface which provides both maneuver and trim control functions as the horizontal stabilizer incidence is fixed. The friction and breakout force characteristics of the existing system are presented in figure 6. The feel system incorporates a computer that varies feel gradient as a function of dynamic pressure, as shown in figure 7. The feel gradient is constant for speeds less than 60 knots. Control column to elevator gearing is shown in figure 8 and control authority and trim limits are shown in figure 9. The nose-up elevator authority decreases with increasing airspeed because of the available aft column travel and a reduction of the power control unit steady-state gain. This reduction in authority and gain is caused by the flexibility of the power control system components.

The directional control consists of a two-panel rudder, the aft panel being hinged to the trailing edge of the forward panel and geared to it in a 2:1 deflection ratio. The rudder is fully powered through an irreversible dual hydraulic actuator controlled by cables from the rudder pedals. The basic Buffalo directional control system was modified to include a stability augmentation system (SAS) actuator which is mechanically summed in series with pilot inputs. The rudder area was slightly reduced (2.5%) when the powered elevator was installed. The rudder pedal force and gearing are shown in figure 10. Maximum rudder deflection (single panel) is ±25°.

The lateral control system is completely new. Three separate surfaces are used to produce the required rolling moments: ailerons with boundary-layer control, spoilers in front of the ailerons, and augmentor chokes. Figure 11 shows the position and function of each element. The ailerons are mechanically programmed to droop as a function of the flap deflection, as shown in figure 12(a). Full droop is 35° and is reached at flap deflection of about 70°. The maximum differential aileron deflection from the droop position is ±17° with flaps up. As flaps are extended, the control wheel to aileron gearing is changed slightly (fig. 12(b)) and ±18.5° of differential aileron is available at 65° flaps with SAS on. Blowing boundary-layer control is used on the aileron to increase the effectiveness of both the ailerons and spoilers. The augmentor chokes are designed to control the lift of the augmented jet flap system by changing the exit area of the augmentor. Full lateral control reduces the exit area as a function of flap deflection to a maximum of 55% on the down-going wing (fig. 12(c)). The chokes function much the same as spoilers on a conventional airplane. Although there are augmentor chokes in each of the four sections of the flap, only the chokes in the outboard section of each wing are used for lateral control. All four chokes may be activated on the ground after landing for lift dump.

The choke and spoiler lateral control surfaces are programmed to give nearly linear effectiveness with control wheel deflection (fig. 12(d)). The spoiler operates from near neutral wheel position and the augmentor choke is phased in at about 11° (flap deflection 65°) control wheel deflection. The spoilers are fully deflected at about 45° wheel deflection.

Lateral control wheel forces are low (fig. 13) and are produced by a simple spring system. The lateral control surfaces are activated by a central dual hydraulic power actuator, located on the rear spar, which drives the ailerons through a cable system. The central lateral power actuator also drives spoilers and augmentor choke control valves through a second cable. The spoiler and choke actuators are powered by separate hydraulic systems.

Approximately midway through the flight-test program several modifications were made to the airplane. The SAS gearing was changed to increase the Dutch-roll damping, the lateral control feel spring was modified to improve the centering and force gradient, and the powered-elevator system was installed. The powered-elevator system installation caused an increase in the airplane's roll, pitch, and yaw moments of inertia and a decrease of 0.14 m^2 (2.5% of total) in rudder area. At a gross weight of 178,000 N (40,000 lb) the moment of inertia about the yaw axis was increased about 5% while the inertia increase about the roll axis was about 1%.

Rolling moment is produced by ailerons, spoilers, and augmentor chokes. Figure 11 illustrates the location and deflection of these controls. Gearing of the pilots control wheel to these surfaces is shown in figure 12.

Maximum control surface rates of deflection are as follows:

Control wheel	≥ 200°/sec
Ailerons	≥ 50°/sec
Spoilers	≥ 120°/sec
Chokes	≥ 35°/sec

With flaps deflected for landing, full lateral control from neutral position can be achieved in about 0.5 sec.

There is an increase in effective gearing of the control wheel to surface deflection from 0 to ±3° of wheel deflection; the increase is produced by a circuit in the SAS system, as shown in figure 14. With SAS turned off this feature is disabled. With SAS on, the gearing is double that of the SAS off case for the first ±3° of wheel deflection. This system was incorporated to reduce any lag in aircraft response at small wheel deflections in the region of small spoiler deflection where they are relatively ineffective. As the flaps are extended, the control wheel to aileron gearing is increased somewhat. Figure 12(b) shows the change in total aileron deflection available at various flap deflections. At 65° flap deflection, the total aileron deflection available is about 10% greater than that with flaps up.

Stability Augmentation System

Two independent stability augmentation systems, one for the lateral and one for the directional aircraft axis are provided. Block diagrams of the SAS systems are shown in figure 14. The SAS actuators are positioned by closed-loop servos and summed in series with the pilot's control system. The SAS electronics is single channel, and relies on limited rate and displacement authority for safety. The lateral rate limit is 50°/sec with the displacement authority limited to ±20° (27%) equivalent wheel displacement. In the first ±3° of equivalent wheel deflection, the SAS to control gearing is double that beyond 3°. The maximum directional SAS rate is 25°/sec of rudder travel, and displacement is limited to ±5° (20%) of fore-rudder deflection. After the present tests were completed, the displacement limit was increased to ±9° rudder-deflection.

The lateral SAS in the normal mode performs the following functions:

1. Spiral stability augmentation, using yaw rate feedback to the lateral controls

2. Roll damping augmentation, using roll rate feedback to the lateral controls

3. Lateral control quickening, using wheel position feed forward (±3° δ_W maximum) to the lateral controls.

The directional SAS in the normal mode performs the following functions:

1. Turn coordination, using roll rate and roll attitude feedback to the rudder
2. Dutch-roll damping, using yaw rate and roll attitude feedback to the rudder.

The SAS gains (fig. 14) are programmed with flap position and are automatically switched off above 100 knots. About midway through the test program the $\dot{\beta}$ gain was increased from a value of 0.4 to 0.8 to alleviate a snaking tendency at STOL approach speeds. Figure 14(c) is the schematic for the lateral control surface quickener, which doubles the lateral control gearing for the first 3° of control wheel travel to improve the control characteristics near the neutral control surface position.

Data Acquisition System

An on-board data acquisition system gathers data on about 95 parameters measured during all ground and flight testing. A pulse code modulated (PCM) digital system records the data on magnetic tape. Recorded flight-test data include stability and control, SAS signals, engine performance, augmentor performance, and guidance information. Each parameter is sampled 100 times per second.

The PCM data are processed on a digital computer programmed with the desired equations for determining such parameters as engine thrust, lift and drag coefficients, flight-path angle, and corrected airspeed.

For certain tests, the on-board data acquisition system also included a recording oscillograph, which is used for recording high frequency data. This was used for flutter, vibration, and loads testing.

FLIGHT-TEST PROCEDURE

The flight tests were initiated from Moffett Field and flown in test areas in the vicinity of Moffett Field and at the Crows Landing Naval Auxiliary Facility. The flights were made by project pilots from NASA, the Canadian Department of Transport, de Havilland Aircraft of Canada Ltd., and The Boeing Company.

The flight tests included the following general categories: calibration, aerodynamics, stability and control, performance, and operational and handling qualities.

Stability and Control Tests

The stability and control test configurations were generally cruise (5.6° flaps) at 150 knots, landing approach (65° flaps) at about 65 knots with engine nozzles at 75°, and takeoff (30° flaps) at about 80 knots airspeed. In general, power for level flight was used for the cruise and landing approach testing, while maximum continuous power (96% *rpm*) was used for the takeoff configuration tests. Simulated engine-out testing was conducted by throttling one engine to idle.

Stability and control tests were performed to determine the following: control system characteristics, control power, control sensitivity, static stability, dynamic stability, acceleration characteristics, and trim changes.

Longitudinal test maneuvers included the following: trim change with speed (with one and two engines); trim change with power and with nozzle deflection; elevator steps, reversals, and doublets; rapid pitch attitude changes; wind-up turns; engine power lever steps; engine nozzle lever steps; trim change with flap deflection; phugoid; trim change in ground effect; and stall behavior.

Lateral-directional test maneuvers included the following, with SAS both on and off: lateral control steps and reversals; directional control steps and reversals; Dutch-roll; spiral stability; rapid bank angle changes; trim change with one engine operating; stalls; and steady sideslips.

Tests were also conducted to determine the effects of partial hydraulic failure on lateral control and on SAS operation. The lateral control augmentor chokes and the spoilers were deactivated separately to test their effect on control power and sensitivity. The directional and lateral control channels of the SAS were deactivated separately, again to determine their effect on stability and control.

Operational and Handling Qualities

Operational and handling-qualities testing was conducted in conjunction with the other tests. In addition, STOL landing, transition, takeoff, and waveoff operation, and ground effect testing were conducted as part of the evaluation of operational and handling-qualities characteristics. Simulated single-engine landing approaches and takeoffs were also conducted.

FLIGHT-TEST RESULTS AND DISCUSSION

The results of the flight investigation of stability and control are discussed under two categories: (1) longitudinal stability and control, and (2) lateral-directional stability and control.

Longitudinal Stability and Control

Longitudinal stability and control characteristics of the airplane are summarized in tables 2 through 7. Stability and control derivatives for the landing approach configuration are tabulated in table 6. These stability and control derivatives are from reference 13 and were obtained from flight-test data recordings using an equation error parameter identification method and from prediction.

After the first 78 hr of flight testing, a powered-elevator system was installed in the airplane to replace the spring-tab system. In addition to the direct effects of the powered elevator on stability and control, the modification changed the airplane's center of gravity and moments of inertia. The pitching moment of inertia was increased about 14% at 178,000 N (40,000 lb) gross weight and the center of gravity was moved aft 0.3%. The variation of center of gravity with gross weight is shown in figure 15.

Longitudinal control– Before modification of the elevator control system the pilots found that the longitudinal control dynamic feel characteristics were unsatisfactory, and the maximum control from trim that could be obtained at STOL airspeeds with reasonable forces was only about +10° to -17° elevator deflection, although statically, full elevator travel was +15° to -25°. For subsequent testing, the elevator control system was modified to a fully powered system (ref. 12). Control characteristics of the aircraft with the spring-tab system are presented in references 10 and 11. The data presented in the following discussion is for the powered elevator configuration except where otherwise noted.

The longitudinal pitch control characteristics of the aircraft are summarized in the following table. (The control power is for -24° elevator deflection.)

LONGITUDINAL PITCH CONTROL CHARACTERISTICS

Airspeed, knots	60	65	75	90
Control power, rad/sec^2	0.41	0.47	>0.6	>0.6
Sensitivity, rad/sec^2/cm	.027	.032	.043	.062
rad/sec^2/in.	.070	.082	.109	.157
Force gradient, N/cm	9.5	10.1	11.1	14.0
lb/in.	5.4	5.8	6.3	8.0
Breakout force,[a] N	25.8	25.8	26.7	27.6
lb	5.8	5.8	6.0	6.2

[a] Includes system friction of 17.8 N (4 lb).

The angular acceleration for determining control power and sensitivity was obtained from longitudinal control reversal maneuvers of various amplitudes. A typical control reversal at 67 knots is illustrated in figure 16. The angular acceleration for a specific change in elevator position from trim was obtained by the slope of the pitch rate at the time pitch rate is zero, where the damping term is zero. Corrections for changes in angle of attack are made where appropriate. The elevator control effectiveness is shown in figure 17. Figure 17(a) presents the data in terms of the variation of the ratio of angular acceleration to the free-stream dynamic pressure ($\dot{q}/\overline{q}$) with the incremental elevator deflection from trim. The variation of angular acceleration with incremental elevator deflection, computed from the data in figure 17(a) at 60, 65, 75, and 90 knots is shown in figure 17(b). The data show that for the landing approach speeds of 60 to 65 knots the maximum control power is between 0.41 and 0.47 rad/sec^2. At 75 knots and above the angular acceleration exceeds 0.6 rad/sec^2. The pilots felt that angular accelerations greater than 0.5 rad/sec^2 could not be used effectively except in emergencies.

The gearing of the longitudinal control was 1.7° elevator per degree of column deflection for small angles at 60 knots. Some small nonlinearity is evident near zero degrees and at high deflection angles, and there is a change in gearing with airspeed. Details of the system are presented in reference 12.

The length of the column is 0.83 m (32.5 in.). The force characteristics are shown in figures 6 and 7 and in the table of longitudinal characteristics (table 2). The pilots considered the control feel characteristics of the powered elevator satisfactory and to be superior to the spring-tab control system.

A comparison of the control effectiveness of the powered elevator and the original spring-tab elevator, figure 18, shows the powered elevator effectiveness is about 14% less than that of the spring-tab elevator. This reduction results from the increase in pitching moment of inertia due to the concentration of the powered-elevator system components in the tail of the aircraft and the addition of ballast in the nose of the aircraft for balance. The aerodynamic features of the horizontal tail and elevator were not significantly changed.

The pilots considered the longitudinal pitch control characteristics satisfactory for all STOL operation. Hysteresis in the engine power control system produced unsatisfactory thrust control in STOL landing approaches. Elevator deflections as high as -18° (about 15° from trim) were noted in some takeoff rotations and landing flares. The control power was adequate to recover from all stalls conducted. However, at very slow stall speeds, 41–43 knots, the pilots used full forward control which gave a slow recovery. The project pilots, therefore, considered 45 knots the minimum flight speed for the airplane to ensure adequate control.

Longitudinal static stability– The installation of the powered-elevator system in the airplane has removed the undesirable stick-free characteristics of the spring-tab elevator system. Stick-free characteristics of the airplane with the spring-tab elevator are presented in reference 11. The stick-fixed stability characteristics will be discussed in the following paragraphs.

The static longitudinal stability characteristics of the airplane were obtained by flying steady trim conditions from flap placard speeds down to and including the stall and measuring the elevator angle required for trim. Tests were conducted over a range of flap, nozzle, and power settings. The center of gravity varied between 30.0% and 30.9% of mean aerodynamic chord. Test weights varied from 178,000 to 205,000 N (40,000 to 46,000 lb). Figures 19 through 21 present elevator-to-trim data for a broad range of conditions, including simulated single-engine operation.

In the landing configuration with flaps at 65° (fig. 19), nozzles either aft or down, with symmetrical power on both engines of between 90 and 99% *rpm*, trim is achieved for all conditions tested with elevator deflections within 6° of neutral at all angles of attack up to the stall. The airplane is statically stable at angles of attack less than 10° for all conditions of constant engine power or constant nozzle deflection tested and for all angles of attack at engine *rpm* below about 93%. Above 93% *rpm* and at high angles of attack, the stability can either be positive, neutral, or negative depending on the combination of nozzle angle and engine power. In general, increasing engine power has a destabilizing effect and increasing nozzle deflection can either be stabilizing or destabilizing. Neutral stability is evident, however, at angles of attack between 10° and 15° with 95% *rpm* and nozzle angle equal to or less than 67°; for the same conditions, positive stability exists with the nozzle deflection equal to or greater than 88°. The airplane is unstable with *rpm* greater than 95% and nozzle deflection equal to or less than 76° at angles of attack between 15° and the stall angle. A strong nose-down pitching moment exists at the stall for most configurations.

In the simulated engine-out configuration with landing flaps (65°), positive stability is evident (fig. 19(d)) for all conditions tested except for a region of neutral stability in the angle of attack range near 15° with the highest engine *rpm* tested (99.6%) with a nozzle angle of 72°. With a similar nozzle deflection (73°) at lower engine *rpm* (96.5%) there is reduced but positive stability in the region between 10° and 15° angle of attack. The reason for the apparent nonlinearity is not understood.

The elevator to trim data for the takeoff flap configuration (30°) with nozzles up is presented in figure 20 for two engines operating and for the simulated one-engine operating conditions. In both cases the airplane is statically stable throughout the angle of attack range tested except for the highest engine power condition (two engines operating). With 99% *rpm* on both engines (fig. 20(a)) there is a neutral stability region near 15° angle of attack with positive stability evident at angles of attack greater than 20° and less than 12°. In the region of the stall there is a strong nose-down pitching moment for conditions tested with less than 94% engine *rpm*. Some nose-down moment near the stall is also indicated at higher engine power. The region of neutral stability at intermediate angles of attack was not evident for simulated one engine operation (fig. 20(b)). At either constant airspeed or angle of attack, increasing engine power produces a nose-up pitching moment.

With the flaps up (climb and cruise configurations), the airplane exhibits positive static stability as shown in figure 21. Figure 21(a) shows elevator-to-trim for 90% *rpm* (approximately cruise power), and for 97% *rpm*, which is 1% higher than maximum continuous power. For both conditions of engine power, the stability becomes quite high at angles of attack above 20° with large aft column deflections required near the stall. The simulated single engine condition also is stable (fig. 21(b)) for the 97%/idle *rpm* case tested.

Longitudinal dynamic stability— The dynamic longitudinal short period stability characteristics were approximated by analyzing the response of the aircraft to control pulses and steps. Aircraft short-period and phugoid characteristics are summarized in table 5 for several configurations. Figure 16 is a typical time history of response to an elevator step at 66 knots airspeed. The data illustrate the low short-period dynamic stability of the airplane at this speed. The response to a step elevator appears to be almost first order with a time constant of about 0.5 sec; pitch rate becomes almost constant after about 1 sec. Stability values shown in table 5 were computed by the method of reference 13 and show the short-period mode to be of the order of 10 to 16 sec and a damping ratio of about 0.90. The pilots state that there seems to be very little if any stability. Figure 22 is a time history of a phugoid oscillation from a trimmed condition of 65 knots with the nozzles deflected 77°. The period of the phugoid mode is over 30 sec with a damping ratio of less than 0.10.

The pilots were not satisfied with the short-period dynamic characteristics of the aircraft because of the high pilot workload required to maintain a desired pitch attitude and to control airspeed on the landing approach at airspeeds of 60 to 70 knots. Approaches and landings under visual flight rules (VFR) were performed in winds as high as 30 knots with gusts. Flight in gusty conditions resulted in only small low-frequency disturbances in attitude because of the low dynamic stability. The pilot workload increased, however, during the approach because of flight-path disturbances.

Flight-path control– The flight path of the airplane in a fixed flap configuration may be controlled by either modulation of engine power (*rpm*) or engine nozzle deflection. Normally, the engine nozzles are used for flight-path control when flying in the landing approach configuration; however, they can be used effectively for longitudinal acceleration control in other flap configurations. The variation of flight-path angle with airspeed for the landing approach configuration is presented in figure 23 for a typical airplane gross weight of 178,000 N (40,000 lb). Reference 11 presents the flight-path/airspeed relationship for the takeoff and cruise configurations which show characteristics similar to those of conventional airplanes. Figure 23(a) shows the change in flight path and angle of attack as a function of airspeed and engine *rpm* for the landing approach configuration (65° flaps) with nozzles set at 90°. The nozzle deflection used for typical STOL landing approaches at 65 knots on a -7.5° flight path is nominally about 75°. The data show that the aircraft exhibits "back-side" characteristics at 93% engine *rpm* required for a -7.5° approach path at airspeeds less than 72 knots. Higher engine *rpm* reduces the onset speed at which "back-side" conditions exist and the converse is true for decreasing engine *rpm*. It is also evident that for a constant airspeed approach in the 65 knot speed region, the flight path may be changed by *rpm* adjustment with a small change in pitch attitude opposite to the direction of the flight-path angle change. If power is increased to decrease rate of sink, a nose-down pitch attitude change is required to maintain airspeed. The trim angle of attack change is also of opposite sign but of similar magnitude to the flight-path angle change. These characteristics are typical of propulsion lift aircraft where a substantial amount of lift is produced by engine thrust.

The flight-path/velocity relationship as a function of engine thrust vector angle is shown in figure 23(b) for the fixed-*rpm* (94%) landing approach configuration. Large changes of flight path can be made by a change of nozzle position at constant airspeed with essentially no change in angle of attack. The flight-path angle change is therefore proportional to pitch angle change when nozzles are modulated to maintain airspeed. It is also evident that "back-side" conditions exist for any nozzle deflection at airspeeds less than about 72 knots. The nozzle control can be used much the same as a throttle in a conventional jet aircraft if pitch attitude is coordinated.

In practice, both the throttles and nozzles are modulated in the control of flight path, airspeed, and/or angle of attack on a landing approach. In general, the nozzles are used to make large flight-path corrections, and pitch attitude is used for airspeed control. Throttles are used to make small corrections to glide path and/or airspeed with pitch attitude used to control angle of attack. A time history of a typical landing approach is shown in figure 24 which shows the last 60 sec of flight before touchdown when the nozzles were used to decelerate from 90 knots to the approach speed of about 66 knots. The nozzles are moved only once after decelerating to near the approach speed while the *rpm* is adjusted several times for flight-path control. The approach angle of attack is nominally about 4° with some random excursions which may be attributed to reported turbulence. Little elevator is used throughout the approach until the final landing flare where a peak deflection of about 14° from trim is used.

Longitudinal maneuvering characteristics– This section covers the aircraft's vertical and longitudinal acceleration responses to control inputs used for flight path, flare, and airspeed control. Four controls are available to the pilot in this propulsive lift aircraft to achieve these responses: (1) changes of angle of attack with elevator control, (2) changes in engine thrust with the throttles, (3) changes in hot thrust vector angle with nozzle control levers, and (4) change in lift and drag with flap deflection. Each of these controls affects the lift, drag, and pitching moment of the aircraft.

The aircraft exhibits stable maneuvering characteristics at constant airspeed, thrust, and nozzle angle for the conditions tested. Figure 25 compares measured maneuvering data with predicted values from reference 14 in terms of angle of attack-per-g, elevator position-per-g, and stick force-per-g variation with airspeed obtained from wind-up turns and pitch attitude steps. Control force data are presented only for the powered-elevator system.

Load factor per unit angle of attack ($n_{z\alpha}$) becomes quite low as airspeed is reduced and is slightly less than predicted. The test values of $n_{z\alpha}$, which were obtained from pitch attitude step maneuvers, are for conditions where $\Delta\alpha_F$ is less than about 4.5°. In the maneuvers in which $\Delta\alpha_F$ was 5° or greater, the airspeed deviation from trim and pilot technique have a large influence on the measured value of Δn_z. The elevator-per-g is greater than predicted. The greater than predicted elevator-per-g may be accounted for by the lower than predicted load factor per unit angle of attack change. Typical wind-up-turn test data are presented in figure 26 for the takeoff configuration.

Figure 27 shows peak normal acceleration achieved during step changes in pitch attitude with flaps at 65°. A comparison of the test data is made with computed values based on the change of C_L with angle of attack at a constant C_J of 0.4. The computed values are based on a trim angle of attack of 5° and a constant airspeed; although test values of trim angle of attack varied up to 10°, the data are applicable because the lift characteristics are quite linear for angles of attack between 5° and 10°. At 63 knots airspeed (fig. 27(a)), good agreement exists between test values and computed values of Δn_z for conditions of $\Delta\alpha_F$ less than about 5°. At 63 knots, for test conditions of $\Delta\alpha_F$ greater than 5°, the measured values of Δn_z tend to be lower than computed due to a reduction in airspeed in the maneuver. At 68 knots airspeed (fig. 27(b)), test values of Δn_z tend to be greater than predicted.

Figure 28(a) shows time histories of 5° and 10° pitch attitude changes with 65° flap deflection at a trim airspeed of 63 knots. For the 10° step, note that as pitch attitude is increased, the airspeed decreases such that the peak value of vertical acceleration does not occur at the peak value of angle of attack. Also, analysis of the test data show that pilot technique, phasing, and amplitude of control inputs has an influence on the peak Δn_z value, particularly for the larger ($>5°$) test values of $\Delta\alpha_F$. These effects account for the scatter in Δn_z with $\Delta\alpha_F$ shown in figure 27. With attitude changes of 5°, acceleration follows angle of attack more closely; airspeed changes are much smaller and do not affect the peak load factor. Figure 28(b) presents similar time history data for nose-down attitude changes.

Figure 29(a) shows aircraft response to thrust vector nozzle rotation downward from the aft position, with the pilot controlling elevator to hold angle of attack nearly constant. The effect is somewhat similar to a decrease of thrust in a conventional aircraft because the main effect on the flight characteristics of vectoring thrust is to change the thrust minus drag relationship. When the nozzle is moved from full aft to 90° deflection on the 7.5° landing approach path, the lift change is only about 35,000 N which is about 20% of the weight of the airplane. As the thrust vector is rotated from aft to vertical position the airspeed decreases quickly with little change in angle of attack, then increases as the aircraft pitches down and rate of sink increases, exciting the phugoid. The new trim speed is lower than initial trim because of the added lift due to thrust deflection. If pitch attitude were held constant, the flight path would steepen, angle of attack would increase, and speed would decrease. An initial increase in positive vertical acceleration would accompany a more rapid thrust (nozzle down) deflection. The effect of rotating nozzles from the near vertical to aft position is shown in figure 29(b). The time history shows that the pilot initially puts in forward column to counter the nose-up trim change. The aircraft sinks momentarily as the lifting force due to thrust is removed (about −0.1 g), speed increases rapidly, and the aircraft climbs as the pilot pitches the aircraft up. With the exception of the initial increased sink rate due to the lift changes, the response is similar to a thrust increase in a conventional aircraft. Figure 29(c) illustrates similar effects for a smaller change in nozzle position. Thrust vectoring was an effective means for deceleration to approach speed and for flight-path control during glide-slope interception. Once on a −7.5° approach path at 60 to 65 knots, modulation of the nozzles in the range 70° to 90° provided a very effective airspeed or flight-path control which could take the place of conventional throttles. The initial tendency for the aircraft to sink when vectoring the thrust aft, however, restricted the use of the nozzles as a control in the final phase of the flare close to the ground. The pilots preferred to revert to throttle and elevator control for the touchdown. A special technique is required in low altitude waveoffs to avoid sinking when the thrust is vectored aft; increasing angle of attack as nozzles are moved aft effectively alleviates a problem with the loss in lift.

Aircraft response to changes in throttle setting is conventional in the cruise configuration. With flaps down, the response is unconventional, particularly in landing configuration with highly deflected flaps and nozzles down. Figures 30(a) and 30(b) illustrate response to a step increase and a step decrease in power, respectively, in the landing configuration. In the time histories shown in figure 30, the pilot is controlling with the elevator to maintain constant pitch attitude. Increasing thrust with nozzles deflected to 83° produces a lifting force, instead of an axial force, thus causing the aircraft to heave upward. Figure 30(a) shows a peak vertical acceleration of 0.10 g for a step from about 92.5% to 98.5% *rpm* at 2060 m (7000 ft) altitude and no change in longitudinal acceleration. Flight path shallows initially, but with a near constant angle of attack the airspeed decreases tending to wash out the change in flight-path angle.

Similarly, the short-term effect of reducing power (fig. 30(b)) with attitude held constant is a decrease in load factor and a steepened flight-path angle, but as speed increases the flight path tends to shallow. With the use of thrust as the primary flight-path control, this adverse speed-path coupling made it necessary for pilots to continually control both attitude and thrust to achieve desired corrections in flight path and speed. Where the required flight-path corrections were large, pilots preferred to revert to a combination of nozzle and thrust control to achieve the desired response. The direct pitching moment produced as a result of engine throttle or nozzle changes is small because of the proximity of the thrust reaction to the airplane center of gravity. The airplane response to changes of flap deflection is docile because the rate of change of flap deflection is low (4°/sec). The elevator required to trim as a function of airspeed for four flap configurations is shown in figure 31 for a gross weight condition of approximately 197,000 N (44,300 lb) at about 95% *rpm*. Shown also in figure 31 is the variation of elevator required at constant angles of attack as flaps and airspeed are varied. The trim change is nose-up at constant airspeed as flaps are lowered requiring forward column deflection for trim. A change of about 5° (airplane nose-down) elevator deflection is required for a transition at constant 5° angle of attack from cruise configuration (148 knots, flaps up) to the landing approach configuration (63 knots, 65° flap deflection, 88° nozzle deflection). Typically, the transition is made with sizeable variations in engine *rpm* and nozzle deflection and small variations of angle of attack.

A time history of a transition from about 30° flaps to landing flaps is shown in figure 32. The data show that although flaps, nozzles, engine *rpm*, and airspeed are all changing, only small elevator angle changes (about 6°) are required. About 7 sec are required to change the flap deflection the first 20°. The last 10° change of flap deflection takes about 14 sec.

Longitudinal response to a simulated engine failure– The airplane response to a simulated engine failure is presented in figure 33 for the takeoff and landing configurations. In the takeoff configuration (fig. 33(a)) the starboard engine is throttled back just after lift-off, with flaps at 24.8° deflection and about 90 knots airspeed. The gross weight was 210,000 N (47,000 lb). As the engine *rpm* spins down to idle, the rate of climb decreases from 7.5 m/sec to near zero and angle of attack increases from 6° to 10°. Only about 2° of up elevator is required to maintain trim. During the entire maneuver the airspeed is held within 5 knots of 90 knots, which was the airspeed at the time the throttle was moved to idle.

The landing approach simulated engine failure time history is shown in figure 33(b) for a 165,000 N (37,000 lb) gross weight condition. The starboard engine is retarded from 95% *rpm* to idle with flaps at 65°, nozzles at 65°, and airspeed about 70 knots. As the engine *rpm* spins down, the nozzles are rotated aft and airspeed is increased to 80 knots, at which time the flap retraction is started. The angle of attack is held near 2° until the start of flap retraction where the angle of attack is increased to about 6°. The elevator required for trim is 2° to 3° until the beginning of flap retraction. At 30° flap deflection (92 knots) the required elevator is -2°. A positive rate of climb is achieved at about 92 knots airspeed with 99% *rpm* on the port engine at a density altitude of 504 m (1654 ft). About 150 m of altitude is lost in the recovery. The pilots considered the trim change and pilot workload with a simulated engine failure little different from conventional aircraft; the performance, however, was quite different. In the simulated engine failure, the thrust change to idle is slow (20 sec) due to the deceleration schedule of the engine. A rapid deceleration of the engine in an actual engine failure would increase the pilot workload as the trim change and lift loss would occur more rapidly. Recognition of engine failure would be different from that experienced in conventional airplanes as little or no side force is noted by the pilots.

Longitudinal characteristics in the stall– The characteristics at the stall are summarized in table 7 for various takeoff, cruise, and landing configurations. Time histories of approach to stalls are presented in figure 34. In general, the stall is characterized by a mild reduction in vertical acceleration preceded by buffeting as the stall is approached. Most configurations exhibit a strong nose-down pitching moment near the stall or just beyond the stall angle of attack. Recorded angles of attack at the stall varied between 17° and 30°, depending on airplane configuration. The lowest angle of attack recorded at the stall (17°) was experienced in the landing configuration with one engine at idle. The highest stall angle of attack recorded was in the cruise configuration. The only adverse longitudinal characteristic observed in the stall was for the landing approach configuration with high engine power, in which case a slight pitch-up tendency was noted. In the case shown in figure 34(a), the pilot used full forward column to recover from the stall and expressed concern because of the sluggishness of the angular response in pitch. For this condition the airspeed was about 43 knots, nozzles were 73°, engine *rpm* was 99.4%, and the trim elevator at 5° to 6° nose-down as the stall was approached; the airplane gross weight was 189,000 N (42,500 lb). In most other configurations the airplane had a tendency to pitch down as stall was approached as shown in figs. 34(b), 34(c), and 34(d). It should be noted that there is considerable uncertainty as to airspeed near the stall. The airspeed calibration (ref. 11) indicates inaccuracy at large values of C_L.

With both engines operating at 96.7% *rpm* in the landing approach configuration (65° flaps) with engine nozzles at 74°, the stall angle of attack is 27° (fig. 34(b)) and airspeed at the stall is 47 knots. The airplane gross weight for this stall was 191,000 N (42,900 lb). As the stall is approached, the airspeed remains constant at 47 to 48 knots and the elevator required for trim is essentially constant from 21° angle of attack to the stall. Recovery from this stall was made using 13° nose-down elevator, which was initiated at 30° angle of attack ($C_L = 5.5$) where C_L has decreased from a maximum of 6.3 at the stall.

The maximum engine power at which the stall was recorded with takeoff flaps (30°) was 93.5% *rpm*. At higher engine power, the pitch attitude became very high (>30°) and the pilots preferred not to conduct full stalls. A time history of the approach to stall is shown in figure 34(c) for a gross weight of 192,000 N (43,200 lb) with 99.6% *rpm*. In this stall approach, the maximum C_L of 4.5 is achieved at 25° angle of attack, 29.5° pitch attitude, and 52 knots airspeed. Stall recovery was initiated at 25° angle of attack. About 3° nose-up elevator is required for trim at maximum lift coefficient and 11° nose-down elevator increment is used to effect the recovery. The extrapolated stall speed that would be predicted at sea level with N_H at takeoff *rpm* ($C_J = 0.92$) and for a weight of 200,200 N (45,000 lb) would be 50 knots and require about $-2°$ of elevator deflection; pitch attitude would be about 27°. The maximum test value of C_J at the stall was 0.62 with N_H at takeoff *rpm* and flap deflection at 30°.

In the cruise configuration (flaps up) with 90.4% engine *rpm*, a maximum lift coefficient of 2.9 is reached at 28° angle of attack. Figure 34(d) is a time history of the approach to stall for this condition. The maximum lift coefficient of 3.1 was reached at 69 knots with an airplane gross weight of 197,500 N (44,400 lb). An increasing amount of aft column deflection is required as maximum lift coefficient is approached, with $-14°$ elevator required for trim at the stall. Beyond maximum lift coefficient at 30° angle of attack the lift coefficient is reduced to 2.7 at which point recovery is initiated using about 7° nose-down elevator.

In general, the pilots found no problem with the control characteristics at the stall and conventional recovery techniques were applicable. There was some lateral and directional unsteadiness at angles of attack near the stall which required constant attention of the pilot. The control task was not considered difficult, but the work load was high.

Ground effect– In the landing configuration, measurements of ground effect show a marked decrease in drag, a nose-down pitching moment, and a slight increase in lift as the airplane descends to ground level. Figure 35 shows the effect of ground proximity on the lift, drag, and pitching moment coefficient obtained from several landings in which the airplane descended slowly to touchdown. The discrete data points shown were derived from test data (assumed quasi-steady-state) collected with flaps 65°, $C_{L_A} = 2.3$ and 3.0, and engine nozzles deflected between 50° and 80°. The data points for $C_{L_A} = 3.0$ are typical of the STOL landing conditions; however, in practice the flight path is much steeper. Separate flight conditions were used for determining lift, drag, and pitching-moment ground effects. The engine power varied between 93% and 96% *rpm*, depending on flight conditions and gross weight. Figure 35 also presents fairings ($C_{L_A} = 2.65$) based on a least-squares fit to the entire data for four runs using a regression parameter identification technique (ref. 15). When the airplane is flying at ground level the drag is about 70% and lift 105% of the basic values ($C_{L_A} = 2.65$ and $C_{D_A} = 0.45$). The nose-down pitching moment at ground level for the same condition is equivalent to about 8° elevator deflection ($\Delta C_m = -0.3$). The pitching moment in-ground effect was not considered excessive by the pilot. Reference 15 further discusses the ground effect and shows a sizeable change in the ground effect (C_{m_G} and C_{L_G}) with angle of attack. These data indicate $\Delta C_{m_G}/\Delta\alpha = -1.1/\text{rad}$ and $\Delta C_{L_G}/\Delta\alpha = -1.0/\text{rad}$ between $-1°$ and 6° angle of attack with the airplane flying at ground level ($\delta_f = 65°$). There was no measurable change in C_{D_G} with angle of attack for the test conditions.

Lateral-Directional Stability and Control

Lateral-directional stability and control characteristics of the airplane are summarized in tables 8 through 12. The stability derivatives for the STOL landing approach condition at 62 knots airspeed are given in table 8. These stability and control derivatives are from flight tests with the SAS turned off, which were performed after the powered elevator was installed. A parameter identification method such as that reported in reference 13 was used to obtain the stability derivatives.

Lateral control– The lateral control effectiveness is a function of several variables in addition to free-stream dynamic pressure (airspeed) and the three separate control surface deflections. The rolling moment due to aileron deflection varies with the momentum coefficient of the boundary-layer control (BLC) air, and, therefore, varies with engine fan thrust (engine speed, altitude, and temperature), and aileron droop angle, which is a function of flap angle. The rolling moment due to spoiler deflection varies, in turn, with the effectiveness of the drooped ailerons. The rolling moment due to the augmentor choke varies also with engine fan thrust and flap angle. In addition, the angular acceleration for a specific total rolling moment depends on the roll moment of inertia which changes significantly with distribution of the fuel load in the wing tanks. Also, under single-engine conditions, only one aileron has BLC because of the cross ducting arrangement. It is difficult, therefore, to define the lateral control effectiveness for all conditions. Data will be presented that are for configurations that are similar to those used in STOL takeoff, landing, and cruise.

Lateral control effectiveness was measured by conducting lateral control reversals with the airplane in various configurations. A force was applied to the control wheel in one direction and then rapidly reversed and held in the opposite direction with rudder pedals neutral. Rolling angular acceleration was measured as roll rate passed through zero. A typical reversal at 65° flaps with SAS off is presented in figure 36(a) and with SAS on in figure 36(b). The measured variation of maximum lateral control power with airspeed for the takeoff, cruise, and landing configurations is presented in figure 37 along with predictions. The predicted values for the flight test points are shown for 65° and 30° flap configurations (figs. 37(a) and 37(b)) and are within 0.01 rad/sec^2 of the test values except the 92% *rpm*, 30° flap case shown. The flight-test measured control power at 92% *rpm* with 30° flaps is about 0.04 rad/sec^2 greater than predicted. Since there is excellent agreement between test and predicted control power, the predicted control power curves shown for sea level standard day conditions are representative of actual airplane performance. An exception is the takeoff flap (30°) condition at reduced engine power (90% *rpm*) where the predicted control power appears conservative. The predicted curve shown in figure 37(c) for lateral control power for the cruise configuration ($\delta_f = 5.6°$) is based on the average of the measured values of the rolling-moment coefficient computed for a rolling moment of inertia of 474,500 kg-m^2 (350,000 slug-ft^2).

In the approach configuration at 65 knots airspeed (65° flaps, 93% *rpm*) the maximum rolling acceleration at 178,000 N (40,000 lb) gross weight is 0.63 rad/sec^2. At 200,000 N (45,000 lb) the maximum rolling acceleration is 0.50 rad/sec^2 at 65 knots and 92% *rpm*. The lower value for the higher gross weight reflects the increase in roll moment of inertia.

In the takeoff configuration (30° flaps) at 90 knots airspeed the maximum rolling acceleration available with 100% *rpm* is 0.71 rad/sec at 200,000 N (45,000 lb) and 0.86 rad/sec^2 at 178,000 N (40,000 lb) gross weight.

The maximum rolling acceleration measured with flaps up was 1.33 rad/sec^2 at 160 knots and 200,000 N (45,000 lb) gross weight. At 120 knots airspeed a value of 0.85 rad/sec^2 was measured at 196,000 N (44,000 lb) gross weight.

Measured values of rolling acceleration as a function of control wheel deflection are shown in figure 38 for the 67° flap configuration at 69 knots. This figure includes data for the complete lateral control system operating and for conditions where the chokes and spoilers were disabled separately to show the influence of each. The faired curves of figure 38(a) were used to construct the curves of figure 38(b), which shows the rolling acceleration produced by each of the three lateral control surfaces. This figure shows that each control surface contributes about one-third of the total rolling moment for wheel deflections greater than 40°. At wheel deflections less than 40°, the contribution of each control surface reflects the gearing schedule shown in figure 12. The effect of engine power and SAS on lateral control is shown in figure 39 for all control surfaces operating at 69 knots airspeed. At 89% *rpm* with 60° of wheel deflection, the rolling acceleration is about 0.58 rad/sec^2; at 93% to 95% *rpm* it is about 5% greater. In the control wheel deflection region up to about 30°, the SAS-on configuration should exhibit a greater rolling acceleration than does the SAS-off condition because of the "quickener" (fig. 14(c)); however, the difference is not discernible in the data. In figure 36(b) it is evident that the SAS input to surface deflection at zero roll rate (the acceleration measuring point) is leading the control wheel deflection. The SAS-on roll acceleration data is corrected to account for this by the inclusion of an equivalent wheel deflection equal to the amount of the SAS input. With all surfaces operating (SAS off), the lateral control sensitivity at 69 knots is about 0.012 rad/sec^2/deg of wheel deflection in the region of less than 20° wheel deflection. Figure 40 presents roll acceleration data measured at a speed of 62 knots, and figure 41 summarizes 65° flap data in terms of the ratio of roll acceleration to dynamic pressure $(\dot{p}/\bar{q})$. Available acceleration decreases as speed decreases, approximately in proportion to dynamic pressure, to about 0.5 rad/sec^2 at 60 knots. The roll control sensitivity is considered satisfactory by the pilots.

Figure 42 presents roll acceleration data for landing flaps; the data were obtained at 69 knots airspeed and a gross weight of about 200,000 N (45,000 lb). Maximum acceleration is reduced to about 0.53 rad/sec^2 at this weight because of the increased inertia.

Figure 43 shows roll acceleration available in a simulated engine-out configuration with flaps at 66°. Lateral controls are still very effective with a maximum of 0.59 rad/sec^2 measured at 72 knots, 176,000 N (39,500 lb) gross weight, with the left engine at 61% *rpm* (idle) and the right engine at 99.7% *rpm*. For this configuration, about 10° right wheel deflection is required for trim and the maximum rolling acceleration to the right is less than to the left. The engine nozzle deflection for this case was 75°, which is a more severe out-of-trim condition laterally than with reduced nozzle deflection. When the nozzles are rotated aft, the asymmetric moment is changed from roll to yaw. With nozzles undeflected the lateral trim required is about half that of the 75° nozzle deflection condition.

Maximum roll rates achieved in the wheel reversal maneuvers at flaps nominally 65° are given in figure 44 for SAS-on and SAS-off conditions at about 173,000 N (39,000 lb) gross weight. Maximum rate available, SAS on, is about 23°/sec at 69 knots.

Figure 45 presents roll angular acceleration data for the 33° and 5.6° flap configuration at gross weights of 196,000 to 200,000 N (44,000 to 45,000 lb). With 33° flaps, the maximum acceleration at 78 knots is 0.53 rad/sec^2. These data are for an engine thrust setting of approximately level flight; the control power with takeoff thrust is 0.59 rad/sec^2 at the same airspeed and gross weight. With flaps up (fig. 45), the measured maximum rolling acceleration is 1.25 rad/sec^2 at 166 knots ($C_l = 0.074$). This high value is due in part to the lower surface of the chokes acting as ailerons. The choke deflection is only 10.4° with flaps up (fig. 12). Figure 46 presents additional data for approximately 30° flaps showing the effect of choke and spoiler on control power. At 60° wheel deflection the spoilers produce about 35%, the chokes about 25%, and the ailerons 40% of the total rolling moment. The control surface to wheel gearing is shown in figure 12.

In figures 36(a) and 36(b) it can be seen that with SAS on or off at STOL airspeeds, the yaw acceleration due to lateral control is very small. However, some adverse sideslip is evident; it will be discussed later.

Directional control– Directional control power was evaluated by conducting rudder reversals with the control wheel at neutral. Maximum yaw acceleration was measured as yaw rate passed through zero. The measured yaw acceleration is corrected to account for the yawing moment produced by the sideslip angle present at the time of measurement. A typical directional control reversal with SAS off is shown in figure 47, and with SAS on in figure 48. Roll acceleration due to directional control with SAS on is small (fig. 48).

The rudder power measurements shown in figure 49 for the landing configuration are about 70% of those predicted for one-half maximum rudder deflection. At 14° of rudder deflection, 0.15 rad/sec^2 yawing acceleration was measured at 72.5 knots airspeed (flaps 65°). The installation of the powered elevator reduced the rudder area by 0.14 m^2 (2.5%) and increased the yawing moment of inertia about 5% at 178,000 N (40,000 lb) gross weight. It is obvious that, aside from the inertia and area change, the empennage modification reduced the rudder power. After modification, the measured rudder power is about 70% of predicted, while it was 90% to 95% of predicted before the modification.

Results of rudder reversal tests with 67° and 33° flaps, which were conducted prior to the empennage modification, are compared with predicted results and are presented in figure 50. At 67° flaps and at an airspeed of 70 knots, a yaw acceleration of 0.22 rad/sec^2 was measured for 17° (68%) of rudder deflection. The measured value is slightly less than the predicted value of 0.23 rad/sec^2. At 33° flaps and 80 knots airspeed, a yawing acceleration of 0.22 rad/sec^2 was achieved at 66% rudder deflection and is about 75% of predicted.

Maximum yaw rates achieved during the rudder reversal maneuvers conducted before the empennage modification are shown in figure 51. At 67° flaps, 69 knots, and SAS off, a yaw rate of 0.17 rad/sec was measured when using 10° rudder deflection. With SAS on, the maximum yaw rate measured was about 0.18 rad/sec with flaps at 33°, 80 knots airspeed, and using 60% of maximum rudder pedal deflection. Higher values of yaw rates are shown in the figure; however, for those cases the control deflection was decreased while the yaw rate was still increasing.

Lateral-directional static stability– The static stability characteristics were assessed by performing steady sideslip maneuvers. Test results are presented for takeoff, approach, and cruise configurations in figures 52 through 56.

Data are shown for tests conducted both before and after the elevator/rudder modification. The aircraft exhibits positive stability about both lateral and directional axes for all configurations tested, and the modification produced no noticeable effect.

Figures 52 and 53 present data for the 65° flap condition. Figure 52 shows variation of rudder deflection, wheel deflection, bank angle, and elevator position with sideslip; figure 53 shows the same data as a function of rudder angle and indicates a positive dihedral effect. The data fall within a range of C_{l_β} as predicted by wind-tunnel tests, correlating better with $C_{l_\beta} = -0.004$ than with $C_{l_\beta} = 0$. The variation of rudder and wheel deflection with sideslip angle is reasonably linear out to ±15°. At 65 knots the sideslip produced by 10° rudder is about 22% less than the predicted value, indicating a higher directional stability than predicted. At speeds below 90 knots, the aircraft exhibited a low-amplitude directional "snaking" characteristic ($\beta = \pm 1°$ to $2°$) indicating that near zero degrees of sideslip the directional stiffness may be very low. Attempts to document any nonlinearities were not successful. About half available rudder and less than half available wheel throw are required to achieve 15° sideslip at 65 to 70 knots.

Figure 54 presents steady sideslip data for the 30° flap configuration at airspeeds of 65, 90, and 97 knots. The rudder deflection with sideslip is linear through the test range of ±15° sideslip; however, the slope of control wheel deflection with sideslip is reduced with increasing angles of sideslip and indicate a reduction in the apparent dihedral effect at increasing angles of sideslip. The 97-knot data were collected after installation of the powered elevator and the data for 75 and 90 knots were from flights made previous to the modification. Since the rudder deflection required for a given sideslip angle is identical for both configurations and because the modification reduced the rudder power, it follows that the directional stiffness was reduced as a result of the modification. This reduction in directional stiffness was nearly proportional to the reduction in rudder power.

In the flaps-up configuration, the reduction in apparent dihedral effect with increasing sideslip angle is more marked, as shown in figures 55 and 56 than for the 30° flap configuration. At 120 knots, about 15° of control wheel is required at 5° sideslip angle while only about double that is required for a threefold increase in sideslip angle (15°). The flaps-up configuration test data show approximately a linear variation of rudder deflection with sideslip over the range of conditions tested.

In the STOL landing configuration, 15° of sideslip is achieved with bank angles of about 5°, indicating low net sideforces. Ratios of bank angle to sideslip angle in steady-state sideslip, were approximately as follows:

δ_f, deg	ν, deg	V_E, knots	N_H, %	ϕ/β
65	6	65	93	0.25
30	6	75	90	.30
5.6	6	120	PFLF	.65
5.6	6	150	PFLF	.85

The low ϕ/β at landing approach speeds below 65 knots results in very little lateral acceleration with sideslip. The absence of the lateral acceleration cue requires the pilot to use the sideslip indicator in the cockpit much more as speed is reduced to maintain low sideslip angles. The low directional stability aggravates this problem.

Longitudinal trim change with sideslip is small for all configurations, requiring a maximum of about 1° elevator deflection change over the range of sideslip tested.

Lateral-directional dynamic stability– Lateral-directional dynamic characteristics were evaluated at flap settings of 65°, 30°, and 5.6° with the roll and yaw SAS on and off (SAS is automatically off above 100 knots). In addition, evaluations were made in the landing approach configuration with only the roll SAS operating (yaw SAS off) and with only the yaw SAS operating (roll SAS off). Dynamic characteristics are summarized in table 9, Dutch-roll characteristics are shown in figure 57, and roll damping characteristics are shown in figures 58 and 59. Figure 60 shows a typical Dutch-roll time history at 67 knots airspeed.

The flagged data points shown in figure 57 are from flights conducted after the elevator/rudder modification and SAS gearing change (fig. 14(a)). At the time of installation of the powered elevator, the rudder area was reduced 2.5%, directional inertia increased about 5% and rolling inertia increased about 1% at 178,000 N (40,000 lb) gross weight. The inertia change had only a small effect on the Dutch-roll characteristics (SAS off), while the SAS gearing change had a large effect. As noted in the discussion on static stability, a residual directional snaking motion was common at speeds below 90 knots even with SAS on. The SAS gearing was changed to increase the $\dot{\beta}$ damping which markedly improved the pilots' opinion of the directional characteristics at landing approach speeds by reducing, but not eliminating, the snaking motion.

At the landing approach flap deflection of 67°, the Dutch-roll damping with SAS off is low with a damping ratio of between 0.1 and 0.2. The Dutch-roll period is 6 to 7 sec and is close to the predicted value at 60 to 70 knots. The measured Dutch-roll period is slightly less than that predicted with flaps 33° at about 100 knots airspeed, indicating a trend toward greater directional stiffness than predicted at higher speed with takeoff flaps. With flaps up, the Dutch-roll period and damping are about as predicted. The oscillation is primarily a yawing motion with $|\phi|/|\beta|$ about 1.0.

With SAS on, the Dutch-roll damping ratio was about 0.3 (flaps 67°) before the SAS modification, and about 0.45 (flaps 62°) after the modification. The Dutch-roll period with SAS on was about 7 sec before and about 9 sec after modification. With either SAS configuration, the roll-to-yaw ratio ($|\phi|/|\beta|$) is about 0.75 with flaps extended (65°) and 60 to 70 knots airspeed.

In the landing condition, with the roll SAS off, there is little effect on the Dutch-roll; however, with the yaw SAS off, the Dutch-roll is similar to that when both roll and yaw SAS are off.

With flaps 33°, the Dutch-roll damping ratio with SAS off is about 0.1 at 78 knots, but with SAS on damping is increased to a satisfactory level of about 0.3 at 79 knots. The Dutch-roll damping ratio was increased to 0.7 as a result of the SAS modification. With 30° flaps the Dutch-roll period is little changed by SAS except that the period is about 2 sec longer for the modified SAS configuration. At 78 knots the period is 6.8 sec with SAS off.

In the cruise configuration, Dutch-roll characteristics are satisfactory with period and damping near predicted values. The damping ratio is about 0.15 and period is 4 to 5 sec.

Figures 61(a) through 61(g) present typical time histories of Dutch-roll oscillations with SAS on and off, for the various configurations tested.

Time histories showing aircraft spiral characteristics are shown in figures 62(a) and 62(b). The spiral time to half or double amplitude is given in table 9 for the various configurations tested.

With SAS off at 67° flaps, and nozzles up, the aircraft is spirally unstable as predicted, with time to double amplitude of about 6 sec at 60 to 75 knots airspeed. With nozzle angle increased to 90°, time to double amplitude appears to increase; measured times varied from about 8 to more than 20 sec. Precise spiral behavior was not always discernible due to small lateral trim offsets produced by poor control centering and atmospheric perturbations. With only the yaw SAS operating, the spiral mode was similar to the SAS-off condition with a tendency to diverge more rapidly, the time to double amplitude being 4 to 6 sec. With only the roll SAS operating, the spiral stability is positive. Times to half amplitude of 7 to 10 sec were noted at 69 knots. With all SAS on, spiral stability at 65° flaps is neutral to slightly positive. Increasing nozzle angle to 90° appears again to give a small increase in stability. With 30° flaps the spiral is unstable with SAS off ($T_2 \sim 8$ sec at 78 knots), and the stability is neutral to positive with SAS on. In the cruise configuration, the spiral stability is neutral to slightly positive at 135 and 168 knots airspeed.

The airplane roll damping characteristics are summarized in figures 58 and 59 and in table 9. The roll damping with 67° flaps, nozzles aft, with SAS off is low with a roll time constant of 1.0 sec as determined from roll reversal maneuvers (fig. 36). The apparent roll time constant with SAS on (67° flaps) is 0.45 sec. With flaps 33° the roll time constant is about 1.0 sec (fig. 59) and is approximately the same SAS on or off. With flaps up the roll time constant is 0.8 sec at 135 knots and 0.7 sec at 168 knots; both are near predicted values.

Turn coordination– Turn entries were conducted with flaps at 65°, 30°, and 5.6° and with SAS on and off. All tests conducted at less than 65 knots were performed after the elevator/rudder and the SAS modifications were made; therefore, it is not evident what effect these modifications had on turn coordination. Based on the Dutch-roll and steady sideslip characteristics, the SAS-off turn coordination was little affected by these modifications; however, the SAS-on characteristics were undoubtedly changed. The turn coordination data obtained are shown in figure 63 as the observed peak sideslip to bank angle ratio ($\Delta\beta/\Delta\phi$) which was measured at the initial entry to the turn. Turn coordination characteristics where $\Delta\beta/\Delta\phi$ is greater than about 0.3 is considered unsatisfactory (ref. 16). With SAS on, the aircraft exhibits satisfactory characteristics at speeds above 65 knots. Between 60 and 65 knots (SAS on) the turn coordination is marginally acceptable with the SAS gearing used in the tests. There is considerable scatter in this region with ratios increasing to about 0.4 at 60 to 65 knots. With SAS off, the turn entry degrades markedly due to adverse sideslip giving $\Delta\beta/\Delta\phi$ ratios at speeds less than 80 knots which are above the maximum level of 0.3 generally considered acceptable.

The time history of a turn entry at 68 knots (fig. 64) shows the large adverse sideslip generated on initiation of the maneuver. Yaw rate lags roll rate by about 2 sec. The large sideslip with bank angle and the lag between bank angle and turn rate greatly increase the pilot's workload when maneuvering laterally during low speed approaches without SAS. With SAS on, turn coordination is much improved, as shown in figure 64. Yaw rate now follows roll rate with a small lag, and adverse sideslip is reduced. The SAS reduces $\Delta\beta/\Delta\phi$ ratios to about 0.3, a value the pilots considered satisfactory. The stability augmentation improves the turn coordination by deflecting the rudder proportional to roll rate. Adverse yaw due to lateral control is negligible in both examples.

At 33° flaps with SAS off, some difficulty was encountered in setting up initial steady-state conditions, with β varying ±1° about a steady bias of approximately $-2°$. The $\Delta\beta/\Delta\phi$ ratio data in figure 63, therefore, showed scatter with an average value of about 0.37 at 77 knots. No adverse yaw due to lateral control deflection was evident. But yaw rate lagged roll rate by 1 to 2 sec due to adverse sideslip, thus giving unsatisfactory turn coordination overall. With SAS on, adverse sideslip and yaw rate lag were reduced and turn coordination was considered satisfactory.

In the flaps-up configuration (with SAS automatically off above 100 knots), $\Delta\beta/\Delta\phi$ has a value of about 0.1 at 165 knots and 0.13 at 135 knots. In flaps-up turn entries, no adverse sideslip was evident and yaw rate followed roll rate without lag, indicating satisfactory turn coordination.

Engine out lateral-directional control– Time histories of control and airplane motion recorded at the time of simulated engine failures are presented in figures 33(a) and 33(b) for a landing approach 165,000 N (37,000 lb) and takeoff at 210,000 N (47,000 lb) gross weight.

In the landing-approach simulated engine failure case shown in figure 33(b), the starboard engine was abruptly throttled back to idle from 95% *rpm* while flying at 70 knots airspeed. Approximately 3 sec later the port engine was advanced from 94.3% to 99% *rpm*. The engine nozzles at the time were deflected 65° to 70°. As can be seen in the time history of wheel and rudder positions, little rolling or yawing is experienced until the port engine thrust is increased. At that time a rolling disturbance to the left is evident. About 15° of right wheel is used to counteract this roll and the rudder does not exceed 5° until 9 sec after the engine is throttled back. As the engine decelerates to idle, which requires about 25 sec, the airspeed is increased to 80 knots and the nozzles brought up to 12°. At this condition 20° to 25° of right wheel and 8° left rudder are required for trim. The angle of sideslip increased to about 9° about 11 sec after the engine was throttled back and the sideslip was then trimmed near zero as the airplane reached 80 knots airspeed.

The simulated engine failure time history for the takeoff configuration is shown in figure 33(a). The starboard engine was throttled back from 99% *rpm* to idle about 4 sec after lift off. The airspeed at the time the throttle was retarded was 90 knots. Four seconds after the starboard throttle was retarded the port engine was advanced to about 101% *rpm* from its takeoff setting of 99%. Immediately after the throttle was retarded, a yaw to the right was experienced; it required about 6° of rudder for correction, and after the initial disturbance only about 3° of rudder was required for trim. In contrast to the lateral control required for the landing configuration case, the control required for 30° flaps appears to be insignificant, with a small amount of left wheel used to establish a 3° bank angle to the left. The sideslip is near zero until the left roll attitude is established where it is erratic around about 5° left sideslip.

Pilots considered the lateral-directional characteristics with a simulated engine failure to be acceptable for an emergency condition.

Lateral-directional control in the stall– The lateral-directional behavior of the airplane in the region of the stall is summarized in table 7 for landing approach, takeoff, and cruise configurations. The lateral-directional characteristics in the stall are considered mild except with 66° flaps, nozzles up, and one engine at idle. In this case, nearly full lateral control is required to keep the wings level. Figures 34(a) through 34(d) show the control used in the stall for various configurations.

In the landing approach configuration with nozzles at 75°, there is some lateral-directional instability apparent as the stall is approached, but it is easily controlled using about 5° rudder deflection and a maximum of about 20° wheel deflection. At the stall there is no additional rolling or yawing evident in a typical time history (fig. 34(b)).

In the takeoff flap configuration with engine *rpm* at 99.6%, there is little roll or yaw as the stall is approached, as shown in figure 34(c). Less than 3° rudder and about 3° wheel deflection is used controlling the airplane at the maximum angle of attack. The airplane was not stalled at this condition because of the extreme nose-high attitudes encountered.

With flaps up and with 90% *rpm*, a yaw and roll to the right is encountered at the stall (see fig. 34(d)). About 25° of control wheel deflection and less than 2° of rudder deflection are used for control in the stall. About 9° left sideslip was experienced at angles of attack 1° to 2° above the stall angle of attack.

CONCLUDING REMARKS

A flight investigation of 200,000 N (45,000 lb) augmented jet flap STOL airplane has shown that the stability, control, and handling qualities are satisfactory for VFR tasks over the low-speed operating envelope (60 to 160 knots). Lateral and directional stability augmentation were required to improve the Dutch-roll damping, spiral stability, roll damping, and turn coordination. The longitudinal characteristics were satisfactory for VFR tasks but some form of augmentation would be required for IFR tasks at the low speed required for STOL operations.

In general, the airplane exhibited conventional flying qualities with the exception of flight-path control in the landing approach. With thrust vectoring capability, an additional control is available to the pilot for flight-path maneuvering. The pilots used the thrust vector control to establish landing approach flight-path angle while the engine throttles and elevator were used to establish the desired airspeed and angle of attack. When thrust vector modulation is used to control small deviations from the flight path in the landing approach, the airplane response is similar to that of conventional airplanes. Control of landing approach flight path by use of the engine throttles produced the tendency for unconventionally large deviations of airspeed from trim.

The stability and control characteristics of the airplane with one engine inoperative (simulated) were acceptable for an emergency condition in landing approach and takeoff. Cross ducting of the augmentor and aileron BLC air provide characteristics that result in satisfactory controllability for the one-engine inoperation condition.

A powered elevator control was required to provide satisfactory feel characteristics and full elevator deflection capability at low airspeeds. This improved pitch control is particularly noticeable in the stall recovery (landing approach configuration) and in the landing flare.

Ames Research Center
National Aeronautics and Space Administration
Moffett Field, California 94035, November 11, 1977

REFERENCES

1. Wick, Bradford H.; and Kuhn, Richard A.: Turbofan STOL Research at NASA. Astronaut. & Aeronaut., vol. 9, no. 5, May 1971, pp. 32–50.

2. Whittley, D. C.: The Augmentor Wing: A New Means of Engine Airframe Integration for STOL Aircraft. ICAS Paper 64-574, presented at Fourth ICAS Conference, Paris, Aug. 24–28, 1964.

3. Middlebrooks, J. E.; Tinney, H. C.; and Whittley, D. C.: The Evolutionary Development and Current Status of the Augmentor Wing Concept. Paper 700812 presented at SAE National Aeronautics and Space Engineering and Manufacturing Meeting, Los Angeles, October 5–9, 1970.

4. Kelley, G. S.; and Gerend, R. P.: Propulsion Systems for Commercial STOL Aircraft. AIAA Paper 71-746, AIAA/SAE 7th Propulsion Joint Specialist Conference, Salt Lake City, June 14–18, 1971.

5. Quigley, H. C.; Sinclair, S. R. M.; Nark, T. C., Jr.; and O'Keefe, J. V.: A Progress Report on the Development of an Augmentor Wing Jet STOL Research Aircraft. SAE Paper 710757, National Aeronautic and Space Engineering and Manufacturing Meeting, Los Angeles, September 1971.

6. Ashleman, R. H.; and Skavdahl, H.: The Development of an Augmentor Wing Jet STOL Research Aircraft (Modified C-8A), Vol. I: Summary, NASA CR-114503, 1972.

7. Spitzer, R. E.; Rumsey, P. C.; and Quigley, H. C.: Use of the Flight Simulator in the Design of a STOL Research Aircraft. AIAA Paper 72-762, August 1972.

8. Innis, Robert C.; and Anderson, Seth B.: Comparisons of Simulator and Flight Results on Augmentor-Wing Jet STOL Research Aircraft. NASA SP-320, 1972, pp. 283–290.

9. Whittley, D. C.: The Aerodynamics of High Lift Illustrated by Augmentor-Wing Research. CASI Paper 72/20, presented at 12th Anglo-American Aeronautical Conference, Calgary, July 1971.

10. Skavdahl, H; and Patterson, D. H.: The Development of an Augmentor Wing Jet STOL Research Aircraft (Modified C-8A). Vol. II: Analysis of Contractor's Flight Test. NASA CR-114504, 1972.

11. Quigley, Hervey C.; Innis, Robert C.; and Grossmith, Seth: A Flight Investigation of the STOL Characteristics of an Augmented Jet Flap STOL Research Aircraft. NASA TM X-62,334, 1974.

12. Glende, W. L. B.: Design of a Powered Elevator Control System – Final Report. NASA CR-114727, 1974.

13. Wingrove, Rodney C.: Estimation of Longitudinal Aerodynamic Coefficients and Comparison with Wind-Tunnel Values. NASA TN D-7647, 1974.

14. Spitzer, R. E.: Predicted Flight Characteristics of the Augmentor Wing Jet STOL Research Aircraft. NASA CR-114463, 1972.

15. Wingrove, Rodney C.: Parameter Estimation of Powered-Lift STOL Aircraft Characteristics Including Turbulence and Ground Effects. NASA TM X-62,382, 1974.

16. Innis, Robert C.; Holzhauser, Curt A.; and Quigley, Hervey C.: Airworthiness Considerations for STOL Aircraft. NASA TN D-5594, 1970.

17. NATO-AGARD: V/STOL Handling-Qualities Criteria. AGARD Report 577, Dec. 1970.

18. Allison, R. L.; Mack, M; and Rumsey, P. C.: Design Evaluation Criteria for Commercial STOL Transports. NASA CR-114454, 1972.

19. Military Specification – Flying Qualities of Piloted Airplanes. MIL-F-8785B(ASG), August 1969.

20. Tentative Airworthiness Standards for Powered Lift Transport Category Aircraft. Part XX, Federal Aviation Administration, August 1970.

21. Military Specification – Flying Qualities of Piloted V/STOL Aircraft. MIL-F-83300, December 1970.

22. Condit, P. M.; Kimbrel, L. G.; and Root, R. G.: Inflight and Ground-Based Simulation of Handling Qualities of Very Large Airplanes in Landing Approach. NASA CR-635, 1966.

TABLE 1. RESEARCH AIRPLANE CHARACTERISTICS

Weights, N(lb)		
Maximum gross	213,000	(48,000)
Maximum gross (STOL takeoff)	200,000	(45,000)
Maximum landing (STOL landing)	191,000	(43,000)
Maximum fuel	62,000	(14,000)
Areas		
Wing area, total including ailerons flaps and 10.31 m^2 (111 ft^2) of fuselage, m^2 (ft^2)	80.36	(365)
Wing flap area, projected, including ailerons aft of wing line, m^2(ft^2)	17.38	(187.10)
Total aileron area aft of hinge line, including trim tab, m^2(ft^2)	4.30	(46.30)
Horizontal tail area, total, m^2(ft^2)	21.65	(233)
Elevator area aft of hinge line, m^2(ft^2)	7.57	(81.5)
Vertical tail area, total, m^2(ft^2)	14.12	(152)
Rudder aft of hinge line		
Fore, m^2(ft^2)	2.65	(28.5)
Trailing, m^2(ft^2)	2.79	(30)
Dimensions and general data		
Wing		
Span, m(ft)	24.00	(78.75)
Root chord, m(ft)	3.83	(12.58)
Tip chord, m(ft)	2.36	(7.74)
Reference aerodynamic chord, m(ft)	3.78	(12.4)
Aerofoil section		
Root	NACA 64_3 A417.5 (MOD)	
Tip	NACA 63_2 A615 (MOD)	
Sweepback at 40 percent chord, deg	0.0	
Dihedral, outer wing only, deg	5.0	
(Note: Wing taper and dihedral each start 5.36 m from plane of symmetry.)		
Aspect ratio	7.2	
Ailerons		
Span, m(ft)	3.51	(11.50)
Chord aft of hinge line, m(ft)	.61	(2.01)
Distance from plane of symmetry to centroid of aileron, m(ft)	10.27	(33.70)
Aerodynamic balance, percent	20.0	
Spoilers		
Span, m(ft)	3.44	(11.30)
Chord, m(ft)	.36	(1.18)
Position of hinge line, percent wing chord (average)	62.4	
Flaps		
Span (each side), m(ft)	7.01	(23.0)
Chord aft of hinge line, m(ft)	.98	(3.2)

TABLE 1. RESEARCH AIRPLANE CHARACTERISTICS – Continued

Horizontal tail	
Span, m(ft)	9.75 (32.0)
Root chord, m(ft)	2.54 (8.33)
Mean aerodynamic chord, m(ft)	1.91 (6.25)
Aerofoil section	
Root	NACA 63_A214 (MOD) (inverted)
Tip	NACA 63-212 (MOD) (inverted)
Sweep of leading edge, deg	4.8
Dihedral, deg	0.0
Aspect ratio	4.4
Vertical tail	
Span, m(ft)	4.14 (13.60)
Root chord, m(ft)	4.27 (14.00)
Tip chord, m(ft)	2.54 (8.33)
Mean aerodynamic chord, m(ft)	3.48 (11.41)
Airfoil section, m(ft)	NACA $63_{(215)}$014 (MOD)
Sweep of leading edge, deg	22.6
Aspect ratio	1.2
Overall height, m(ft)	8.75 (28.7)
Overall length (with nose boom of 4.88 m) m(ft)	28.44 (93.32)
Distance, wing MAC, 1/4C, to horizontal tail MAC, 1/4C, m(ft)	14.11 (46.3)
Distance, wing MAC, 1/4C, to vertical tail MAC, 1/4C, m(ft)	13.23 (43.4)
Wing incidence angle, deg	+2.5
Horizontal tail incidence angle (ground adjustable), deg	+1.0
Control surface deflections and rates	
Flaps	5.6° down to 72° down 4°/sec extension and retraction
Conical nozzles	6° to 104° (down from aft of aircraft) 90°/sec
Ailerons (65° flap deflection)	±19° about +35° max droop angle 50°/sec
Spoilers	48° 120°/sec
Augmentor choke	55% choke gap area closure at 75° flap deflection 35°/sec
Rudder	±25° forward segment ±25° trailing segment -50°/sec
Elevator (at 65 knots)	-24° +15°

TABLE 1. RESEARCH AIRPLANE CHARACTERISTICS – Concluded

Maximum design speeds, knots	
Dive speed (V_D)	180
Maximum operating speed (V_{mo})	160
30° flaps-down speed (V_{f30})	120
>50° flaps-down speed ($V_{f>50°}$)	90

Moments of inertia, at 178,000 N (40,000 lb) gross weight

With powered elevator, kg-m^2 (slug-ft^2)

I_x = 361,000 (266,300)
I_y = 316,000 (233,100)
I_z = 620,000 (457,300)

With spring-tab elevator, kg-m^2 (slug-ft^2)

I_x = 357,000 (263,300)
I_y = 278,000 (205,000)
I_z = 587,000 (432,900)

TABLE 2. ELEVATOR RESPONSE AND FLIGHT-PATH CONTROL FOR THE STOL APPROACH CONDITIONS (65 knots)

	Subject airplane	Criterion	
		Value	Reference
Elevator control power			
(F_{COL} = 180 N ≈ 40 lb), rad/sec^2	0.47, −0.37	>0.05 to 0.20	17
Pitch control sensitivity			
($\dot{q}/\varepsilon_{COL}$), rad/sec^2 cm	.03	- - -	
rad/sec^2 in.	.08	>.08	17
Stick force per g, N/g	191	- - -	
lb/g	43	<20 to 40 > 3	17
Effective vertical speed crossover time ($t_{\dot{h}}$), sec	.9	$\leqslant$.8	18
Load factor response time constant (τ_{n_z}), sec	~1.5	<1.5	16
Load factor per unit control deflection (n_z/δ_{COL}), g/cm	.04	- - -	
g/in.	.10	~.1	18
Load factor per unit angle of attack (n_z/α_F), g/rad	1.8	>2.3	18
Flare control load factor, g	>1.20	$\geqslant$1.20	18
Pitch angle after 1 sec, deg (F_{COL} = 180 N ≈ 40 lb)	3.1	>2 to 4	17

TABLE 3. ELEVATOR SYSTEM CHARACTERISTICS AT STOL APPROACH SPEED (65 knots)

	Subject airplane	Criterion	
		Value	Reference
Elevator deflection from trim at 180 N (40 lb) F_{COL}, deg	−24, +14	- - -	
Control column deflection, cm	+19, −13	- - -	
in.	+7.5, −5	>±4, <±6.5	17
Elevator to column gearing, deg/cm	1.9	- - -	
deg/in.	4.8	- - -	
Force gradient ($\Delta\delta_e < 10°$), N/cm	10.1	- - -	
lb/in.	5.8	>2, <5	17
Column force at T.E.U. maximum δ_e, N	190	- - -	
lb	42	<75	20

TABLE 4. LONGITUDINAL STABILITY CHARACTERISTICS AT STOL APPROACH SPEED
(65 knots, 178,000 N Gross Weight)

	Subject airplane	Criterion	
		Value	Reference
Stick-fixed stability ($\Delta\delta_e/\Delta V_E$), deg/knot	0.1	>0	20
Change of flight path with velocity ($\Delta\gamma/\Delta V_E$) deg/knot	0	$\leq .06$	19
Short-period natural frequency (ω_n), rad/sec	1.03	$>.47$	21
Short-period damping ratio (ζ)	.9	>1.06	21
Phugoid natural frequency (ω_n), rad/sec	.2	. . .	
Phugoid damping ratio (ζ)	.1	>0	21
Change of θ with velocity ($\Delta\theta/\Delta V_E$), deg/knot	−.8	<0	18

TABLE 5. AIRPLANE SHORT PERIOD AND PHUGOID CHARACTERISTICS

						Short period			Phugoid		
δ_f, deg	ν, deg	V_E, knots	Weight		C_J	ω_n, rad/sec	ζ	P, sec	ω_n, rad/sec	ζ	P, sec
			N	lb							
67	9	62	184,000	41,400	0.39	1.00	0.72	9.1	0.17	0.09	37.1
66	40	64	172,000	38,700	.38	.87	.90	16.5	.19	.09	33.2
67	77	65	167,000	37,500	.49	1.03	.90	14.1	.19	.10	33.2
33	14	78	178,000	40,000	.22	1.20	.86	10.1	.18	0	34.9

TABLE 6. STABILITY AND CONTROL DERIVATIVES FOR THE LANDING APPROACH CONFIGURATION

δ_f = 67° α_F = -2° to 10°
ν = 14° V_E = 66 to 79 knots
N_H = 94.5% I_y = 281,000 kg-m^2 (207,000 slug-ft^2)
C_J = 0.3 to 0.4

Stability and control derivatives	Flight measured	Predicted
$C_{Z_{\alpha_F}}$	5.07	4.79
$C_{Z_{\delta_e}}$	-.68	-.55
C_{Z_q}	-17.0	-10[a]
$C_{Z_{C_J}}$	-3.00	-3.45
$C_{X_{\alpha_F}}$	1.32	1.33
$C_{X_{\alpha_F^2}}$	2.22	3.56
$C_{X_{\delta_e}}$	.18	. . .
C_{X_q}	1.57	1.0[a]
$C_{m_{\alpha_F}}$	-.55	-.52[b]
$C_{m_{\delta_e}}$	-2.05	-2.05[b]
C_{m_q}	-29.7	-35[a]

[a] Predicted tail contribution only, $q + \dot{\alpha}_F$

[b] Adjusted for c.g. location and $C_{m_{\alpha_F}}$

TABLE 7. STALLING CHARACTERISTICS

Flap deflection δ_f, deg	Nozzle deflection ν, deg right/left	Engine rpm N_H, % right/left	Gross weight, W		Stall angle of attack, α_F deg	Stall airspeed V_E, knots	Buffet	Behavior at stall (typical)
			N	(lb)				
65.0	76/72	96.6/96.9	191,000	(42,900)	27	47	Slight	G break, some directional snaking, pitch-up tendency
64.5	7/12	95.0/95.8	193,000	(43,400)	24	51	Moderate	Slight G break, yaw and roll to right, full fwd. control used
65.7	73/72	Idle/99.6	197,000	(44,300)	18	65	Moderate	G break, roll and yaw to left, lat.-dir. oscillation
65.8	9/13	Idle/97.0	187,000	(42,000)	21	63	Mild	G break, yaw left, pronounced lat.-dir. oscillation, full lat. control required
31.0	12/11	93.0/94.0	192,000	(43,200)	23	58	Mild	Slight G break, roll and yaw to left
30.3	7/8	97.0/Idle	192,000	(43,200)	22	66	Slight	Slight G break, yaw left, roll right, lat.-dir. oscillation
5.8	8/7	90.1/90.6	197,000	(44,300)	28	69	Heavy	Slight G break, roll and yaw to right
5.6	10/10	97.3/Idle	178,000	(40,000)	26	67	Heavy	G break, roll and yaw to right

TABLE 8. LATERAL-DIRECTIONAL STABILITY AND CONTROL DERIVATIVES

δ_f = 65°
W = 182,000 N (40,900 lb)
α_F = 5.6°
C_J = 0.47
C_{l_p} = -0.502
C_{n_β} = 0.272
C_{n_r} = -0.727
C_{y_p} = -0.044
V_E = 62 knots
N_H = 96.5%
ν = 87°
C_{l_β} = -0.169
C_{l_r} = 0.436
C_{n_p} = -0.937
C_{y_β} = -1.32
C_{y_r} = 1.12

TABLE 9. LATERAL–DIRECTIONAL DYNAMIC CHARACTERISTICS

SAS	δ_f	ν	V_E, knots	Weight, N × 10^{-3}	C_J	Dutch roll mode			Spiral mode		Roll mode
						P, sec	ζ	ω_n, rad/sec	$T_1/_2$, sec	T_2, sec	τ_A, sec
OFF	67°	~10°	~70	165 to 178	0.23-0.35	6	~0.15	1.06	- - -	5-7	1.0
Roll on/yaw off	↓	↓	↓	169	.34	7	.13	.91	8	- - -	- - -
Roll off/yaw on				169	.34	- - -	- - -	- - -	- - -	5	- - -
ON				173	.35	6.8	.33	.98	Neut - pos	- - -	0.45
ON		90°	60	173	.40-.45	- - -	- - -	- - -	Neut - pos	- - -	- - -
ON[a]		74°-85°	62-66	173 to 196	.43-.49	8.8	.46	.80	Neut - pos	- - -	- - -
OFF[a]		90°	62	173 to 182	.43	7.0	.14	.90	- - -	8-20	- - -
OFF	33°	~10°	102	178	.15	4.9	.16	1.3	- - -	- - -	~1.0
↓	↓	↓	105	178	.21	4.3	.12	1.45	- - -	- - -	- - -
			78	198	.27	6.8	.10	.94	- - -	8	- - -
ON			79	195	.29	6.4	.31	1.03	Neut - pos	- - -	~1.0
ON[a]	30°		77	200	.32	8.4	.71	1.06	- - -	- - -	- - -
Not applicable	6°	~10°	168	200	.06	4.2	.16	1.51	Neut - pos	- - -	.70
Not applicable	6°	~10°	135	178 to 196	.075	5.0	.15	1.27	Neut - pos	- - -	.80

[a] These three conditions from flights conducted after the elevator/rudder and SAS modifications; all others from flights conducted before the modifications.

TABLE 10. LATERAL AND DIRECTIONAL CONTROL CHARACTERISTICS

	Subject airplane	Criterion	
		Value	Reference
Lateral			
Control wheel travel at max $\dot{p}$, deg	±75	±60	16
Control travel, cm	±28.5	- - -	
in.	±11.2	- - -	
Breakout force, N	±22.2	- - -	
lb	±5.0	1/2 to 4	21
Force gradient ($\delta_w < 20°$), N/cm	1.40	- - -	
lb/in.	.8	1 to 3	17
Maximum force at max $\dot{p}$, N	20.0	- - -	
lb	4.5	<20	16
Control response (full control), sec	.3	<0.3 for 63% $\dot{p}$ max	17
Directional			
Rudder pedal travel, cm	±9.9	- - -	
in.	±3.9	2.5 to 4.5	17
Force gradient (±25% rudder pedal travel), N /cm	79	- - -	
lb/in.	45	10 to 35	17
Maximum force, N	436	- - -	
lb	98	<130	20
Control response (full control), sec	0.7	<0.3 for 63% $\dot{r}$ max	17

TABLE 11. LATERAL AND DIRECTIONAL CONTROL POWER CHARACTERISTICS FOR LANDING APPROACH AND TAKEOFF CONDITIONS

	Subject airplane			Criterion	
	Landing		Takeoff	Value	Reference
	SAS on	SAS off	SAS on		
Lateral					
$\dot{p}$ max, rad/sec^2	0.67	0.70	0.60	>0.4	16
ϕ_1/δ_w, deg/cm*	.39	.57	.49	. . .	
deg/in.*	1.0	1.46	1.25	>0.8	22
Time to 30°ϕ, sec*	2.4	1.75	1.9	<2.4	16
$\dot{p}/\delta_w$, ($\delta_w < 40°$)					
rad/sec^2/cm	.042	.043	.037	. . .	
rad/sec^2/in.	.106	.110	.095	>0.07	22
Directional					
$\dot{r}_{max}$, rad/sec^2	0.37	0.37	0.40	>0.15	17
β_{max}, deg	20	20	20	>25	18
Decrab ($\Delta\psi_{2.0}$), deg	21	23	. . .	10 to 15	18
Decrab time ($\Delta\psi = 15°$), sec	1.6	1.5	. . .	<2.0	17
Sensitivity ($\delta_p < 2.54$ cm)					
rad/sec^2/cm	.047	.047	.051	. . .	
rad/sec^2/in	.12	.12	.13	>0.05	17

*Based on a ramp wheel input (ramp time = 0.5 sec)

TABLE 12. LATERAL-DIRECTIONAL DYNAMIC CHARACTERISTICS FOR LANDING APPROACH AND TAKEOFF CONDITIONS

	Subject airplane			Criterion	
	Landing		Takeoff	Value	Reference
	SAS on	SAS off	SAS on		
Dutch roll damping ($\zeta\omega_d$), 1/sec	0.37	0.15	0.75	>0.087	16
Dutch-roll frequency (ω_d), 1/sec	.80	.90	1.06	>.523	16
Roll time constant (τ_R), sec	.45	1.1	1.0	<1.4	19
Spiral time constant (τ_s), sec	~0	$-.05$	~0	$> -.035$	16
Turn coordination ($\Delta\beta/\Delta\phi$)	.25	.65	.15	<0.3	16
Dihedral effect ($d\delta_w/d\beta$)	1.2	1.2	1.4	>0	17
Dihedral effect ($F_{w_{\beta max}}$), N	35	35	35	. . .	
lb	8	8	8	<10	17

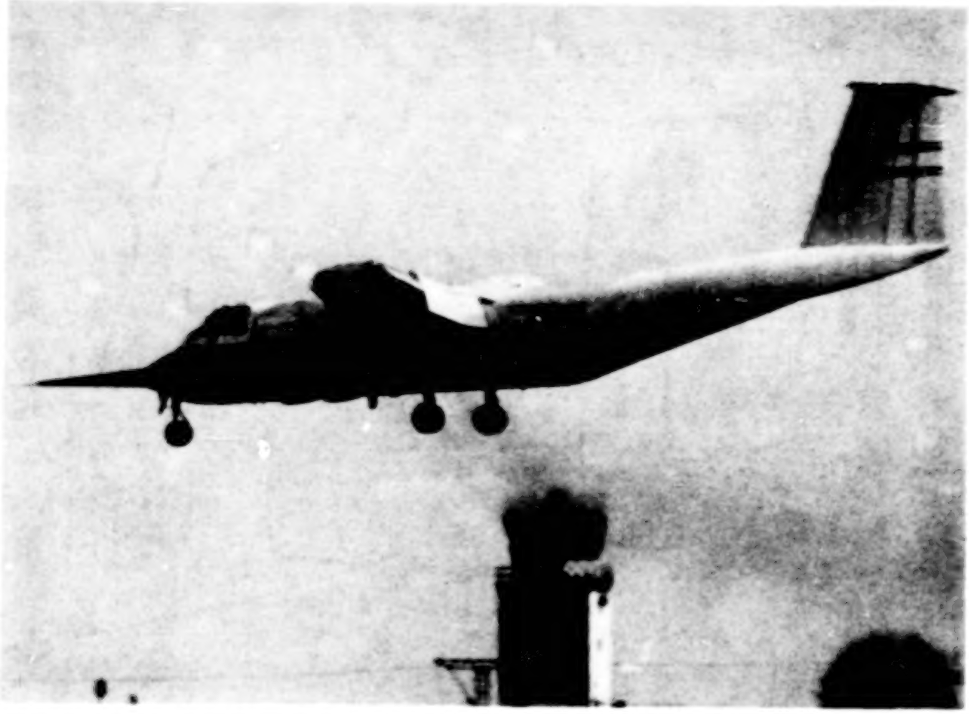

(a) Landing configuration.

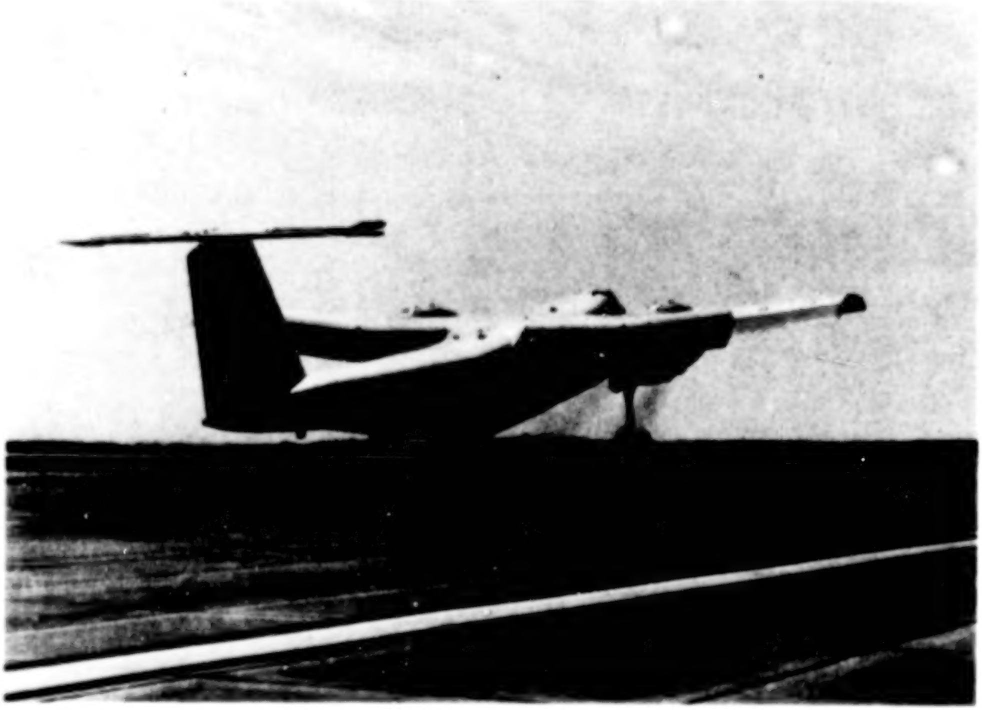

(b) Takeoff configuration.

Figure 1.– Augmentor wing jet STOL research airplane.

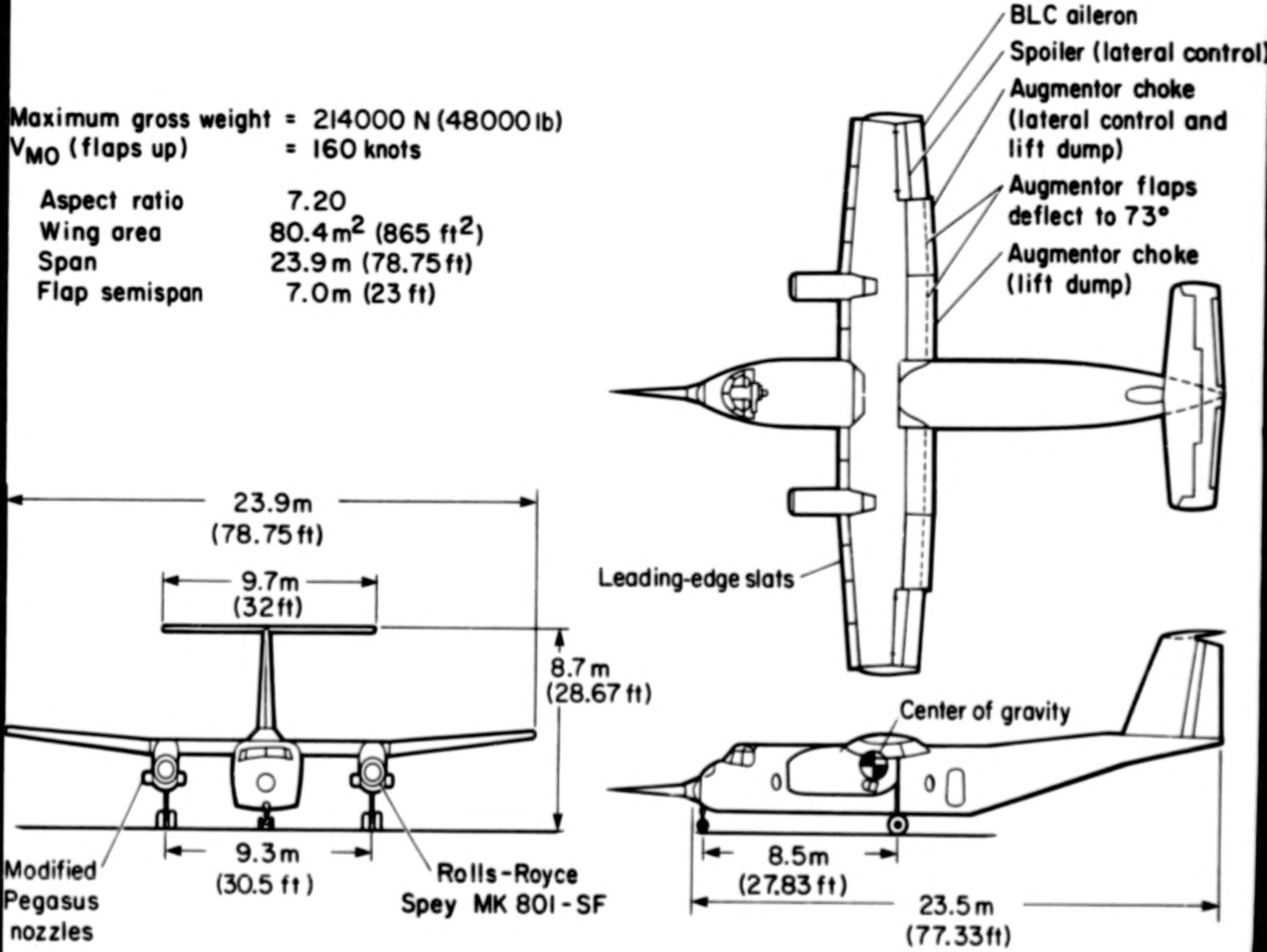
Maximum gross weight = 214000 N (48000 lb)
V_{MO} (flaps up) = 160 knots
Aspect ratio 7.20
Wing area 80.4 m^2 (865 ft^2)
Span 23.9 m (78.75 ft)
Flap semispan 7.0 m (23 ft)
BLC aileron
Spoiler (lateral control)
Augmentor choke (lateral control and lift dump)
Augmentor flaps deflect to 73°
Augmentor choke (lift dump)
Leading-edge slats
23.9m (78.75 ft)
9.7m (32 ft)
8.7 m (28.67 ft)
9.3 m (30.5 ft)
Modified Pegasus nozzles
Rolls-Royce Spey MK 801-SF
Center of gravity
8.5 m (27.83 ft)
23.5 m (77.33 ft)

Figure 2.– Three-view drawing of modified C-8A.

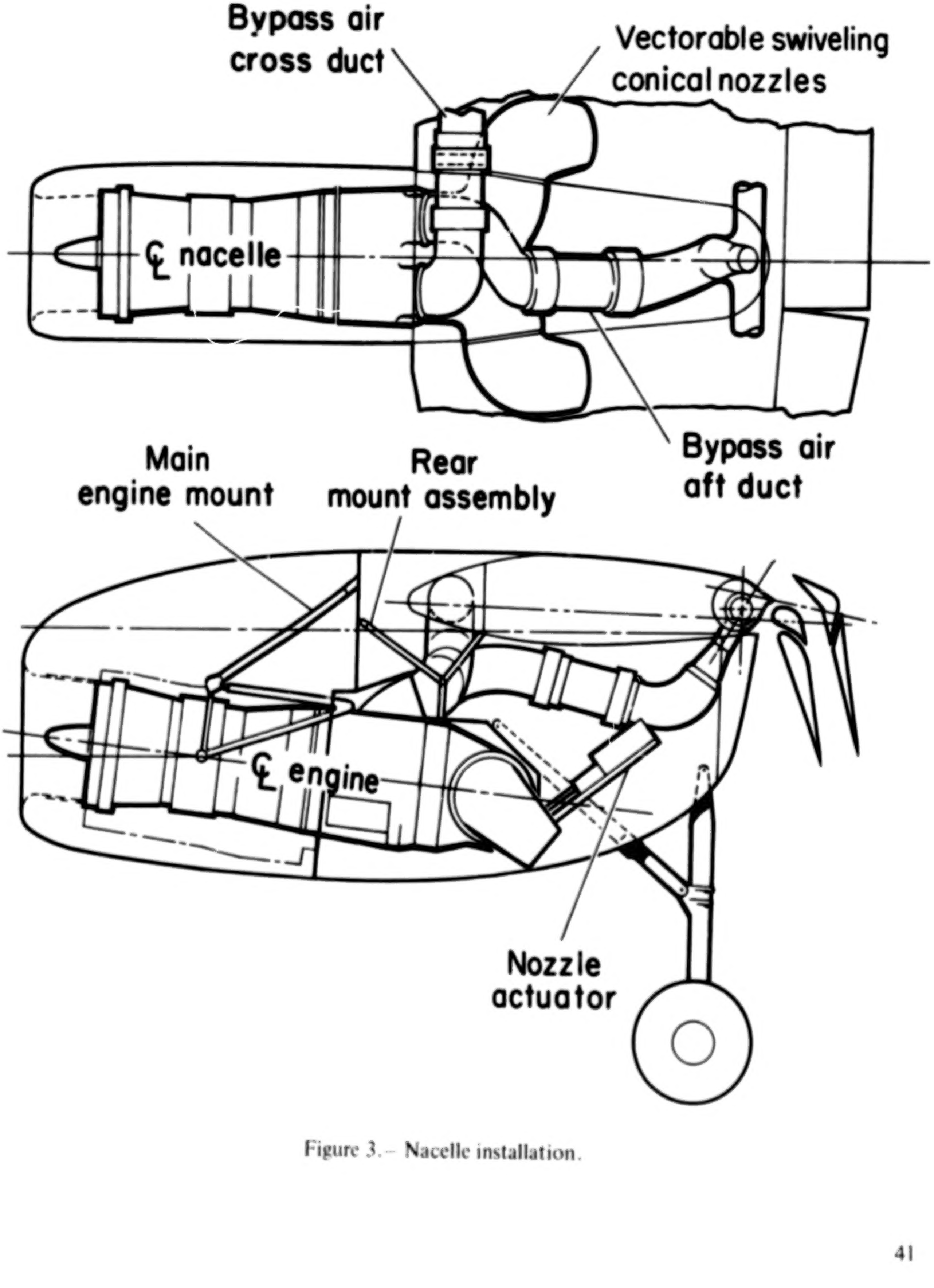
Bypass air cross duct
Vectorable swiveling conical nozzles
℄ nacelle
Bypass air aft duct
Main engine mount
Rear mount assembly
℄ engine
Nozzle actuator

Figure 3.– Nacelle installation.

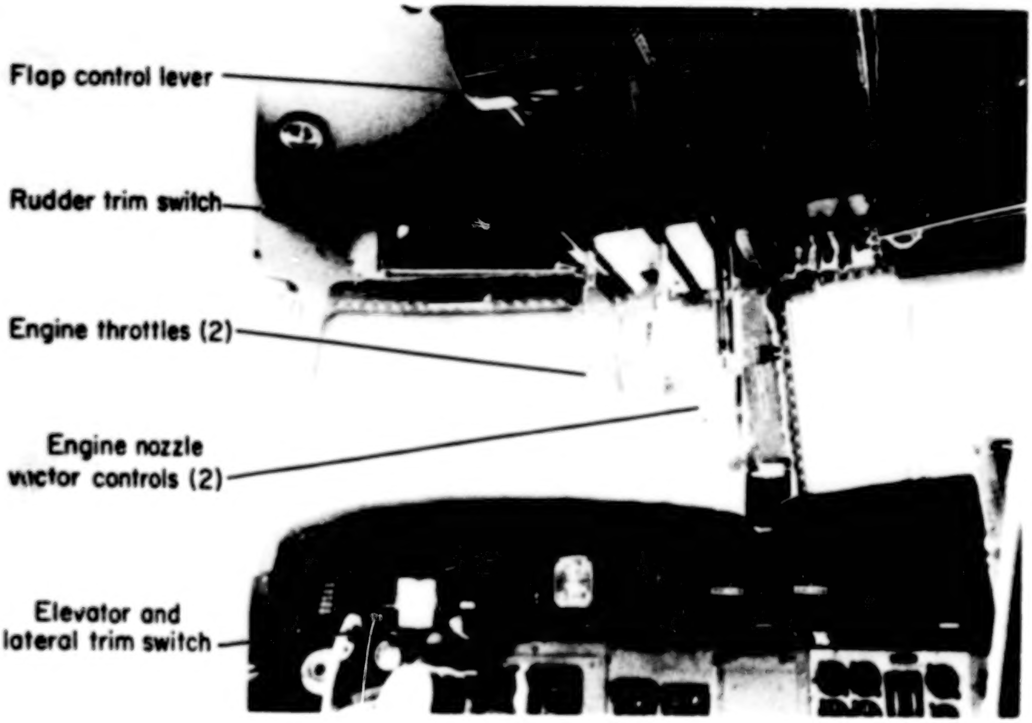
Flap control lever
Rudder trim switch
Engine throttles (2)
Engine nozzle vector controls (2)
Elevator and lateral trim switch

(a) Overhead console.

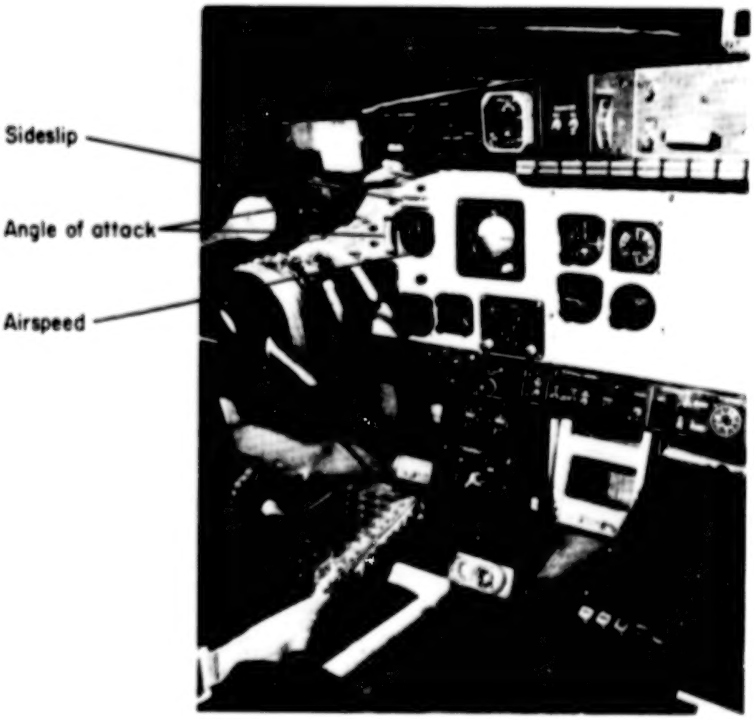
Sideslip
Angle of attack
Airspeed

(b) Pilot's instrument panel.

Figure 4.– Cockpit interior.

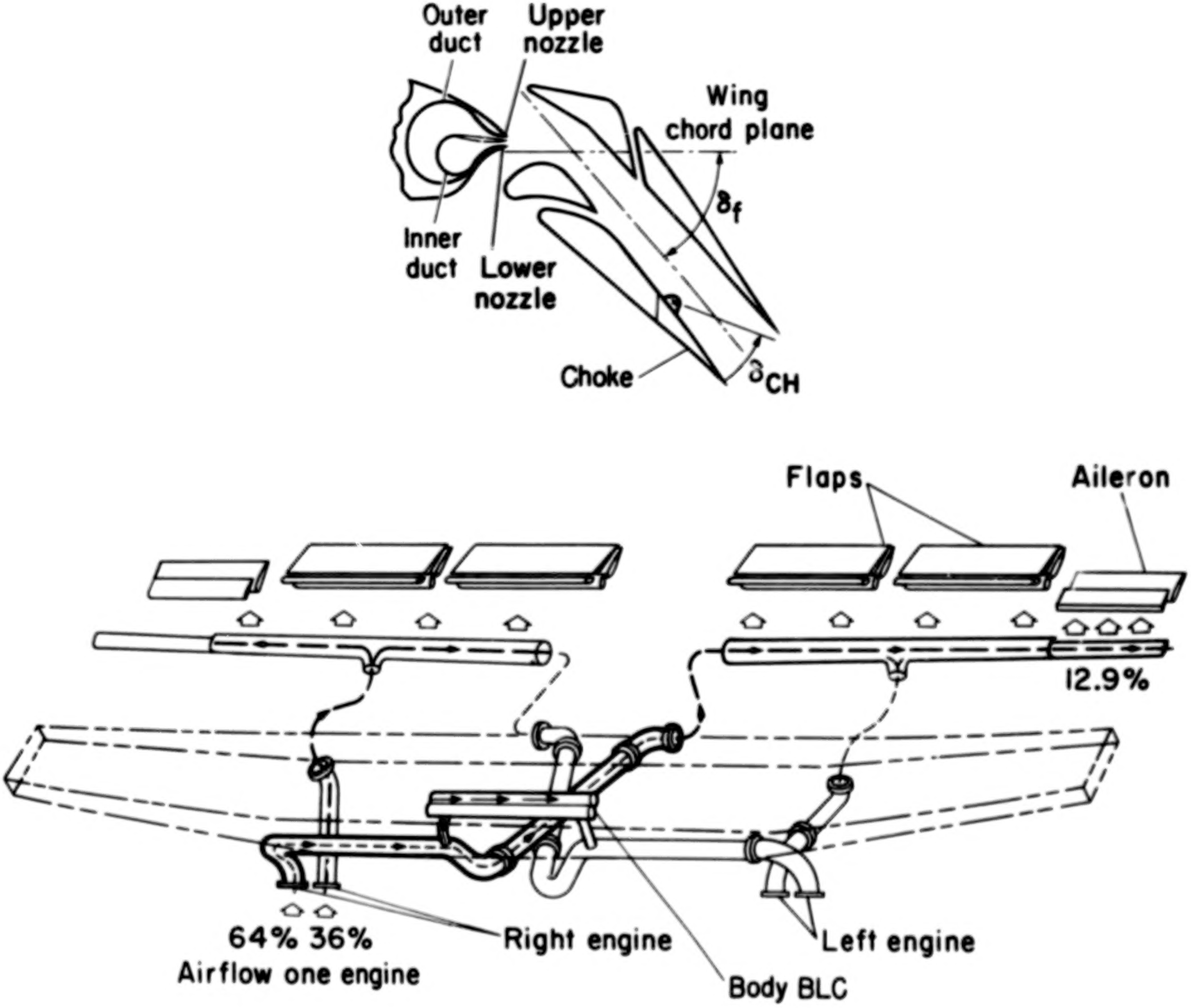
Outer duct
Upper nozzle
Wing chord plane
δf
Inner duct
Lower nozzle
Choke
δCH
Flaps
Aileron
12.9%
64% 36%
Airflow one engine
Right engine
Body BLC
Left engine

Figure 5.– Air distribution system.

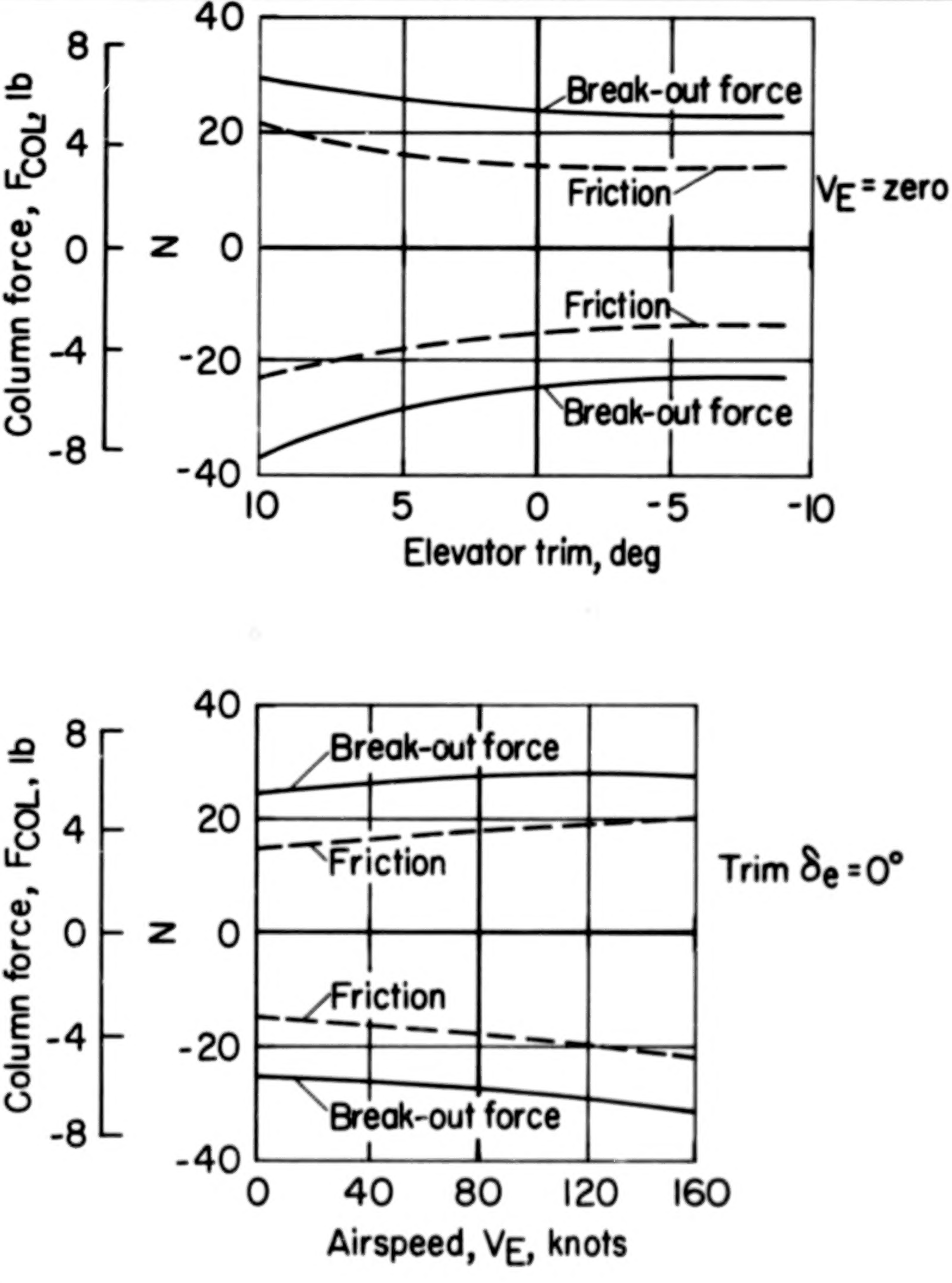

Figure 6.– Elevator control breakout and friction forces.

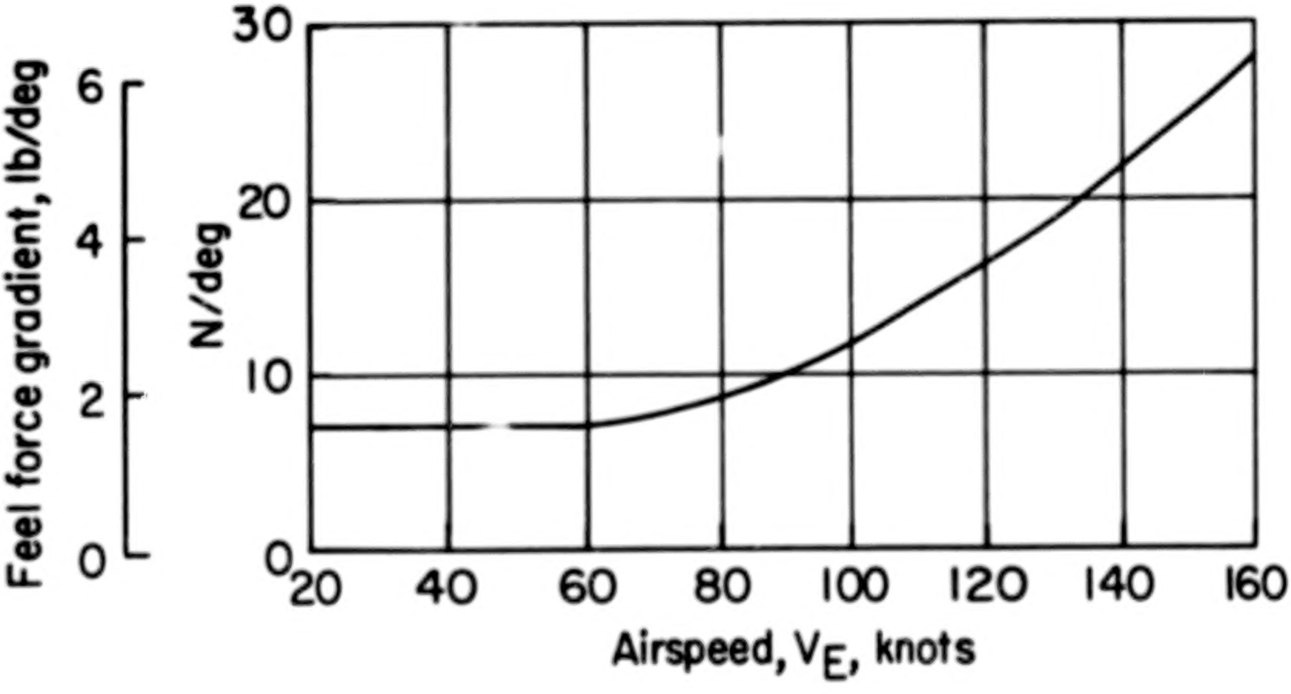

Figure 7.– Elevator control feel force gradient.

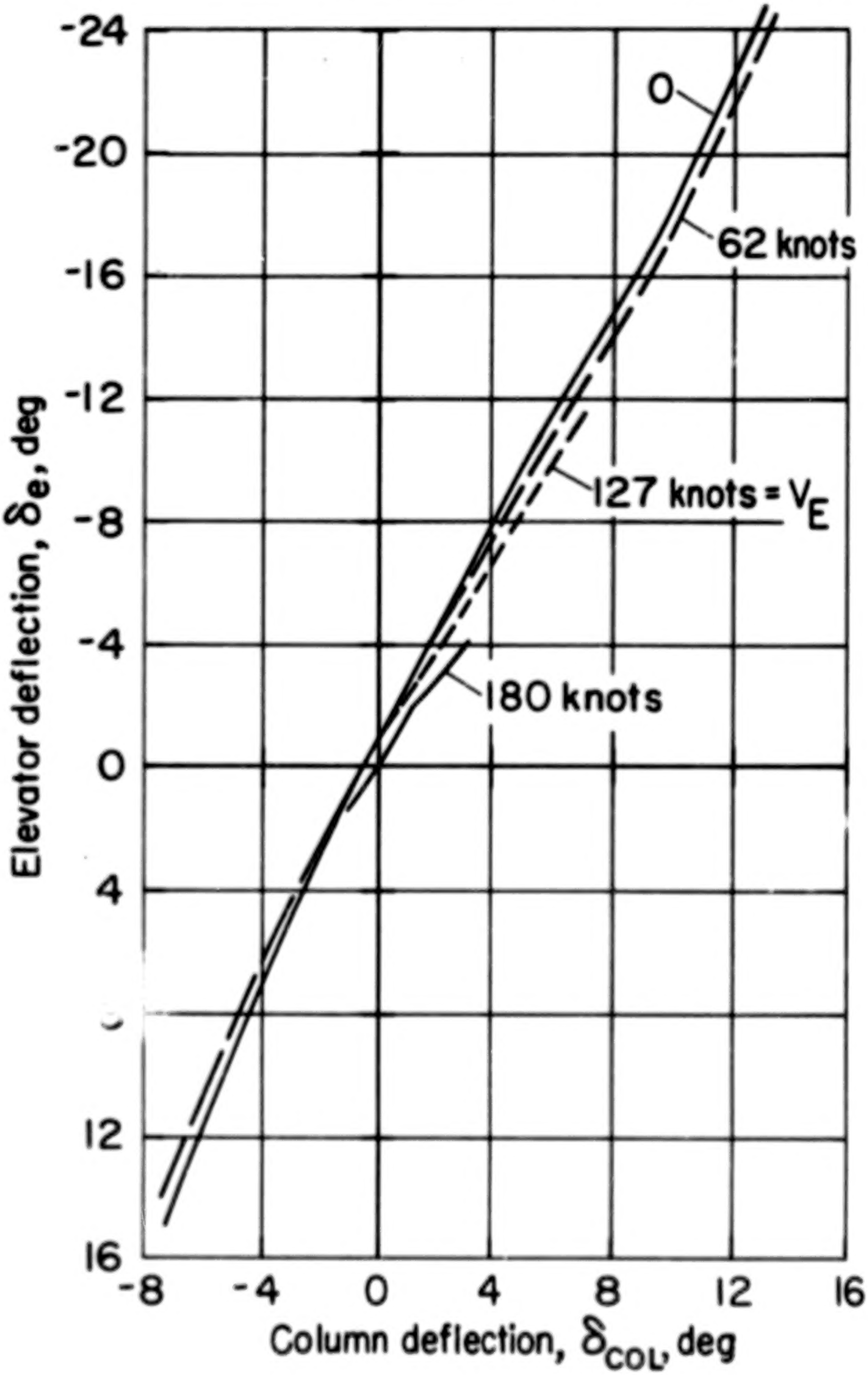
Column length= 82.7 cm

Note: 180 knot curve offset by -1° δ_e for clarity

Figure 8.– Elevator to control column gearing.

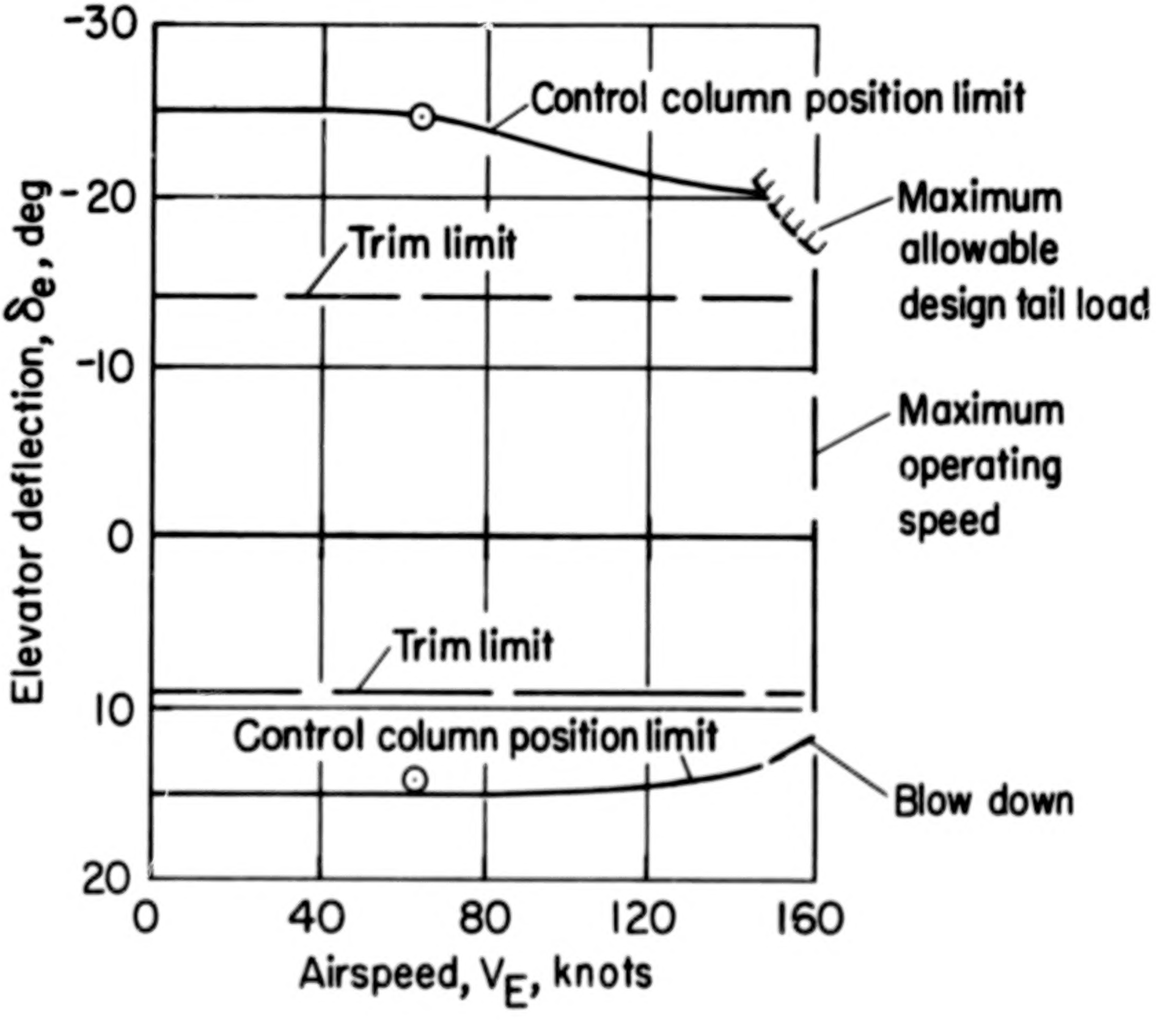

Figure 9.– Elevator control and trim authority.

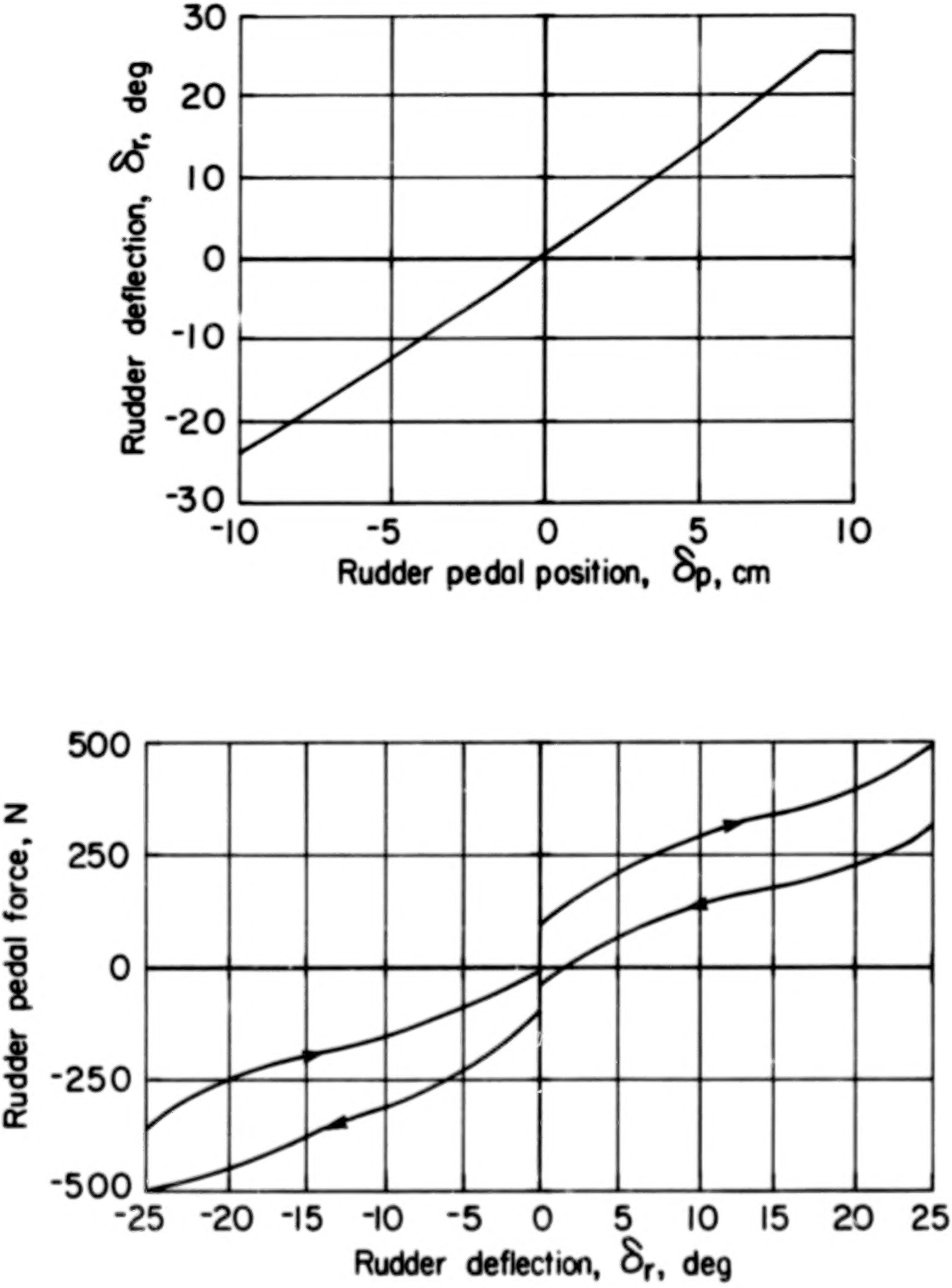

Figure 10.– Directional control characteristics, pedal force and gearing.

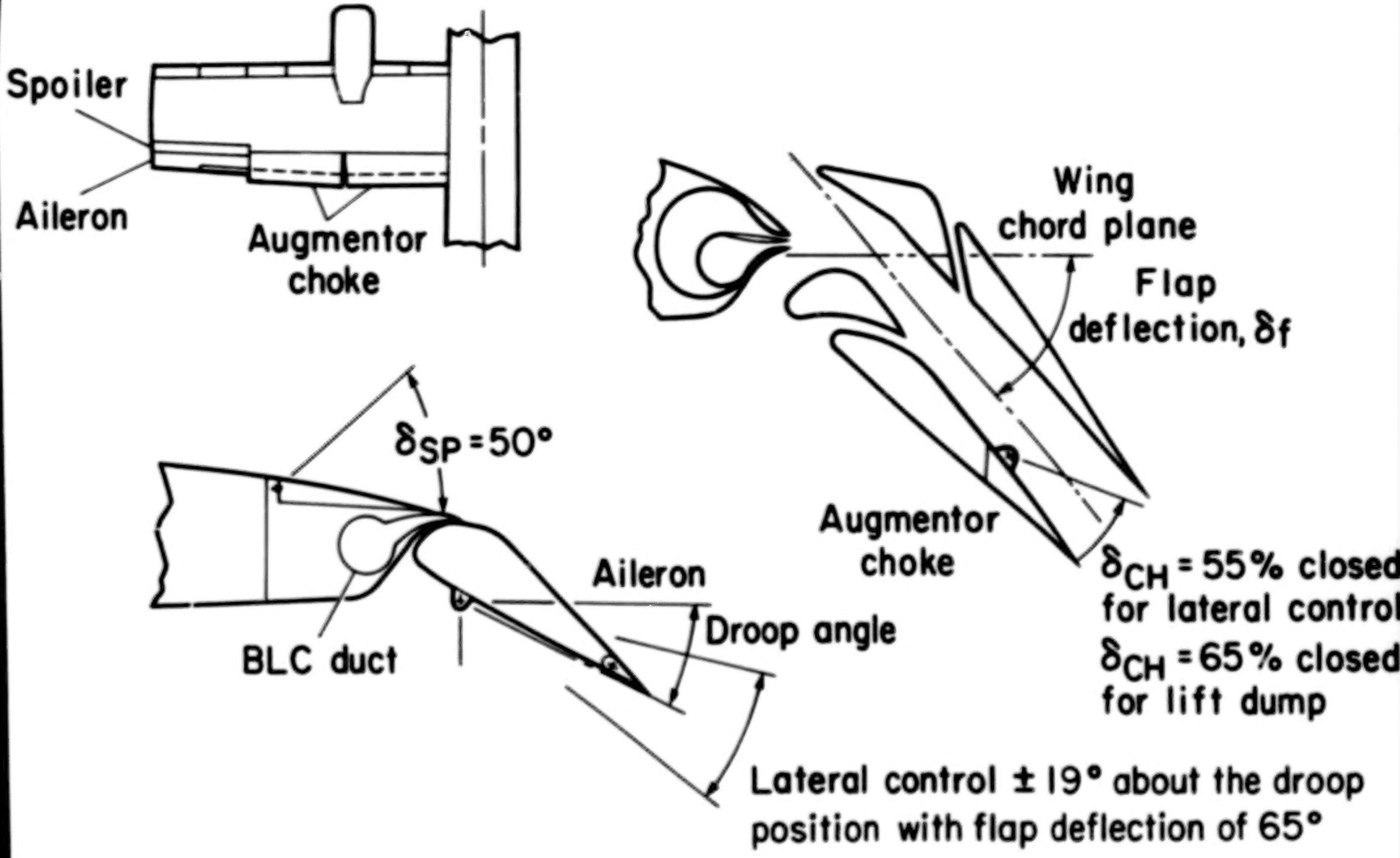
Spoiler
Aileron
Augmentor choke
Wing chord plane
Flap deflection, δ_f
$\delta_{SP} = 50°$
Augmentor choke
$\delta_{CH} = 55\%$ closed for lateral control
$\delta_{CH} = 65\%$ closed for lift dump
Aileron
Droop angle
BLC duct
Lateral control ± 19° about the droop position with flap deflection of 65°

Note: Outboard choke – lateral control and lift dump
Inboard choke – lift dump only

Figure 11.– Augmentor flap and lateral control geometry.

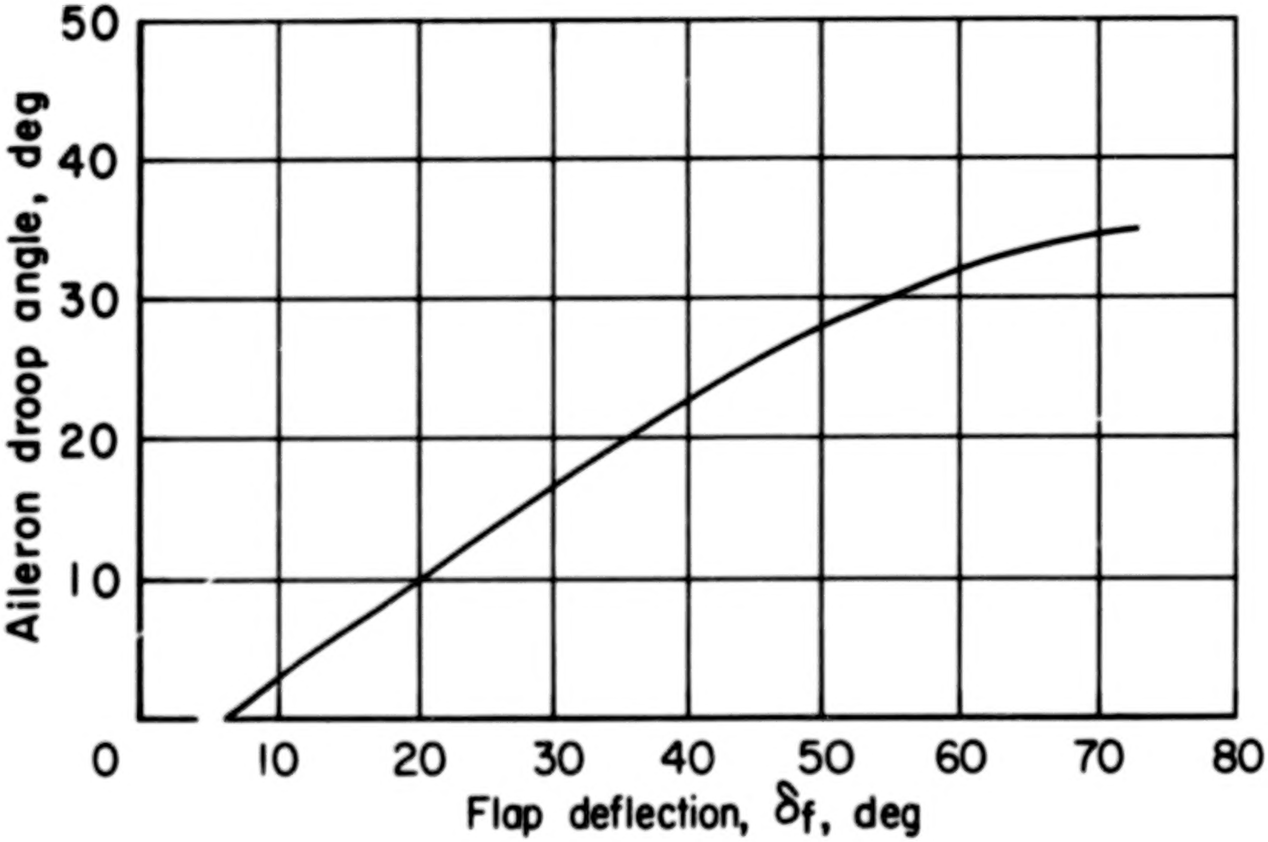

(a) Aileron droop program.

Figure 12.– Aileron mechanical characteristics.

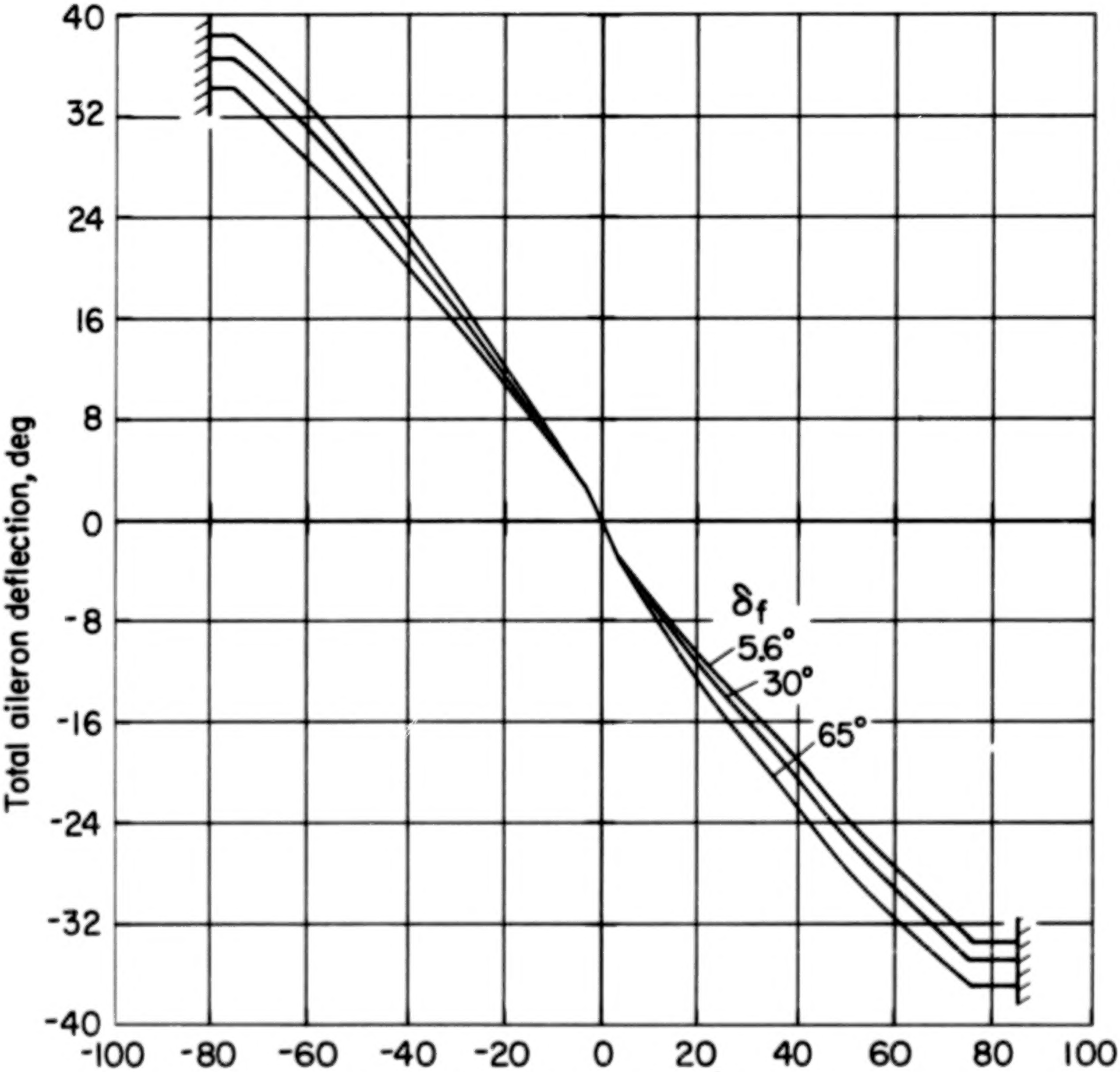

(b) Control wheel to aileron gearing, SAS on.

Figure 12.– Continued.

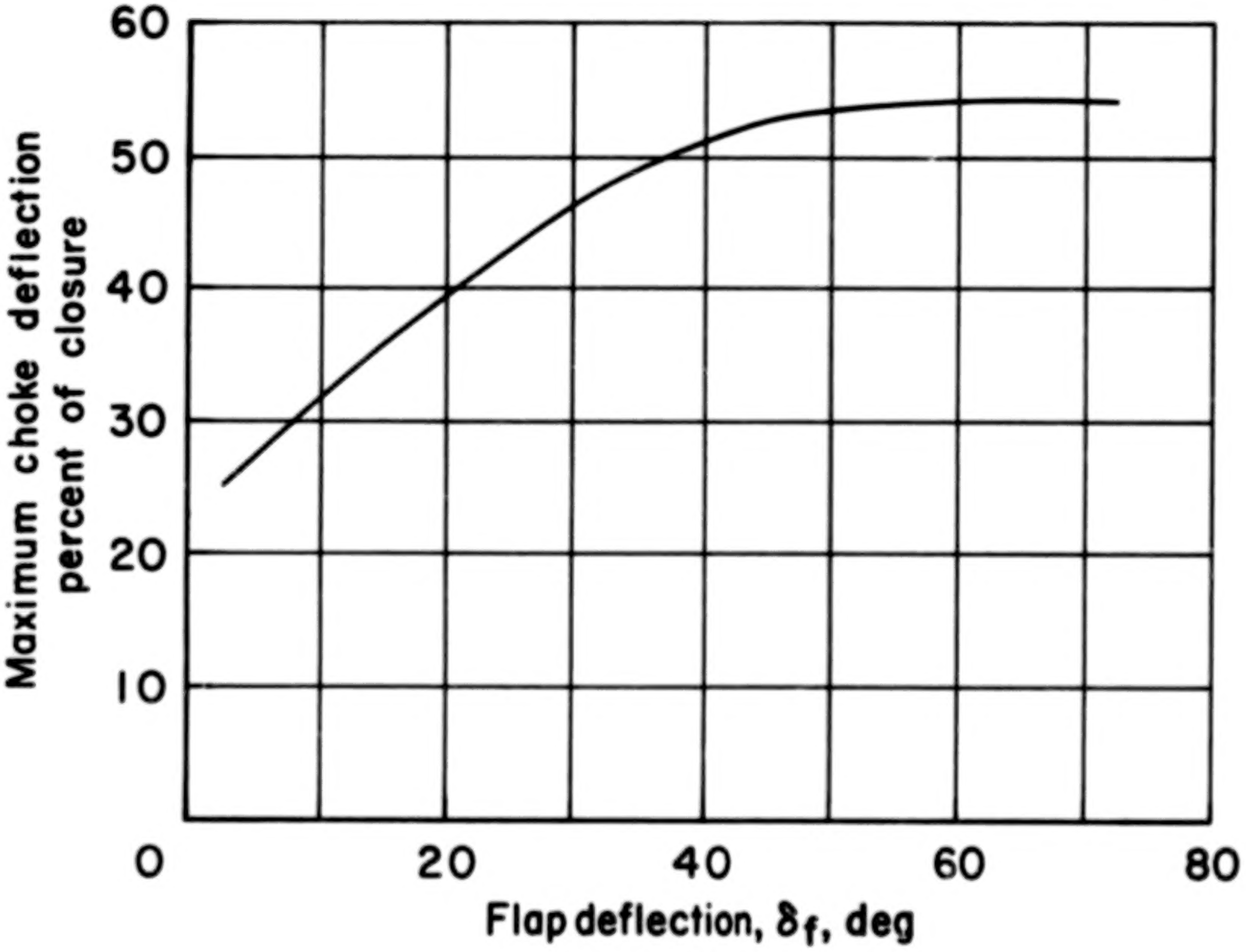

(c) Maximum choke deflection program.

Figure 12.– Continued.

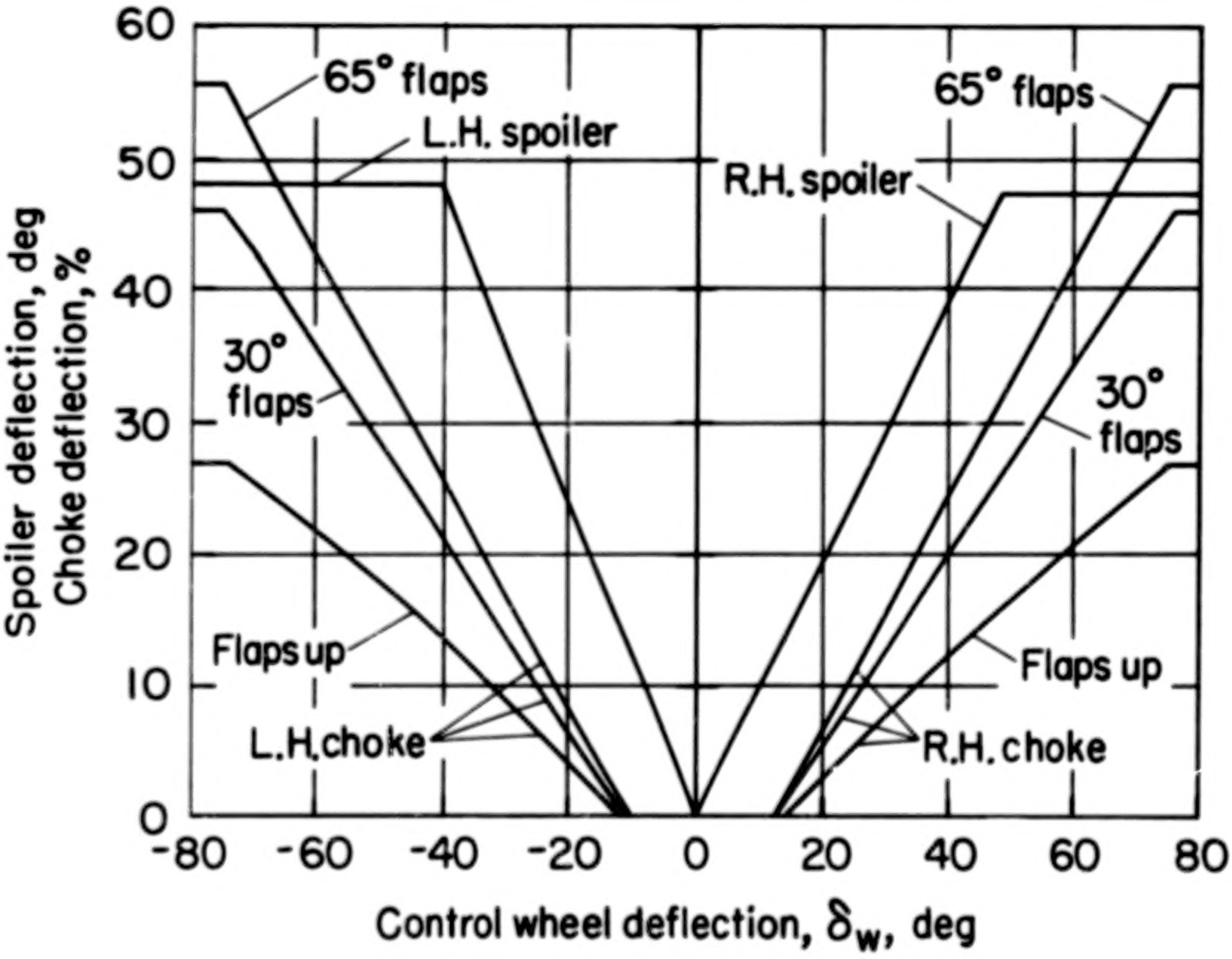

(d) Choke and spoiler gearing, SAS on.

Figure 12.– Concluded.

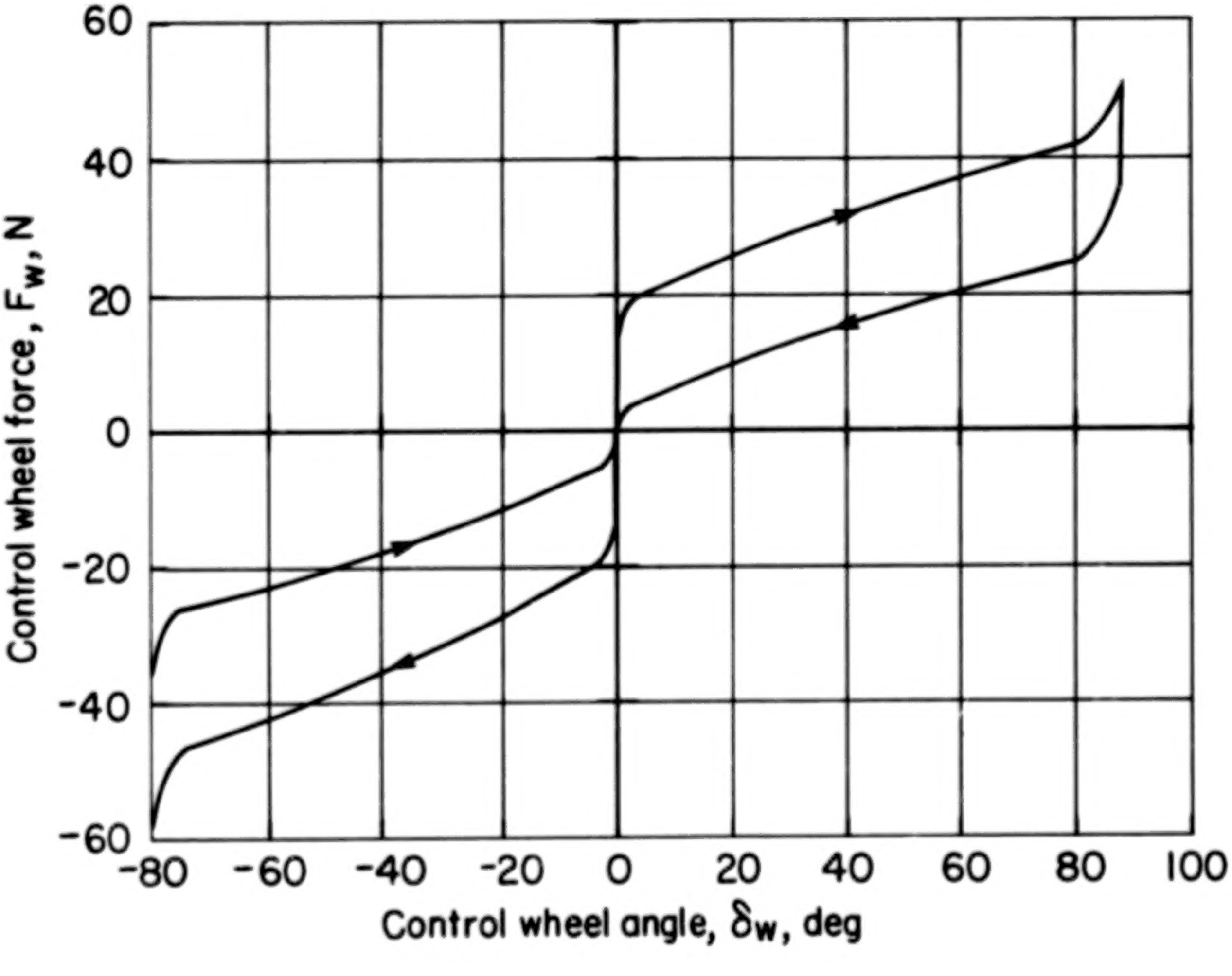

Figure 13.– Control wheel forces.

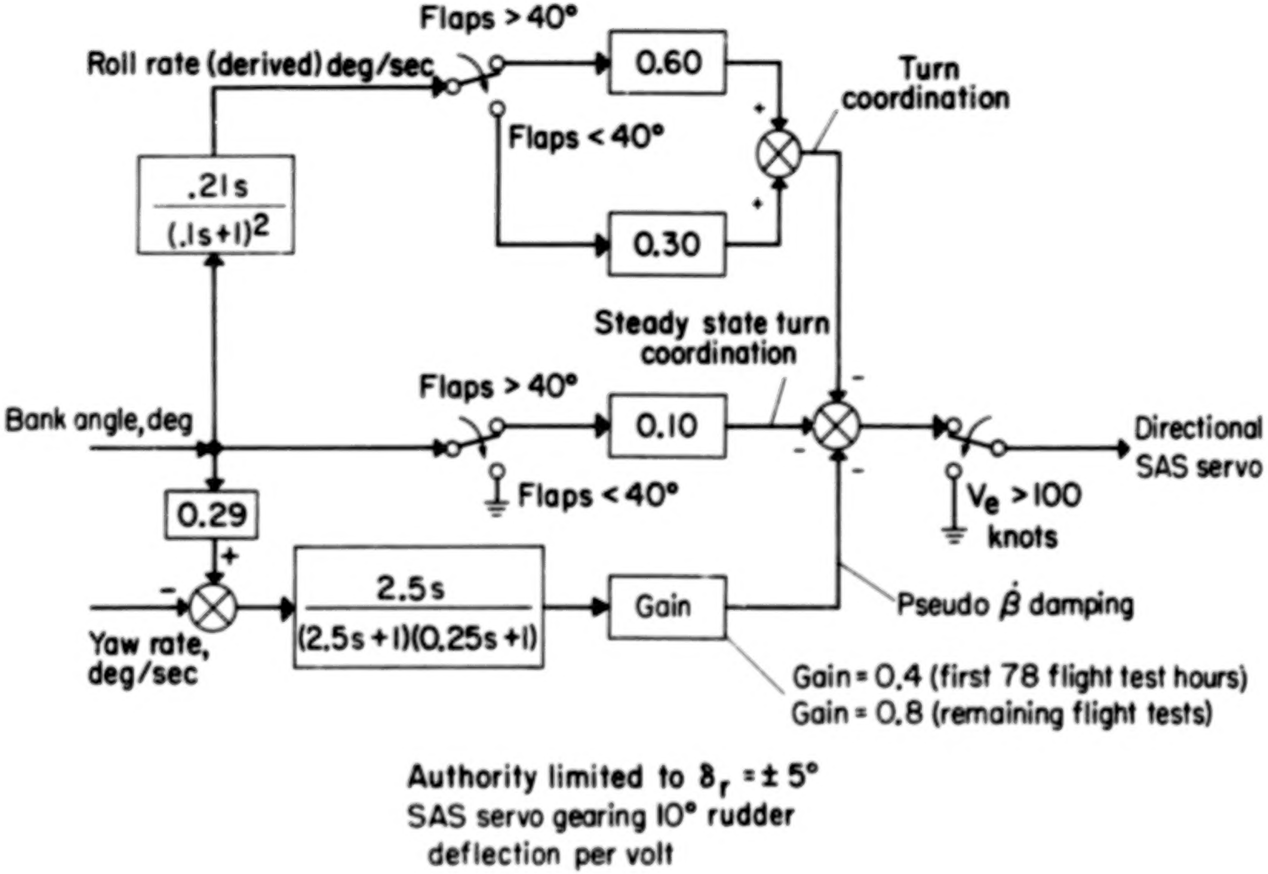
Flaps > 40°
Roll rate (derived) deg/sec
0.60
Turn coordination
+
Flaps < 40°
.21s / (.1s+1)²
+
0.30
Steady state turn coordination
-
Flaps > 40°
Bank angle, deg
0.10
-
-
Directional SAS servo
0.29
Flaps < 40°
V_e > 100 knots
+
-
2.5s / (2.5s+1)(0.25s+1)
Gain
Pseudo $\dot{\beta}$ damping
Yaw rate, deg/sec
Gain = 0.4 (first 78 flight test hours)
Gain = 0.8 (remaining flight tests)
Authority limited to δ_r = ± 5°
SAS servo gearing 10° rudder deflection per volt

(a) Directional axis.

Figure 14.– Stability augmentation (normal mode).

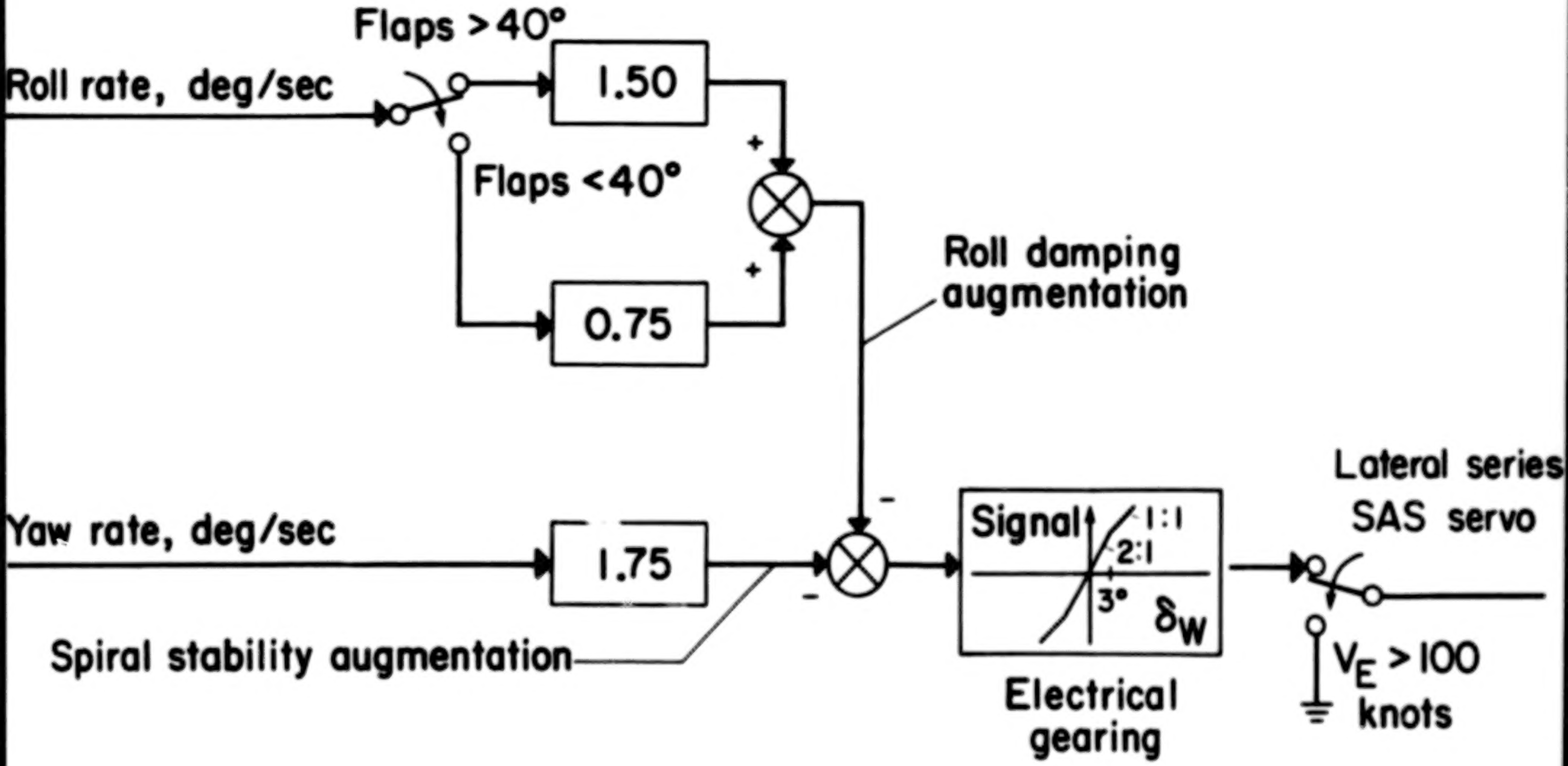
Flaps > 40°
Roll rate, deg/sec
1.50
Flaps < 40°
0.75
+
+
Roll damping augmentation
Yaw rate, deg/sec
1.75
–
–
Spiral stability augmentation
Signal
1:1
2:1
3°
δ_W
Electrical gearing
Lateral series SAS servo
V_E > 100 knots

Authority limited to an equivalent wheel deflection (δ_W) of ± 20°

SAS servo gearing 10° (equivalent wheel deflection) per volt

(b) Lateral axis.

Figure 14.– Continued.

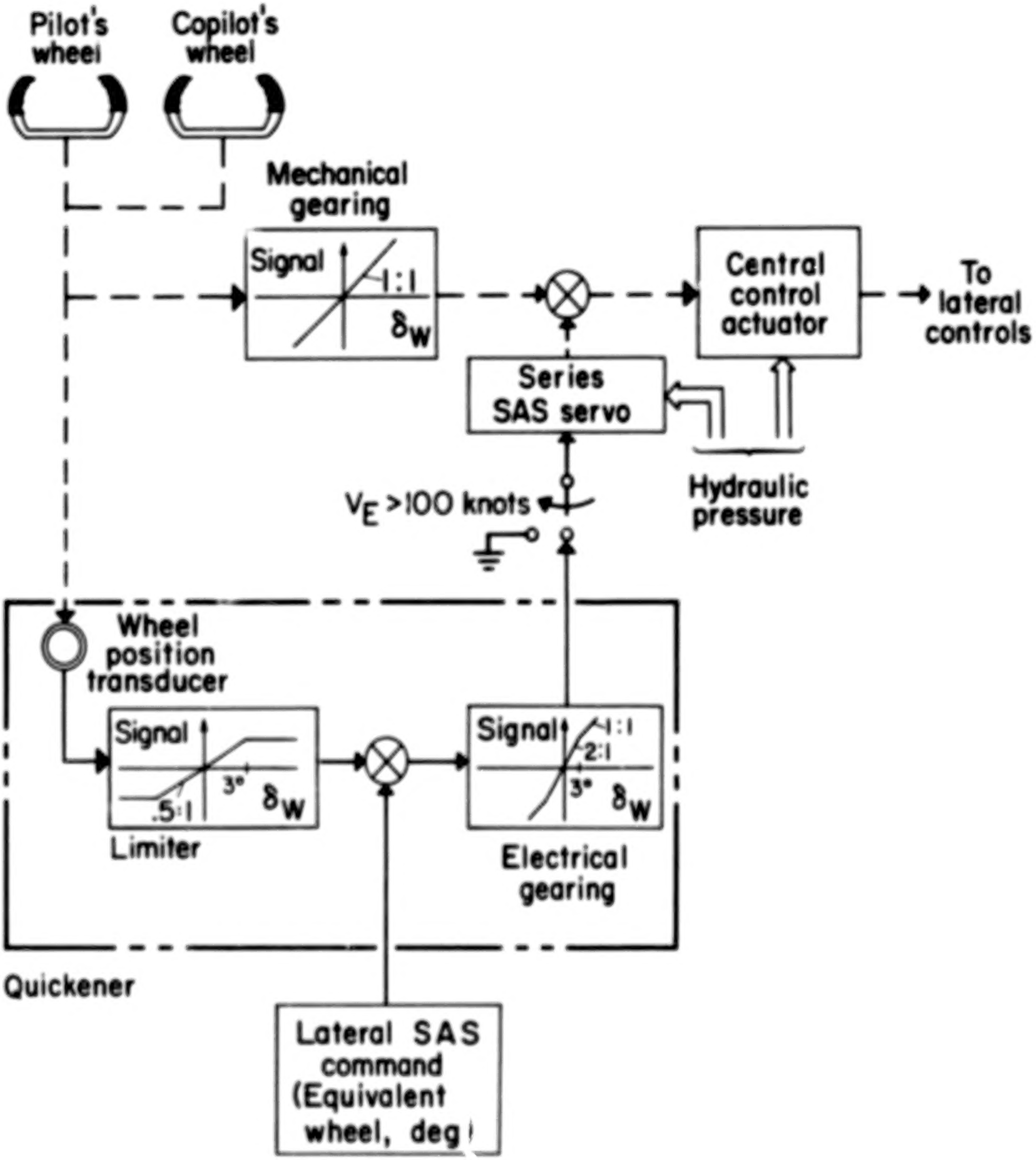
Pilot's wheel
Copilot's wheel
Mechanical gearing
Signal
1:1
δ_W
Central control actuator
To lateral controls
Series SAS servo
Hydraulic pressure
V_E >100 knots
Wheel position transducer
Signal
3°
δ_W
.5:1
Limiter
Signal
1:1
2:1
3°
δ_W
Electrical gearing
Quickener
Lateral SAS command (Equivalent wheel, deg)

(c) Lateral control quickener.

Figure 14.– Concluded.

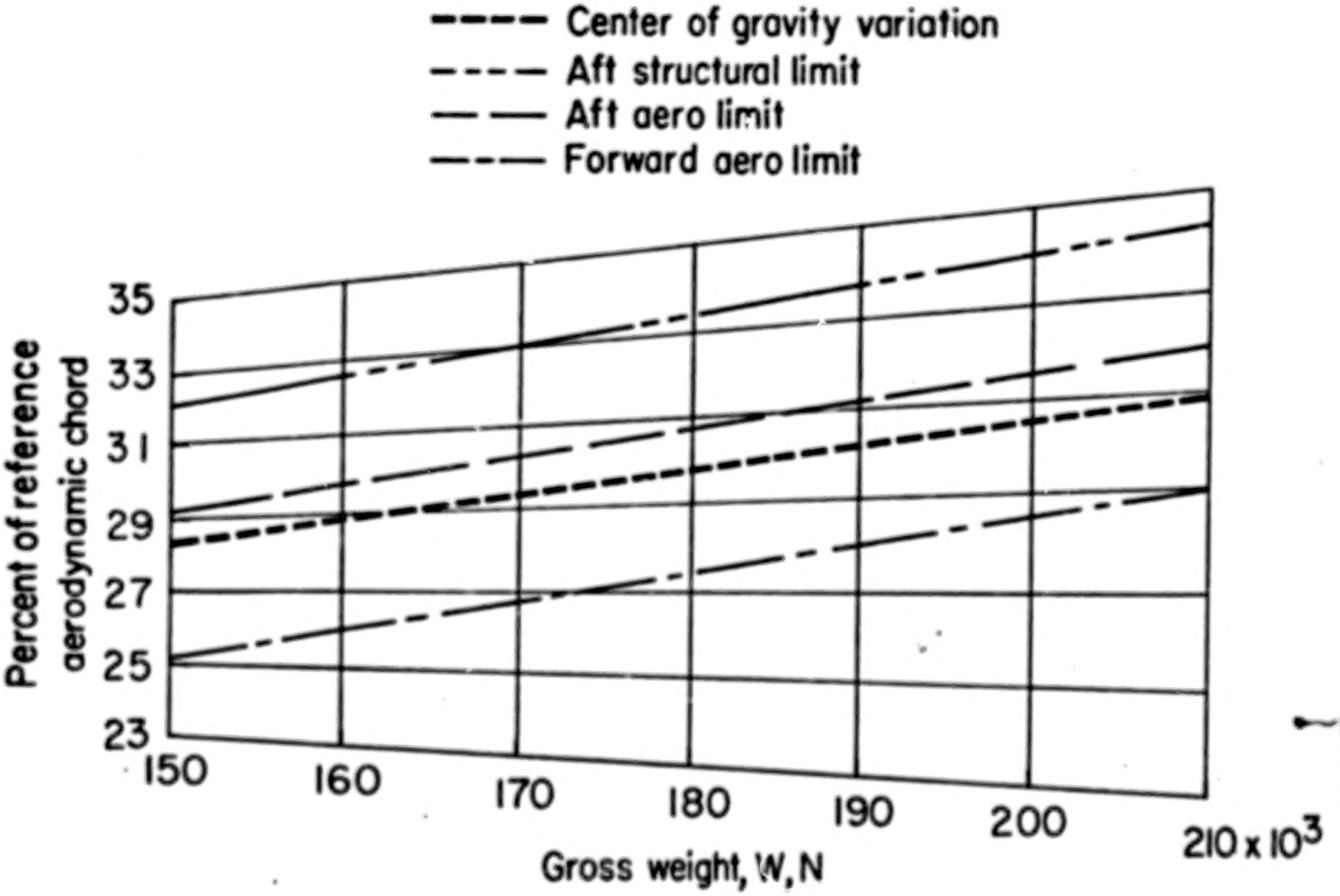

Figure 15.– Variation in center-of-gravity location with gross weight. Gross weight changes with fuel only.

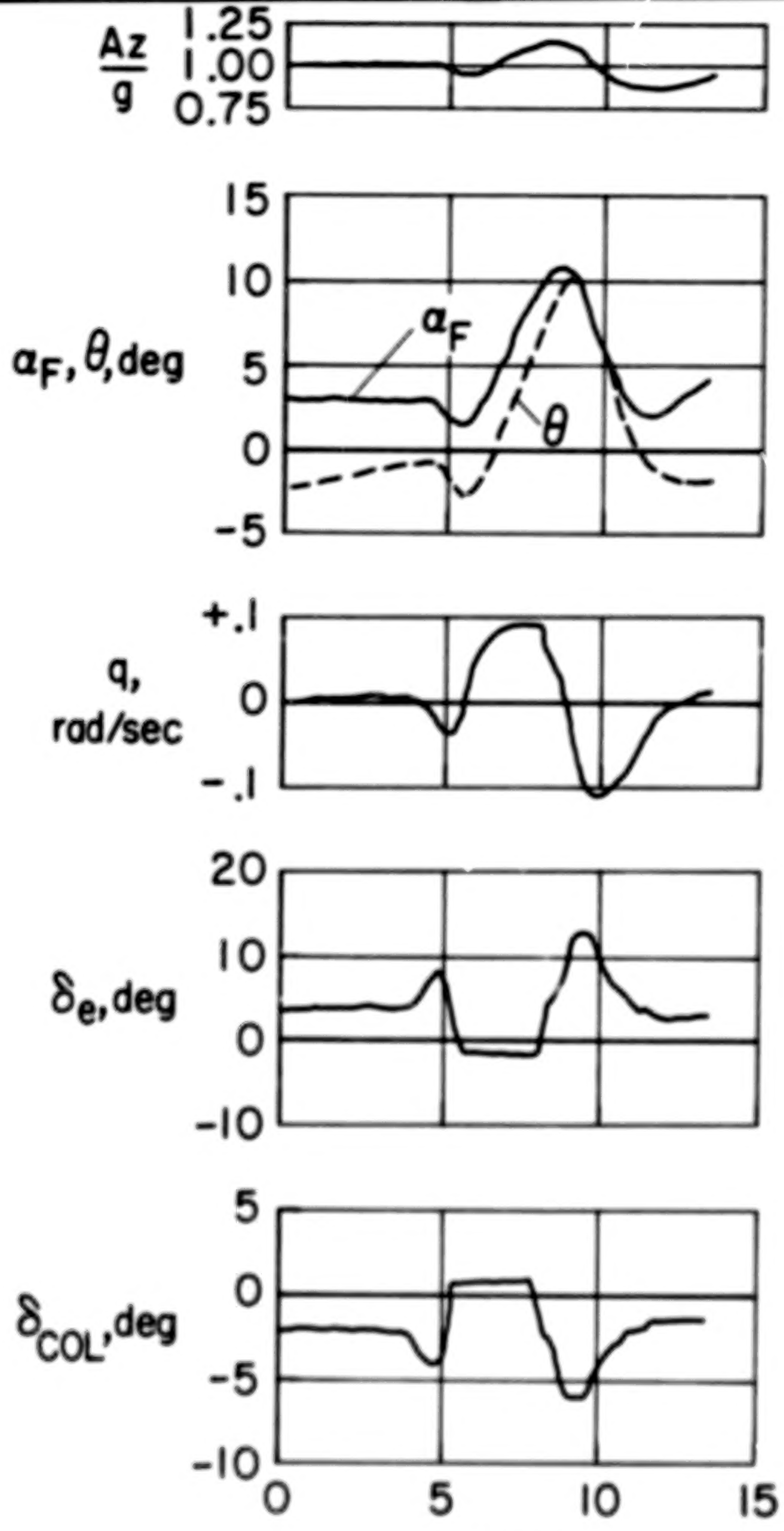

Figure 16.– Response to elevator reversal, 66 knots V_E, 64.8° δ_F, 71° ν, W = 182,000 N, C_J = 0.39.

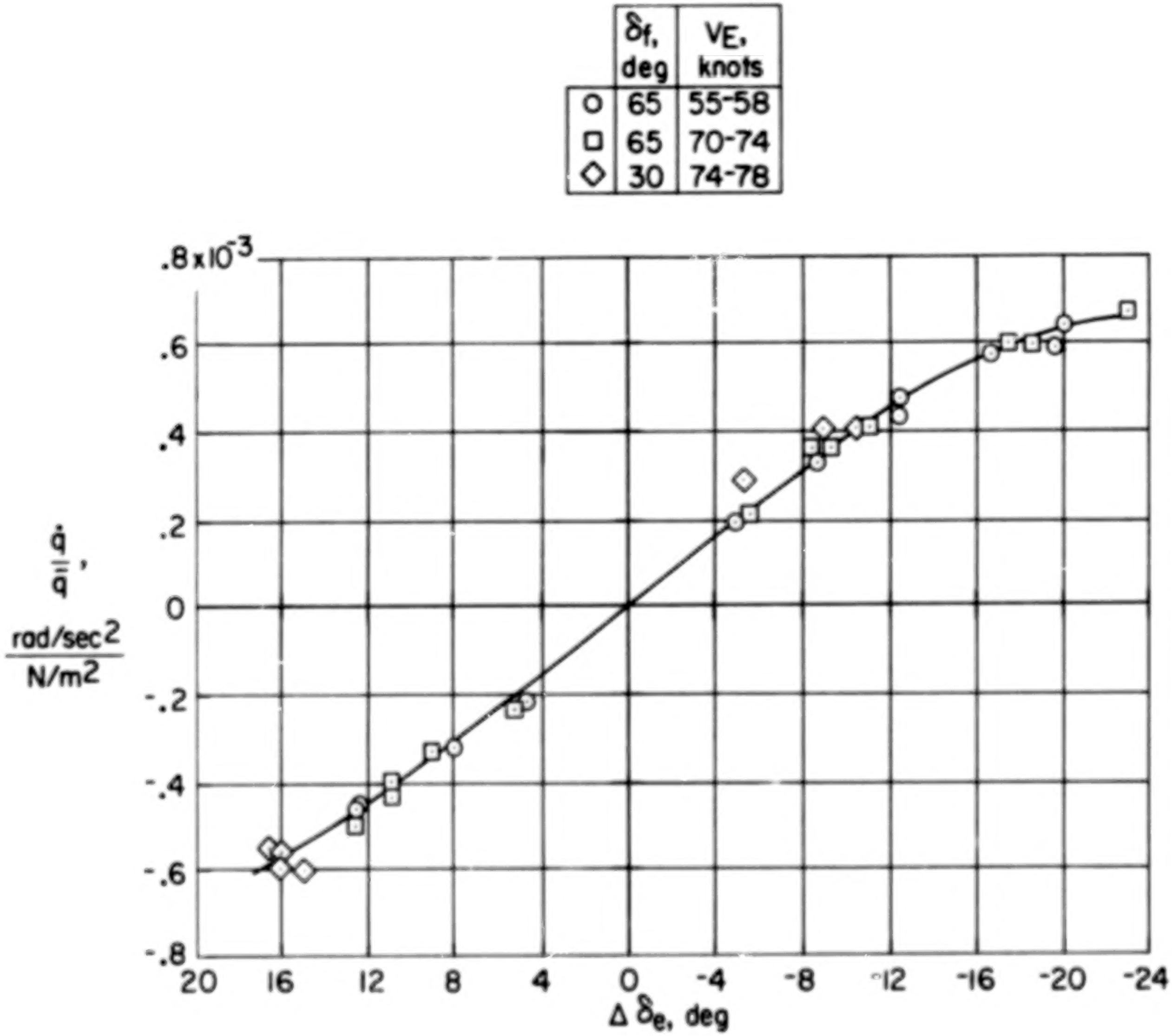

(a) Variation of normalized angular acceleration with incremental elevator deflection.

Figure 17.– Longitudinal control effectiveness with powered elevator.

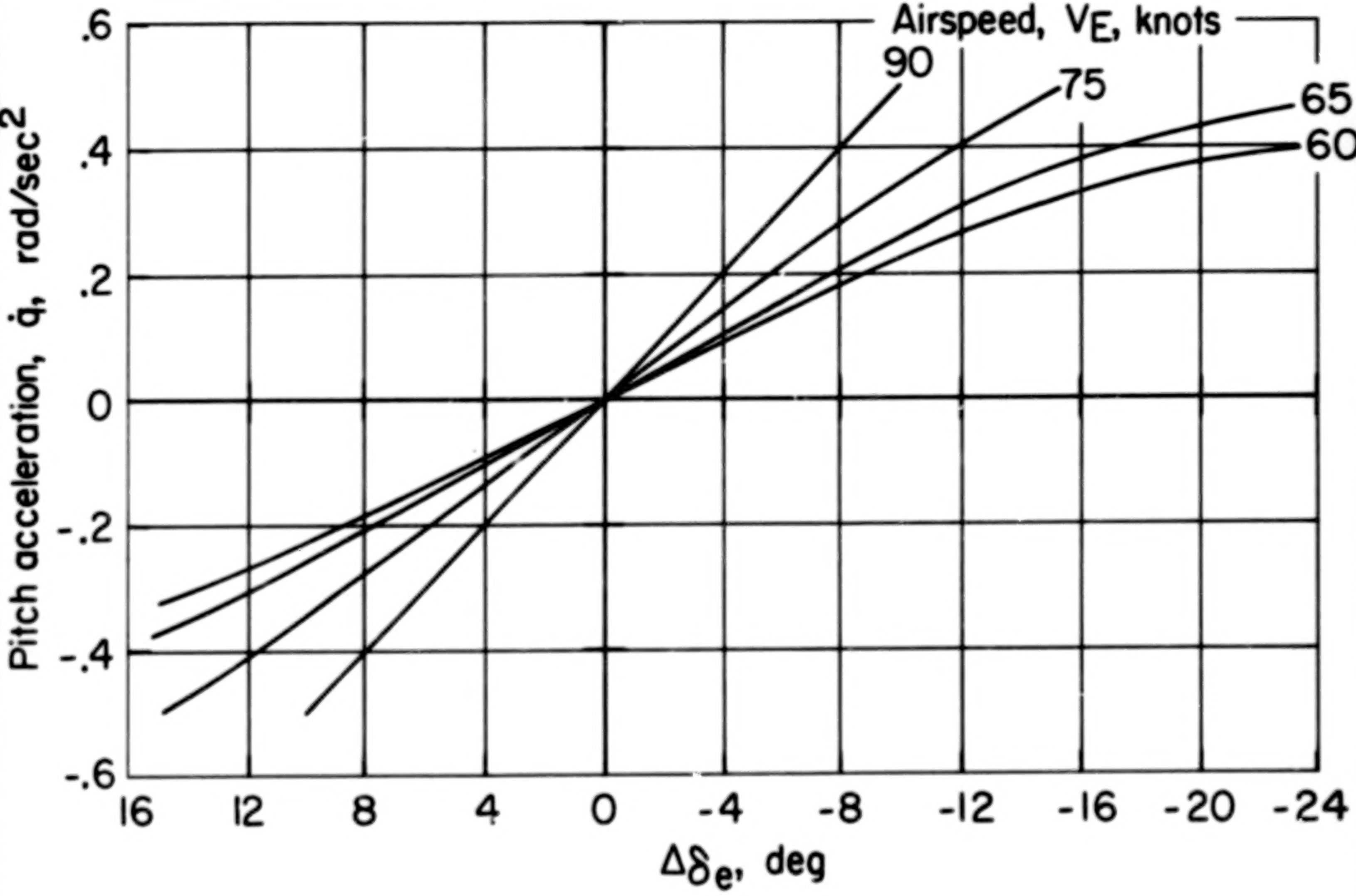

(b) Longitudinal control power for various airspeeds.

Figure 17.– Concluded.

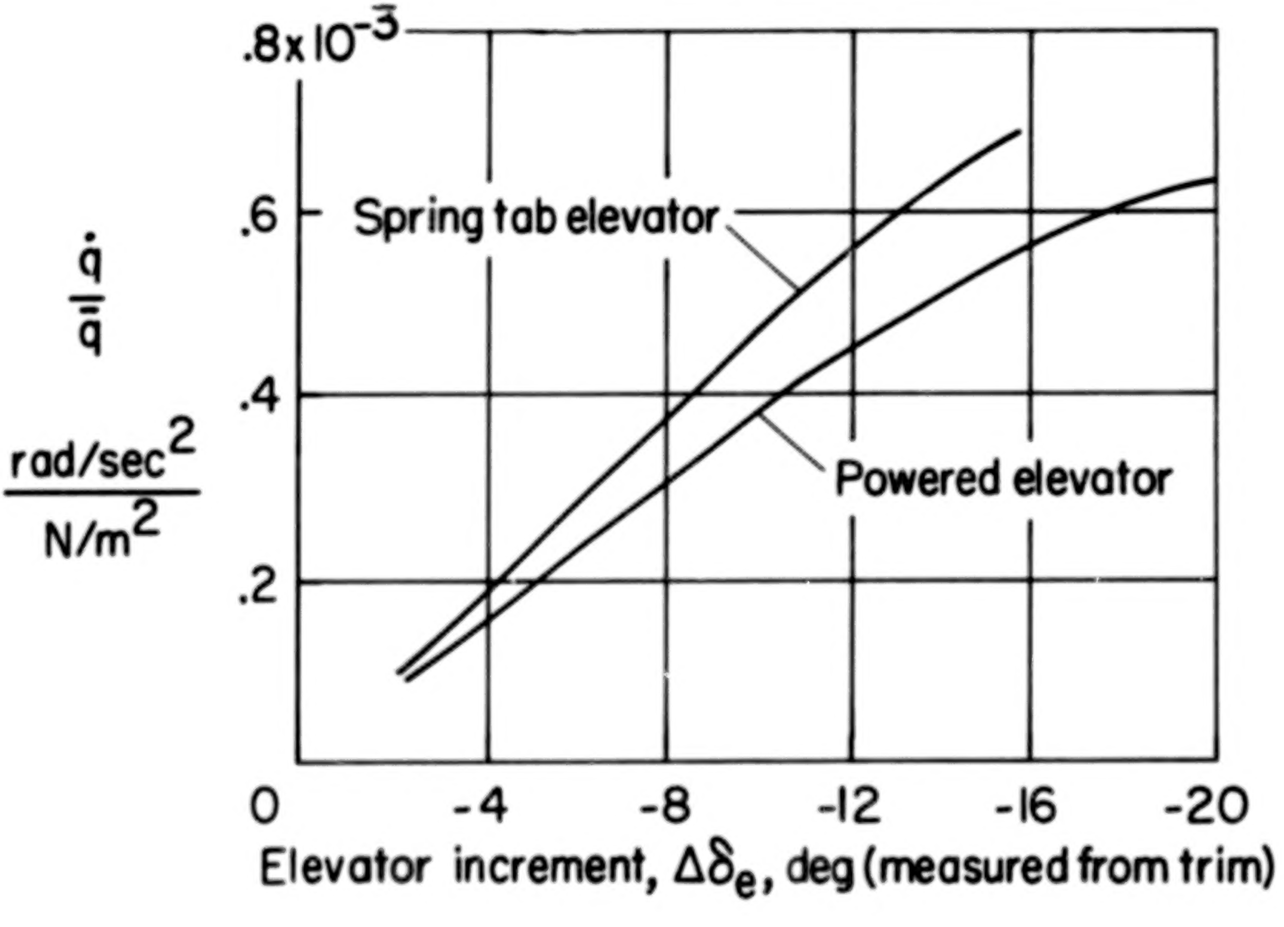

Figure 18.– Longitudinal control effectiveness.

62

	δ_f, deg	ν, deg	N_H, %	Weight, N	Altitude, m	CG, % $\bar{c}$
○	66.5	10	90.2/90.7	203000	2100	30.9
□	65.0	8	92.8/93.3	193000	2300	30.5
◇	64.6	10	95.0/95.8	195000	2200	30.6
△	66.1	12	99.5/99.8	186000	1900	30.4

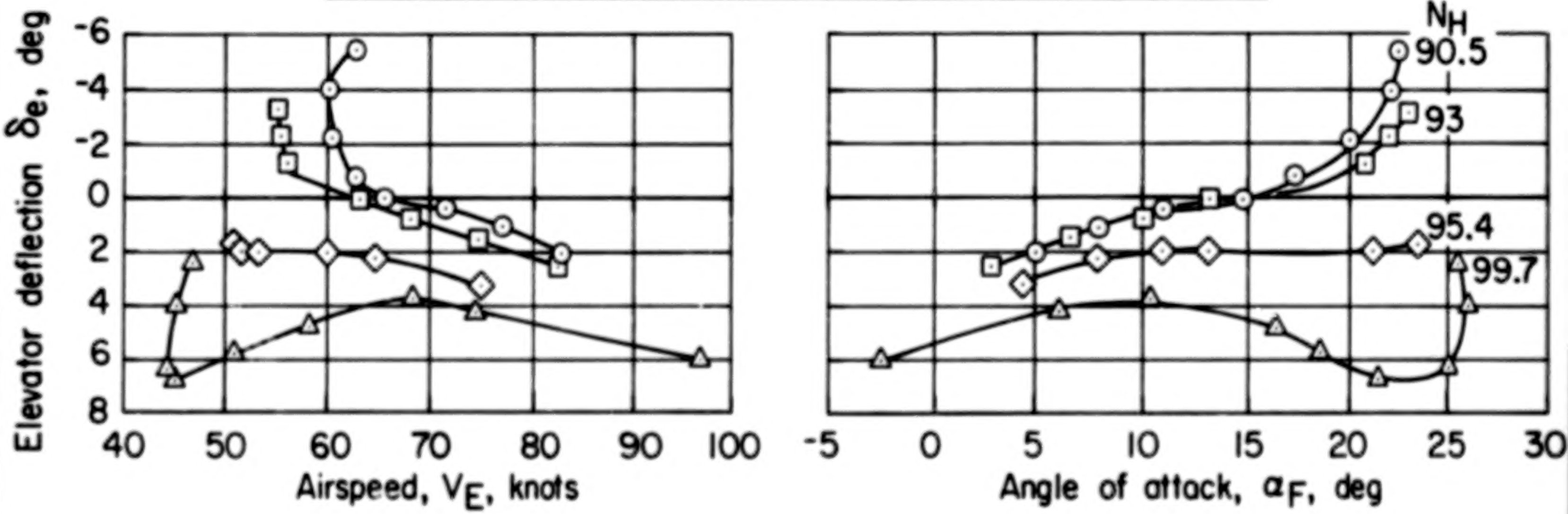

(a) Nozzle deflection 10°.

Figure 19.– Variation of longitudinal static stability with engine *rpm* and nozzle deflection, flap deflection 65°.

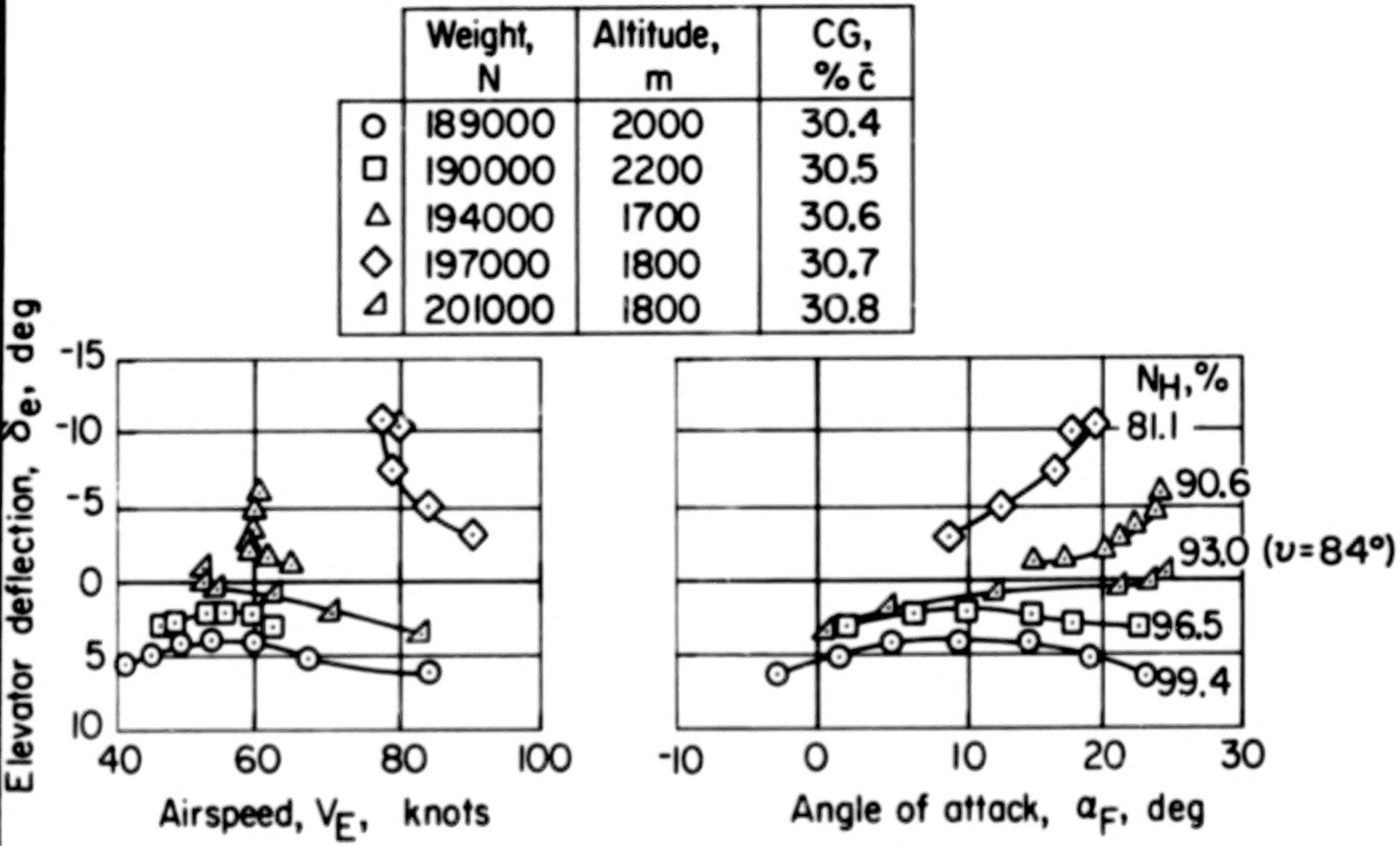

	Weight, N	Altitude, m	CG, % $\bar{c}$
○	189000	2000	30.4
□	190000	2200	30.5
△	194000	1700	30.6
◇	197000	1800	30.7
⊿	201000	1800	30.8

(b) Nozzle deflection 73°.

Figure 19. – Continued.

	δ_f, deg	ν, deg	N_H, %	Weight, N	Altitude, m	CG, % $\bar{c}$
○	64.6	10	95.0/95.8	195000	2200	30.6
□	65.1	27	94.9/95.5	196000	2300	30.7
◇	65.0	55	95.6/95.9	198000	2300	30.7
△	65.1	67	95.7/96.1	191000	2300	30.5
⌓	64.5	88	94.8/95.5	187000	2100	30.3
⌂	67.0	102	94.2/95.1	186000	2100	30.0

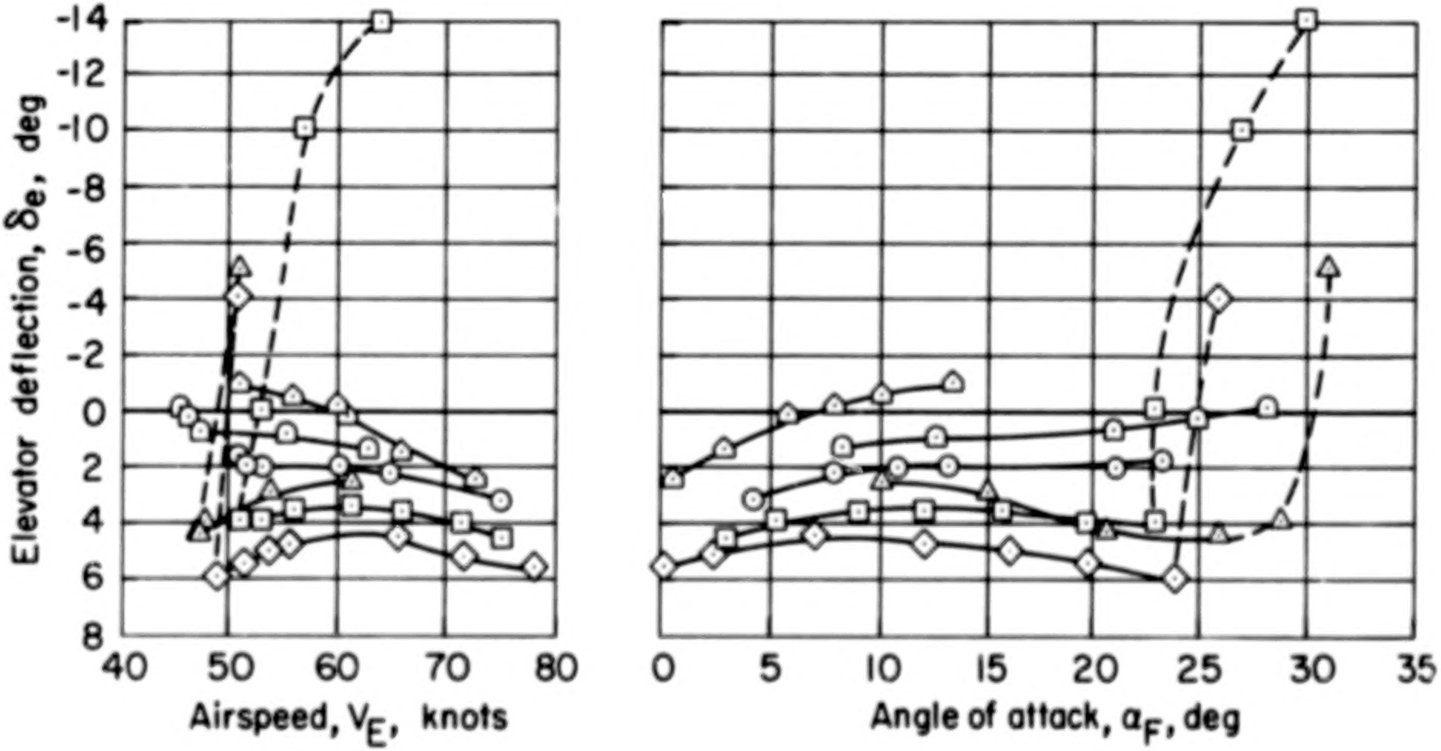

(c) Engine *rpm* approximately 95%.

Figure 19.– Continued.

	ν, deg	N_H, %	Weight, N	Altitude, m	CG, $\%\bar{c}$
○	72	Idle/99.6	197000	2100	30.7
△	73	Idle/96.5	186000	2100	30.3
□	65	Idle/96	177000	2300	30.0
◇	10	Idle/97	186000	2300	30.4

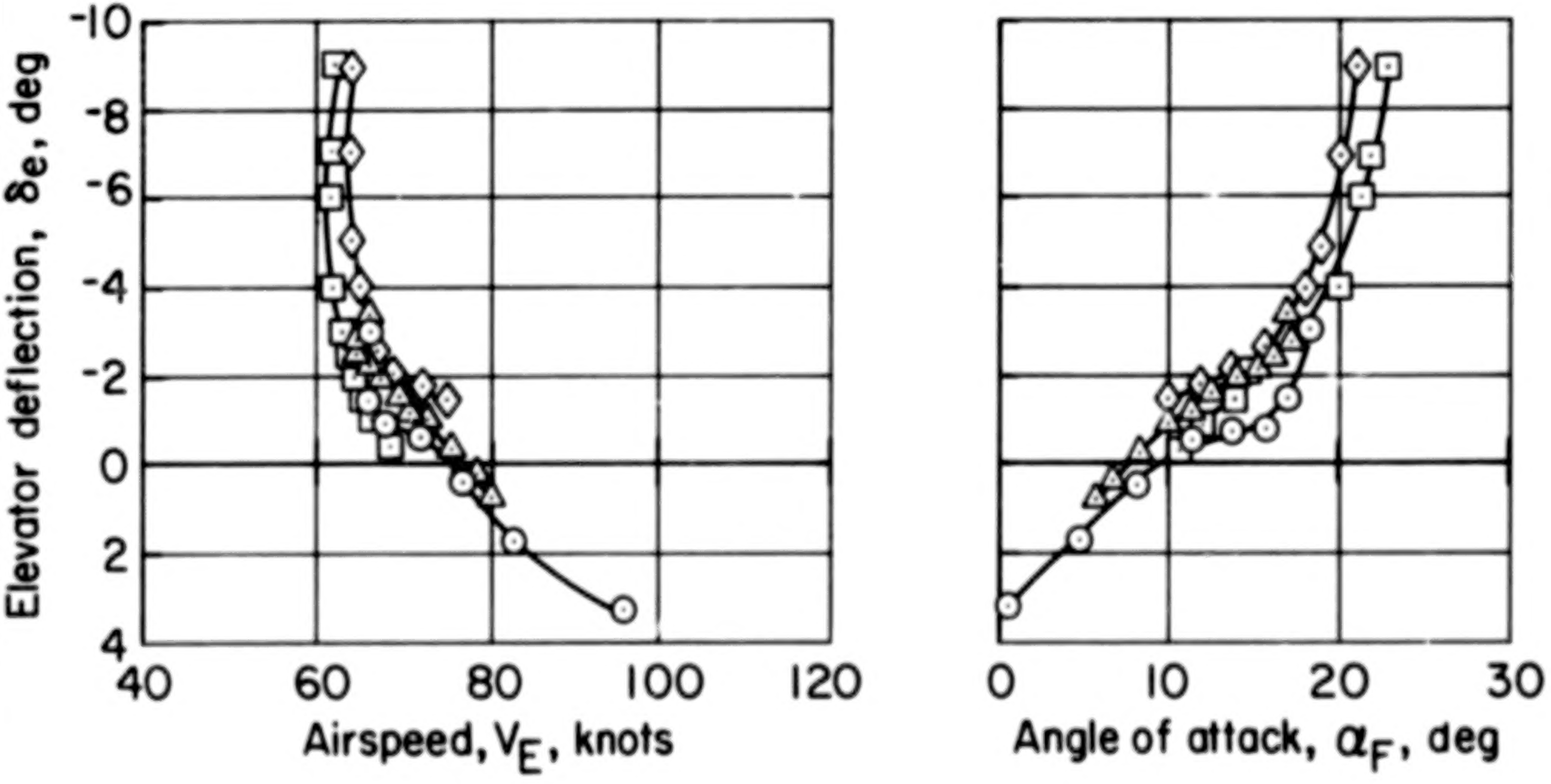

(d) One engine simulated failed.

Figure 19.– Concluded.

	δ_f, deg	ν, deg	N_H, %	Weight, N	Altitude, m	CG, %$\bar{c}$
○	28.7	10	90.1/90.5	196000	2300	30.6
□	31.2	12	91.6/92.0	186000	2400	30.3
⊿	30.8	10	93.2/93.8	191000	2400	30.5
◇	30.8	10	94.4/94.9	189000	1900	30.5
△	30.5	10	96.4/96.9	196000	2200	30.9
ᗝ	28.6	10	99.5/99.7	202000	2100	30.9

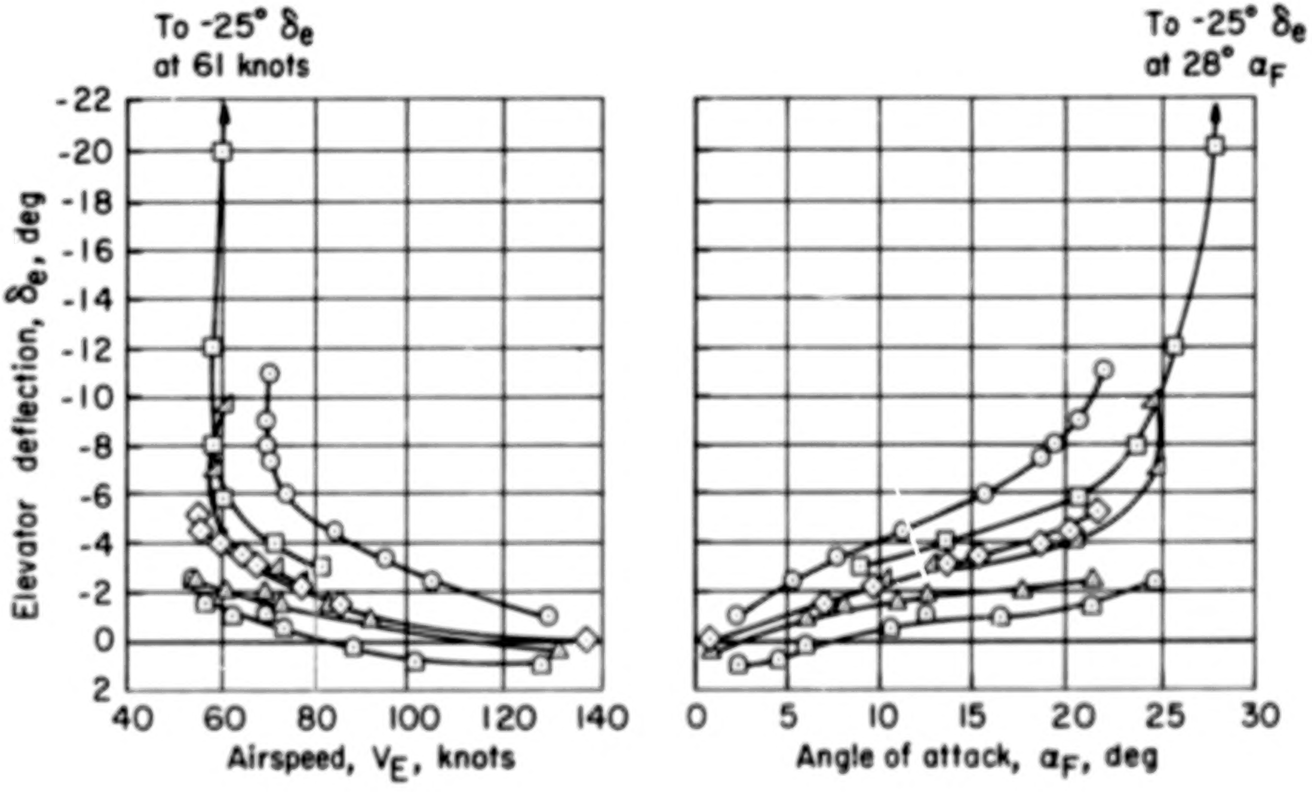

(a) Nozzle deflection 10°.

Figure 20.– Variation of longitudinal stability with engine *rpm*, flap deflection 30°.

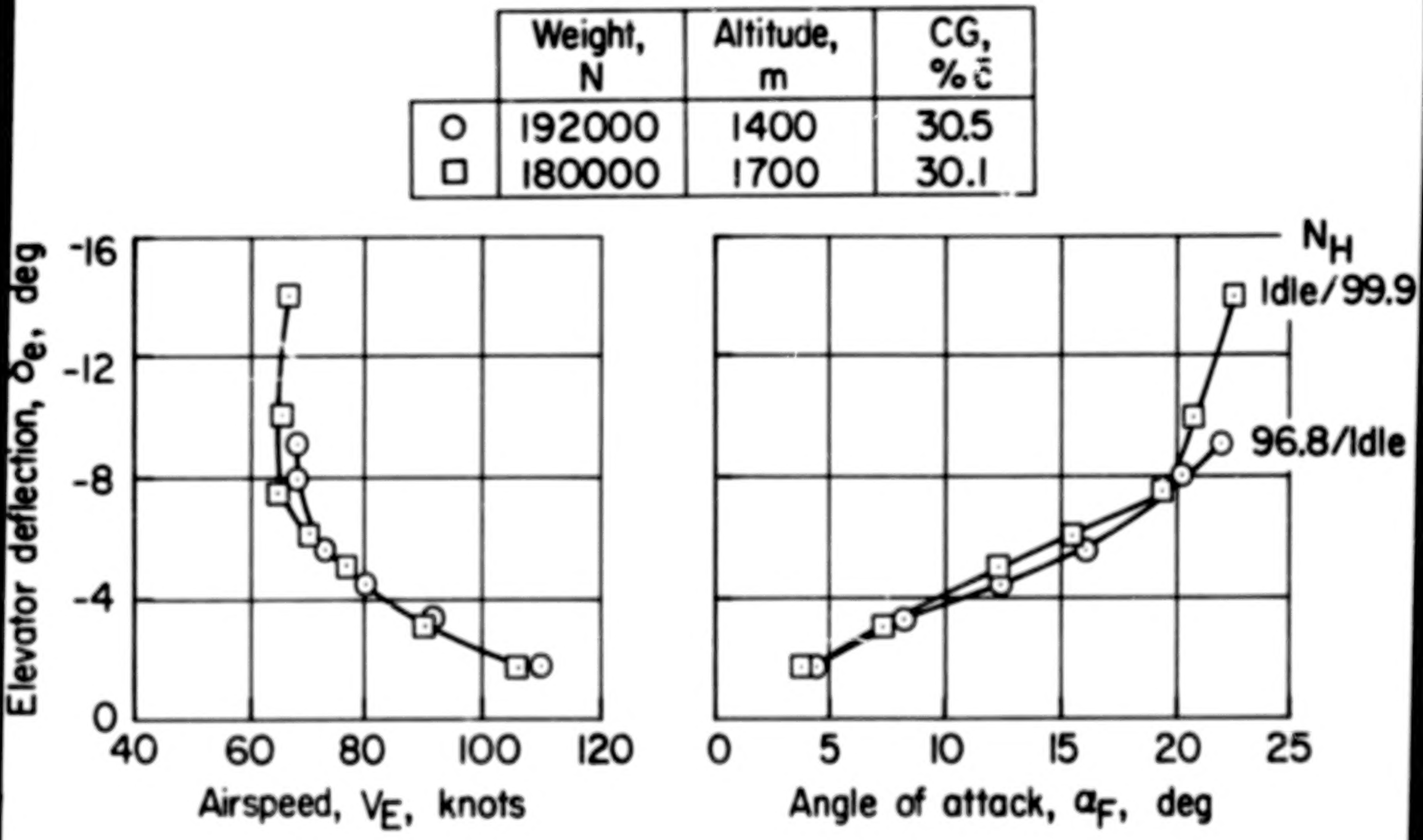

(b) Nozzle deflection 10°, one engine simulated failed.

Figure 20.– Concluded.

	N_H, %	Weight, N	Altitude, m	CG, % $\bar{c}$
○	90.3	205000	1400	30.9
□	94.3	197000	2100	30.4
△	97.4	201000	2100	30.8
◇	90.4	198000	2700	30.7

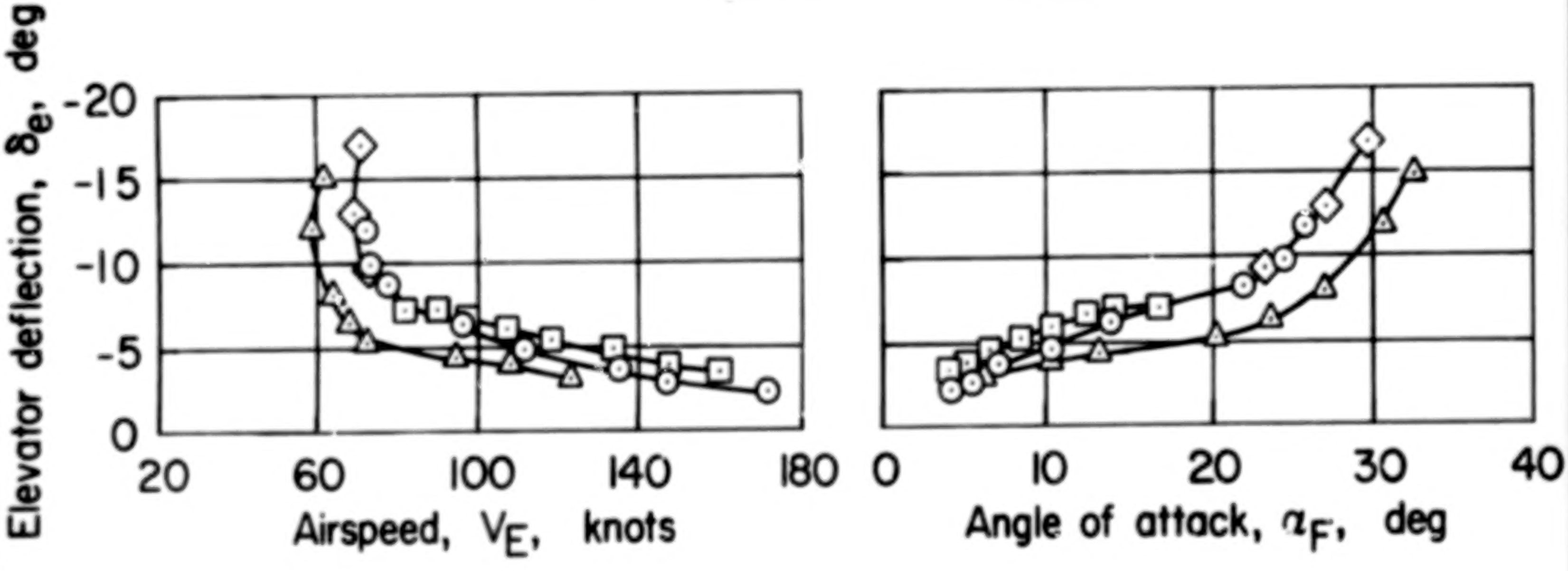

(a) Nozzle deflection 10°.

Figure 21.– Variation of longitudinal stability with engine *rpm*, flap deflection 5.6°.

Weight, N	Altitude, m	CG, %$\bar{c}$
178000	1600	30.0

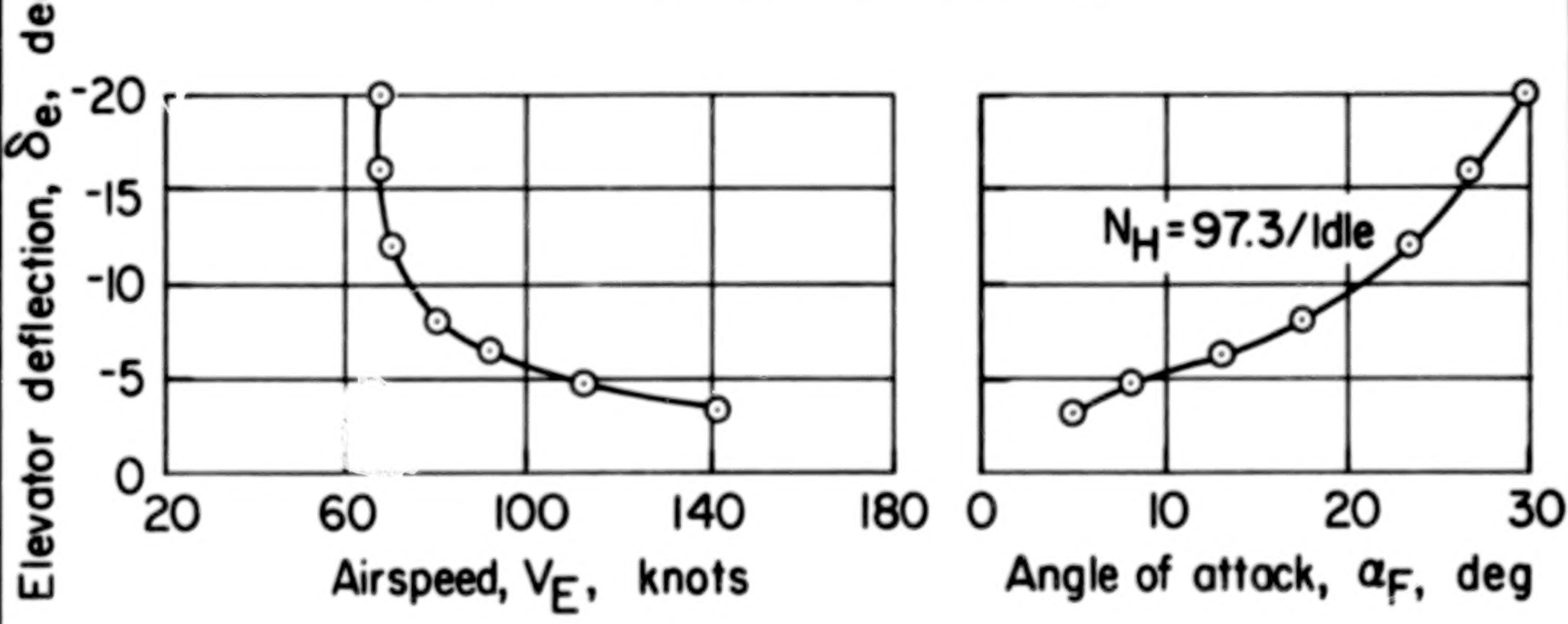

(b) Nozzle deflection 10°, one engine simulated failed.

Figure 21.– Concluded.

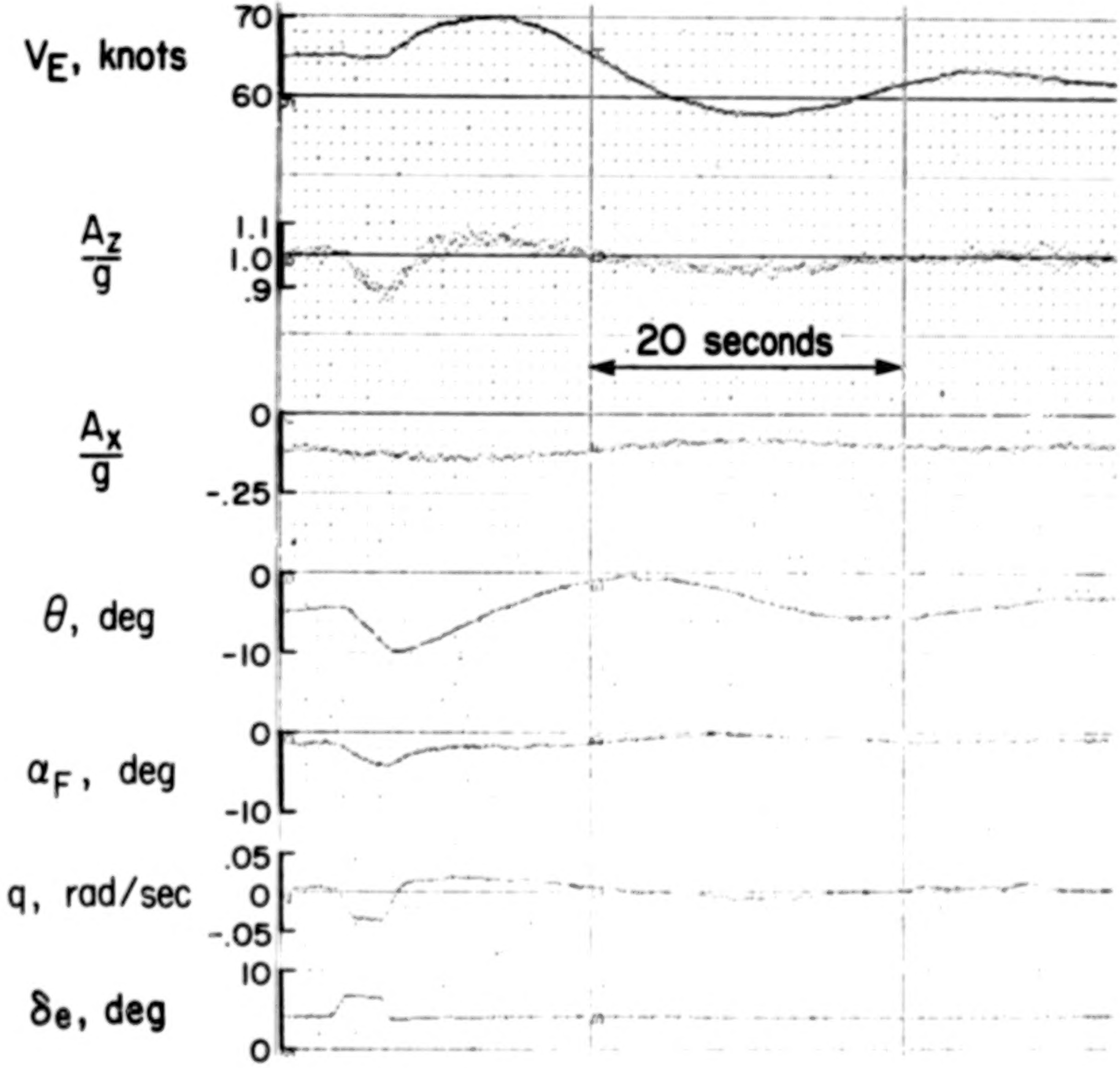

Figure 22.– Elevator pulse – flaps deflection 67°, nozzles deflection 77°, 65 knots.

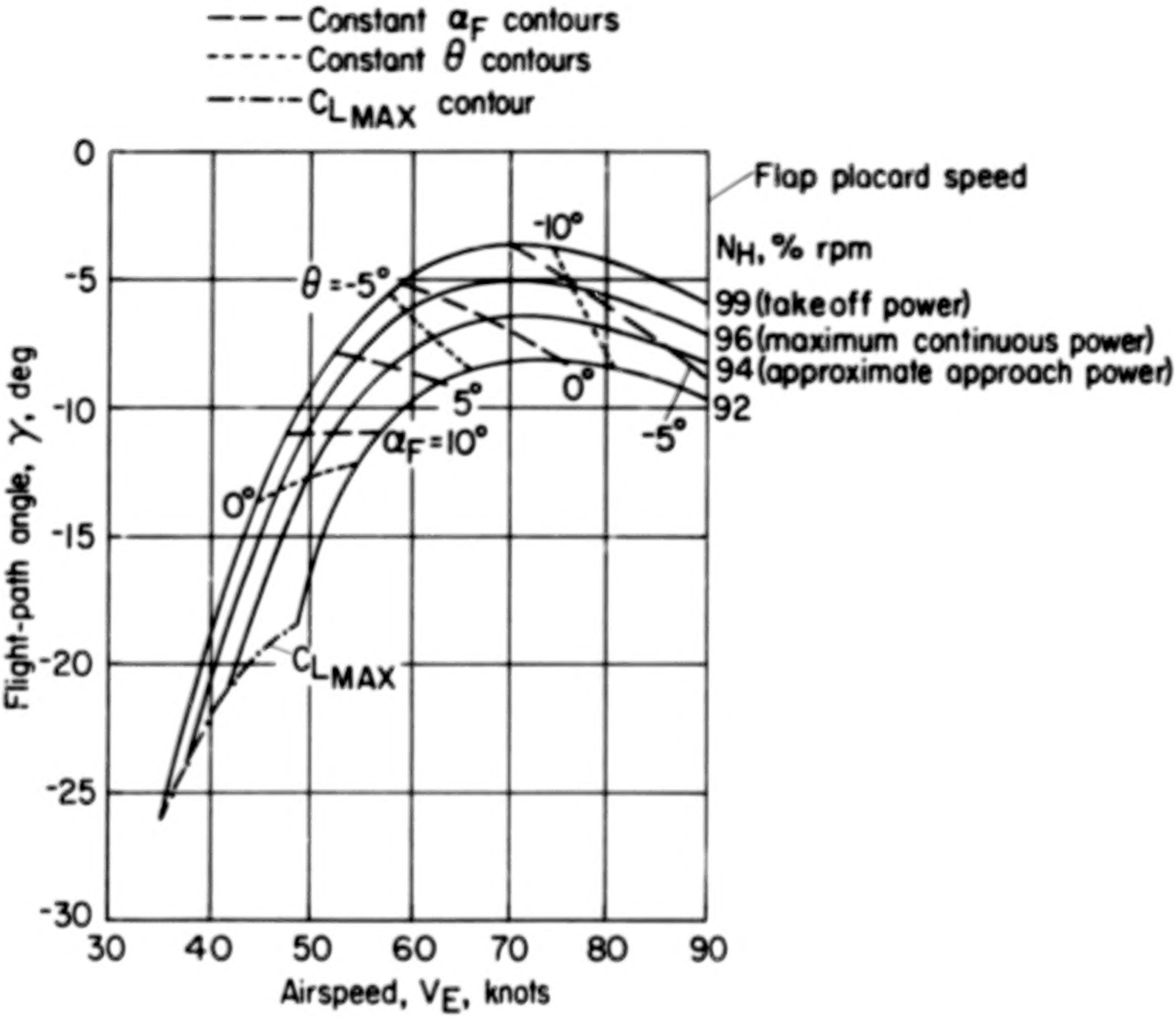

(a) Nozzle deflection constant at 90°.

Figure 23.– Landing operational envelope, flap deflection 65°, W = 178,000 N, sea level standard day.

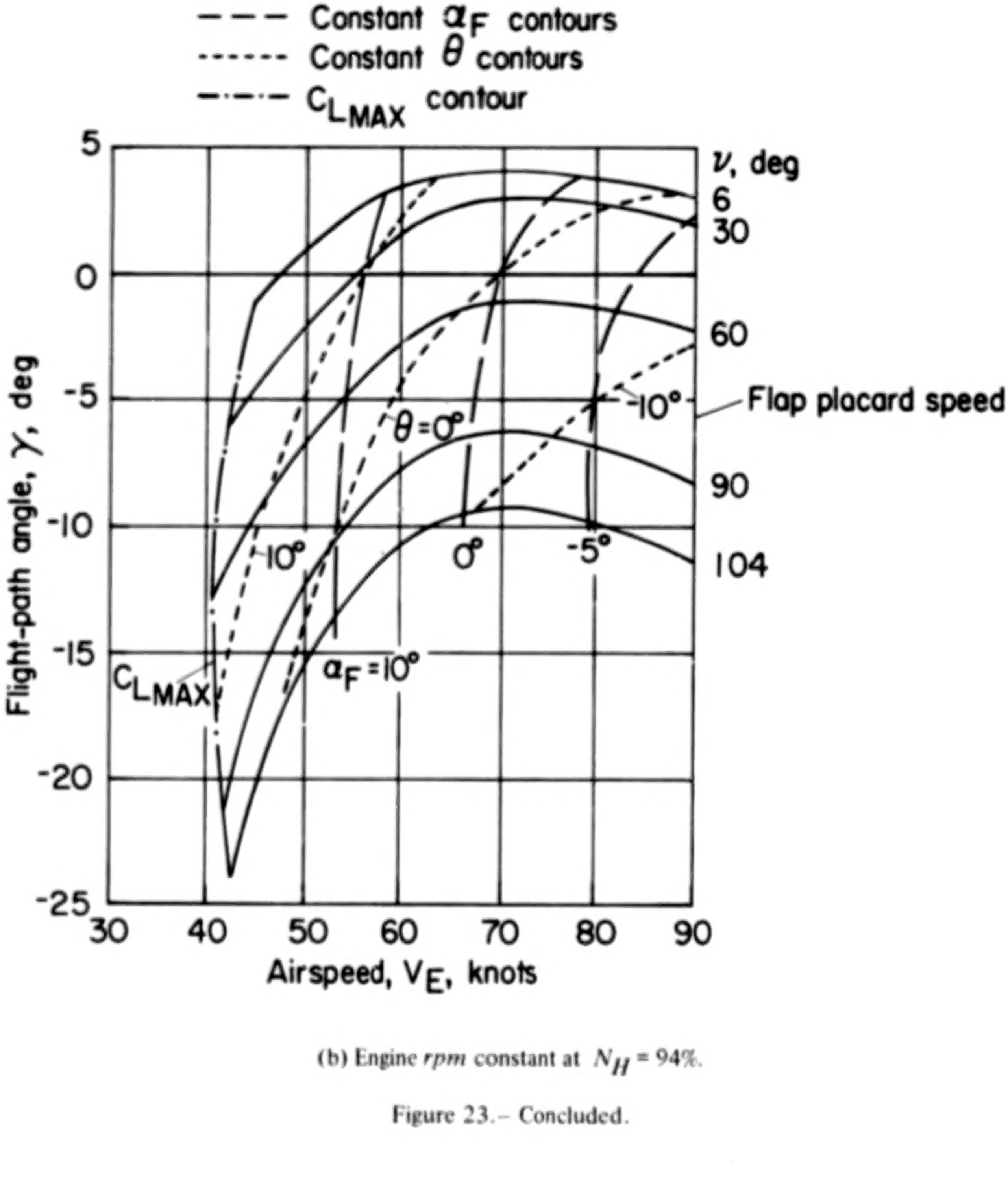

(b) Engine *rpm* constant at $N_H = 94\%$.

Figure 23.– Concluded.

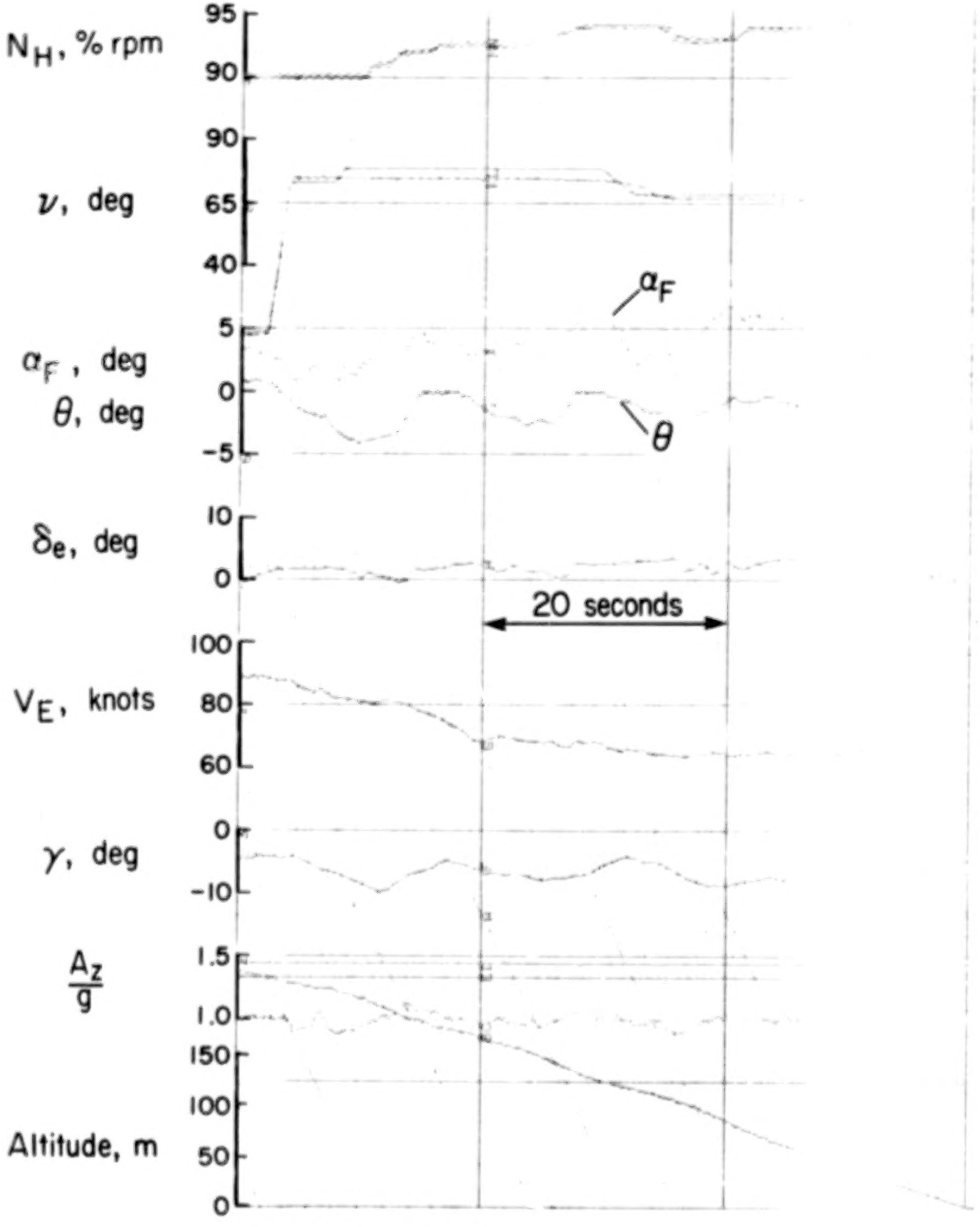

Figure 24.– Landing approach time history, $\delta_f = 64.7°$, $W = 193{,}000$ N.

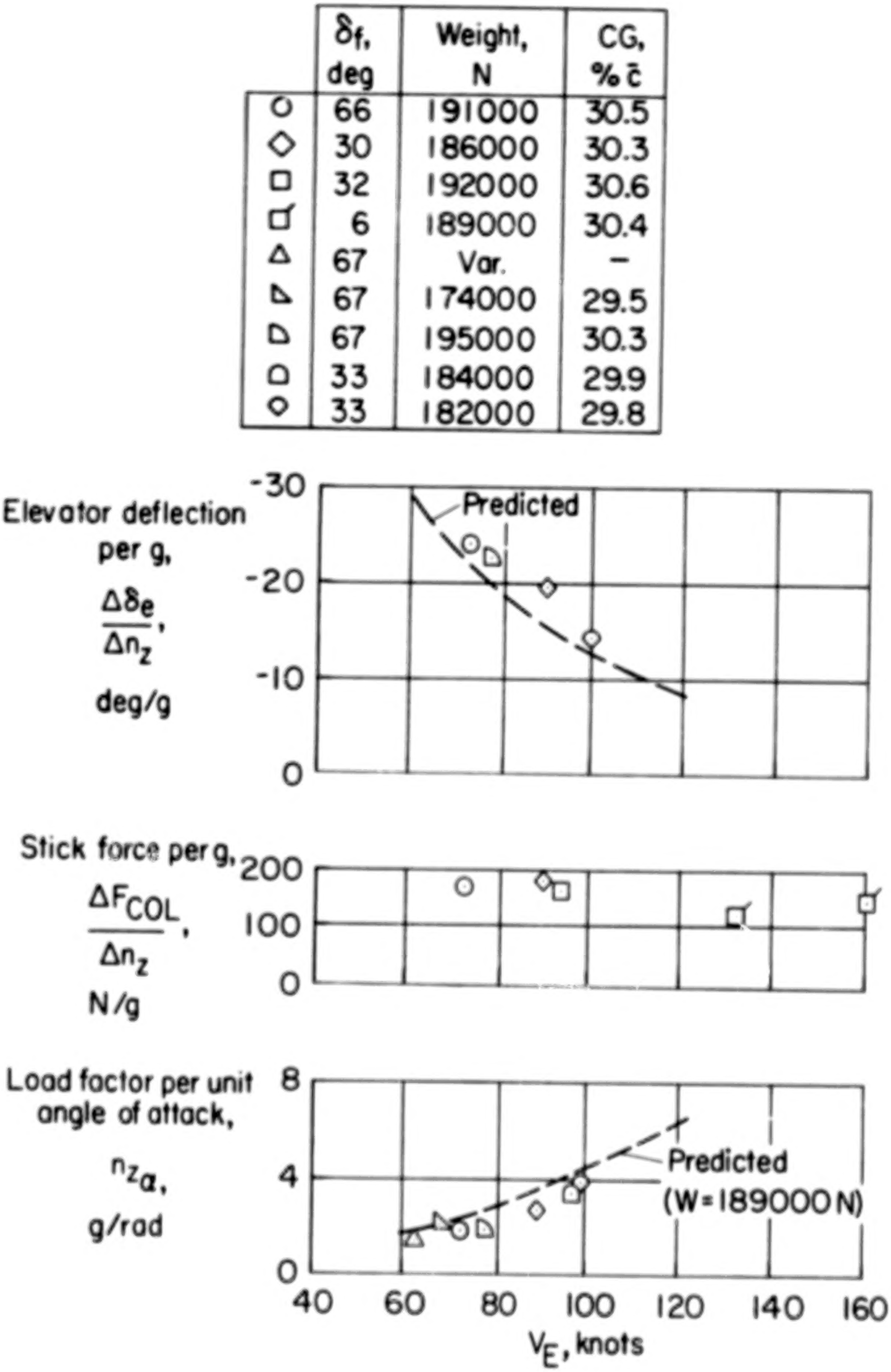

Figure 25.– Maneuvering stability summary.

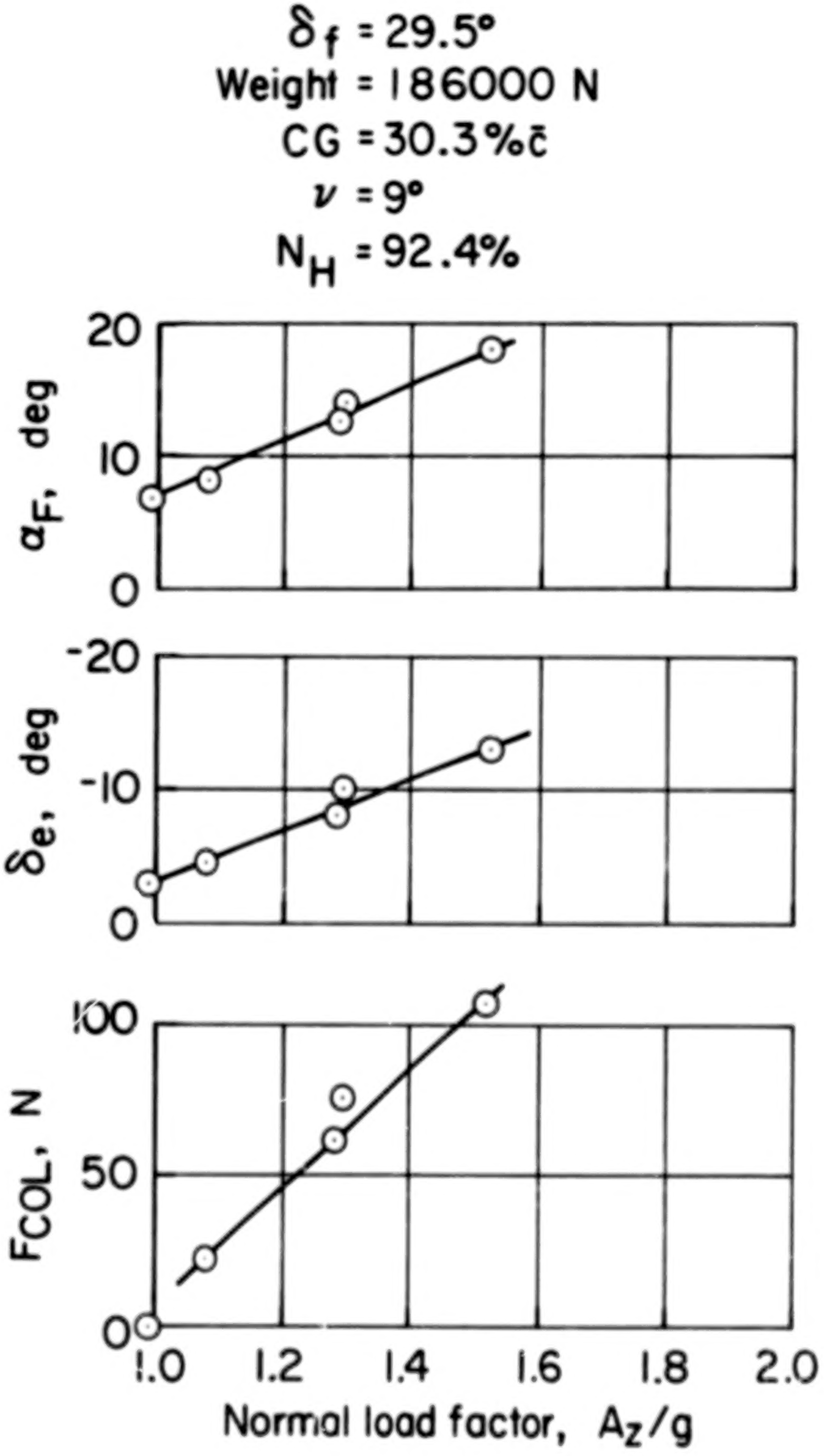

Figure 26.– Wind-up turn, flaps 30°, 90 knots, powered elevator installed.

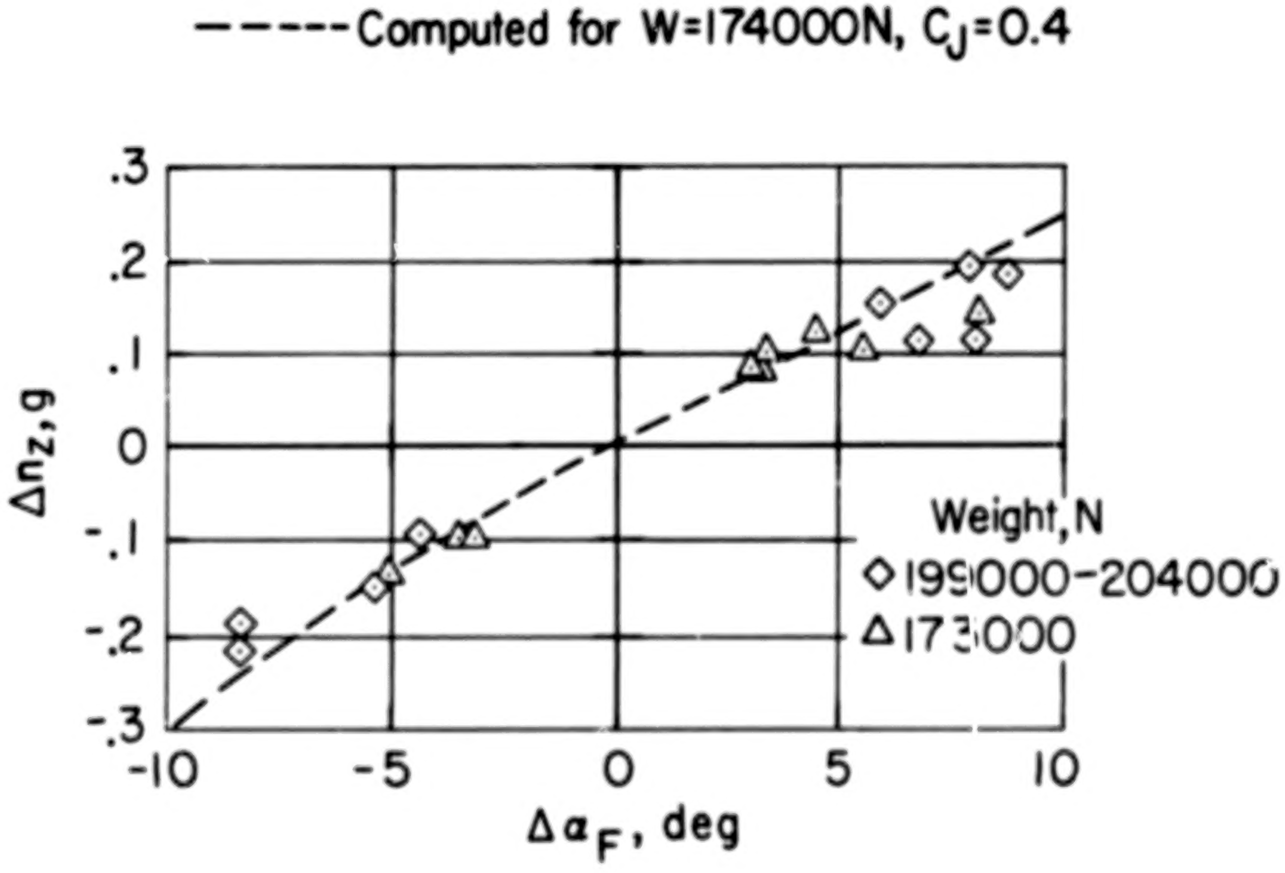

(a) Airspeed 63 knots.

Figure 27.– Variation of vertical acceleration with changes in angle of attack, $\delta_f = 65°$, $\nu = 60°$ to $90°$.

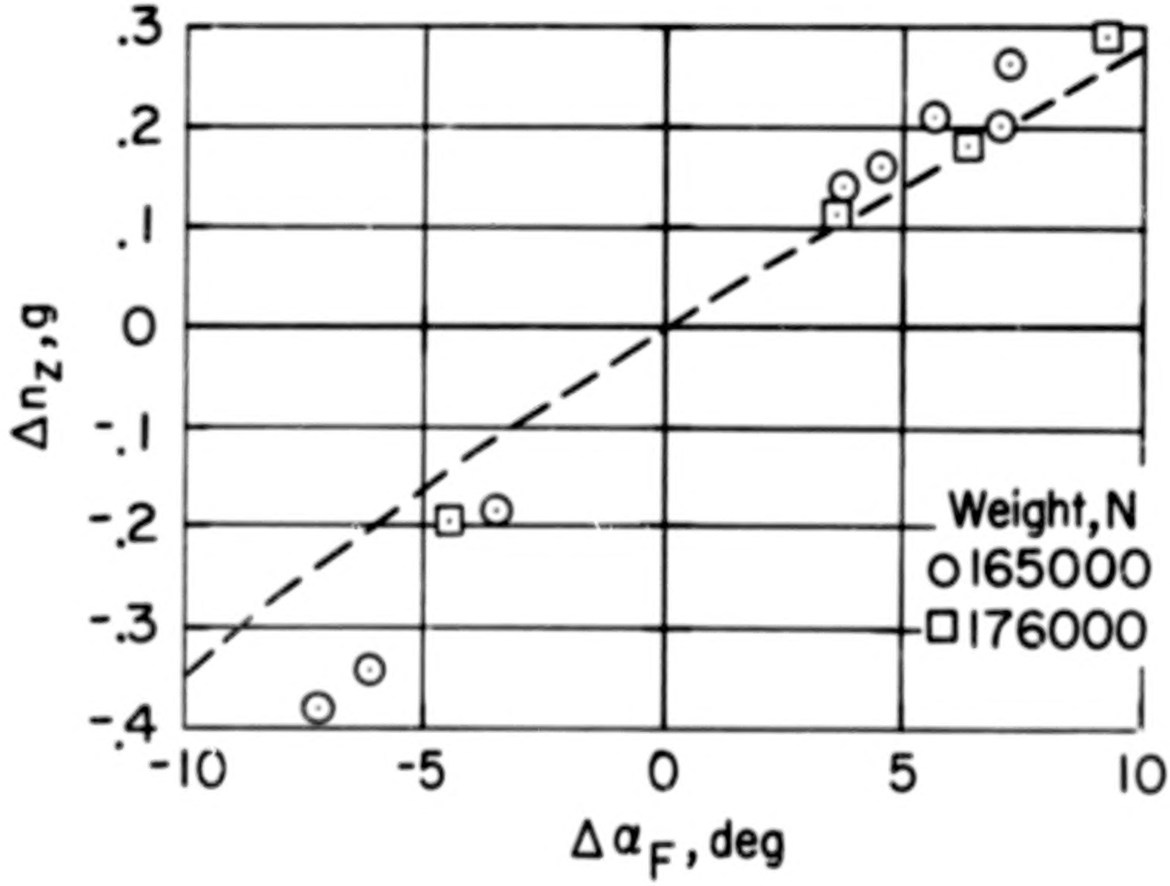

(b) Airspeed 68 knots.

Figure 27.– Concluded.

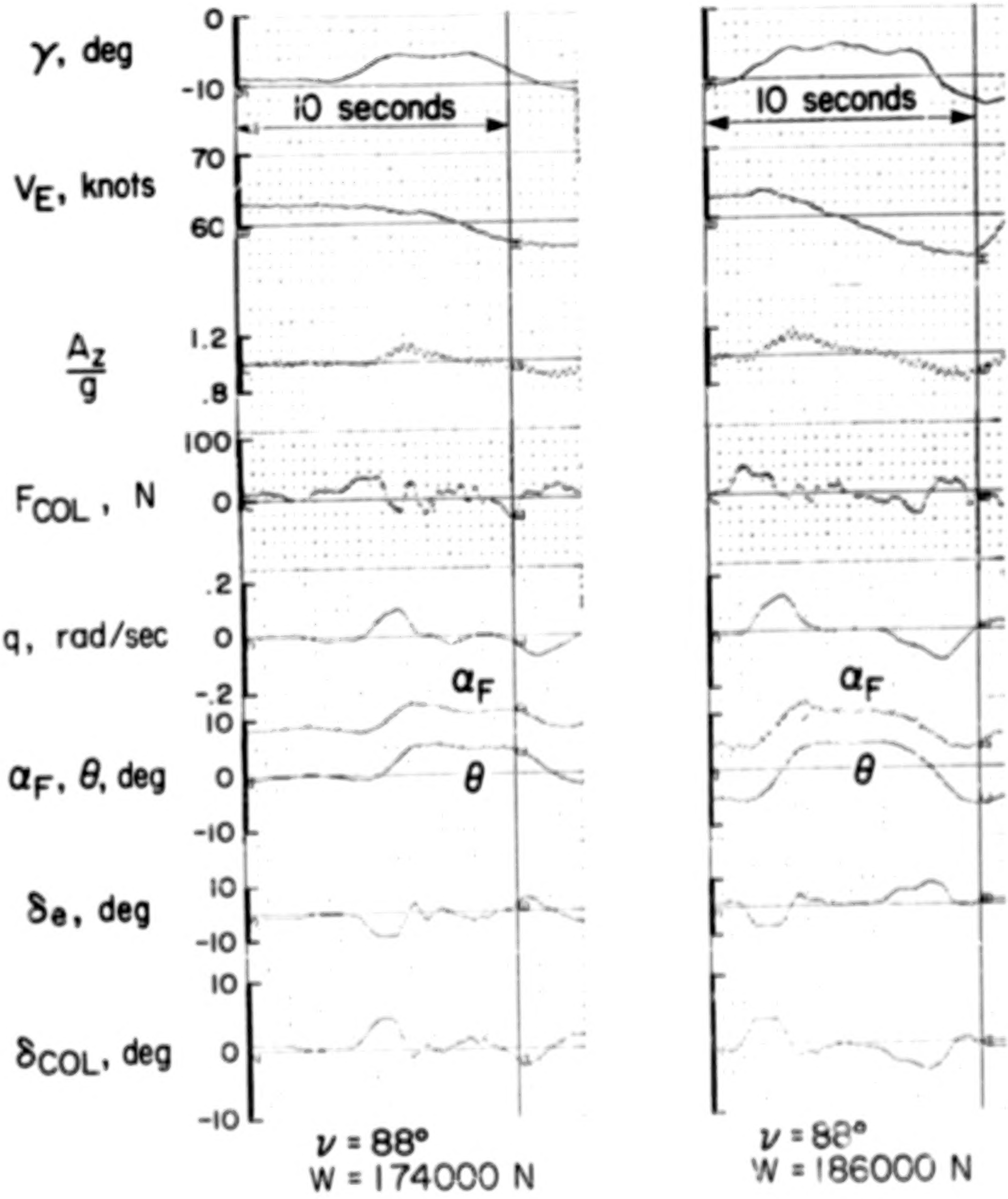

(a) Airplane nose-up steps.

Figure 28.– Pitch attitude steps.

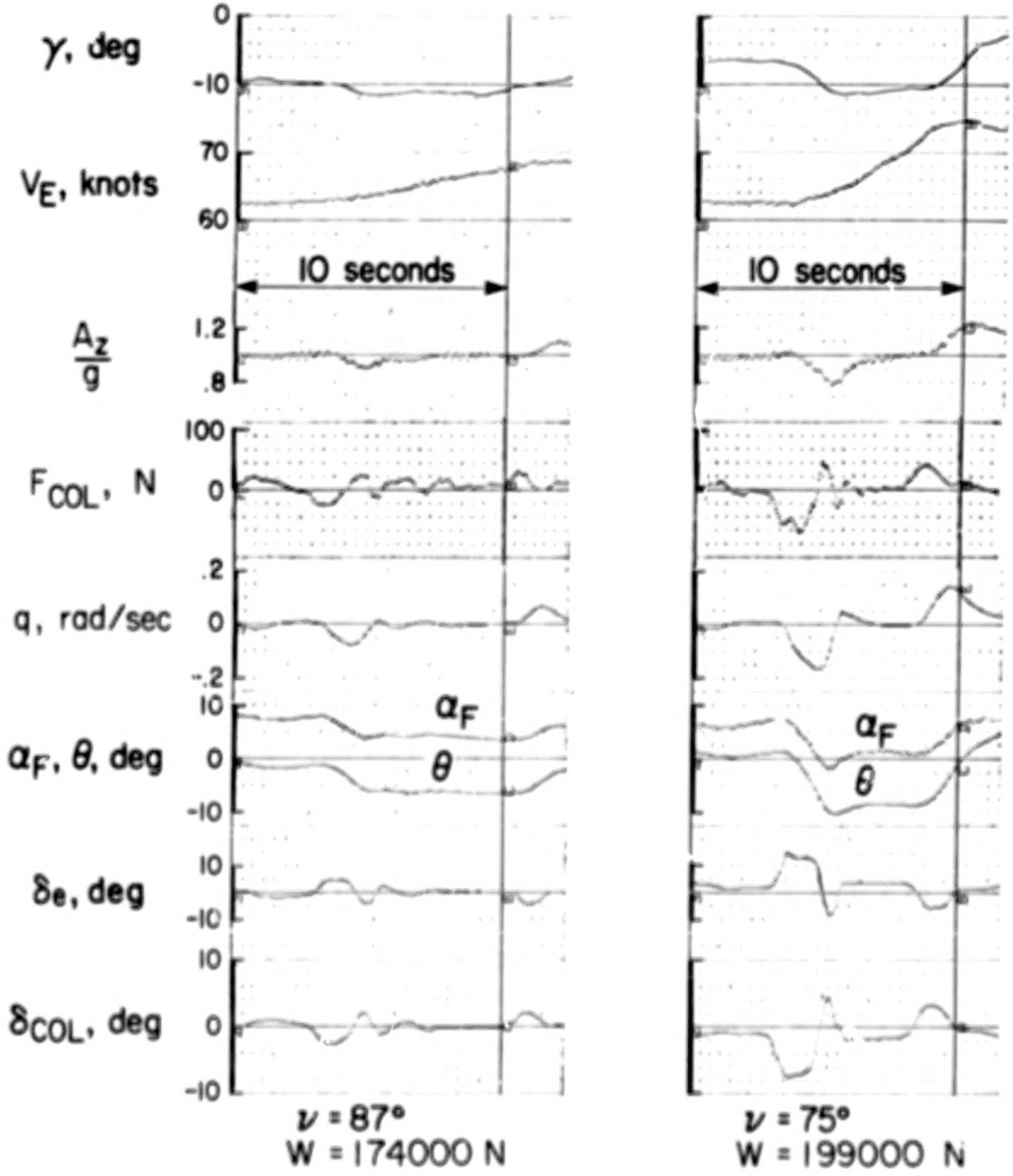

(b) Airplane nose-down steps.

Figure 28.– Concluded.

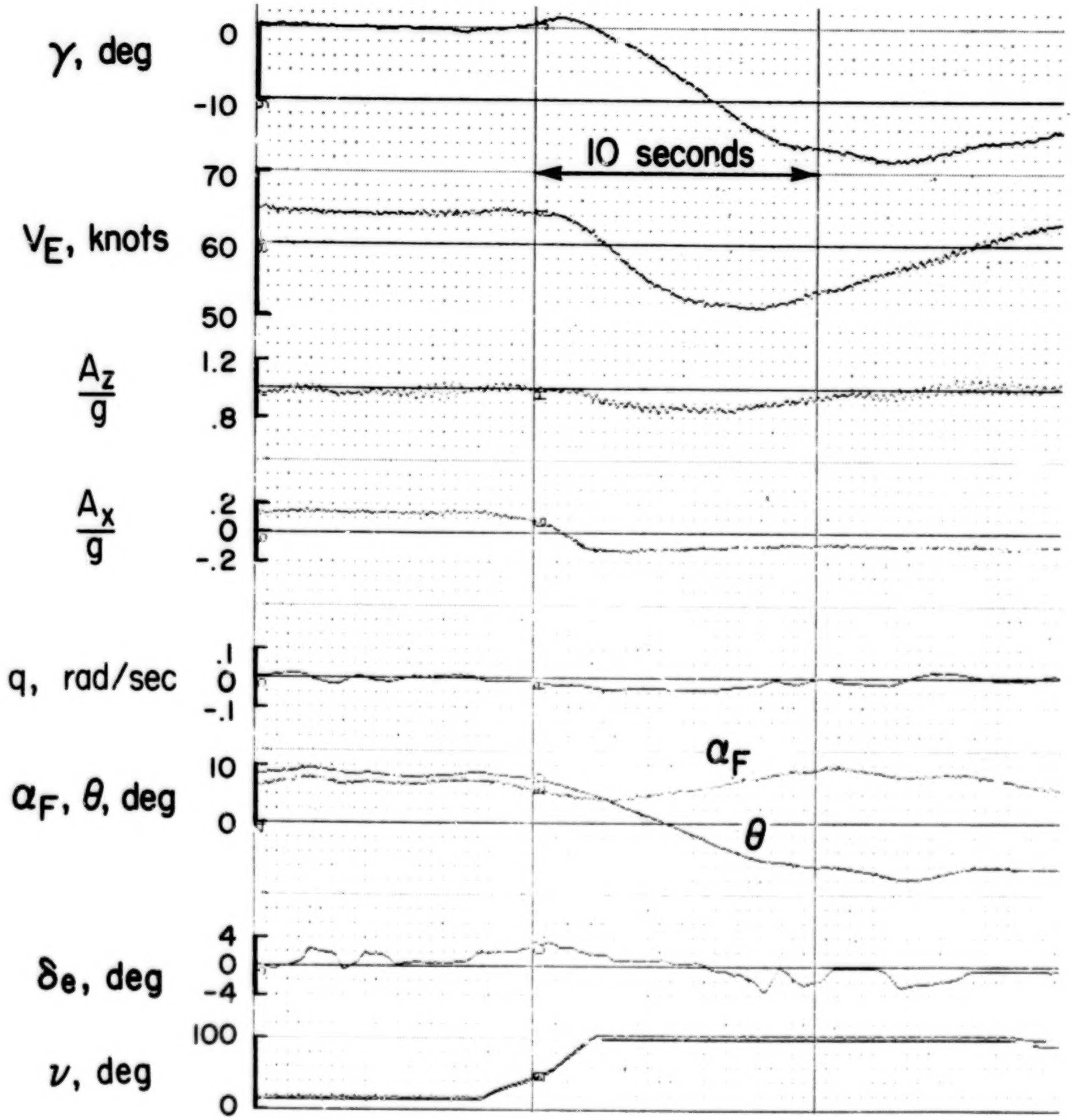

(a) Forward nozzle rotation.

Figure 29.– Response to nozzle rotation, flaps 65°.

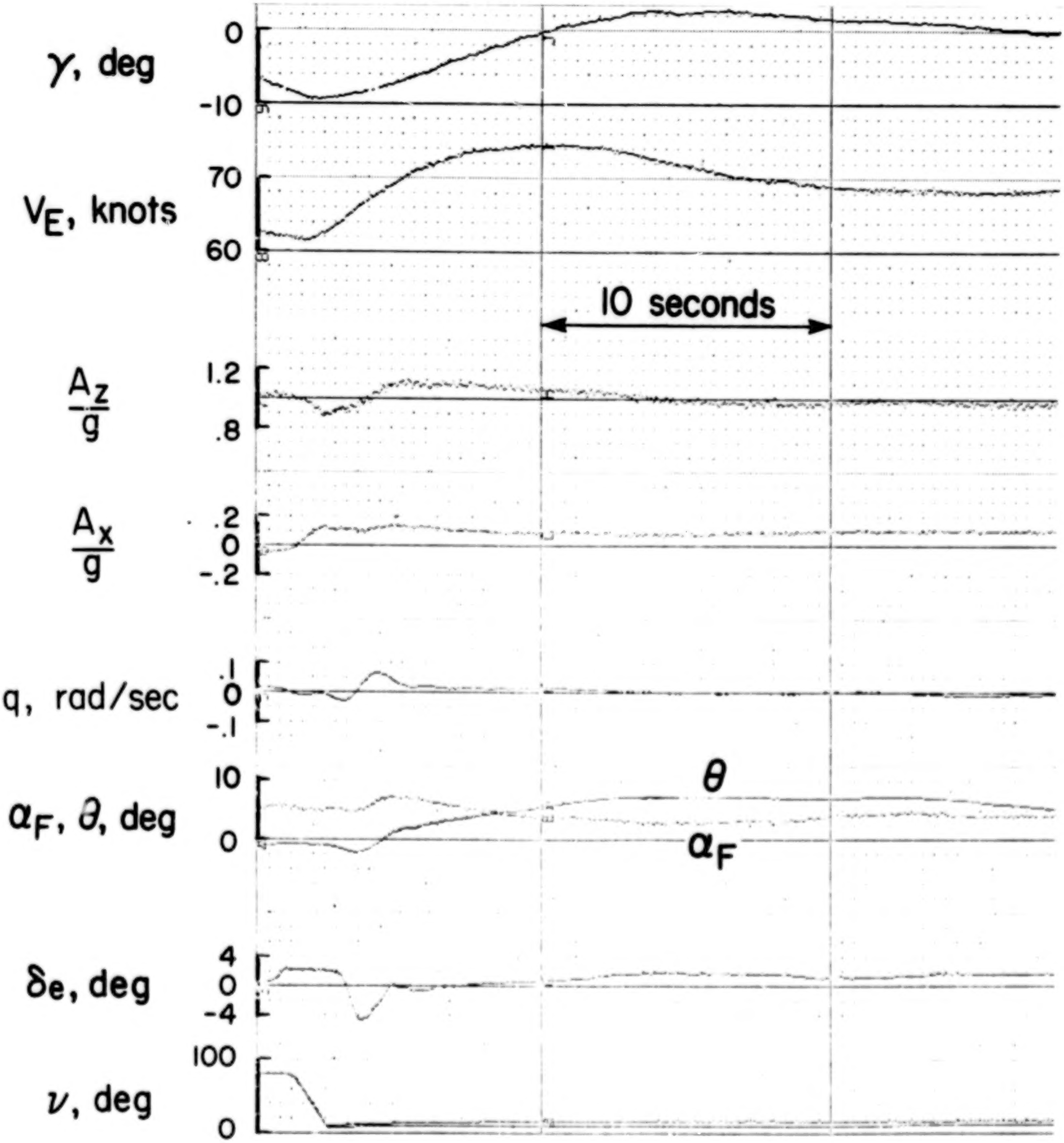

(b) Aft nozzle rotation.

Figure 29.– Continued.

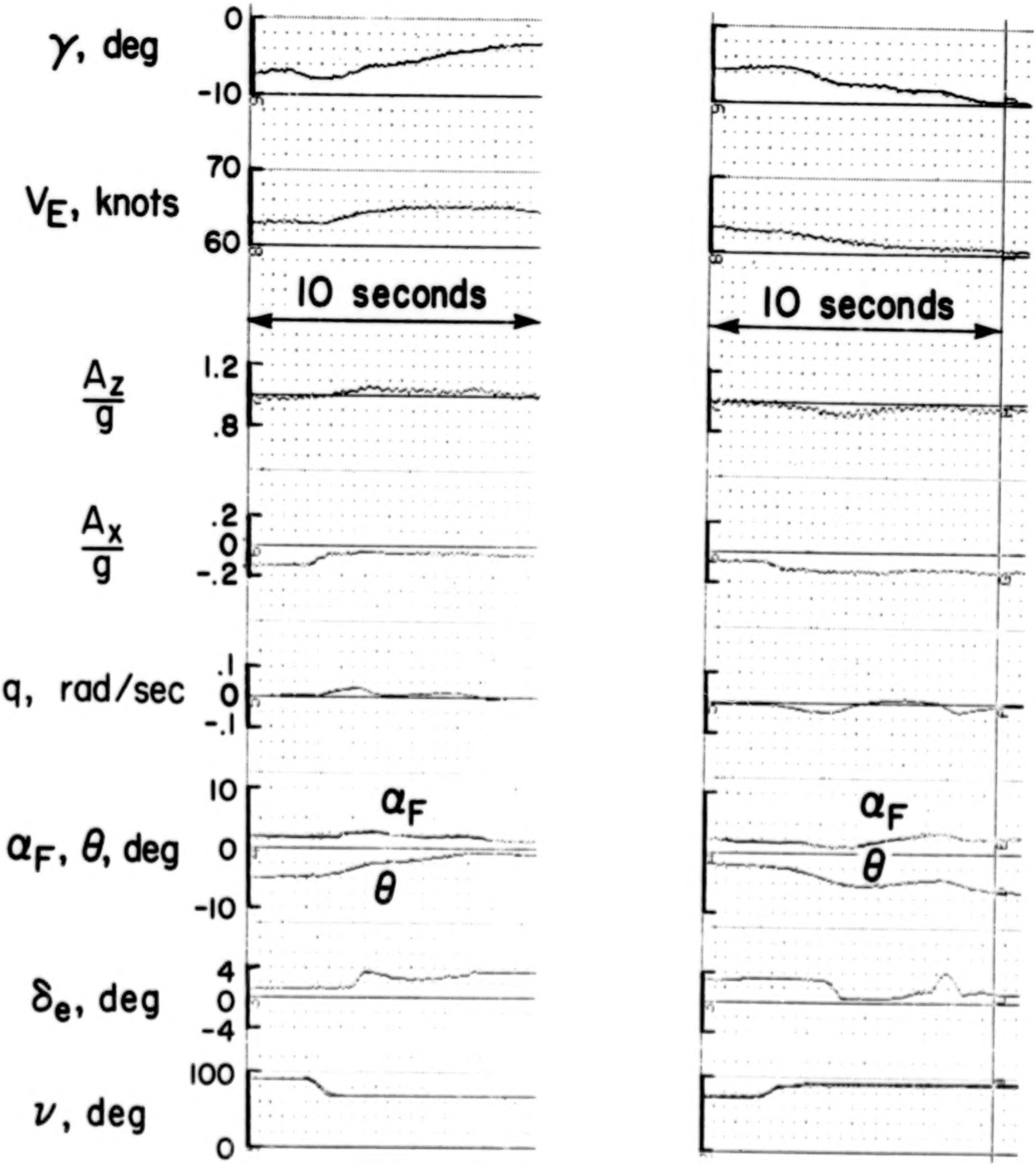

(c) Small nozzle step.

Figure 29.– Concluded.

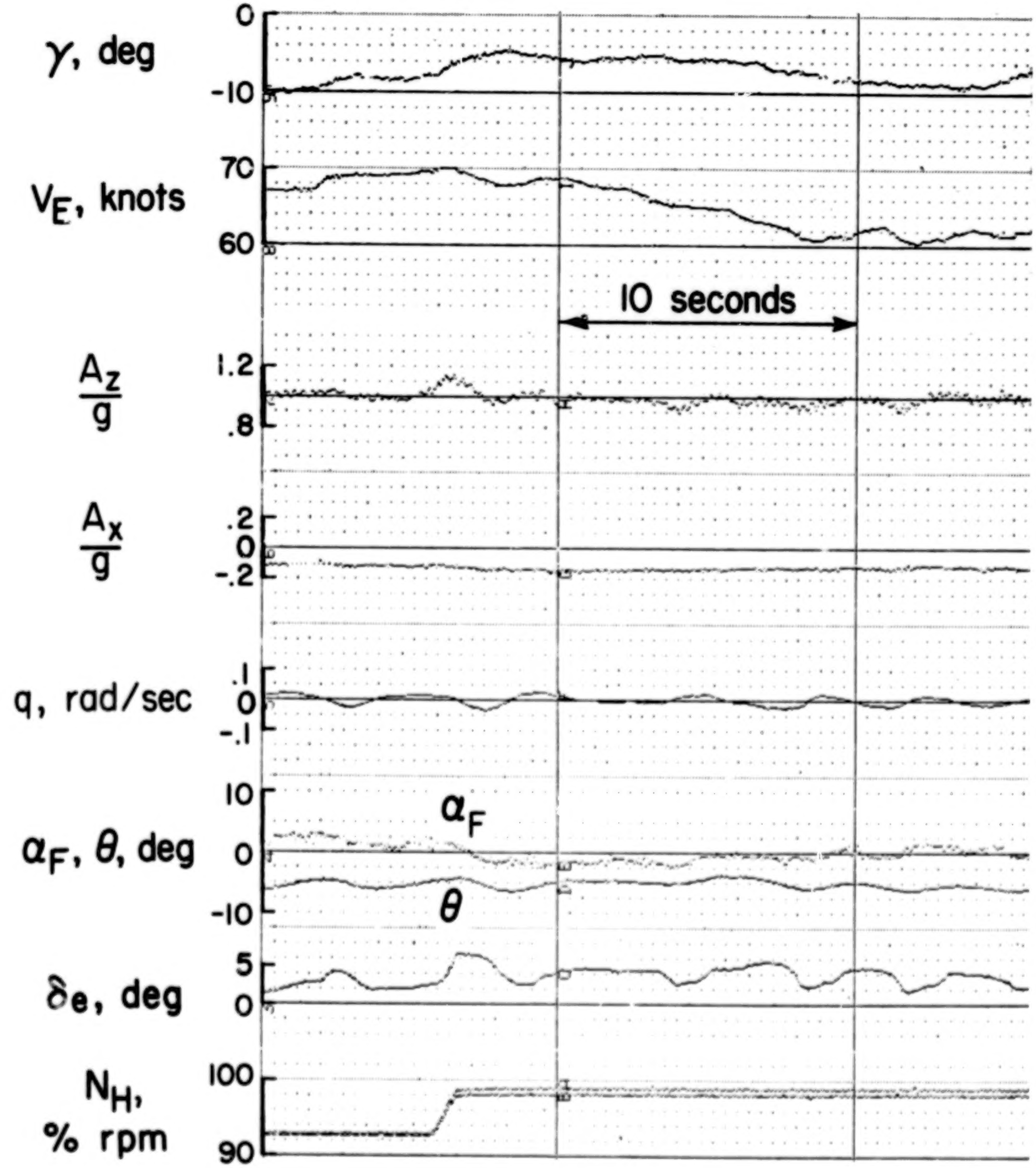

(a) *rpm* increased, $\nu = 83°$.

Figure 30.– Response to a throttle step, flaps 65°.

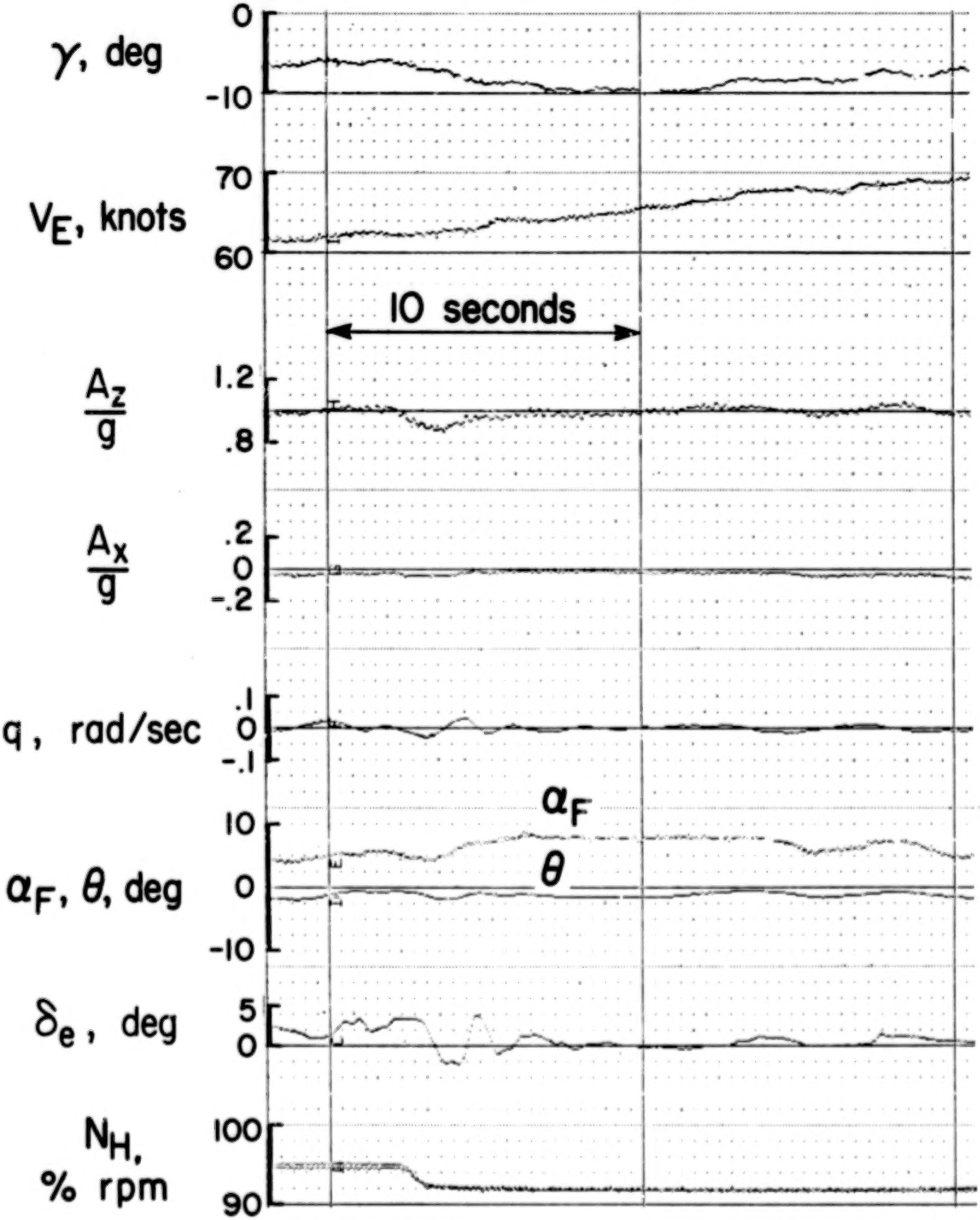

(b) *rpm* decreased, $\nu = 75°$.

Figure 30.– Concluded.

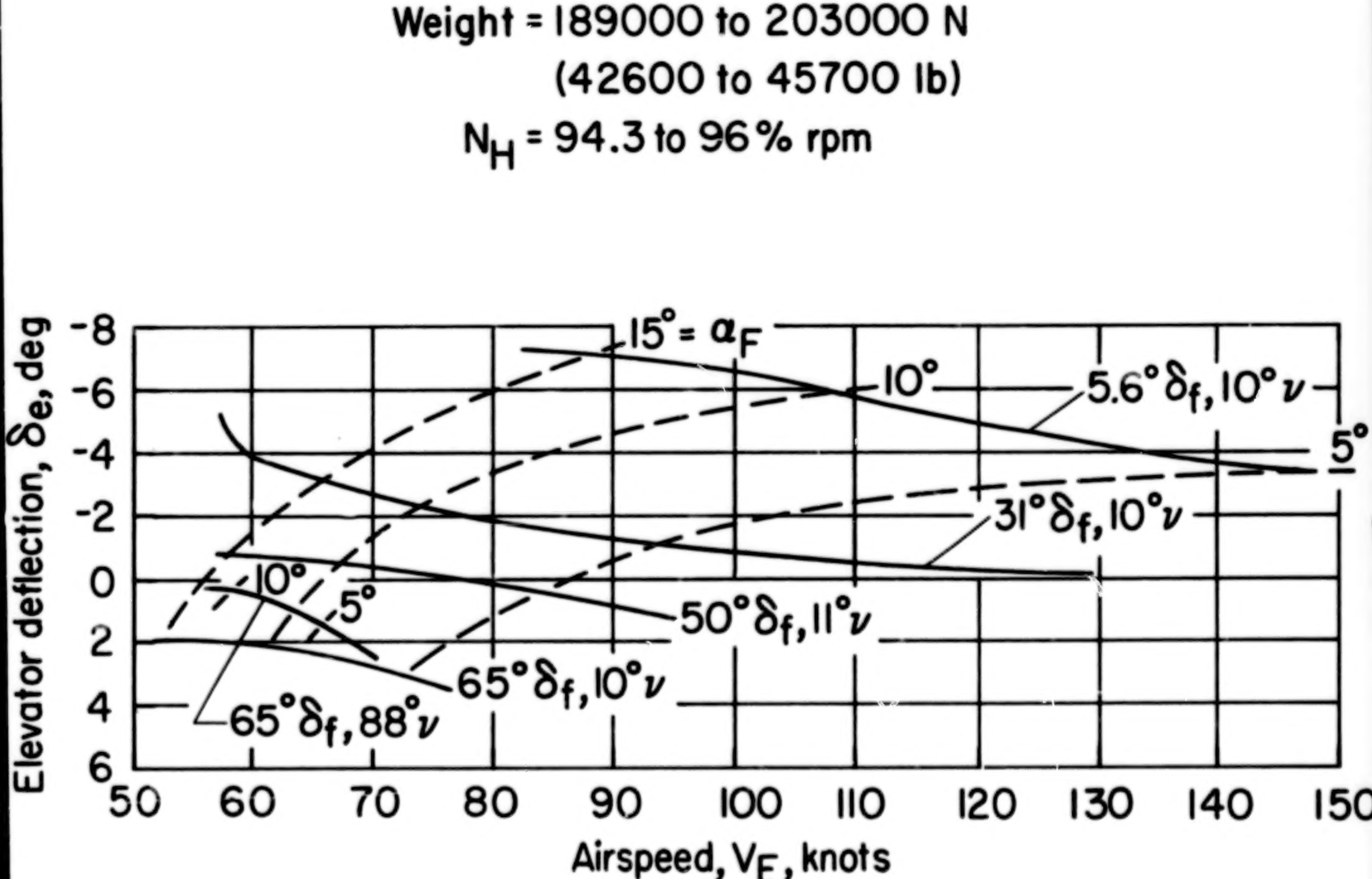

Figure 31.– Elevator required for trim for various flap and nozzle deflections.

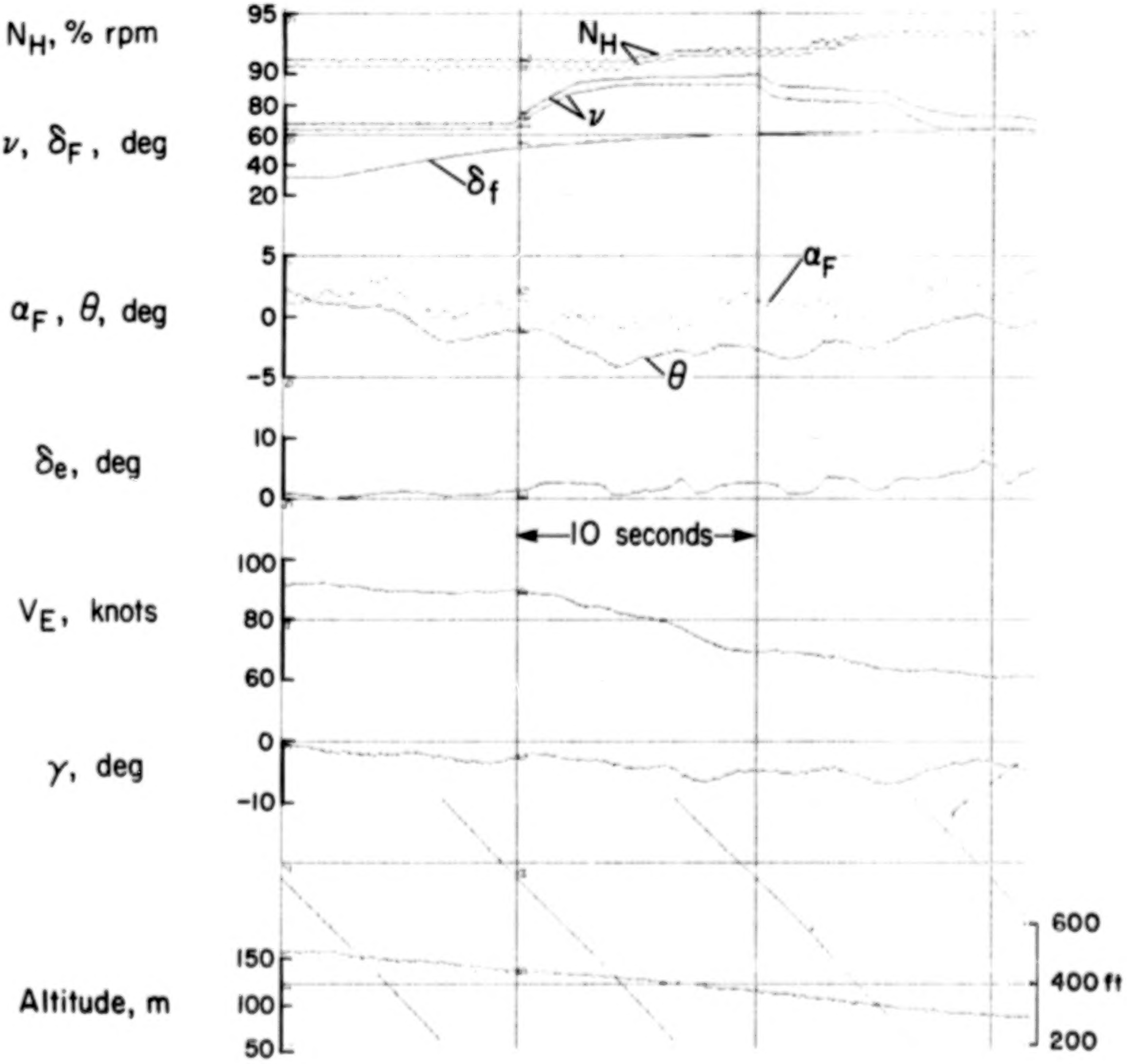

Figure 32.– Transition to handing configuration, $W = 195{,}000$ N.

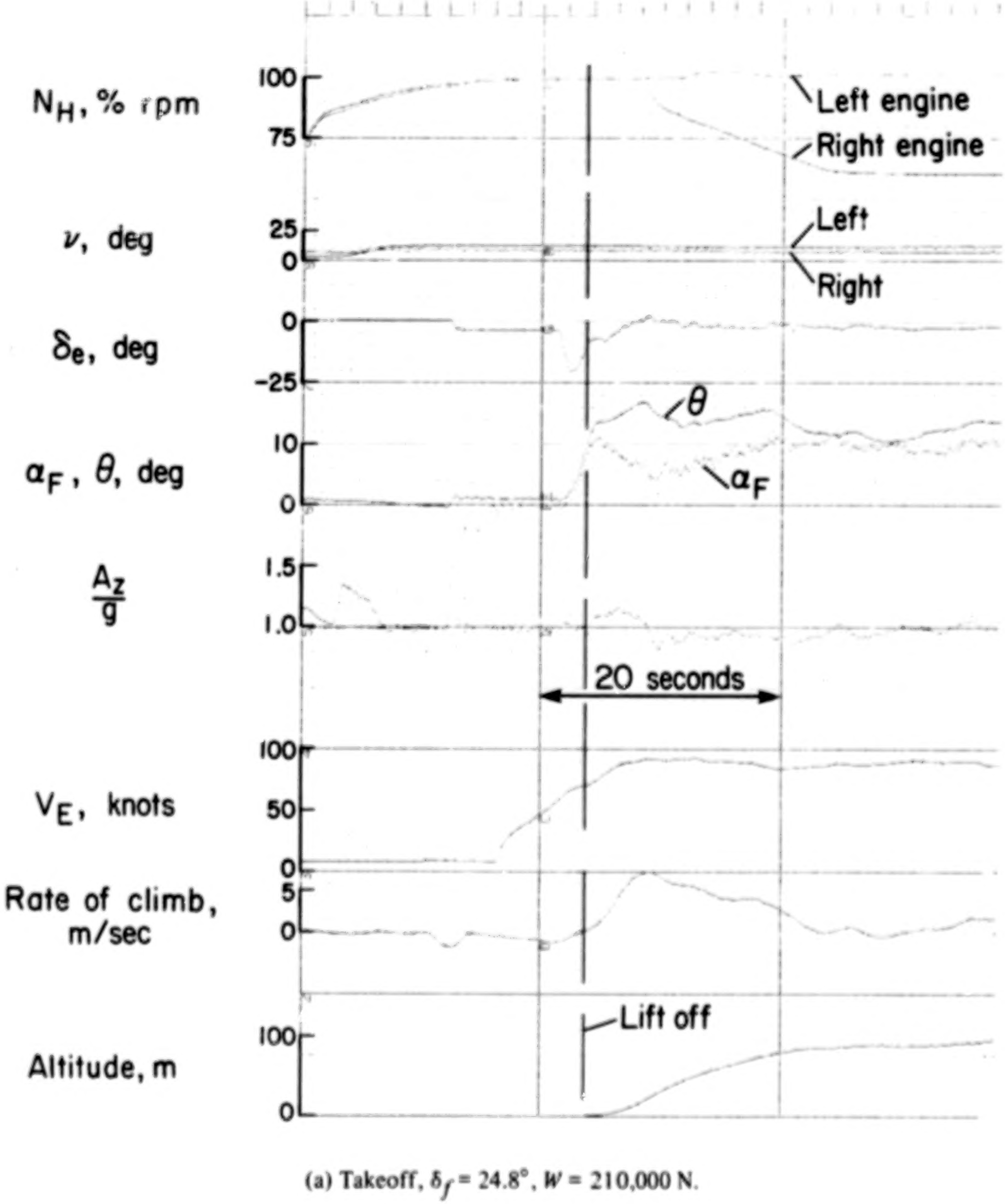

(a) Takeoff, $\delta_f = 24.8°$, $W = 210{,}000$ N.

Figure 33.– Simulated engine failure time histories.

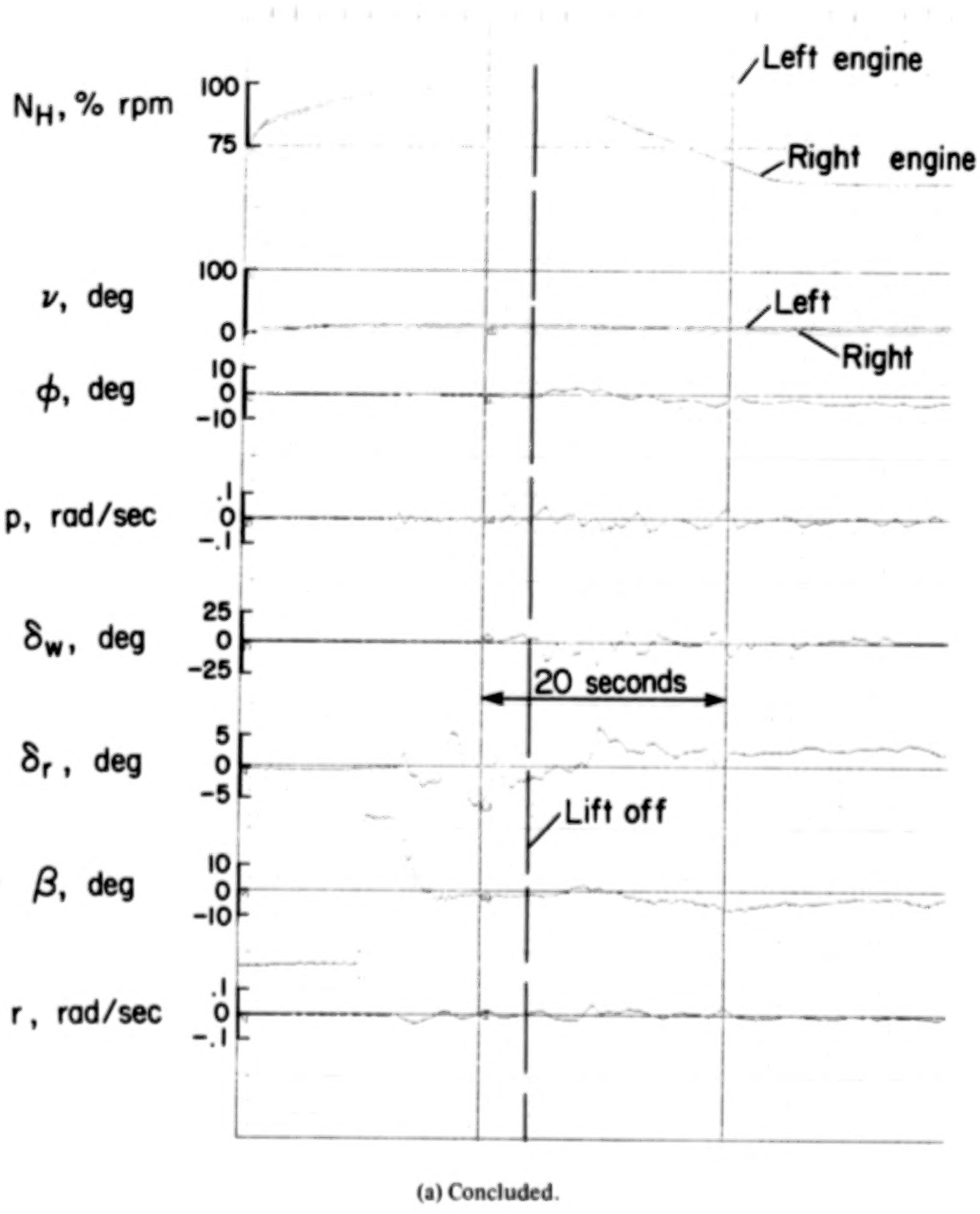

(a) Concluded.

Figure 33.– Continued.

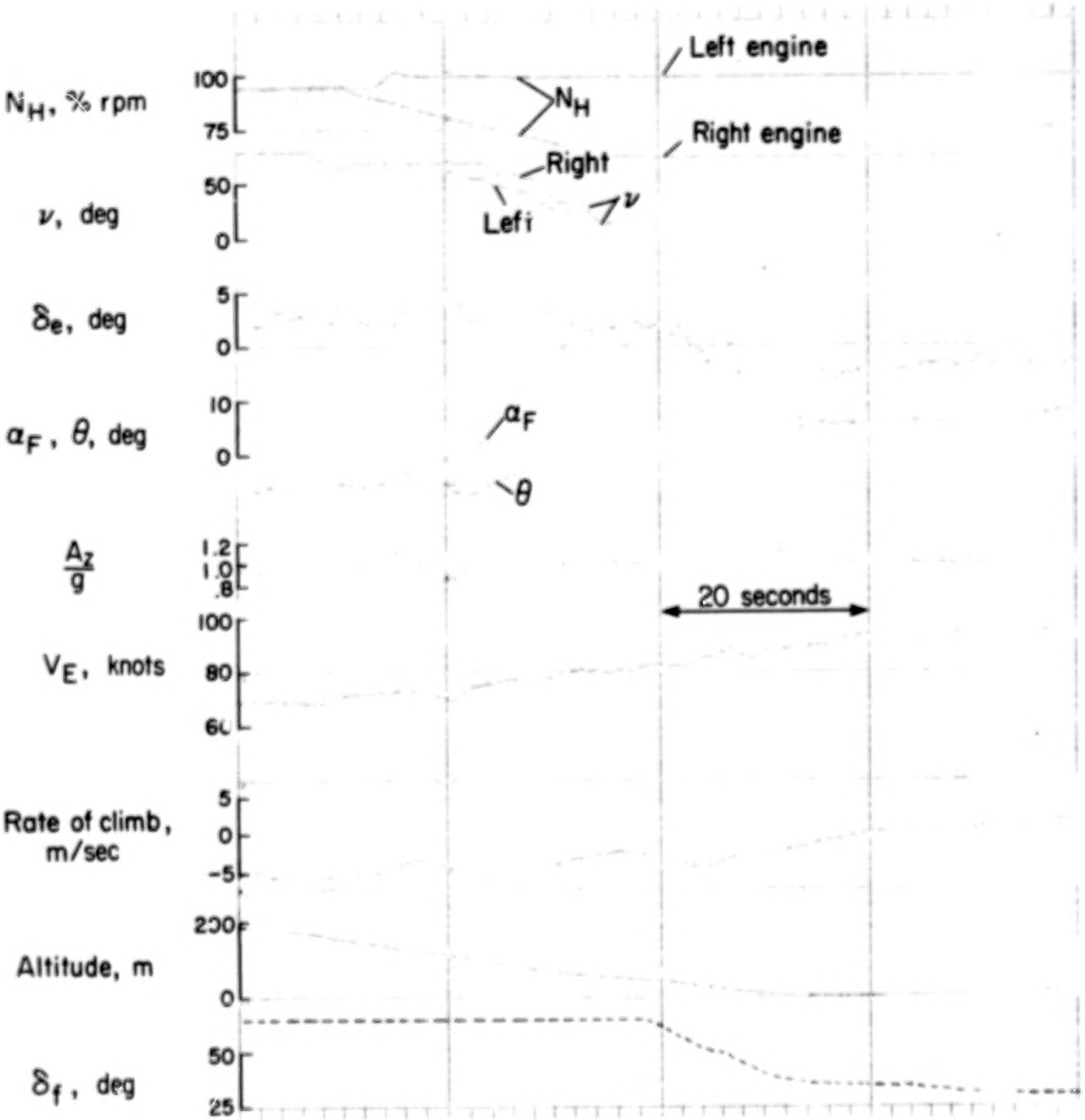

(b) Landing approach, W = 165,000 N.

Figure 33.– Continued.

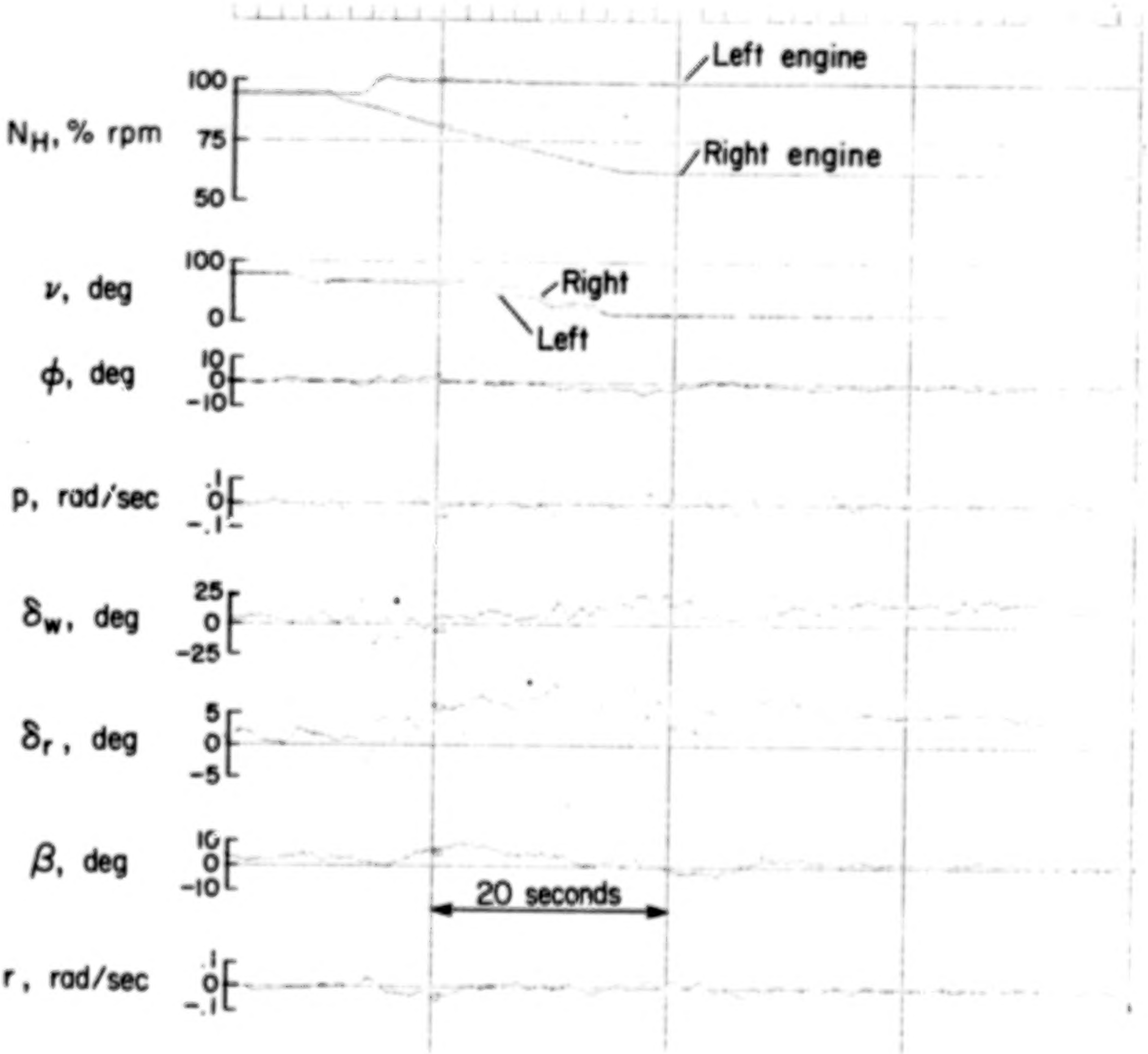

(b) Concluded.

Figure 33.– Concluded.

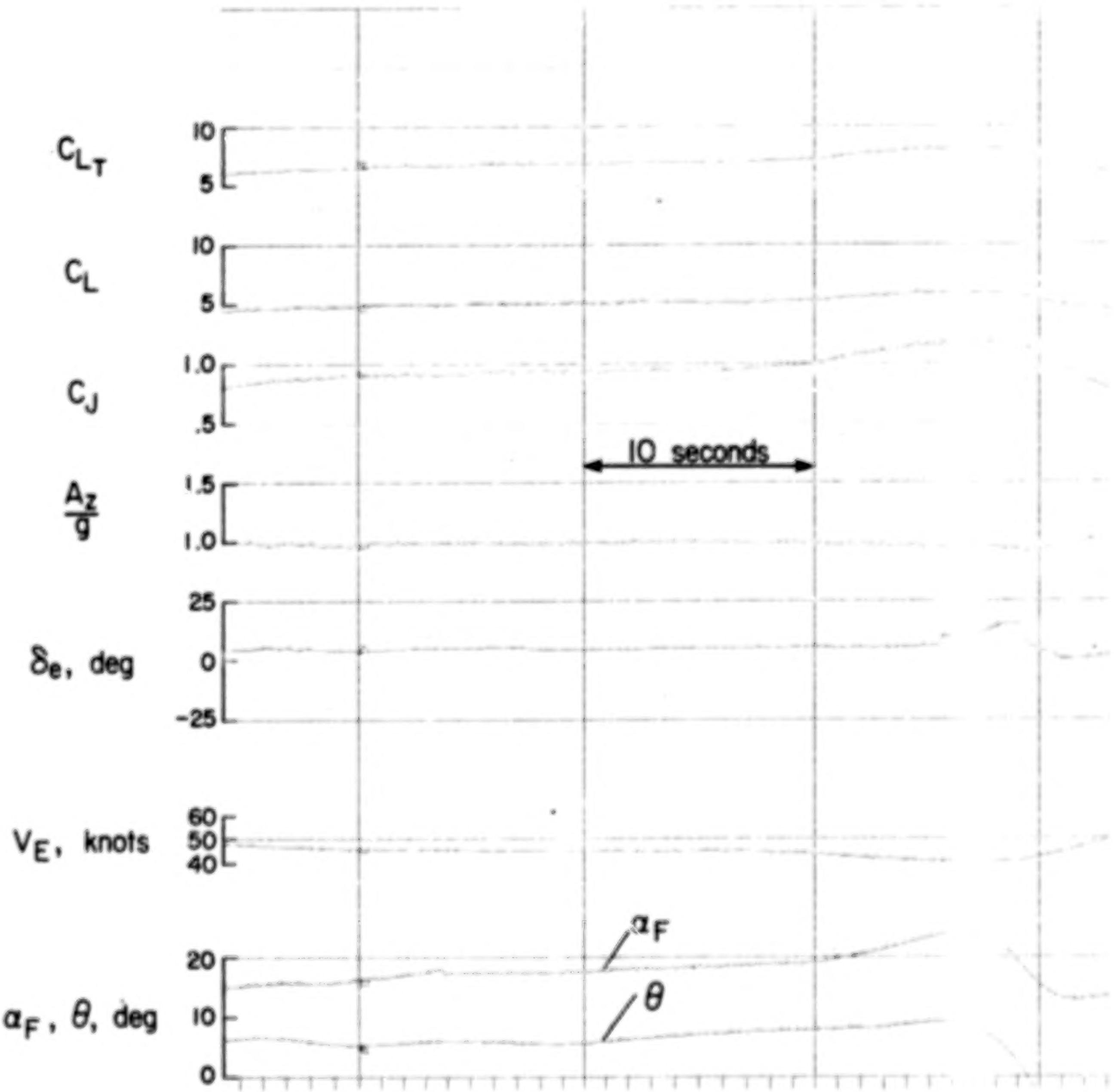

(a) Landing approach, $\delta_f = 64.7°$, $\nu = 73°$, $N_H = 99.4\%$, $W = 189{,}000$ N.

Figure 34.– Stall time histories.

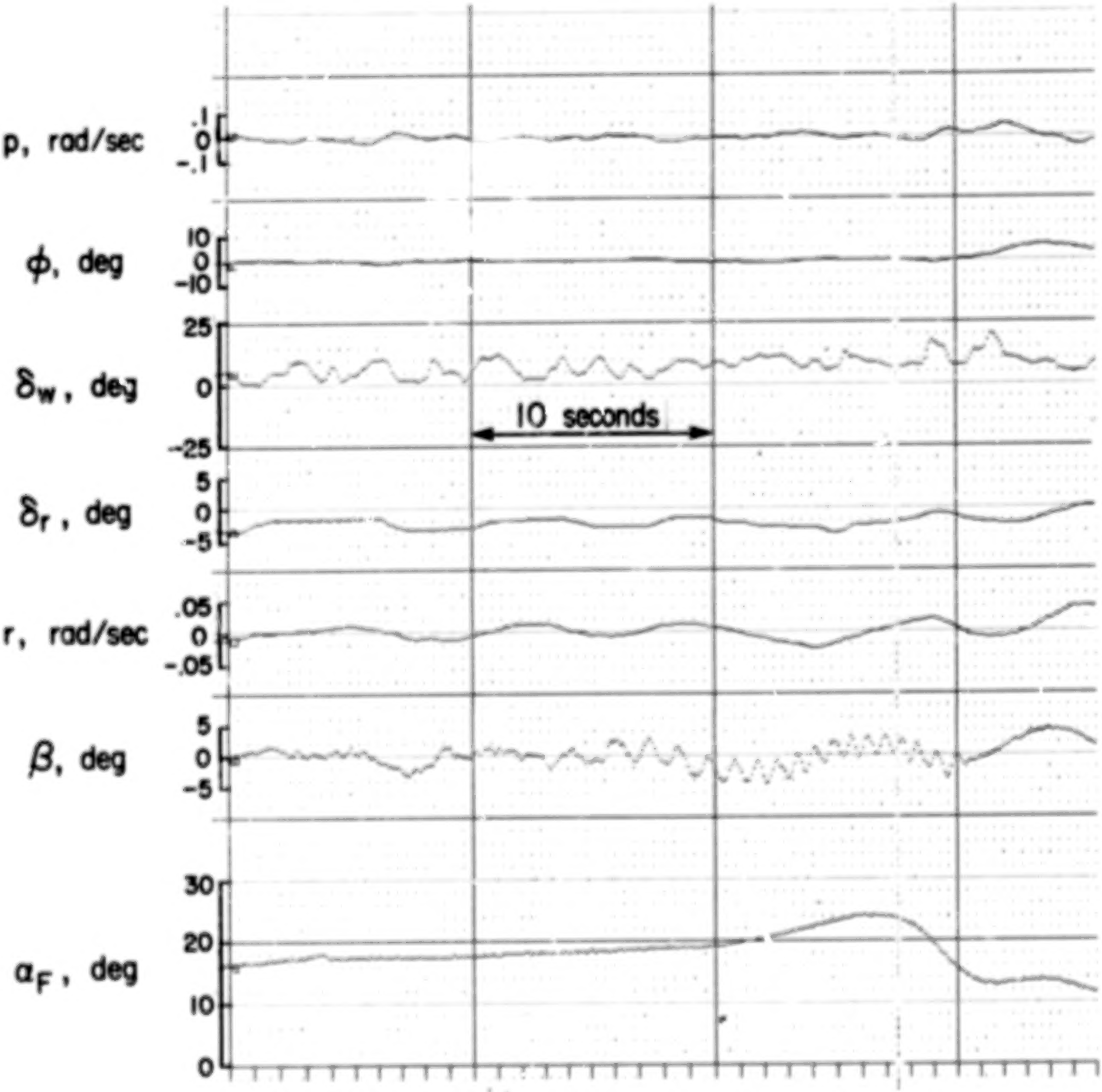

(a) Concluded.

Figure 34.– Continued.

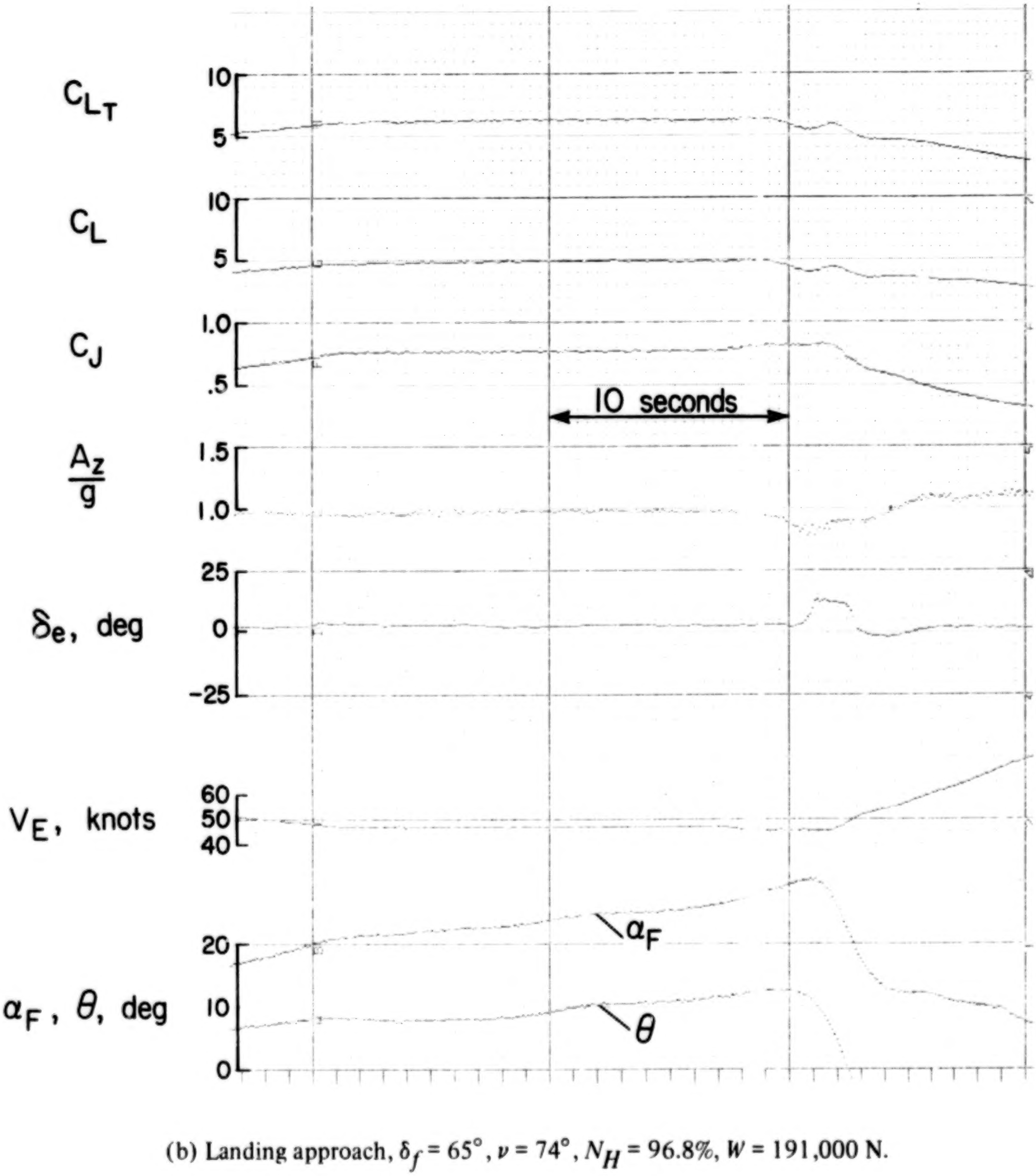

(b) Landing approach, $\delta_f = 65°$, $\nu = 74°$, $N_H = 96.8\%$, $W = 191{,}000$ N.

Figure 34.– Continued.

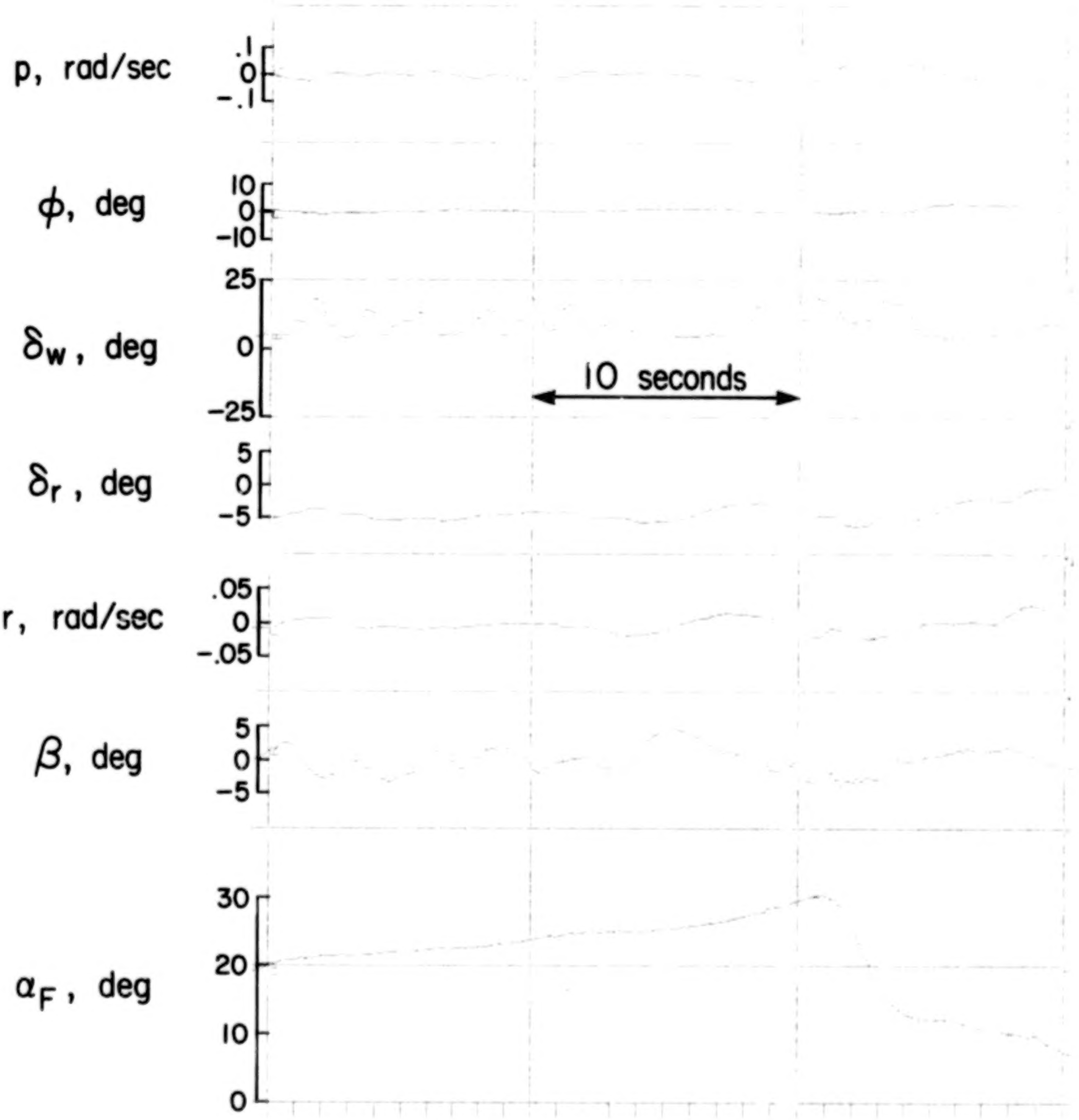

(b) Concluded.

Figure 34.– Continued.

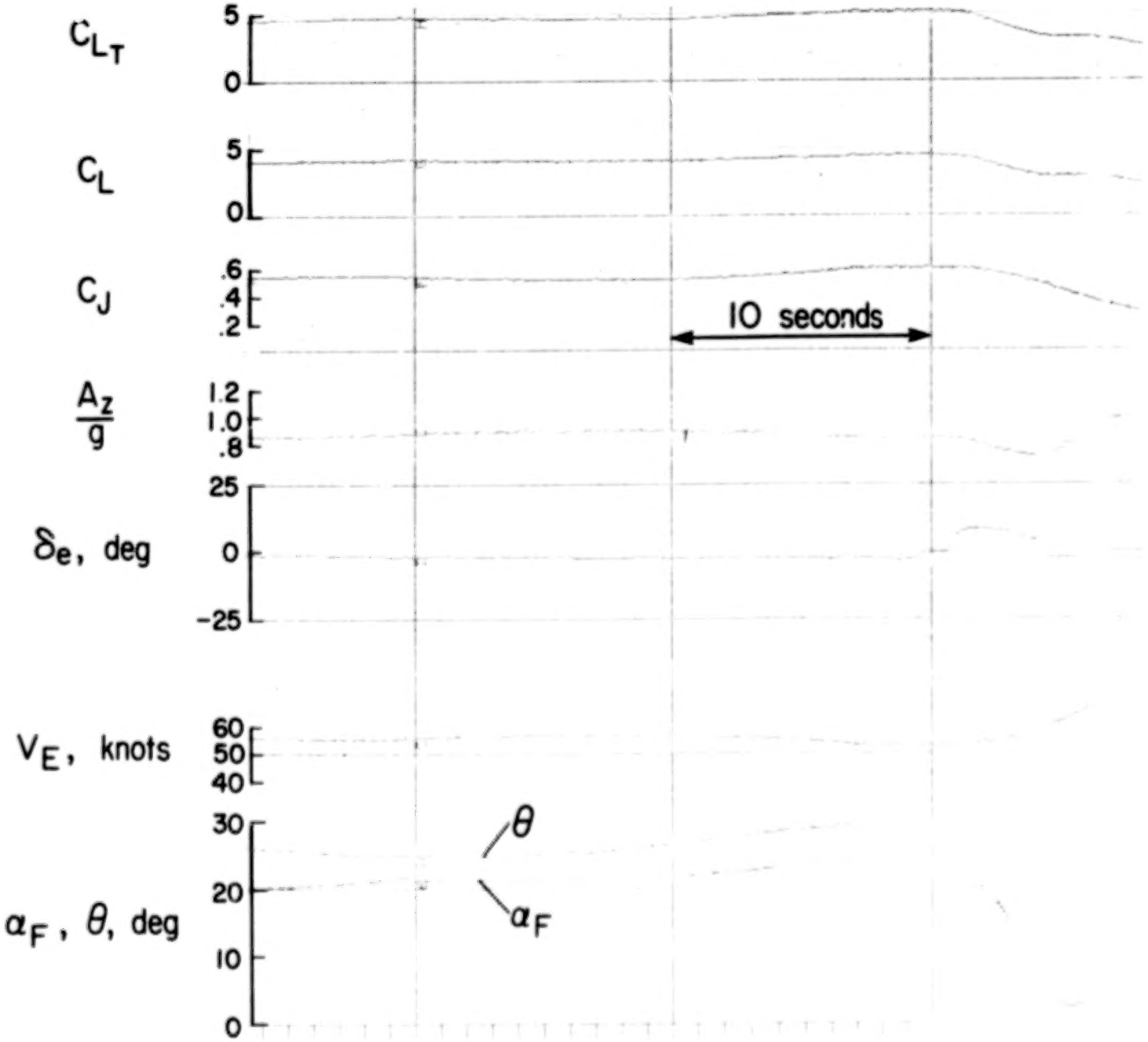

(c) Takeoff, $\delta_f = 28.6°$, $\nu = 11°$, $N_H = 99.6\%$, $W = 192{,}000$ N.

Figure 34.– Continued.

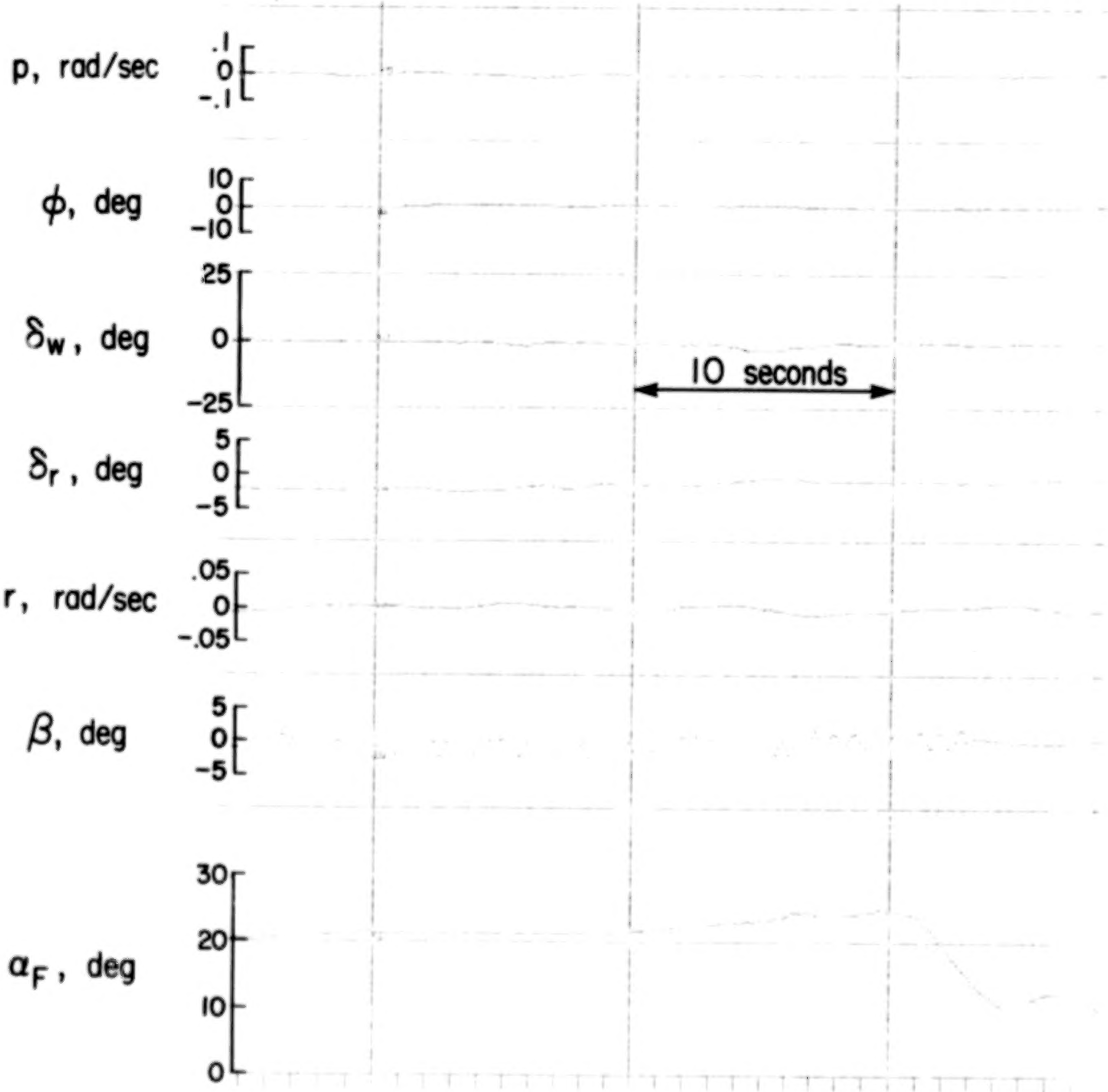

(c) Concluded.

Figure 34.– Continued.

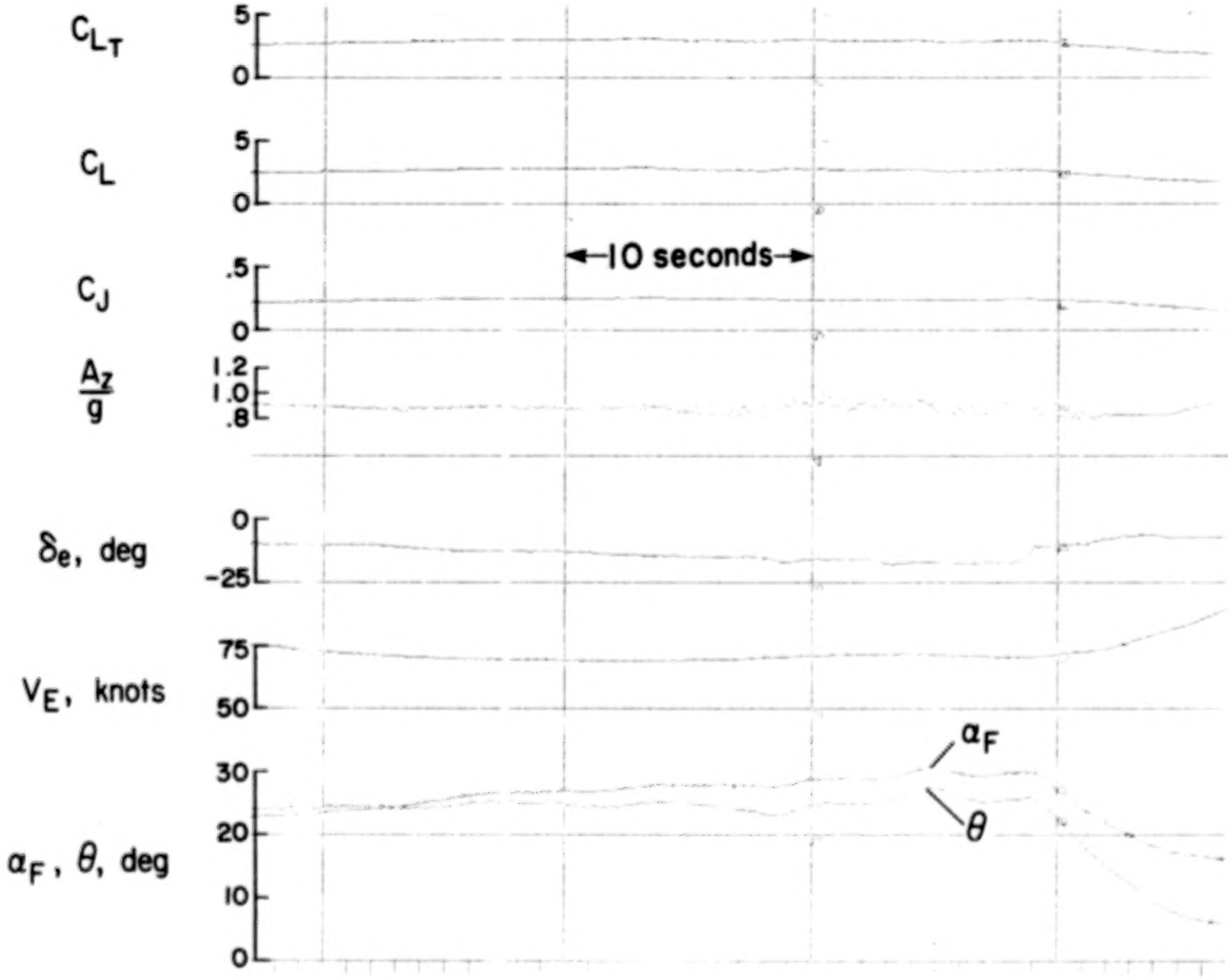

(d) Cruise, $\delta_f = 5.8°$, $\nu = 7°$, $N_H = 90.4\%$, $W = 197{,}500$ N.

Figure 34.– Continued.

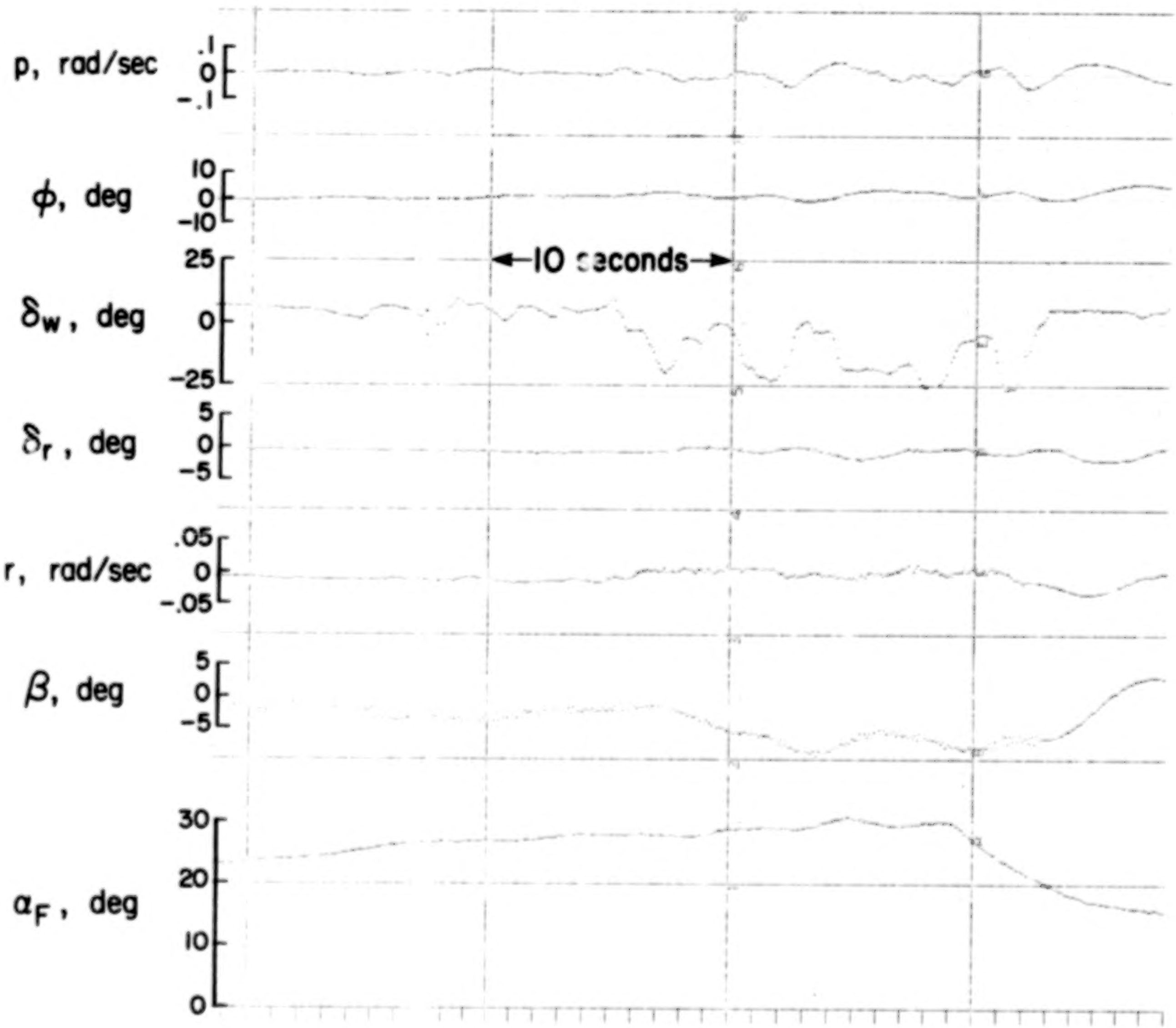

(d) Concluded.

Figure 34.– Concluded.

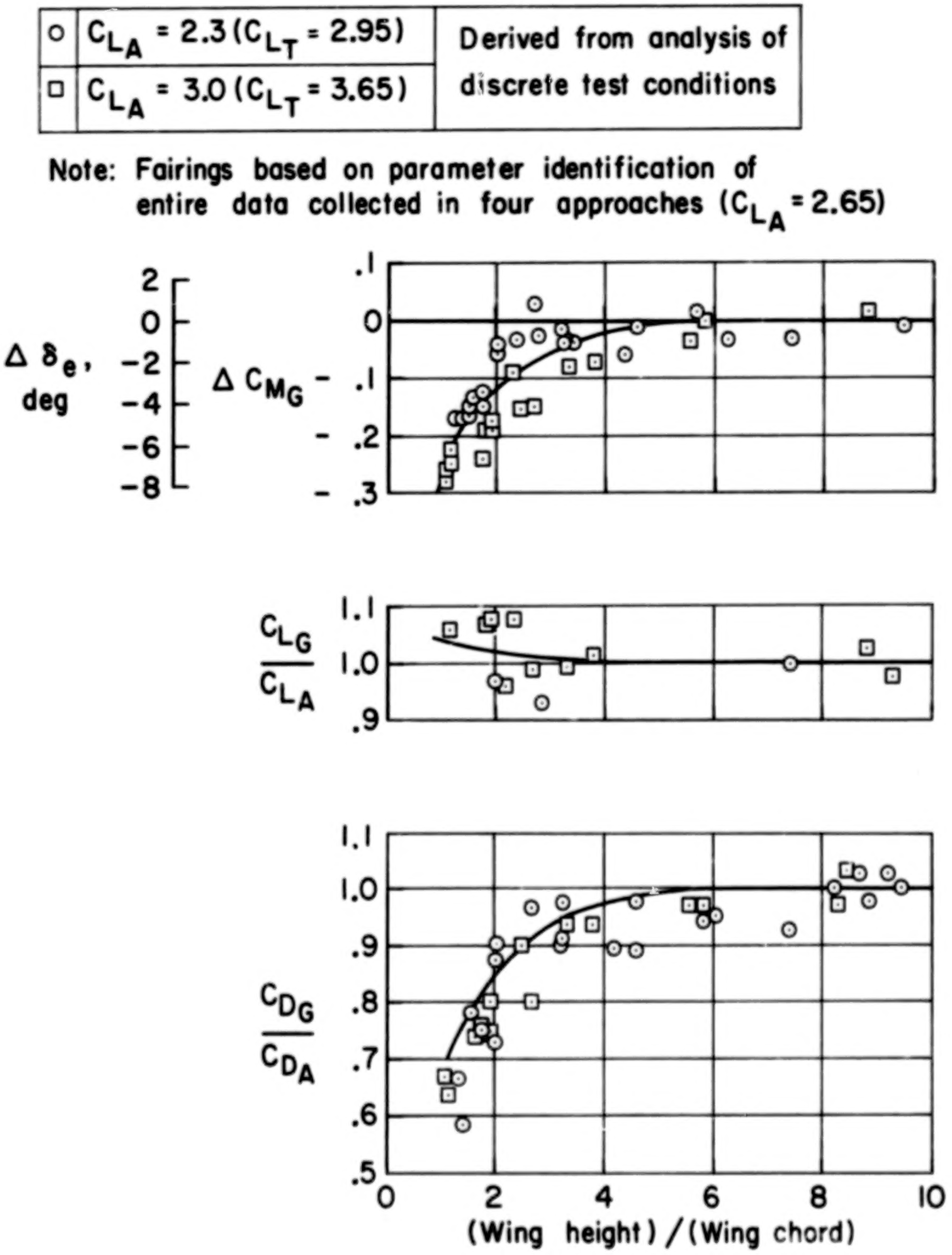

Figure 35.– Ground effect derived from flight-test data: $\delta_f = 65°$; $\nu = 50°$ to $80°$; N_H = 93 to 96% *rpm*; V_E = 60 to 70 knots.

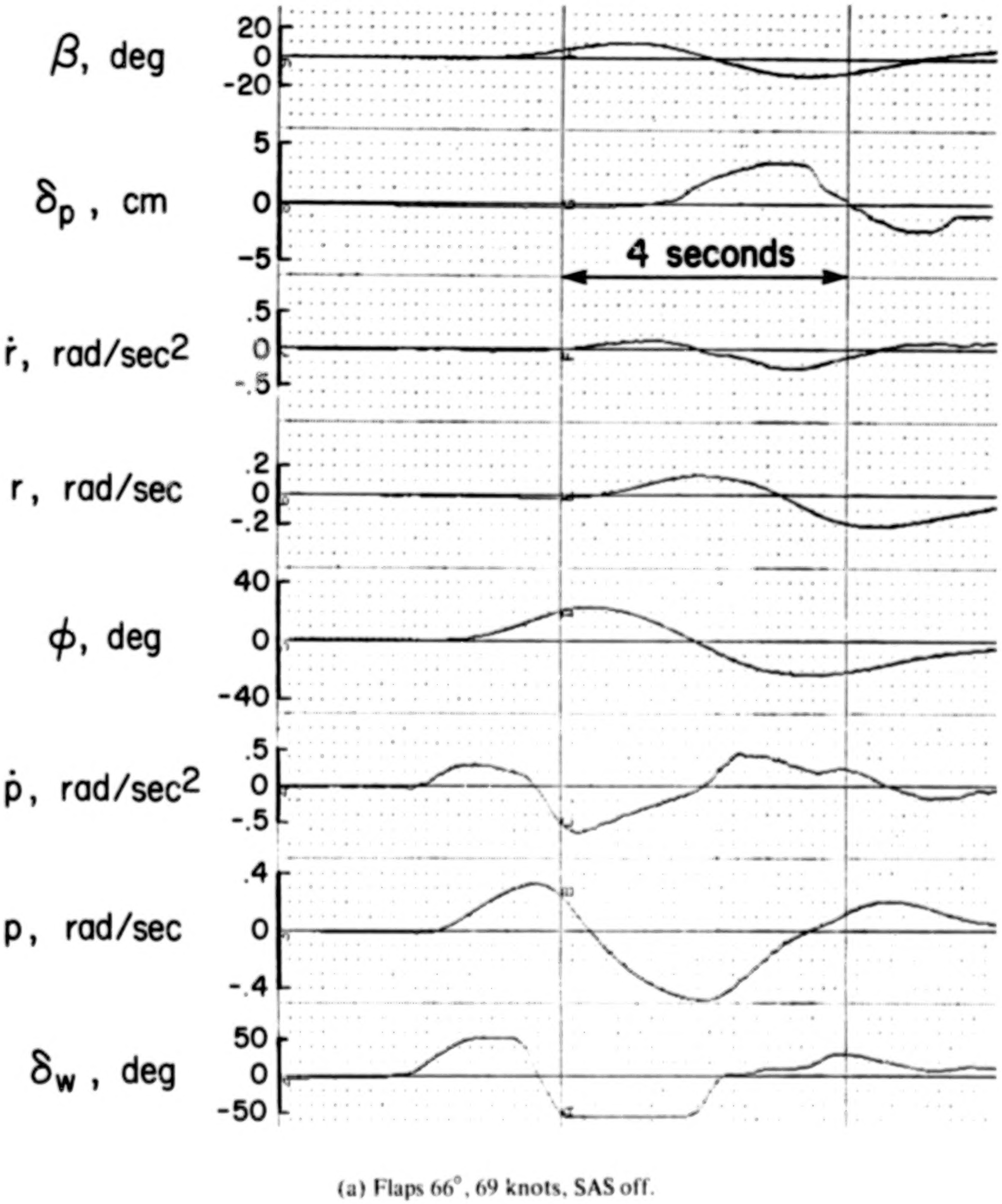

(a) Flaps 66°, 69 knots, SAS off.

Figure 36.– Roll reversal, landing configuration.

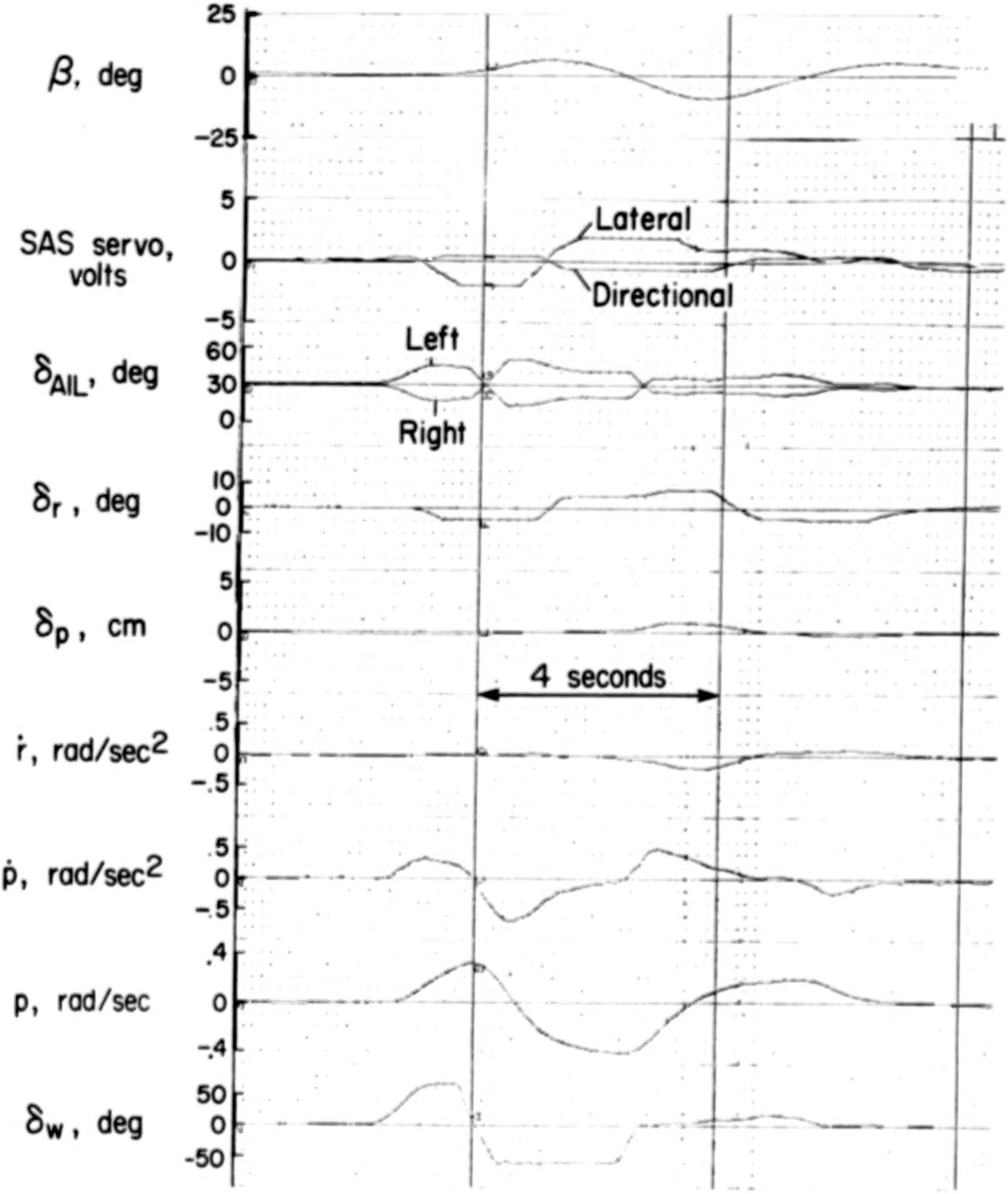

(b) Flaps 66°, 70 knots, SAS on.

Figure 36.– Concluded.

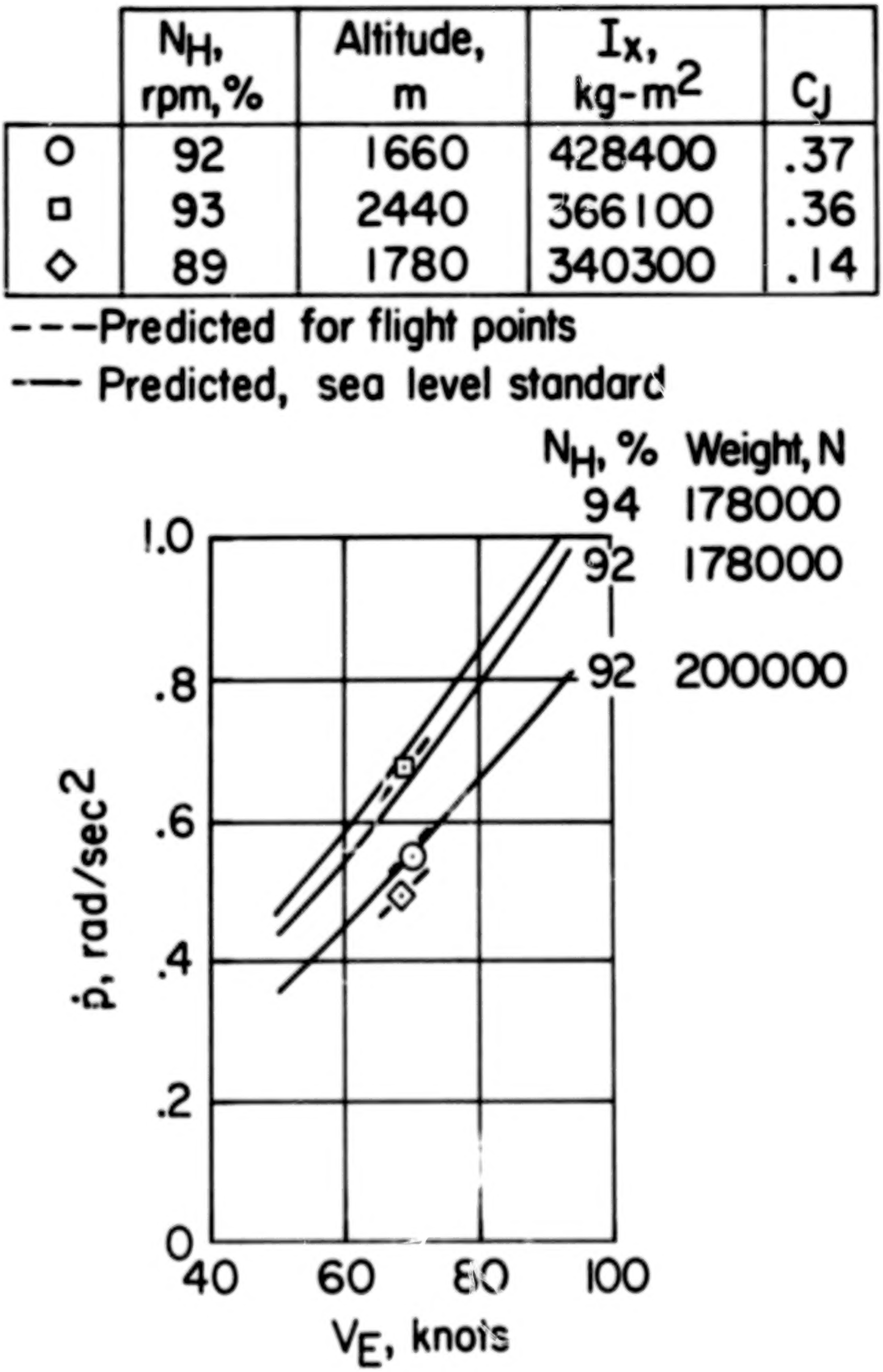

	N_H, rpm,%	Altitude, m	I_x, kg-m^2	C_J
○	92	1660	428400	.37
□	93	2440	366100	.36
◇	89	1780	340300	.14

(a) Flaps 65°.

Figure 37.– Lateral control power.

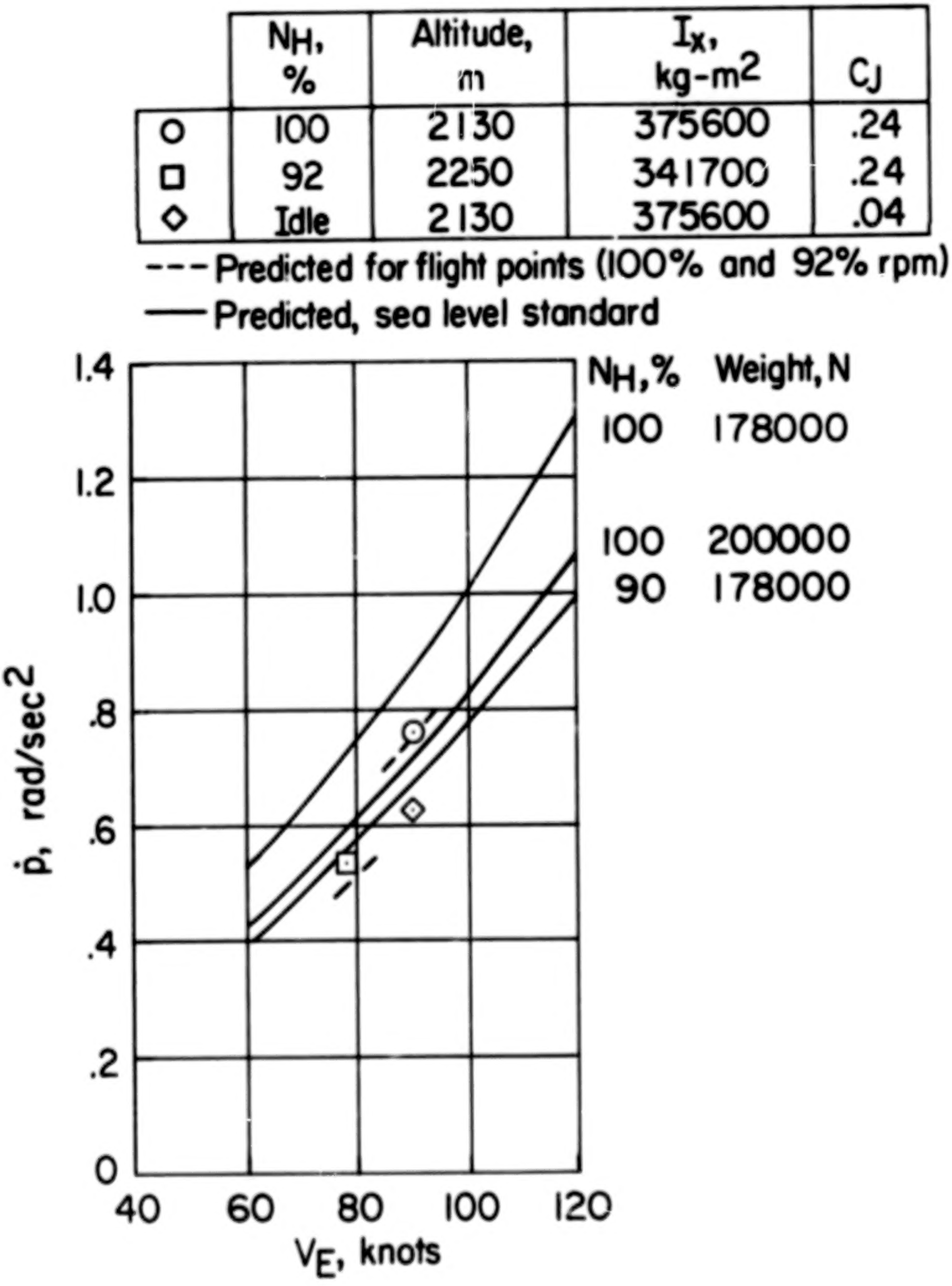

	N_H, %	Altitude, m	I_X, kg-m^2	C_J
○	100	2130	375600	.24
□	92	2250	341700	.24
◇	Idle	2130	375600	.04

(b) Flaps 30°.

Figure 37.– Continued.

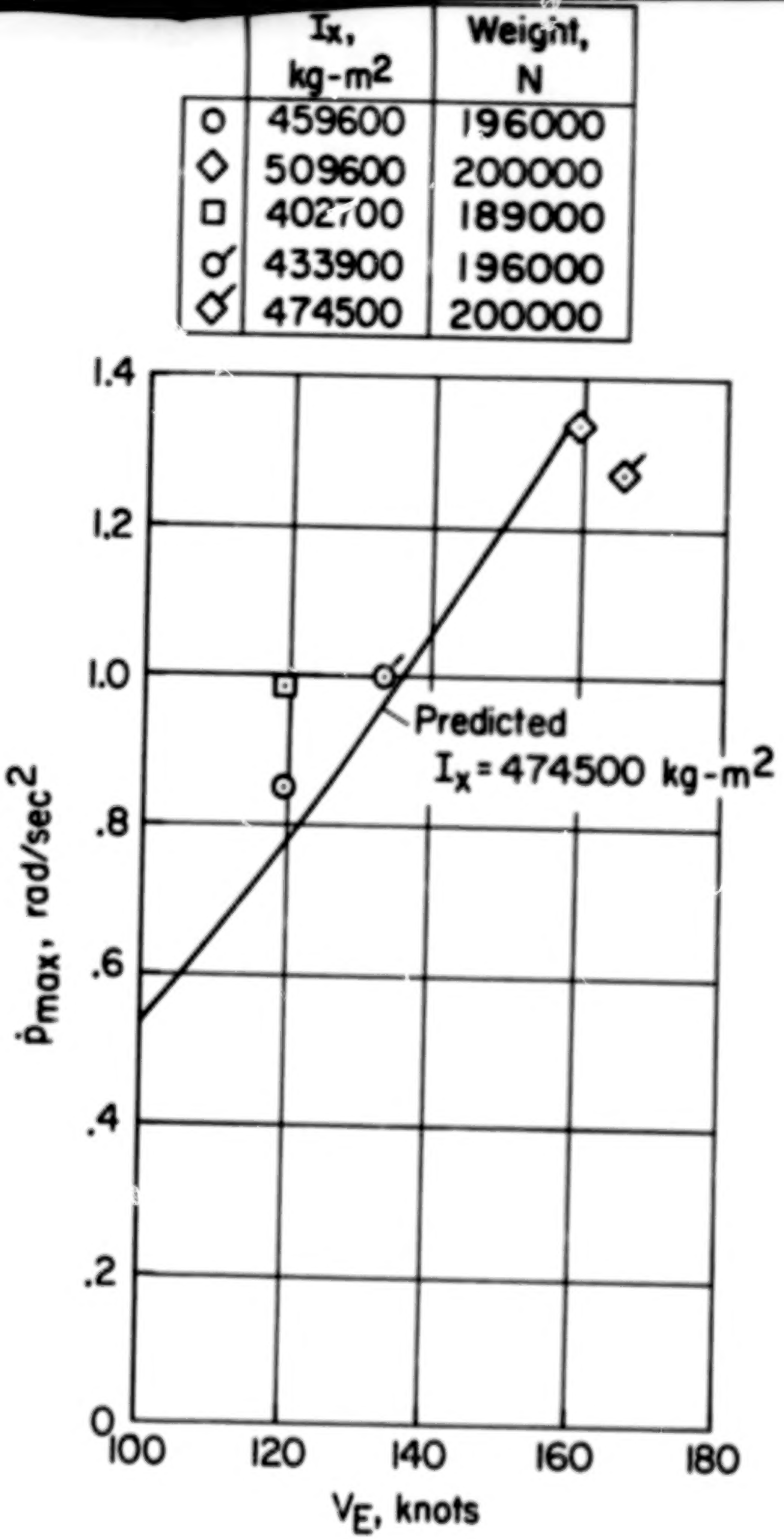

(c) Flaps 5.6°.

Figure 37.– Concluded.

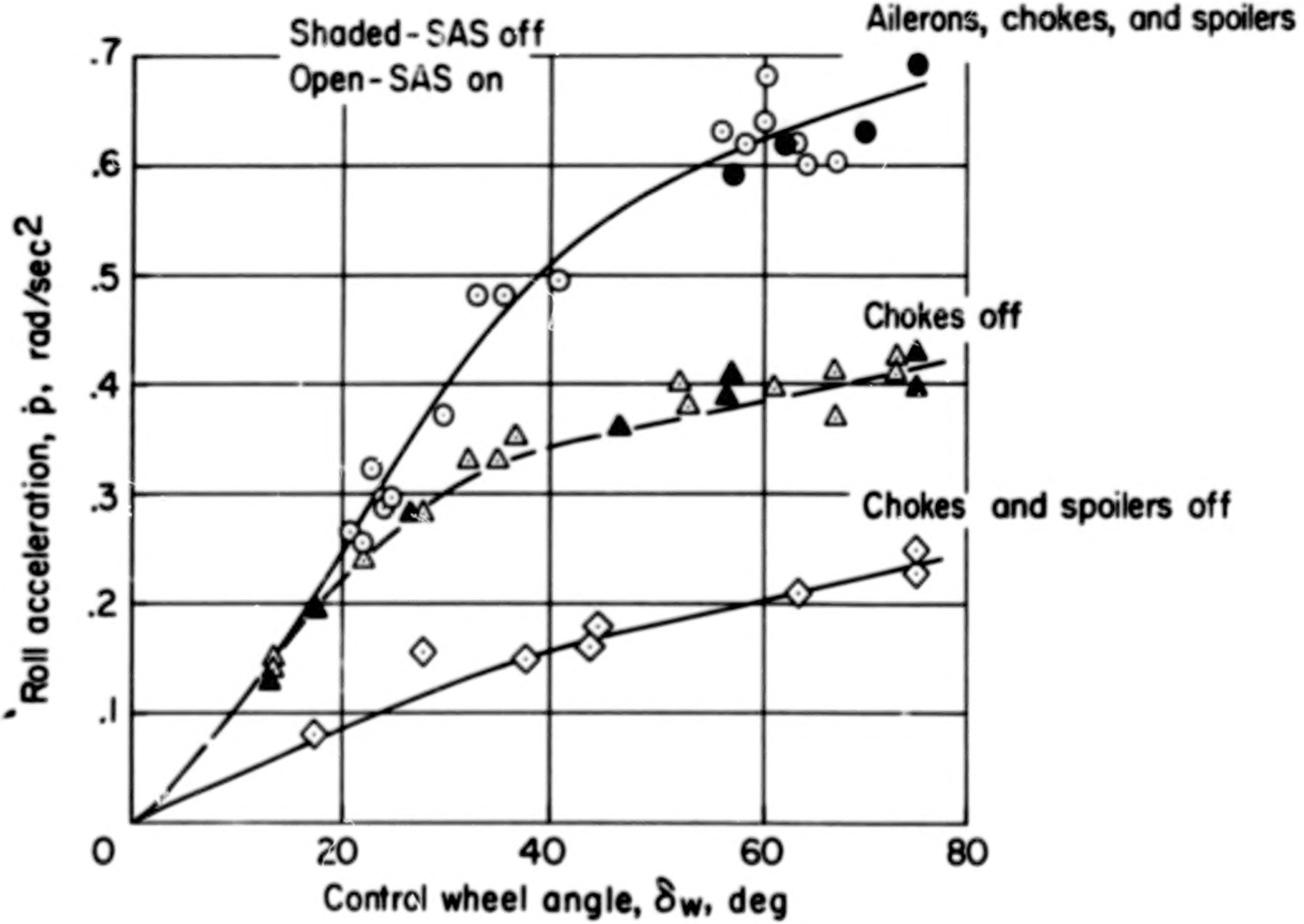

(a) Effectiveness of combined lateral controls.

Figure 38.– Lateral control effectiveness, flaps 67°, airspeed 69 knots, 15° nozzle, W = 165,000 to 178,000 N, N_H = 93 to 95% rpm.

104

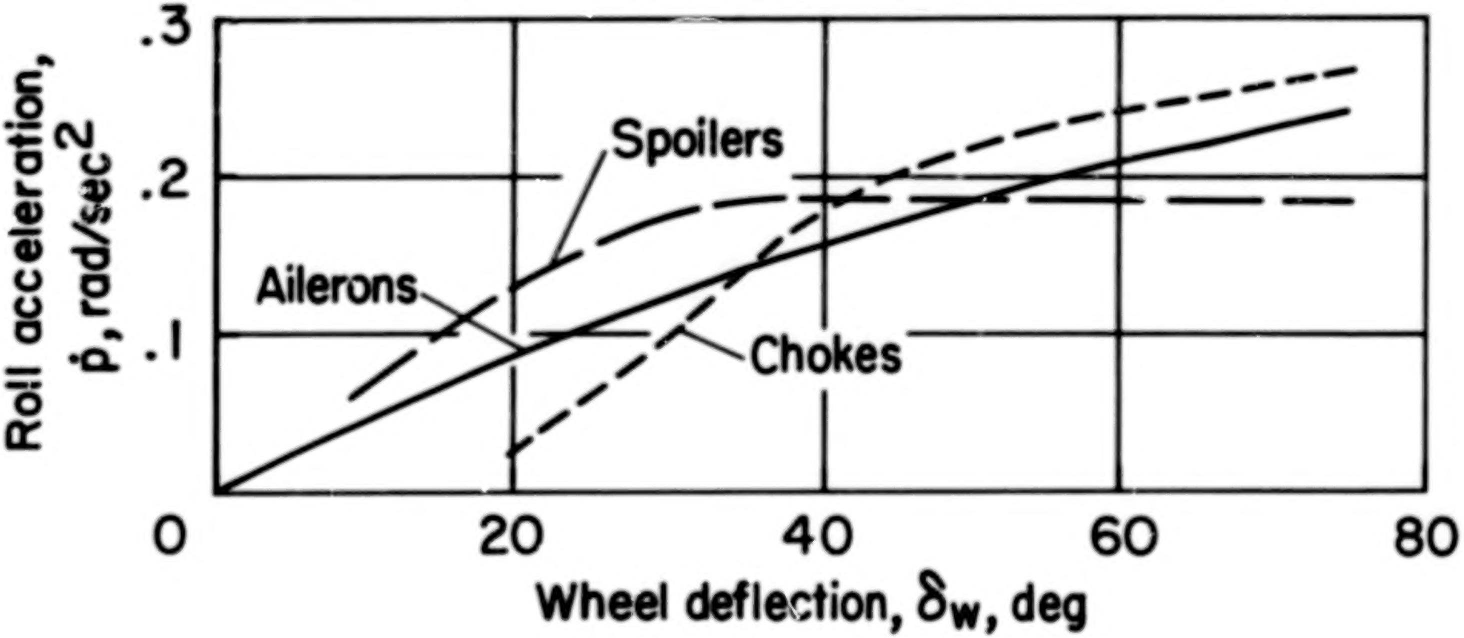

(b) Effectiveness of individual lateral controls.

Figure 38.– Concluded.

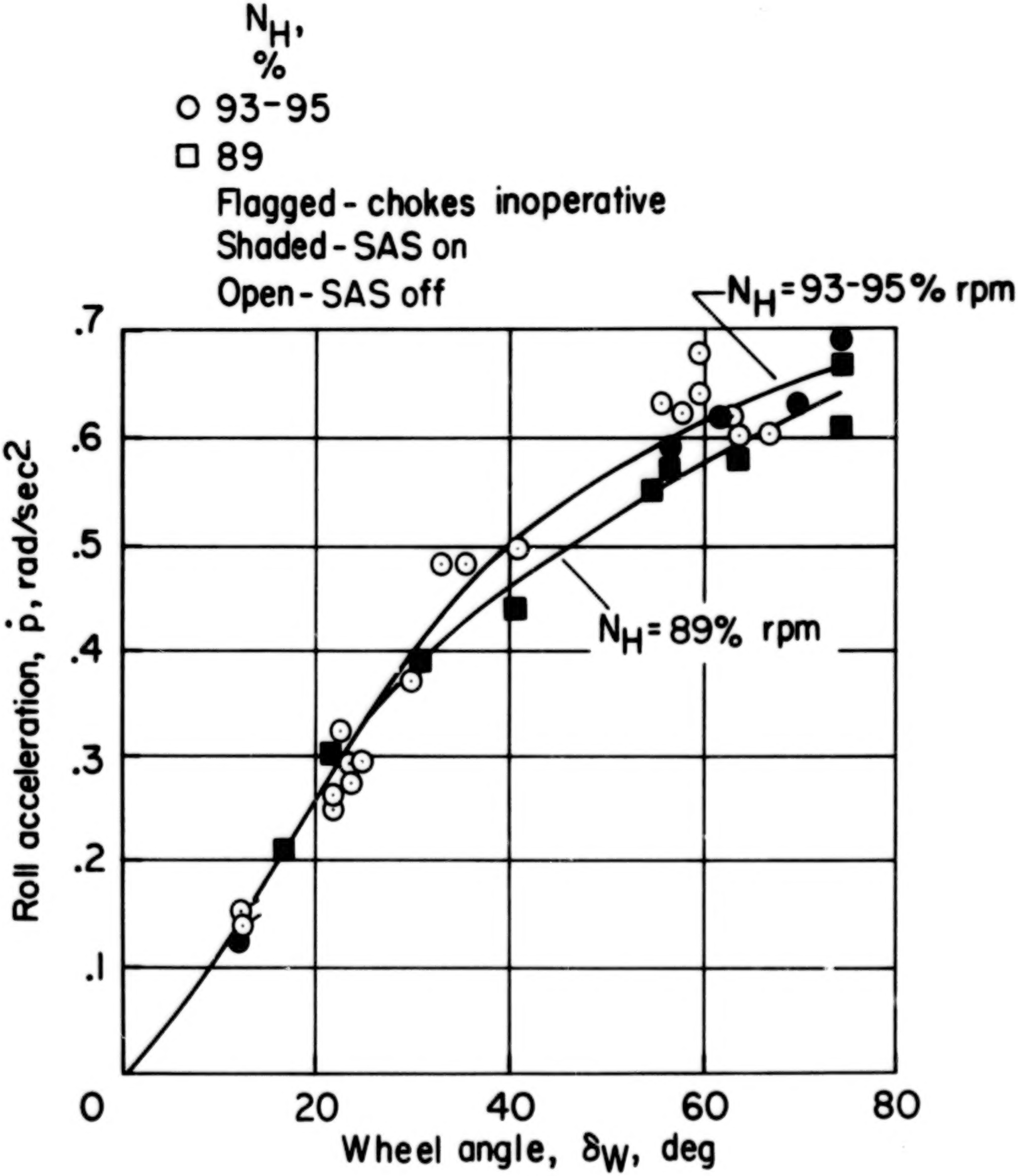

Figure 39.– Effect of engine power and SAS on lateral control effectiveness, flaps 67°, 69 knots, $\nu = 15°$, W = 165,000 to 178,000 N.

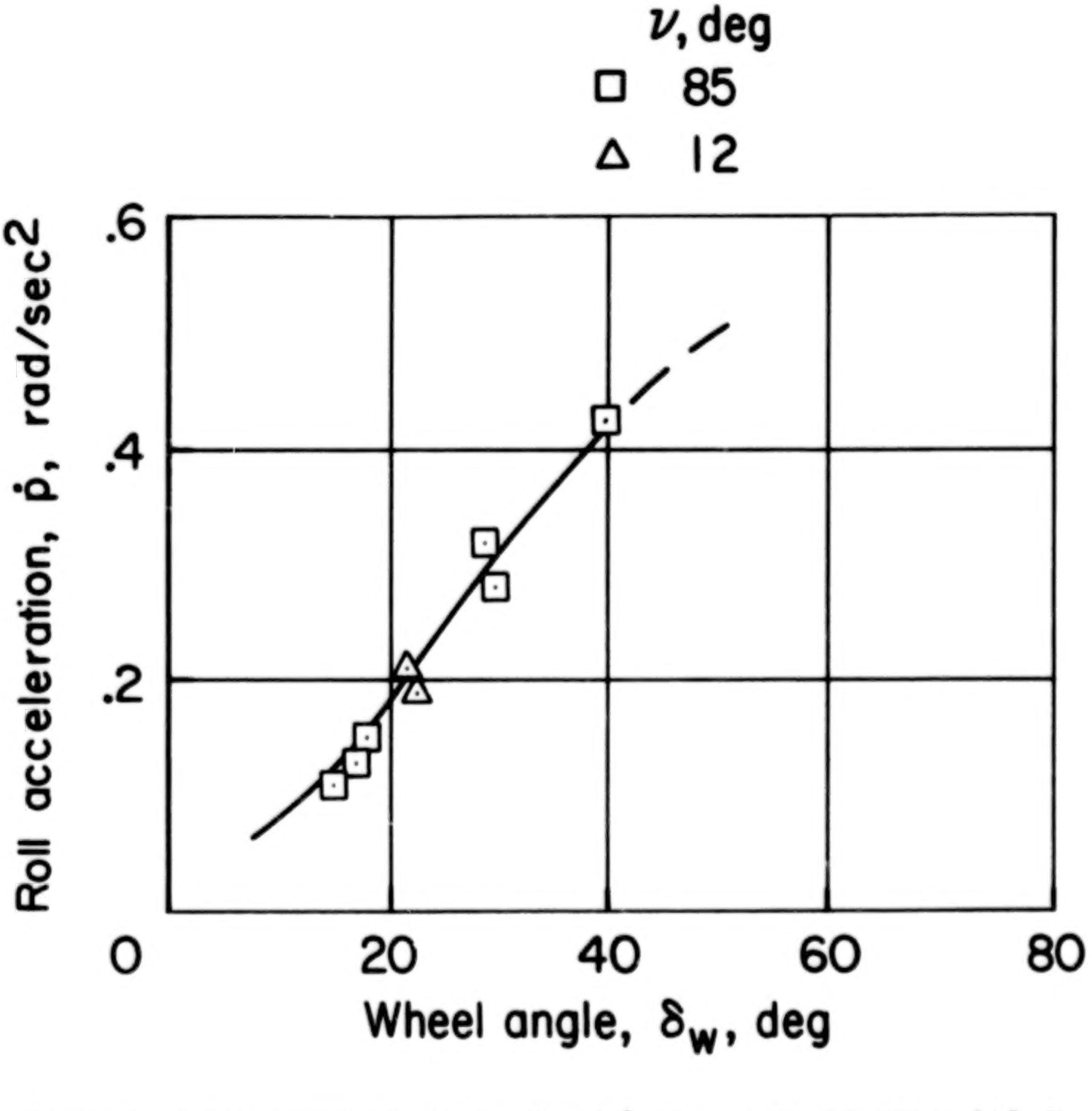

Figure 40.– Lateral control effectiveness, flaps 65°, 62 knots, W = 181,000 N, SAS off, N_H = 96.5%.

	N_H, %	V_E, knots	C_J
●	96.5	62	.46
□ ■	93	69	.35
▲	89	69	.14
◠	93	72	.34
⬟	95	71-77	—
◇	93	69	.35
◿	96	72	.34

Shaded – SAS off
Open – SAS on

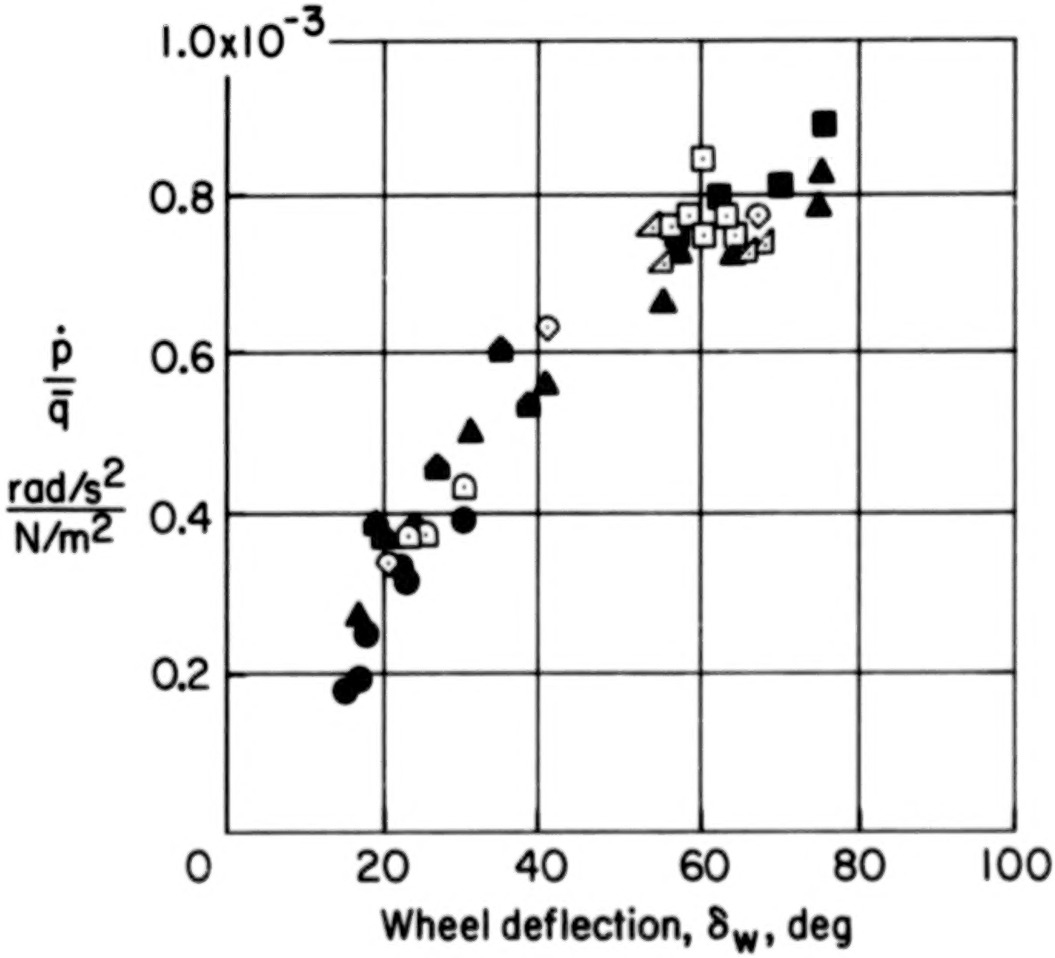

Figure 41.– Lateral control effectiveness, flaps 65°, W = 168,000 to 182,000 N.

	δ_f, deg	ν, deg	V_E, knots	Weight, N
○	67	15	70	199000
□	66	13	68	202000

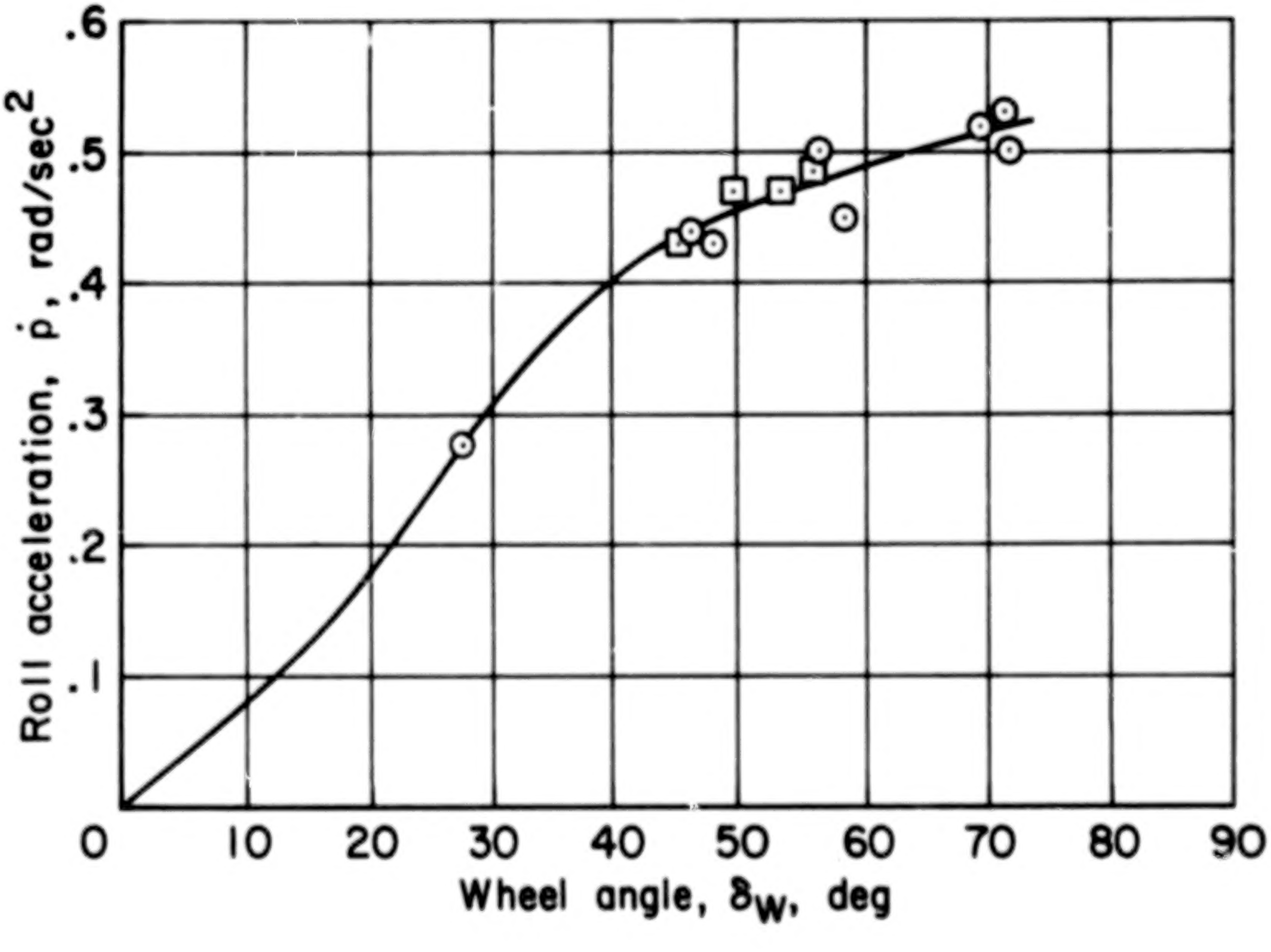

Figure 42.– Lateral control effectiveness, landing flaps, 69 knots, N_H = 95%, SAS on.

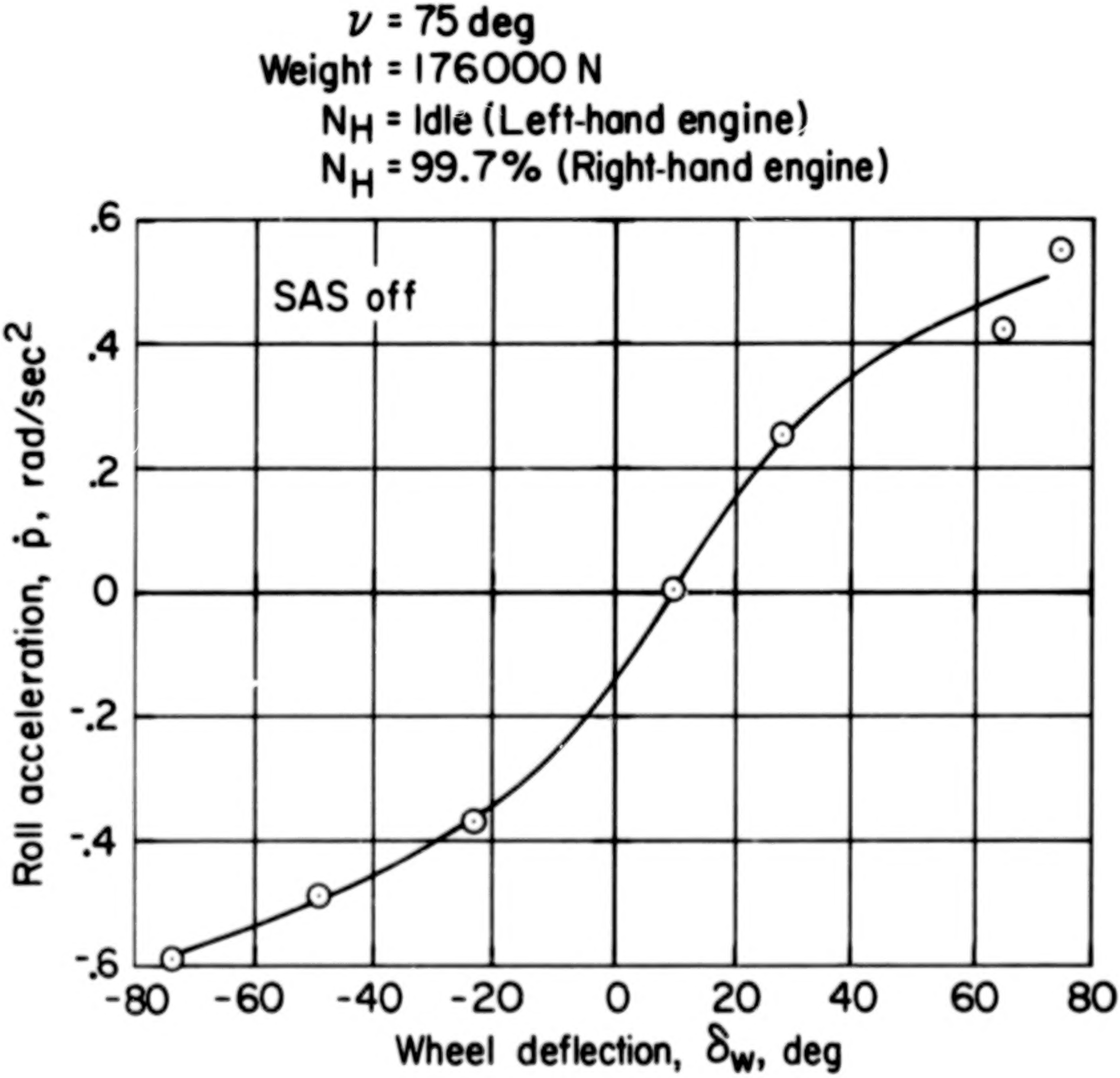

Figure 43.– Lateral control effectiveness for simulated one engine inoperative, flaps 66°, 72 knots.

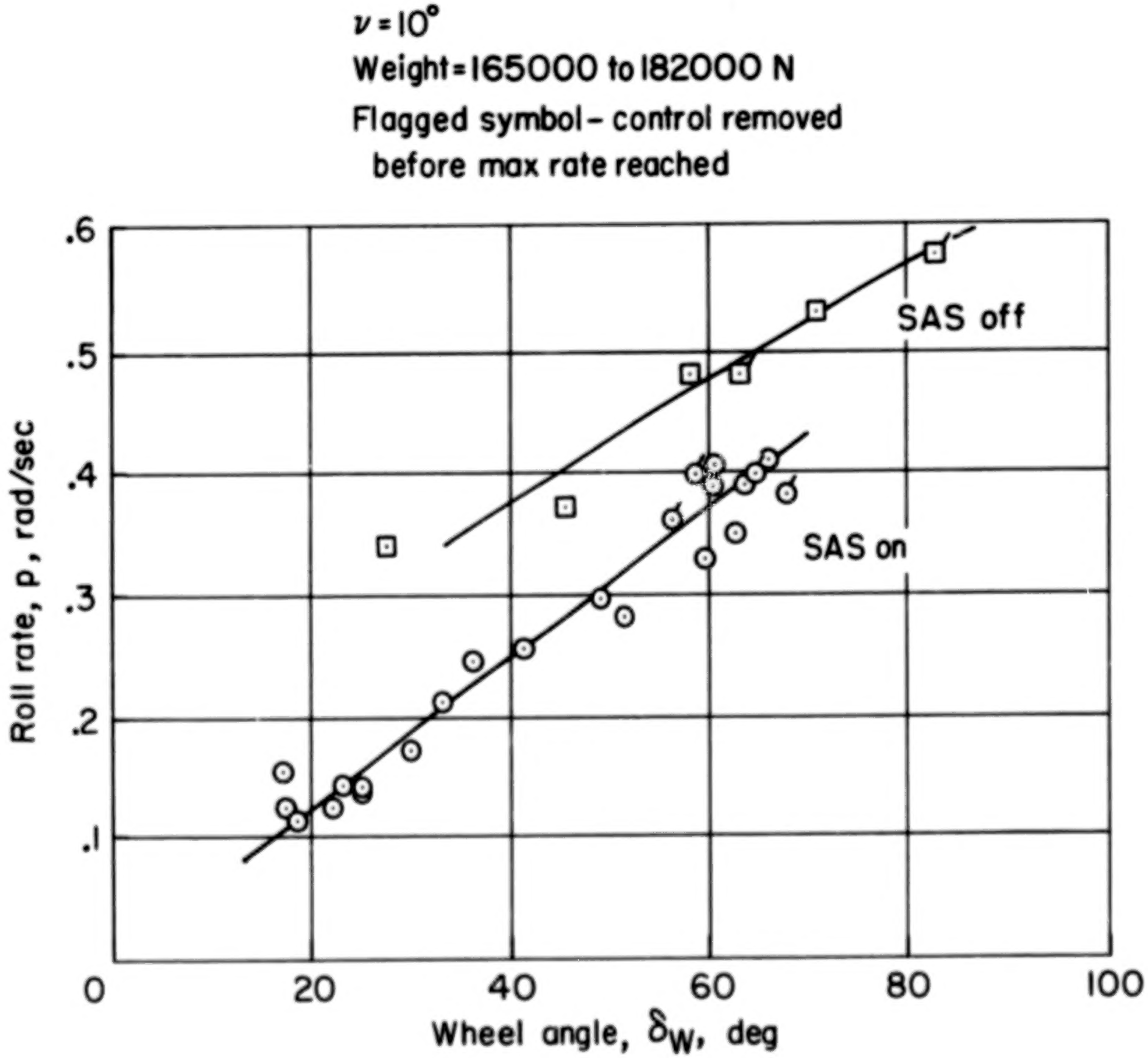

Figure 44.– Maximum roll rate from lateral control reversals, flaps 65°, 69 knots, W = 165,000 to 182,000 N, nozzle deflection = 10°.

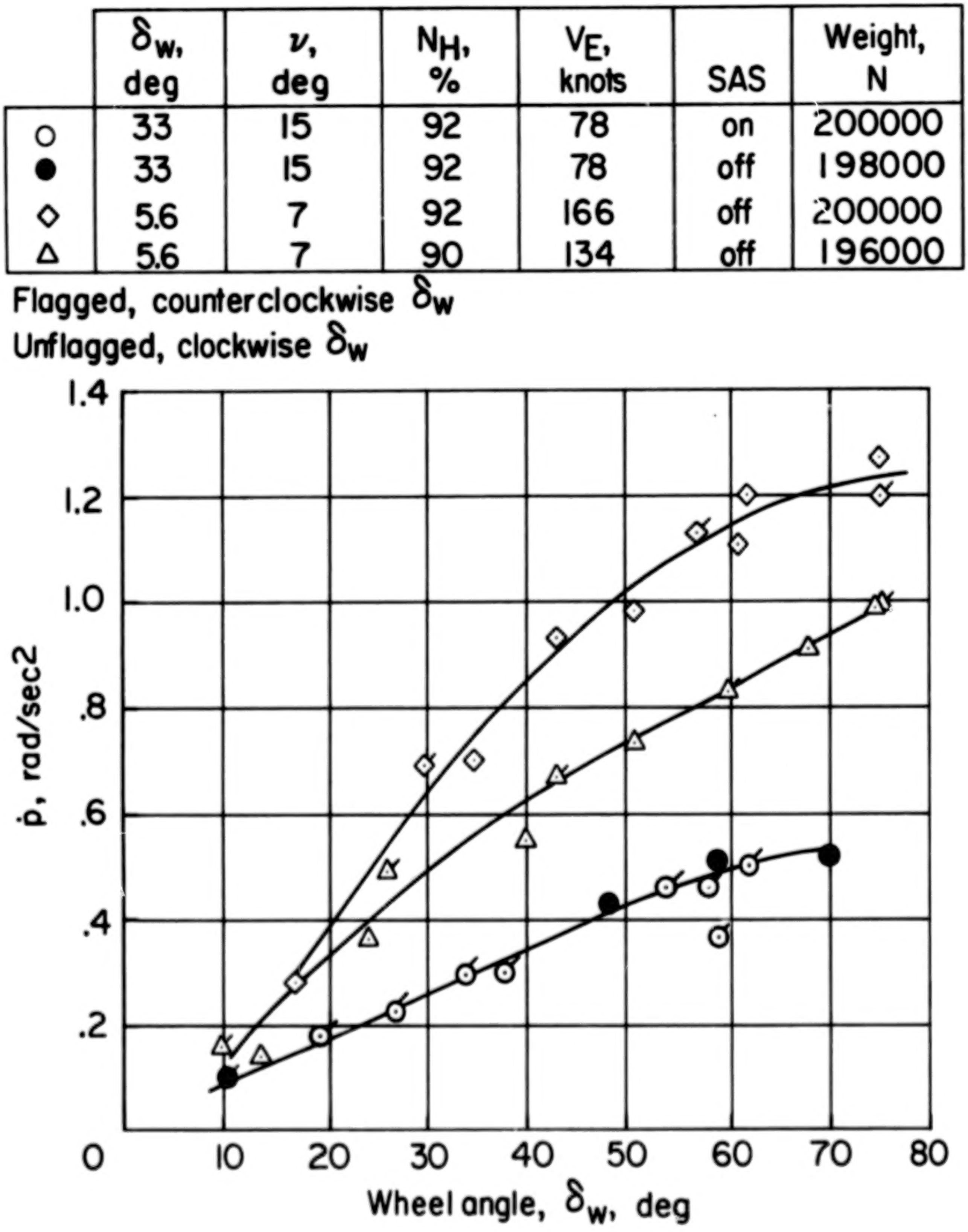

	δ_w, deg	ν, deg	N_H, %	V_E, knots	SAS	Weight, N
○	33	15	92	78	on	200000
●	33	15	92	78	off	198000
◇	5.6	7	92	166	off	200000
△	5.6	7	90	134	off	196000

Flagged, counterclockwise δ_w
Unflagged, clockwise δ_w

Figure 45.– Lateral control effectiveness, flaps 33° and 5.6°.

	δ_f, deg	ν, deg	N_H, %	Weight, N
● ○	32.7	15	92	200000
■ □	28.6	8	92	198000
◆ ◇	28.6	8	92	200000

Shaded - SAS off
Open - SAS on
Unflagged - clockwise δ_w
Flagged - counterclockwise δ_w

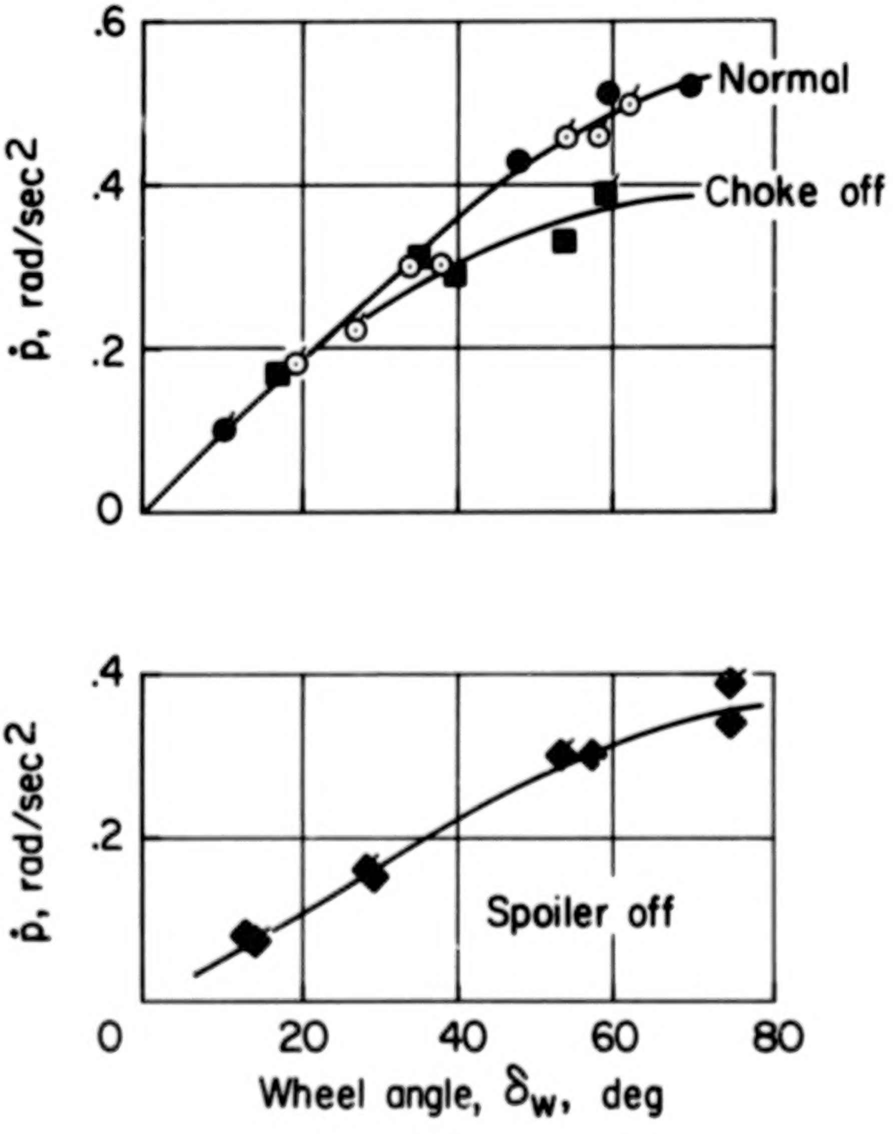

Figure 46.– Lateral control effectiveness, flaps ~30°, 78 knots.

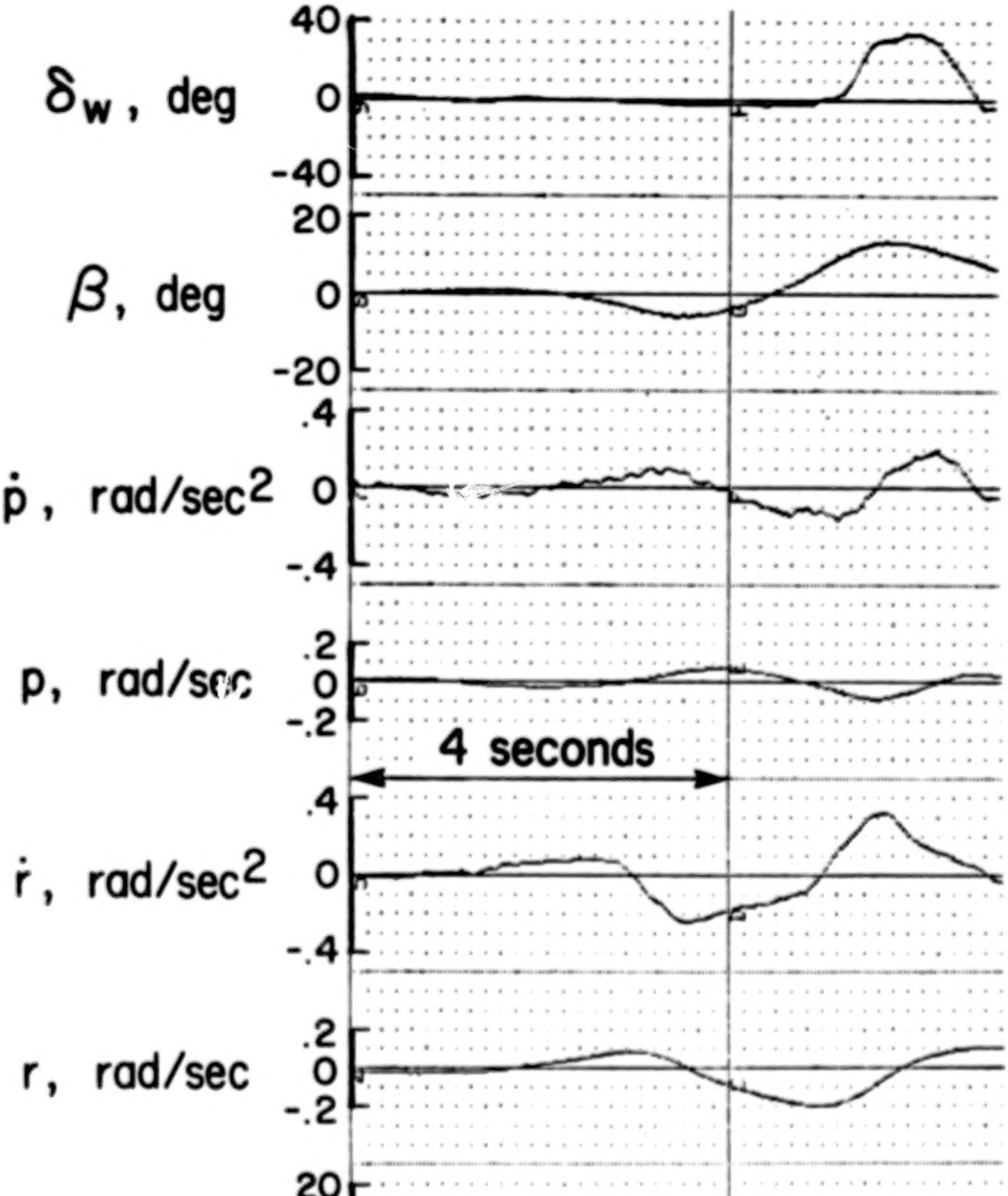

Figure 47.– Rudder reversal – flaps 67°, 68 knots, SAS off.

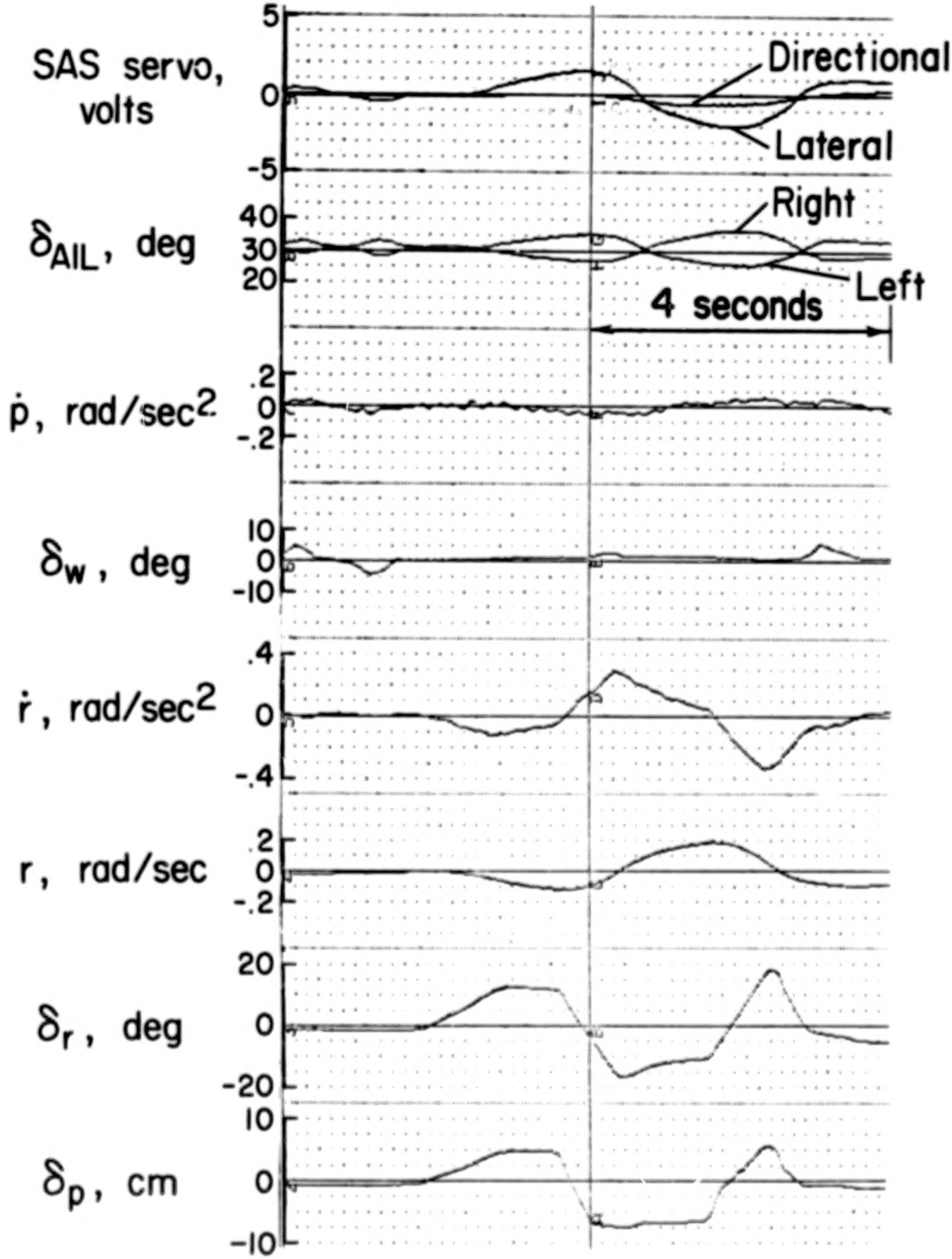

Figure 48.– Rudder reversal – flaps 67°, 70 knots, SAS on.

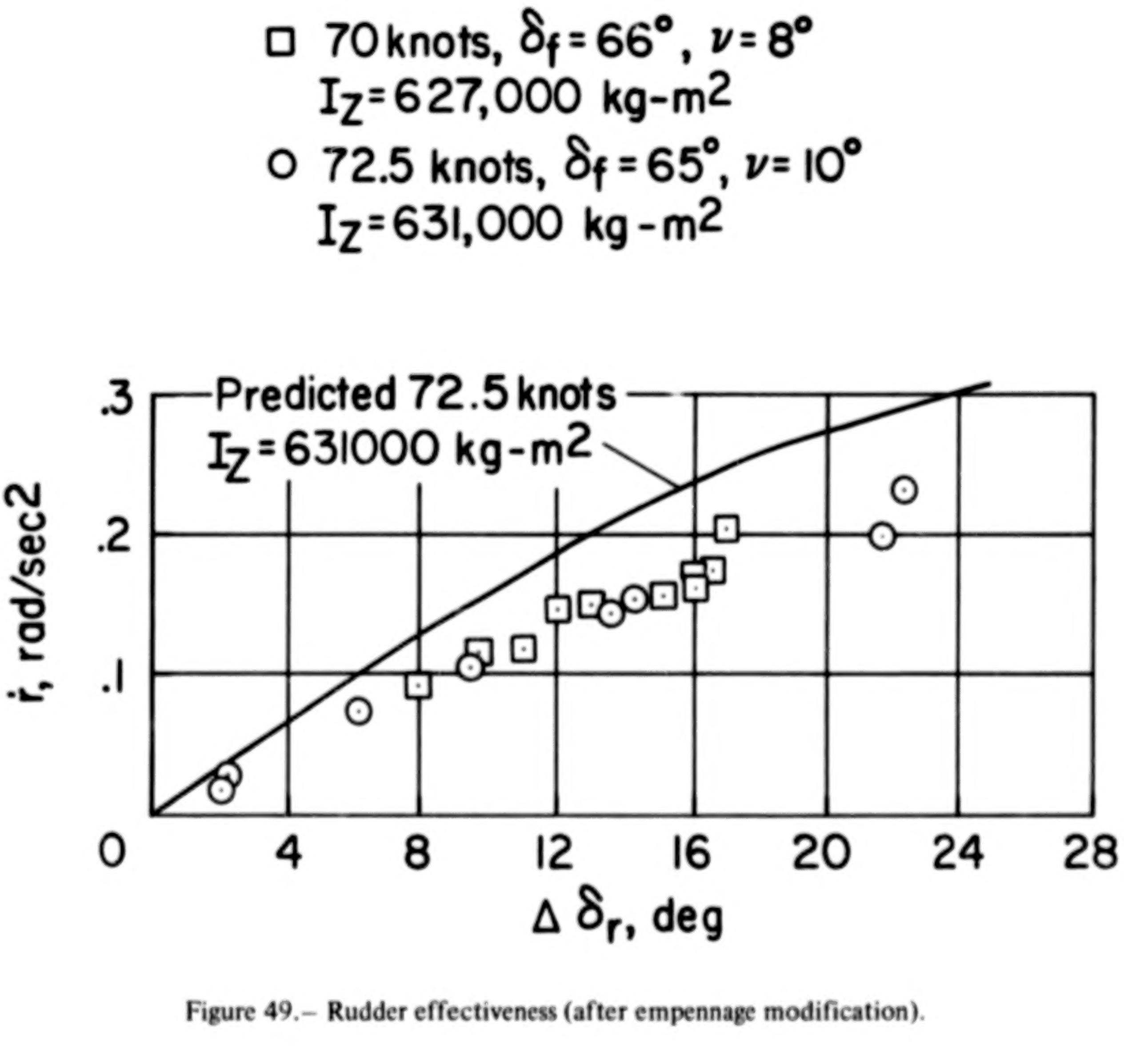

Figure 49.– Rudder effectiveness (after empennage modification).

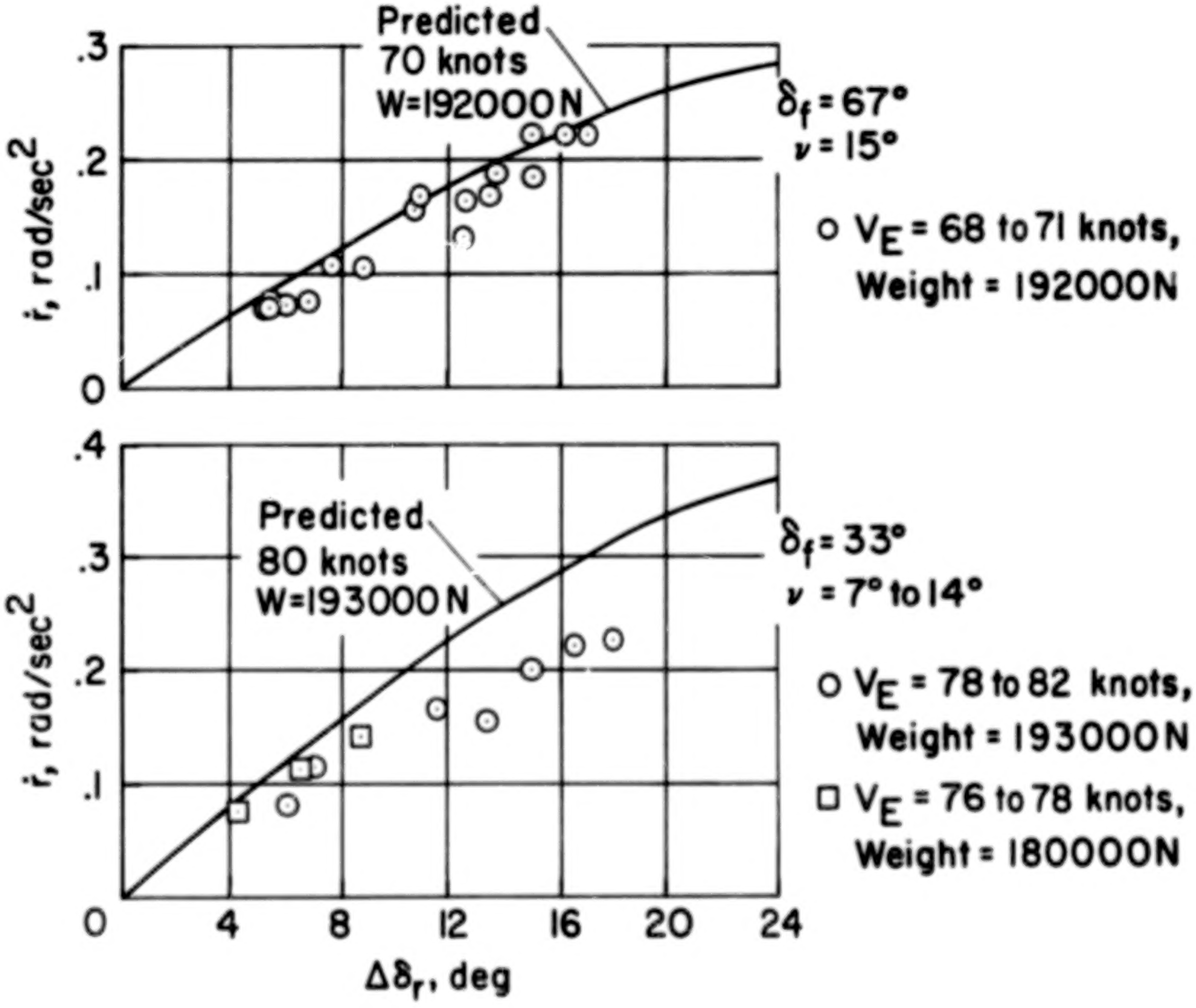

Figure 50.– Rudder effectiveness (before empennage modification).

	δ_f, deg	ν, deg	V_E, knots	Weight, N
○	67	15	69	191000
□	67	15	70	196000
△	33	7	80	194000

Flags: Control removed before max rate reached

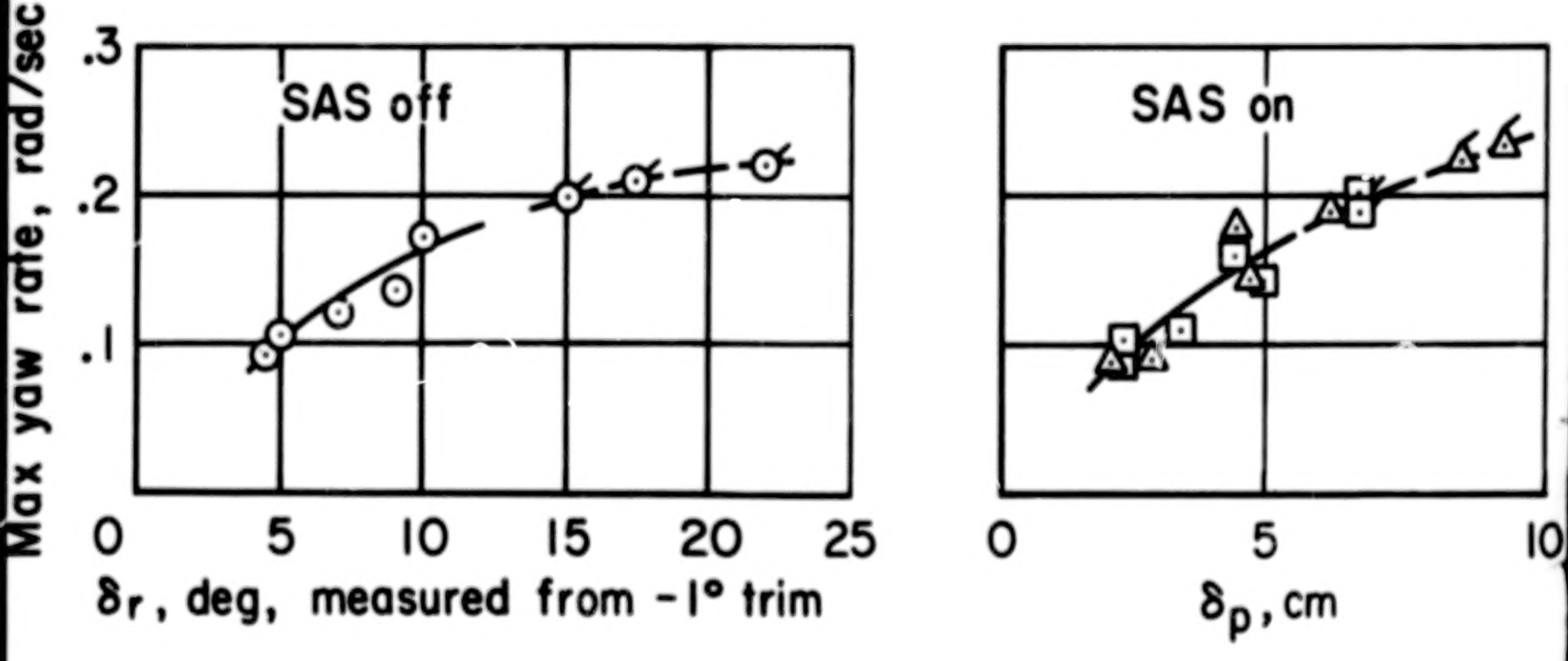

Figure 51.– Maximum yaw rate from directional control reversals (before empennage modification).

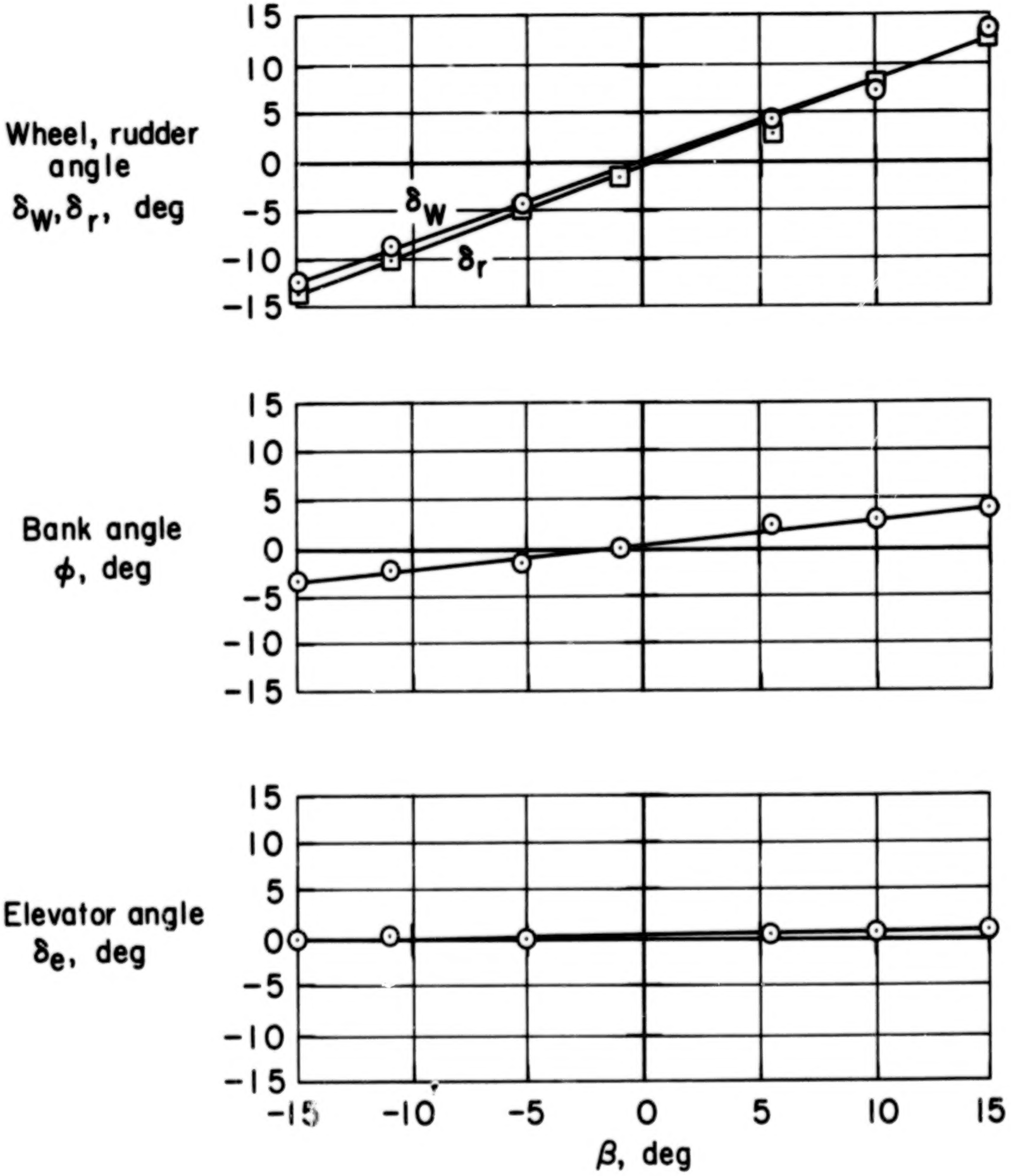

Figure 52.– Steady sideslip – $\delta_f = 65°$, $\nu = 15°$, $V_E = 65$ knots, $N_H = 93\%$.

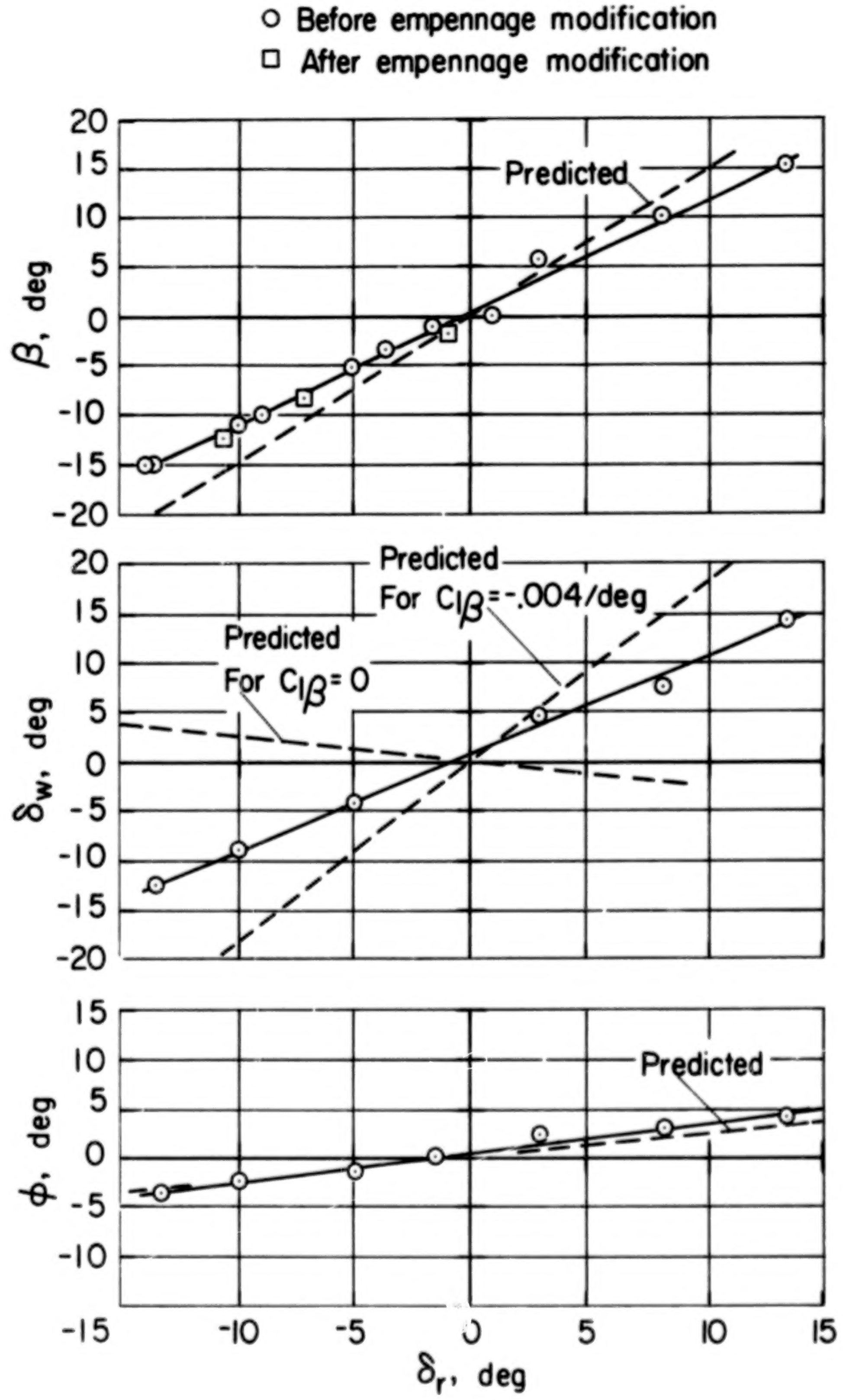

Figure 53.– Steady sideslip, flaps 65°, V_E = 65 knots, ν = 15°, N_H = 93%.

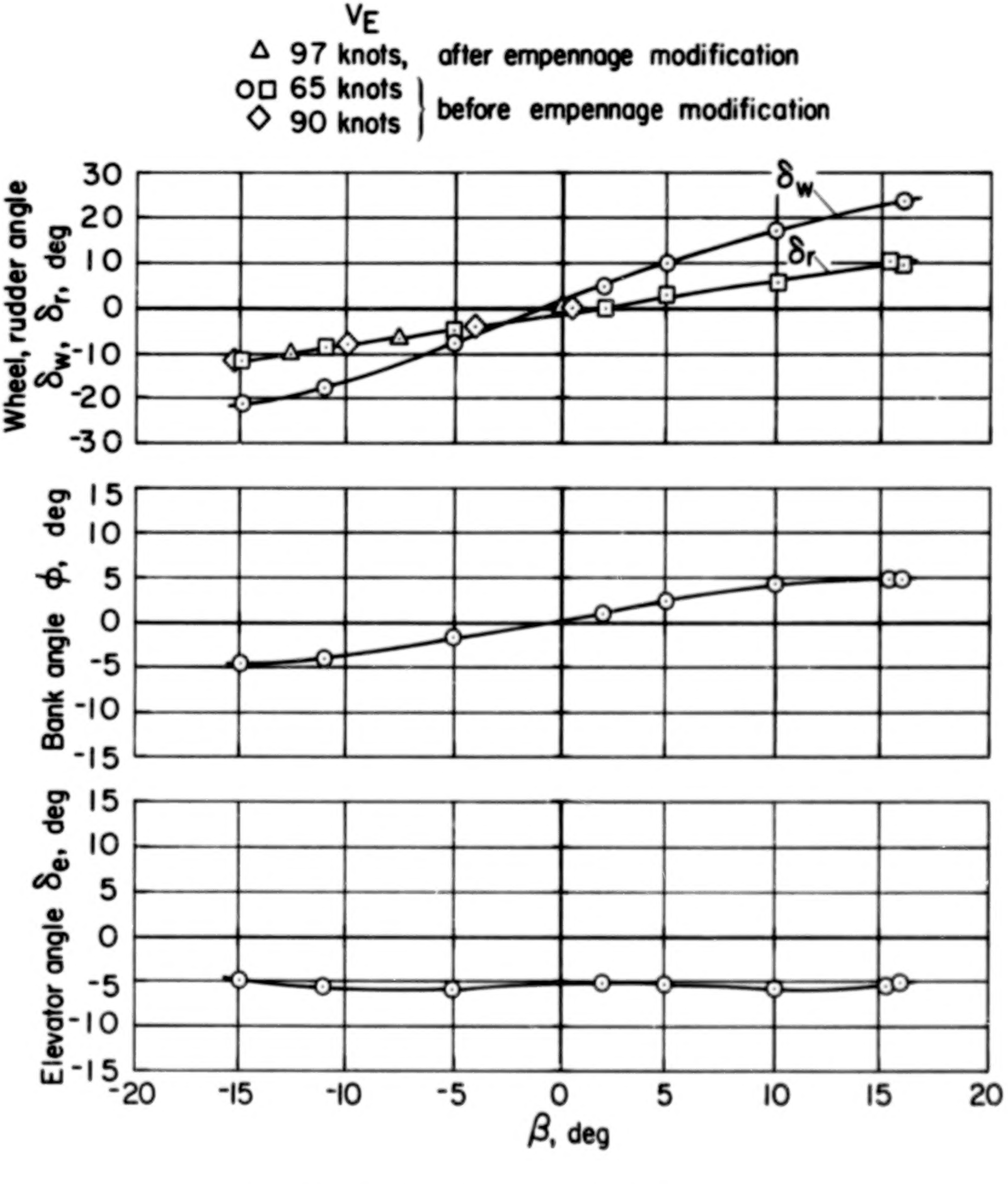

Figure 54.– Steady sideslip, flaps 30°, $\nu = 6°$, $N_H = 90\%$.

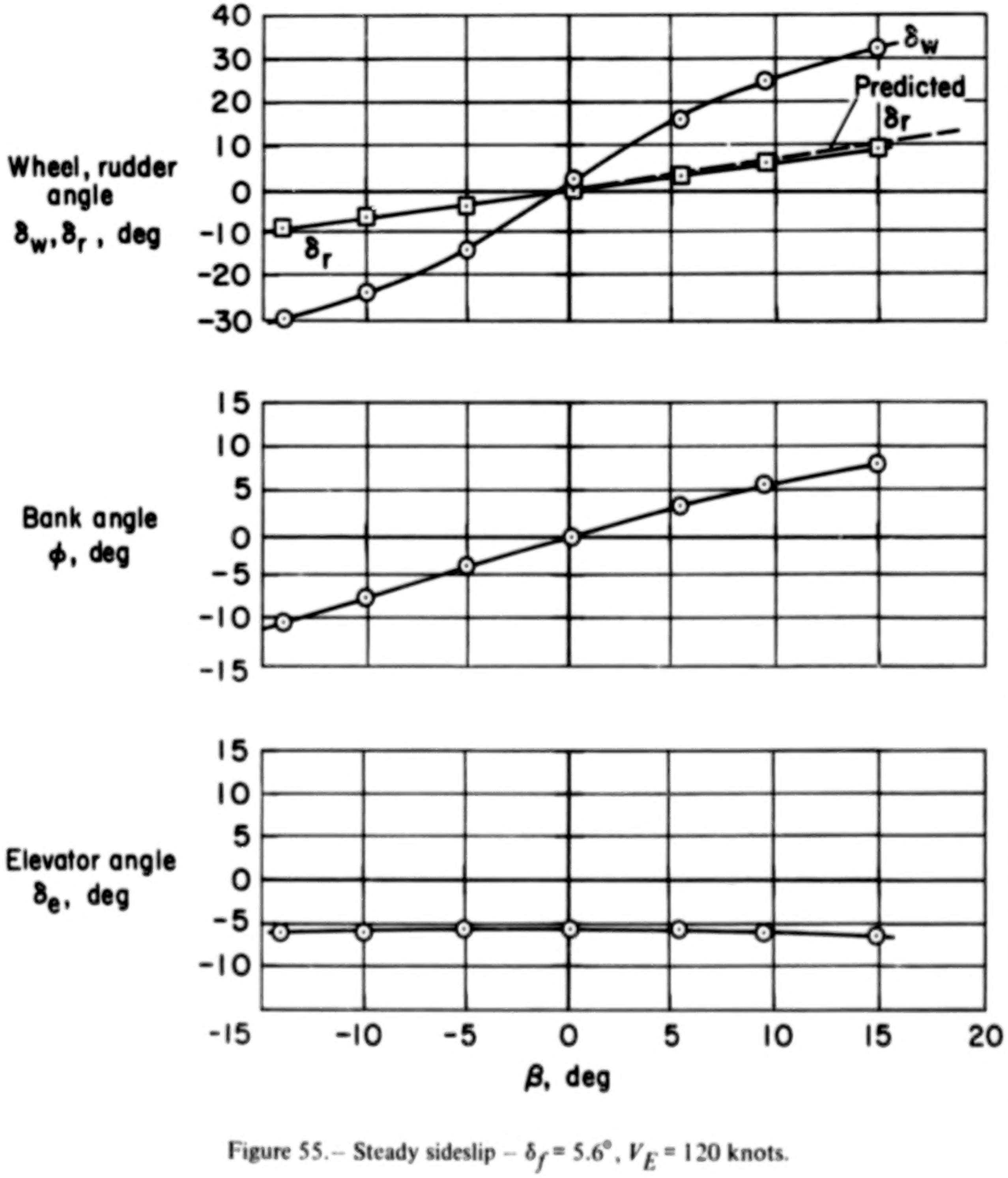

Figure 55.– Steady sideslip – $\delta_f = 5.6°$, $V_E = 120$ knots.

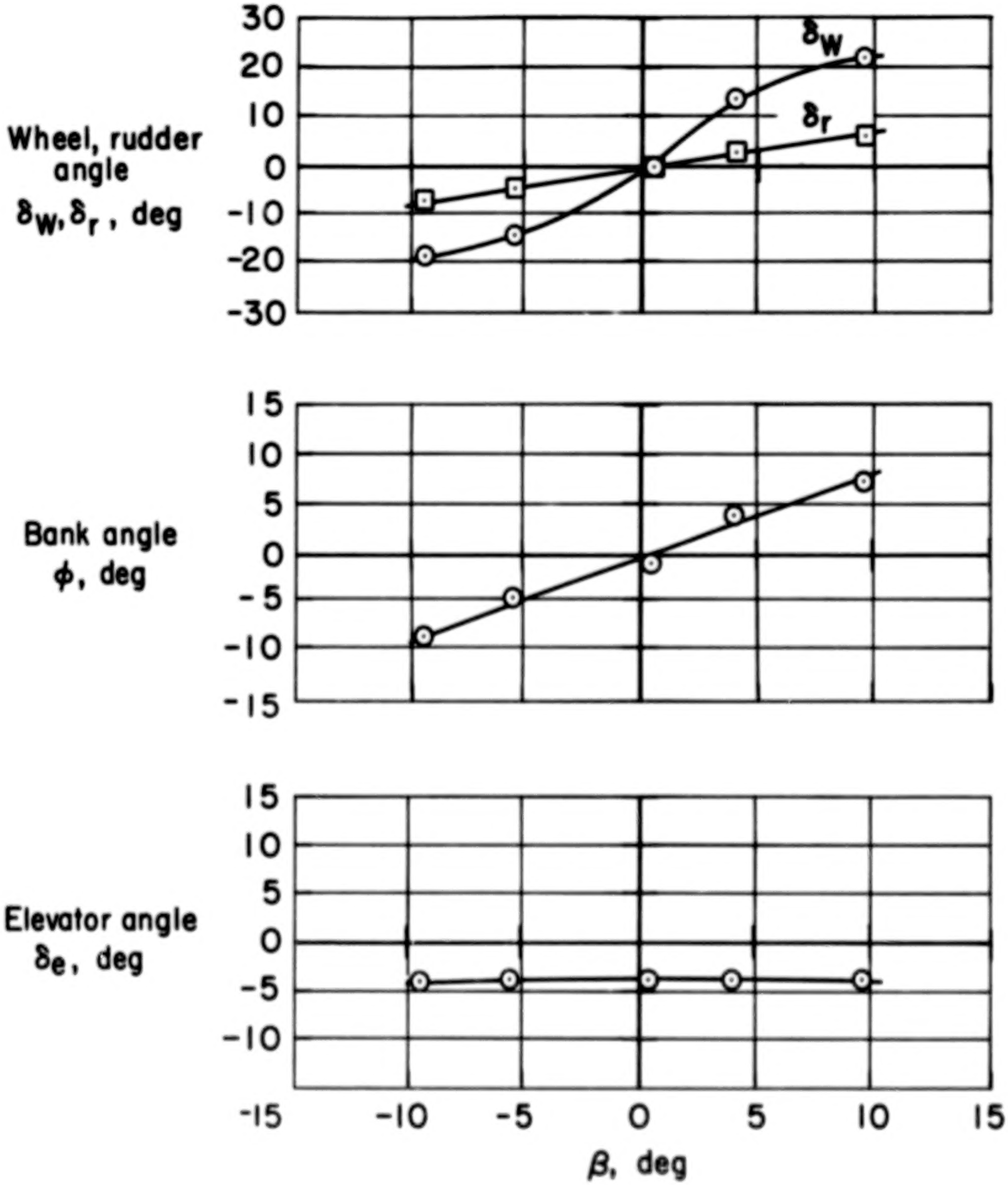

Figure 56.– Steady sideslip – $\delta_f = 5.6°$, $V_E = 150$ knots.

	δ_f, deg	ν, deg	Weight, N	SAS
○	67	~10	165000 to 182000	off
⍜	67	57-86	165000 to 182000	off
■	67	17	172000	on
■′	62	82	194000	on *
◺	33	15	202000	off
△	33	9	176000	off
◆	33	15	195000	on
◆′	30	11	200000	on *
⌂	6	11	196000	off
◗	6	11	176000	off

* Flagged - SAS modified
Shaded - SAS on
Open - SAS off

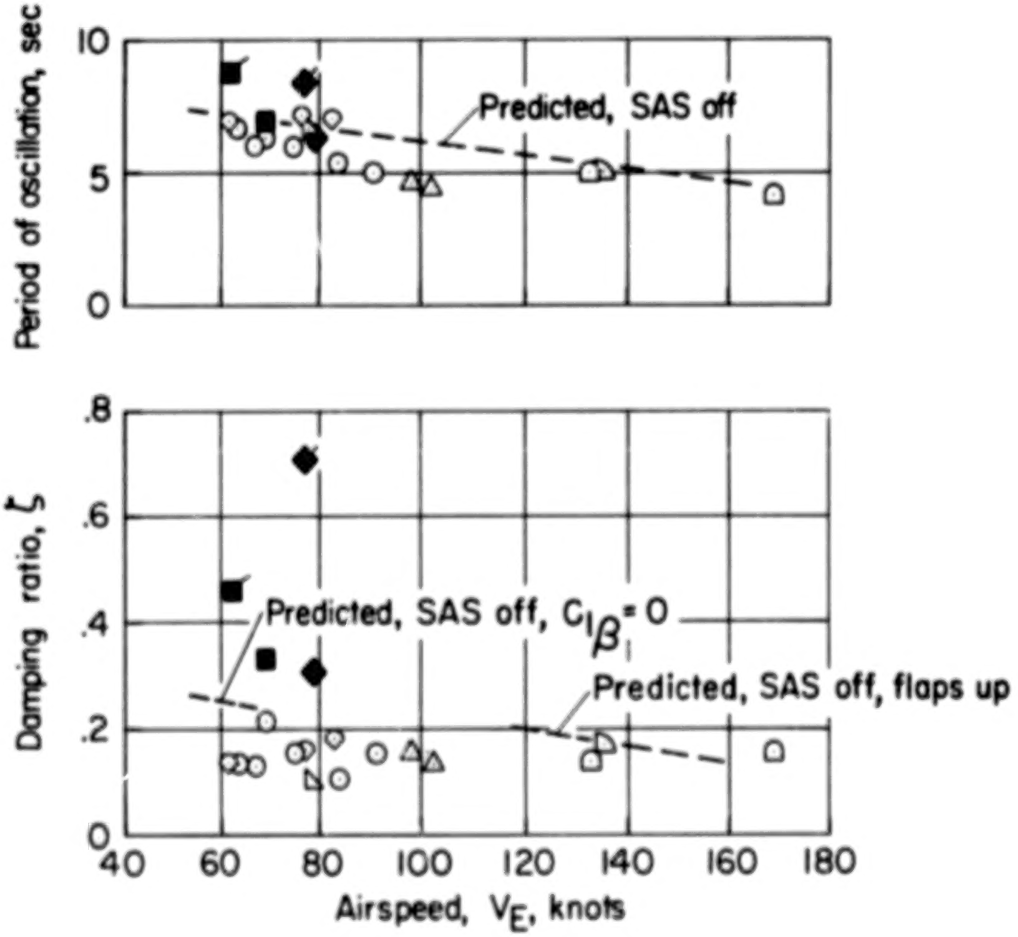

Figure 57.– Dutch-roll characteristics.

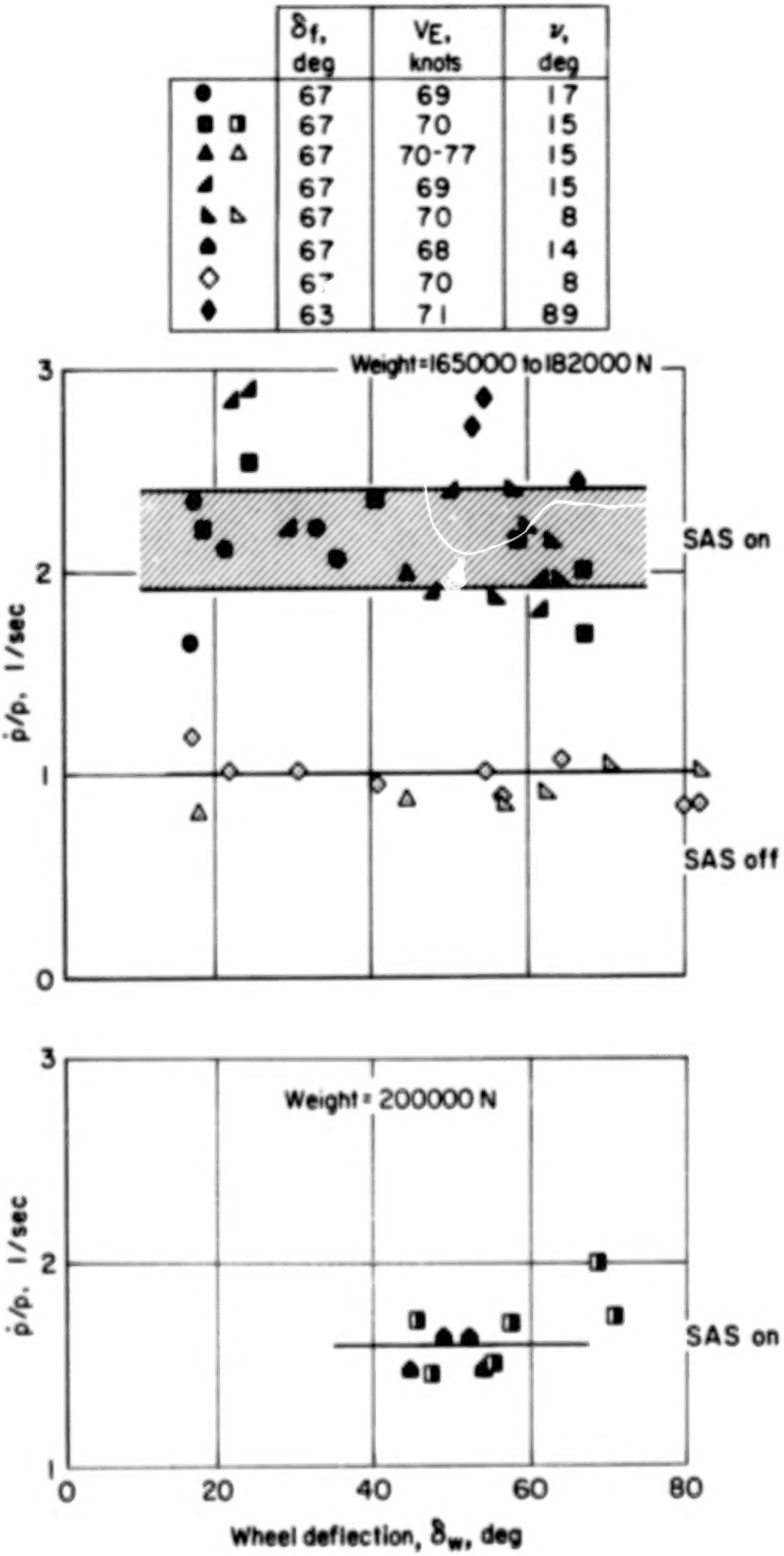

Figure 58.– Roll-damping characteristics, landing flaps.

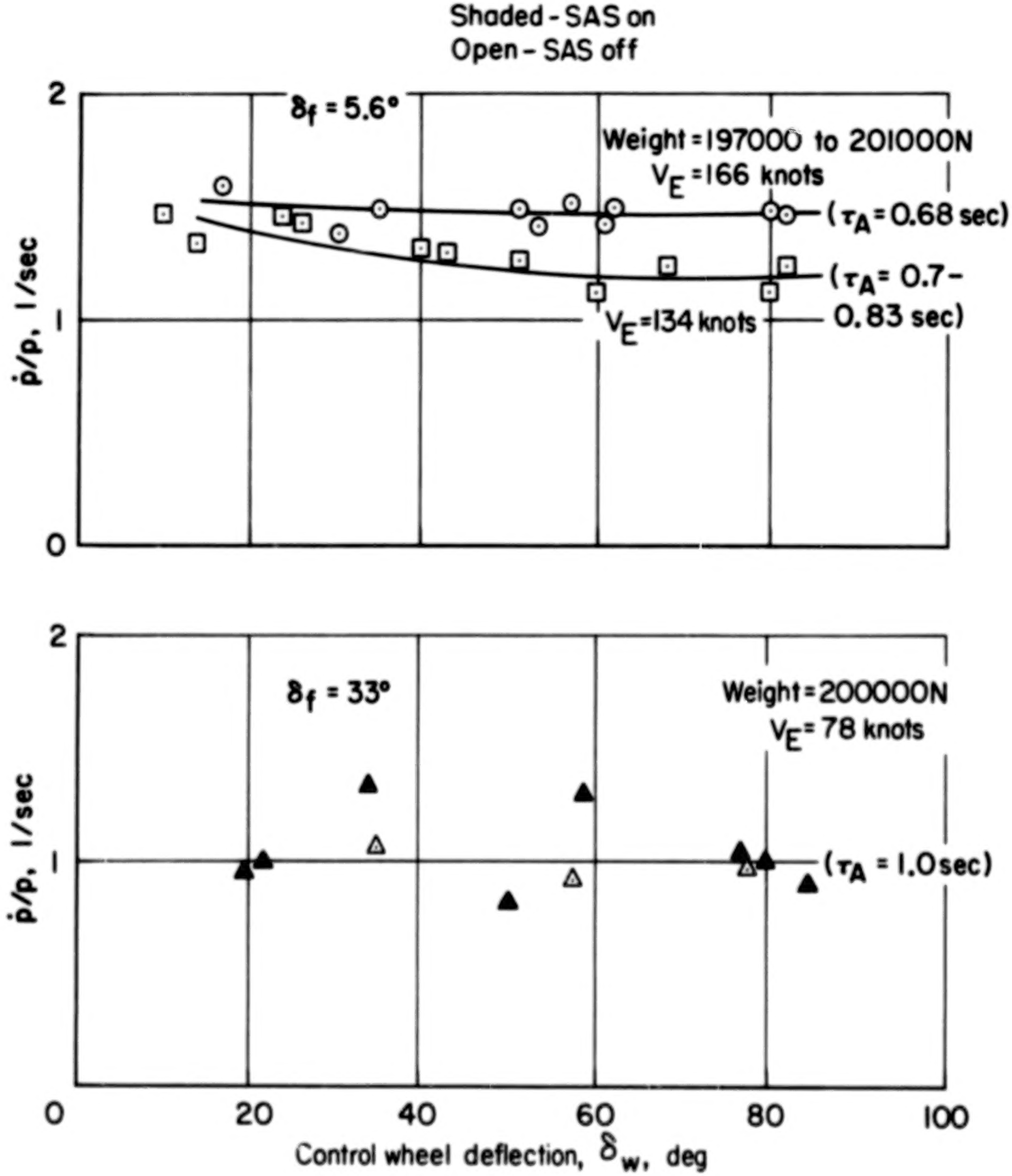

Figure 59.– Roll-damping characteristics – flaps 33° and 5.6°.

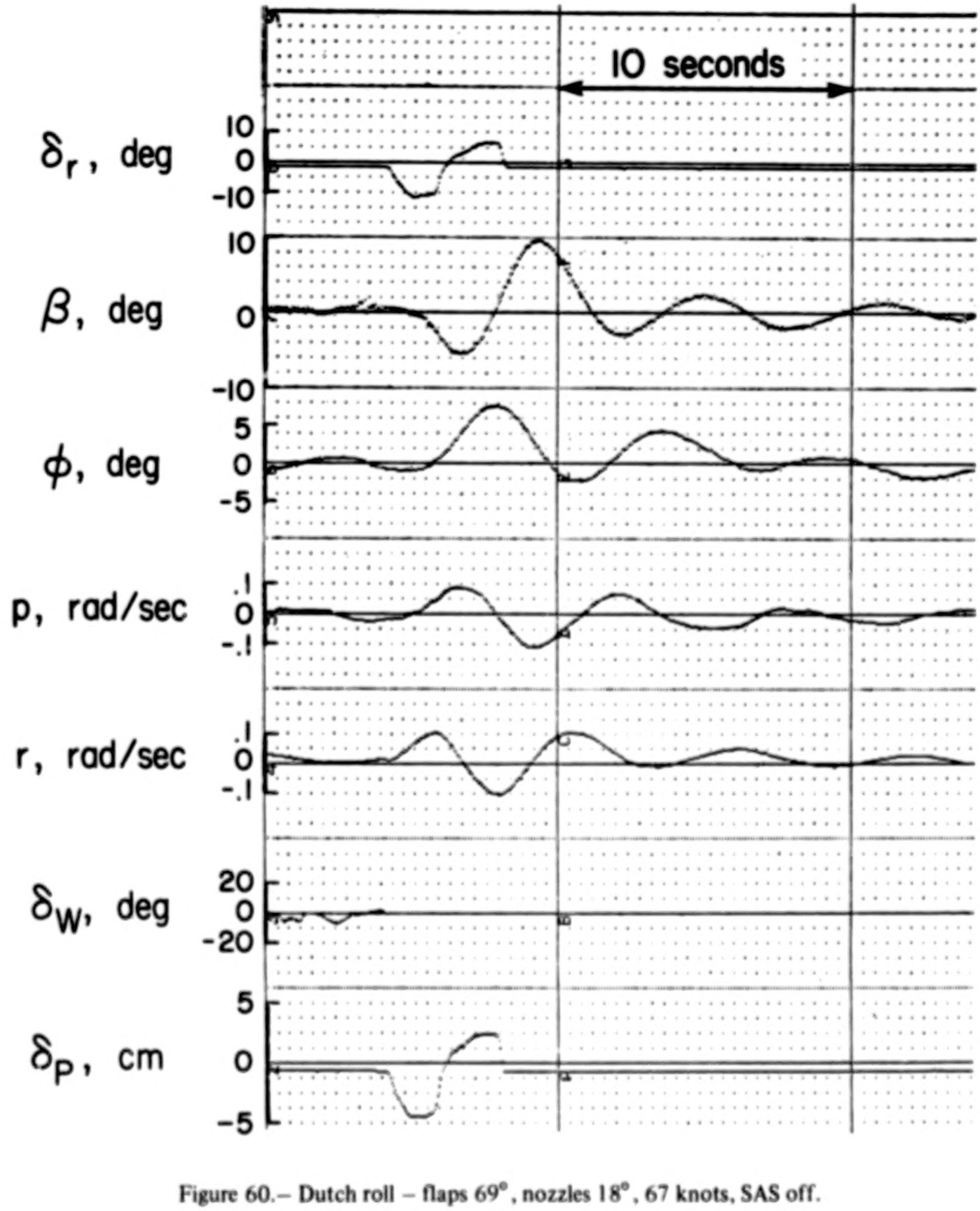

Figure 60.– Dutch roll – flaps 69°, nozzles 18°, 67 knots, SAS off.

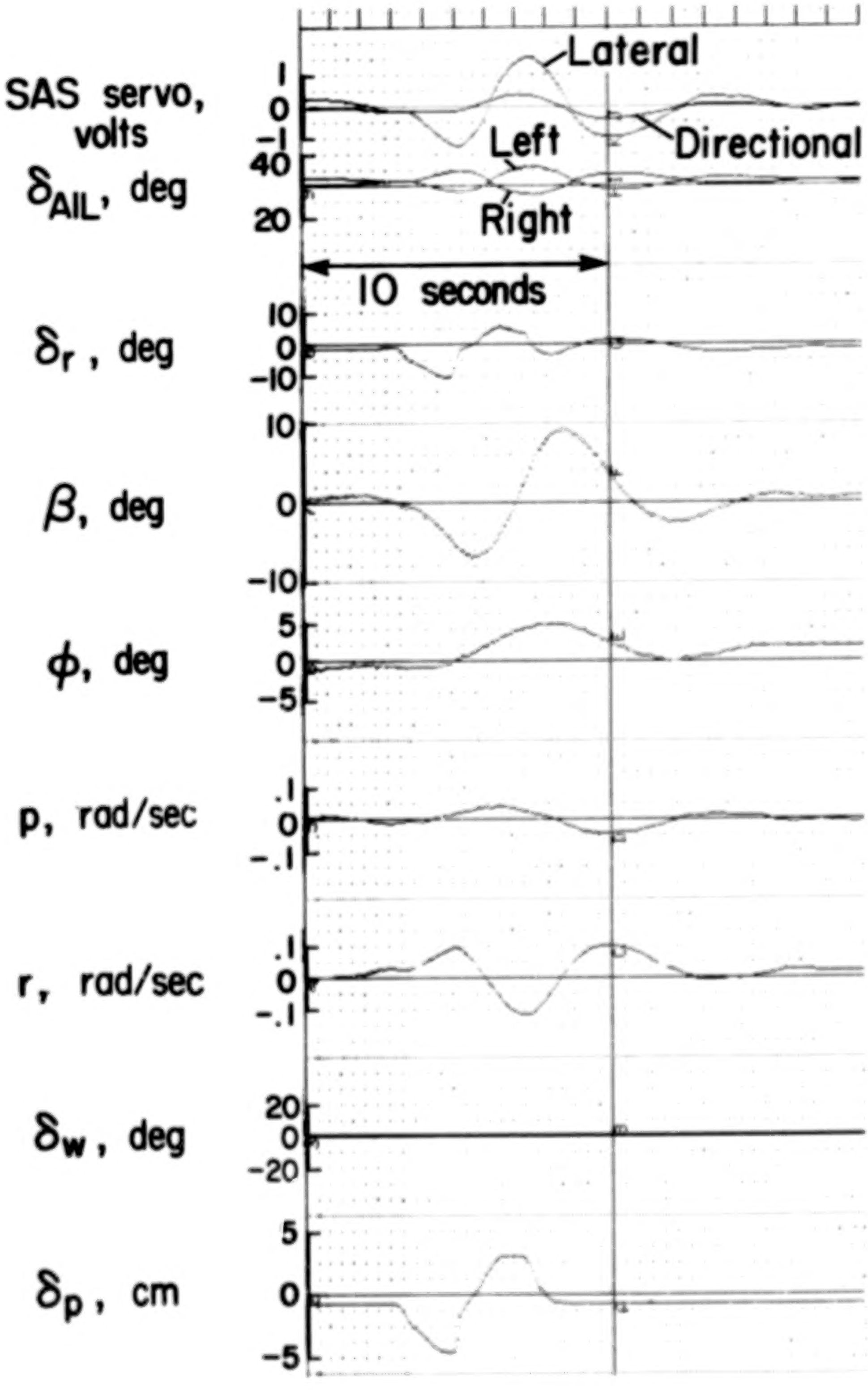

(a) Flaps 69°, $\nu = 18°$, $V_E = 69$ knots, SAS on, before SAS modification.

Figure 61.– Dutch-roll time history.

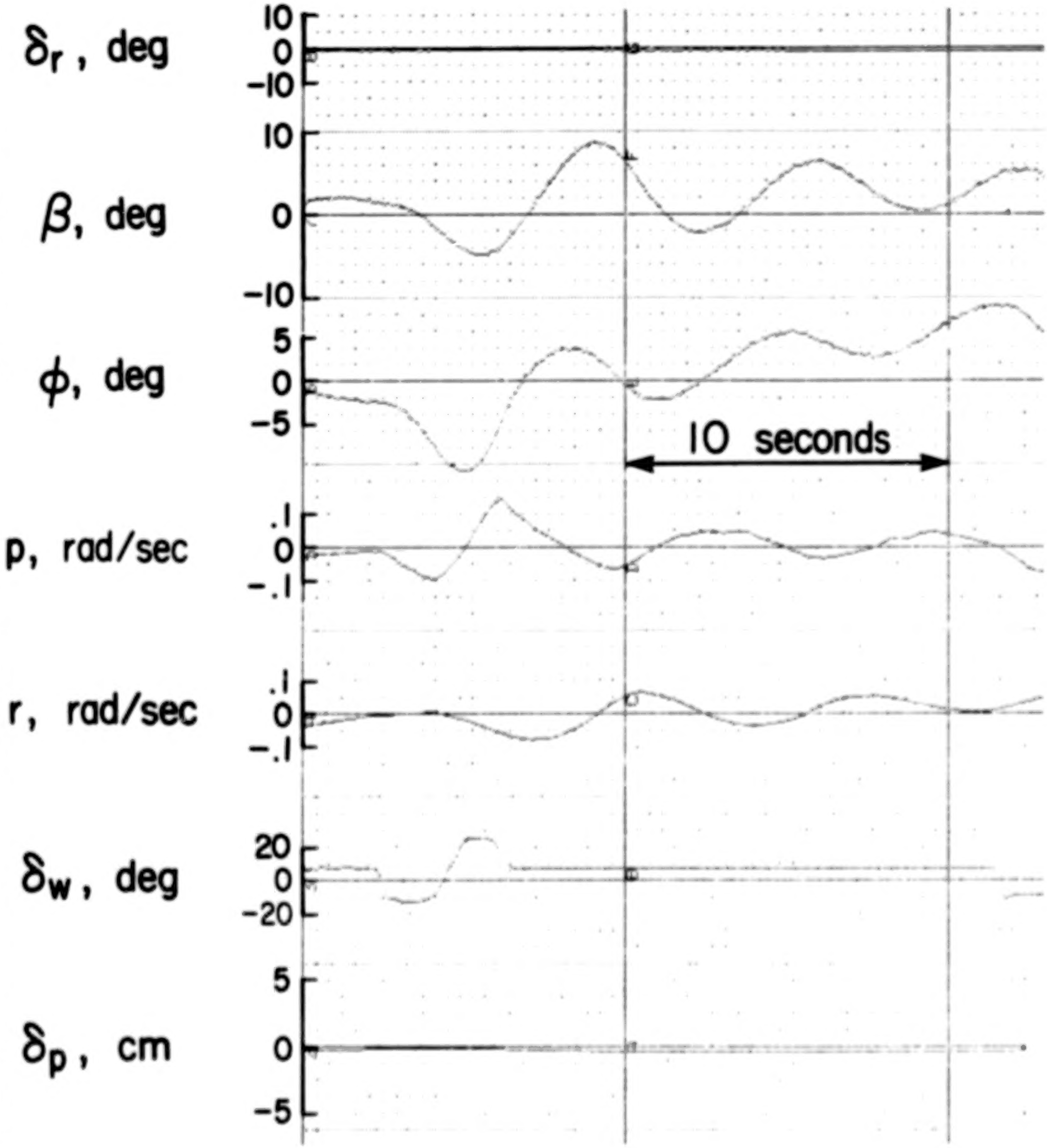

(b) Flaps 65°, $\nu = 87°$, $V_E = 61$ knots, SAS off.

Figure 61.– Continued.

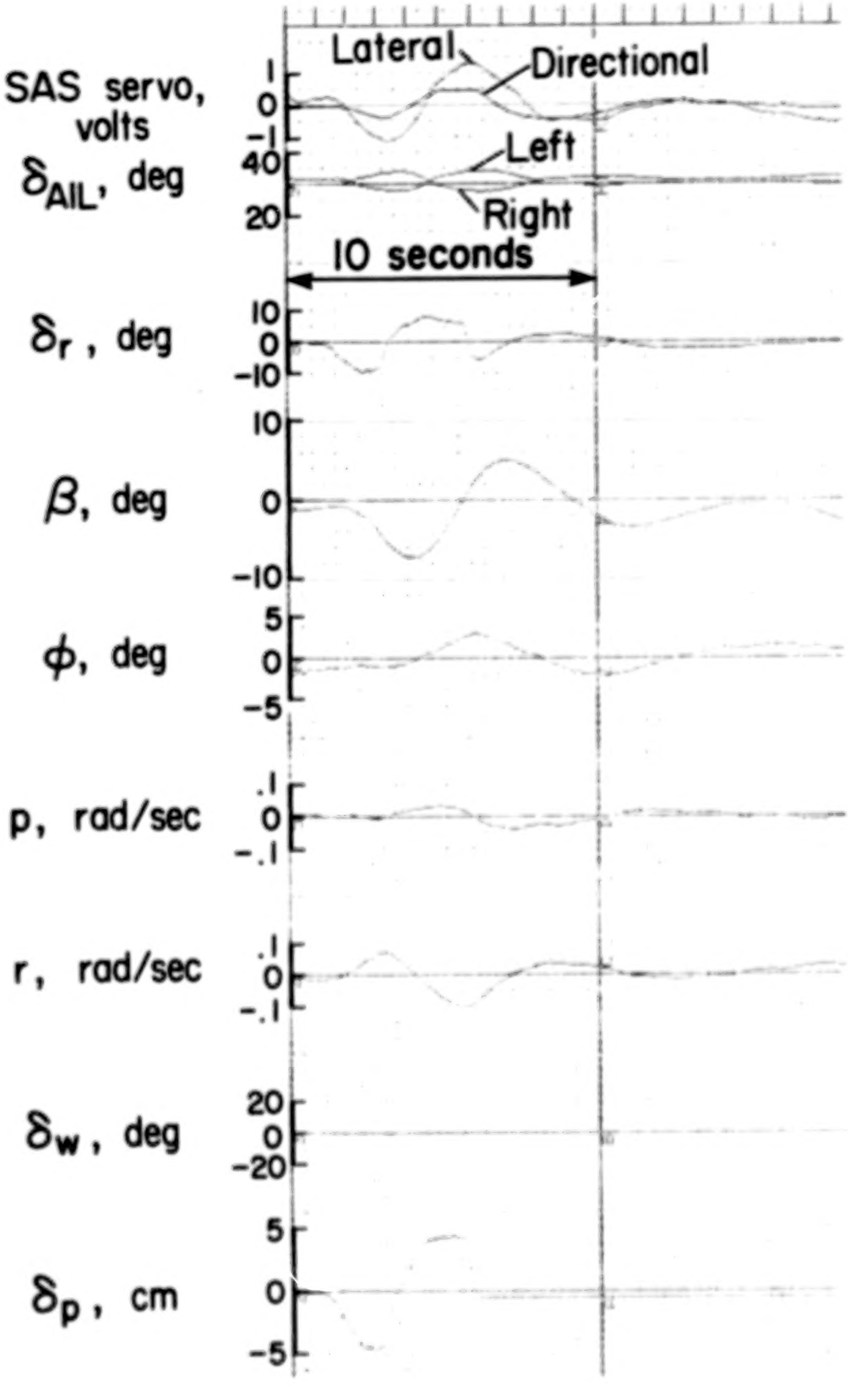

(c) Flaps 65°, $\nu = 82°$, $V_E = 62$ knots, SAS on (after SAS modification).

Figure 61.– Continued.

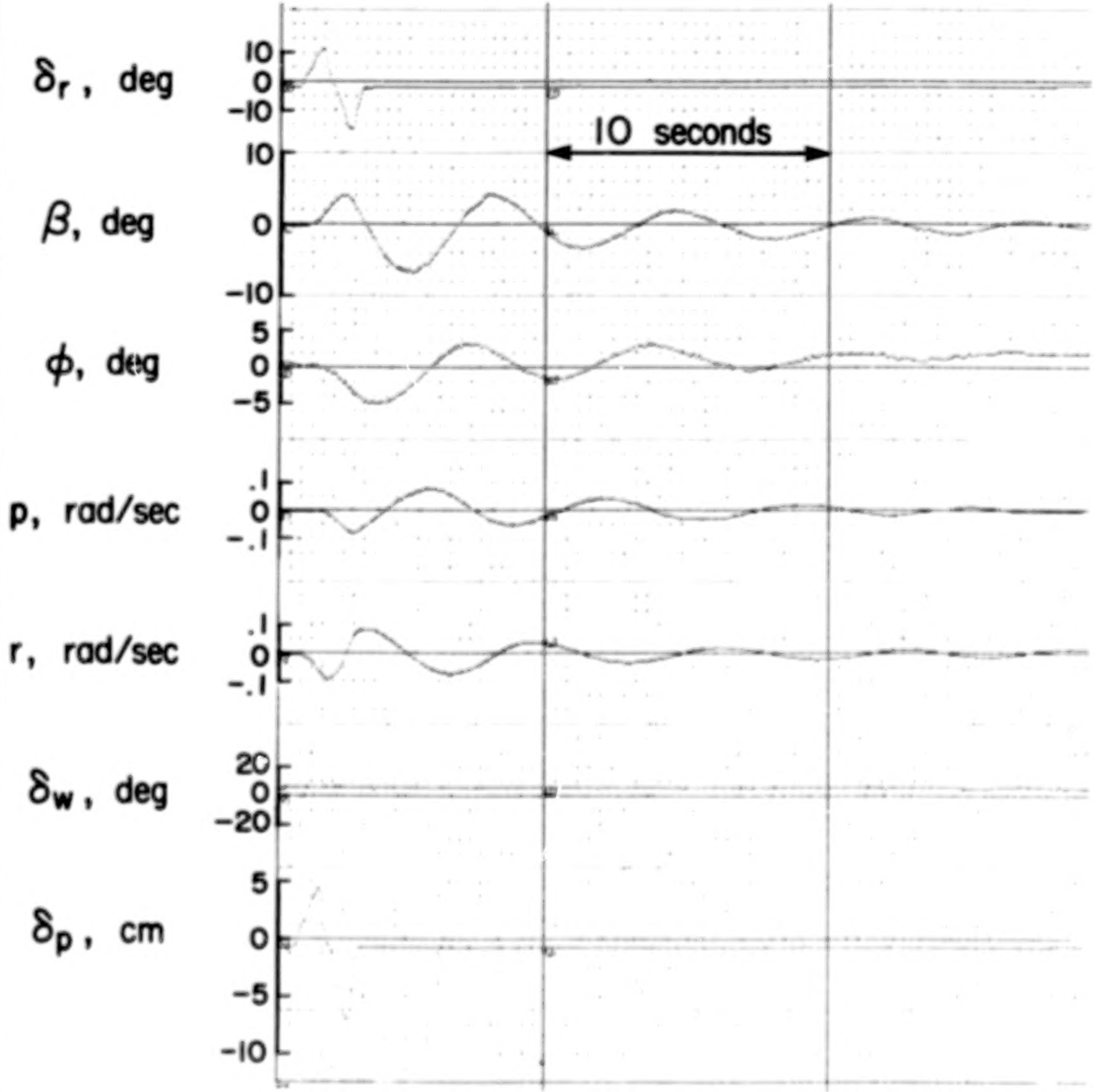

(d) Flaps 33°, ν = 15°, V_E = 78 knots, SAS off.

Figure 61.– Continued.

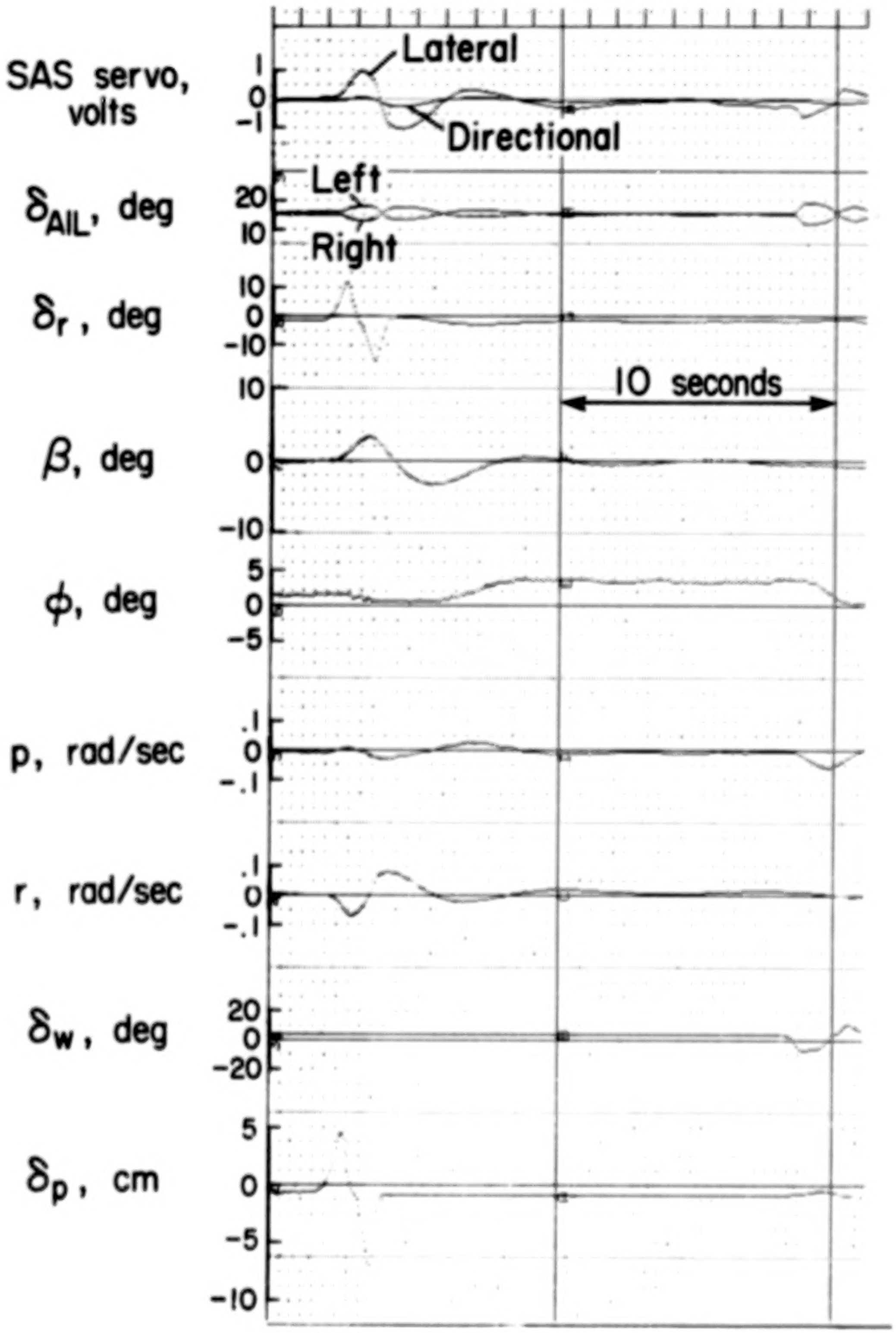

(e) Flaps 33°, $\nu = 15°$, $V_E = 78$ knots, SAS on (before SAS modification).

Figure 61. – Continued.

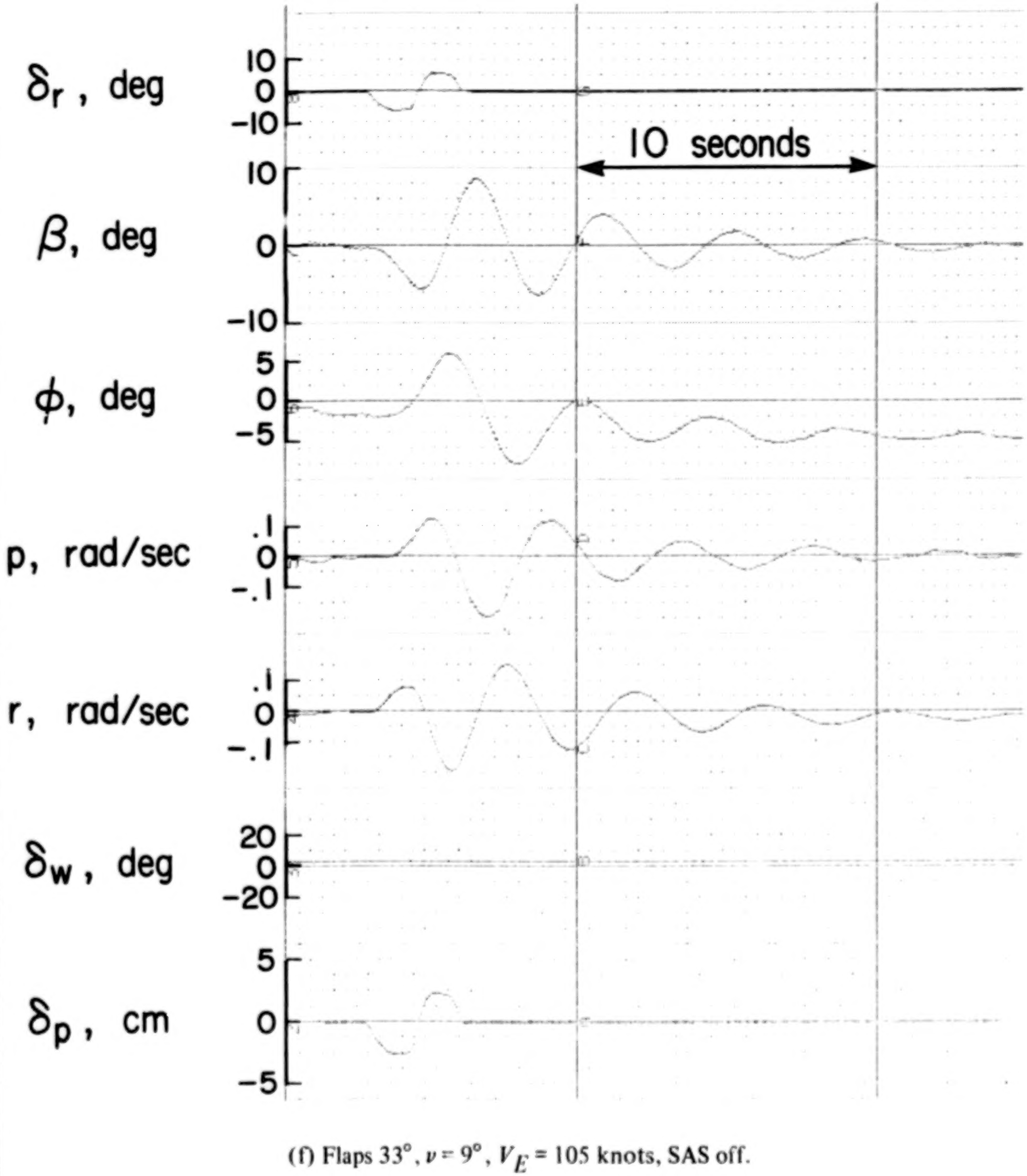

(f) Flaps 33°, $\nu = 9°$, V_E = 105 knots, SAS off.

Figure 61.– Continued.

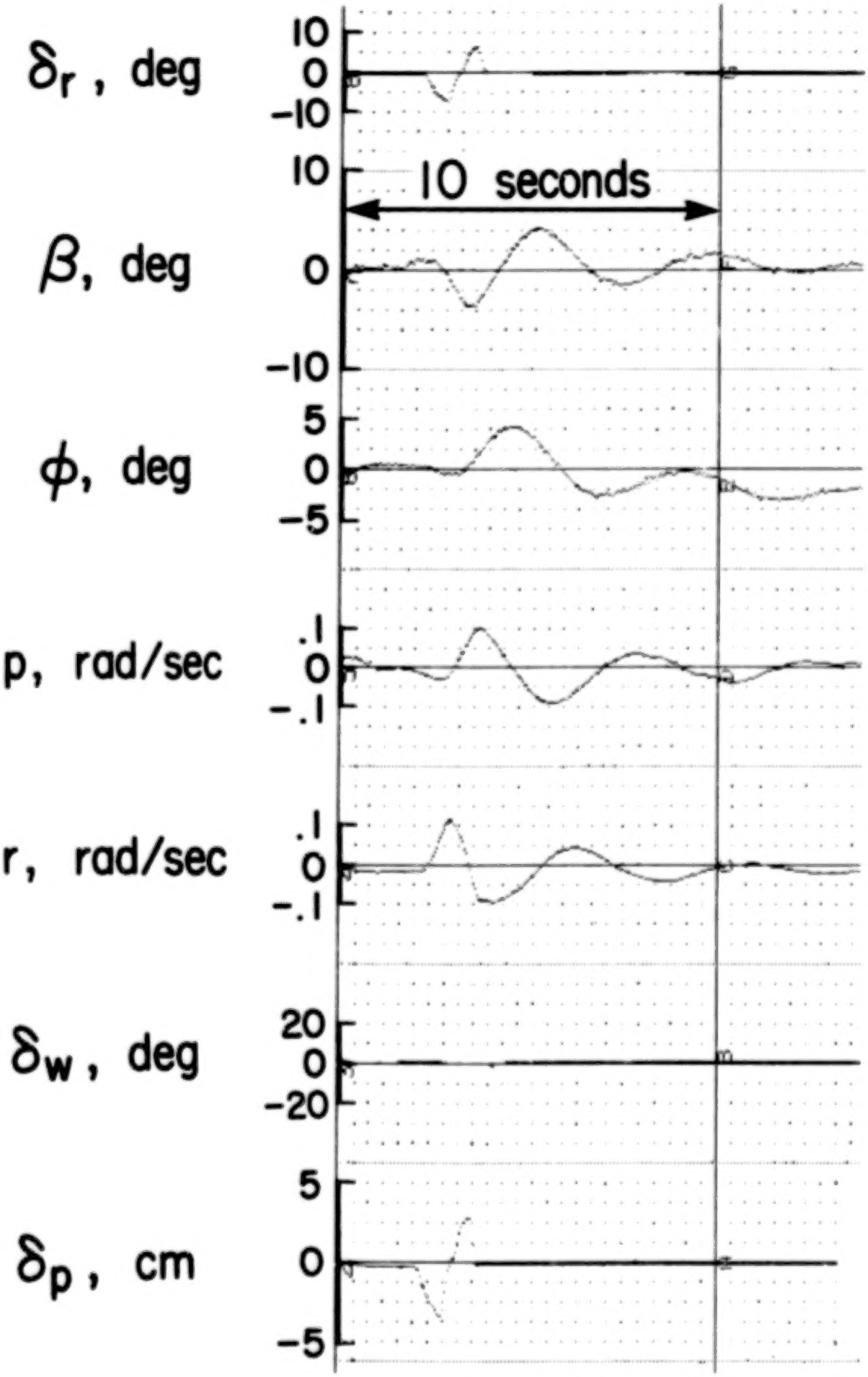

(g) Flaps 6°, $\nu = 15°$, $V_E = 135$ knots, SAS off.

Figure 61.– Concluded.

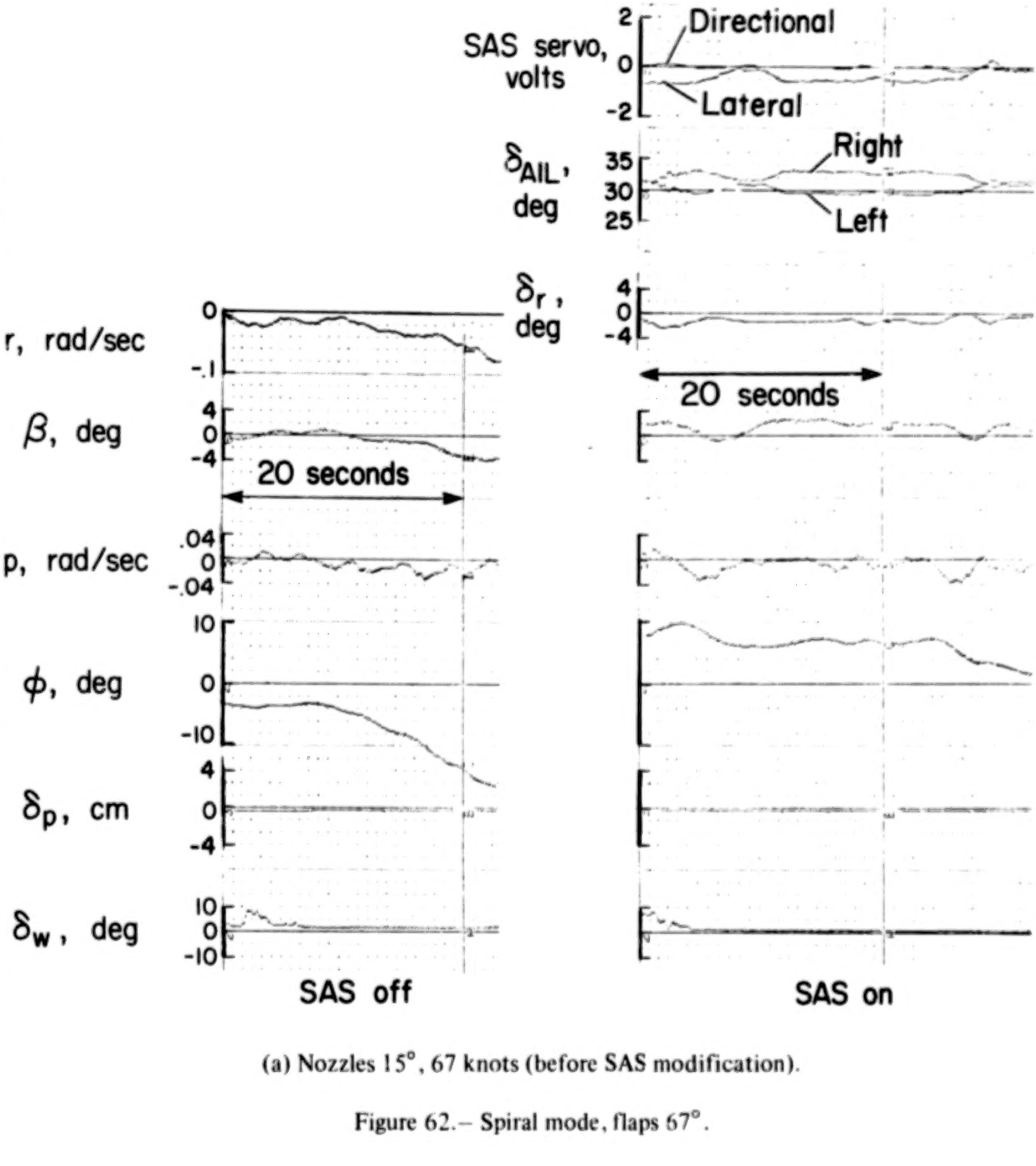

(a) Nozzles 15°, 67 knots (before SAS modification).

Figure 62.– Spiral mode, flaps 67°.

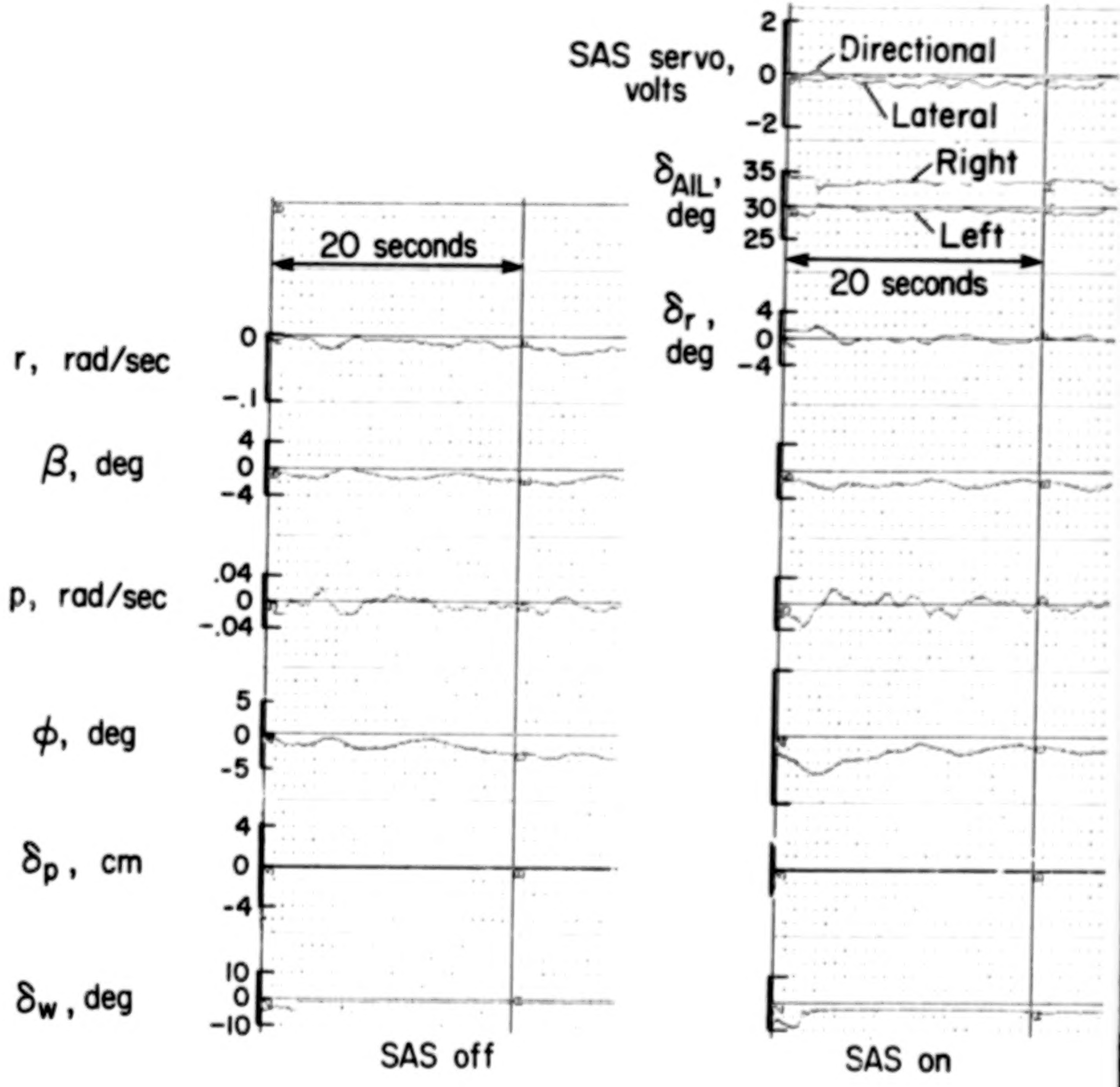

(b) Nozzles 90°, 62 knots (before SAS modification).

Figure 62.– Concluded.

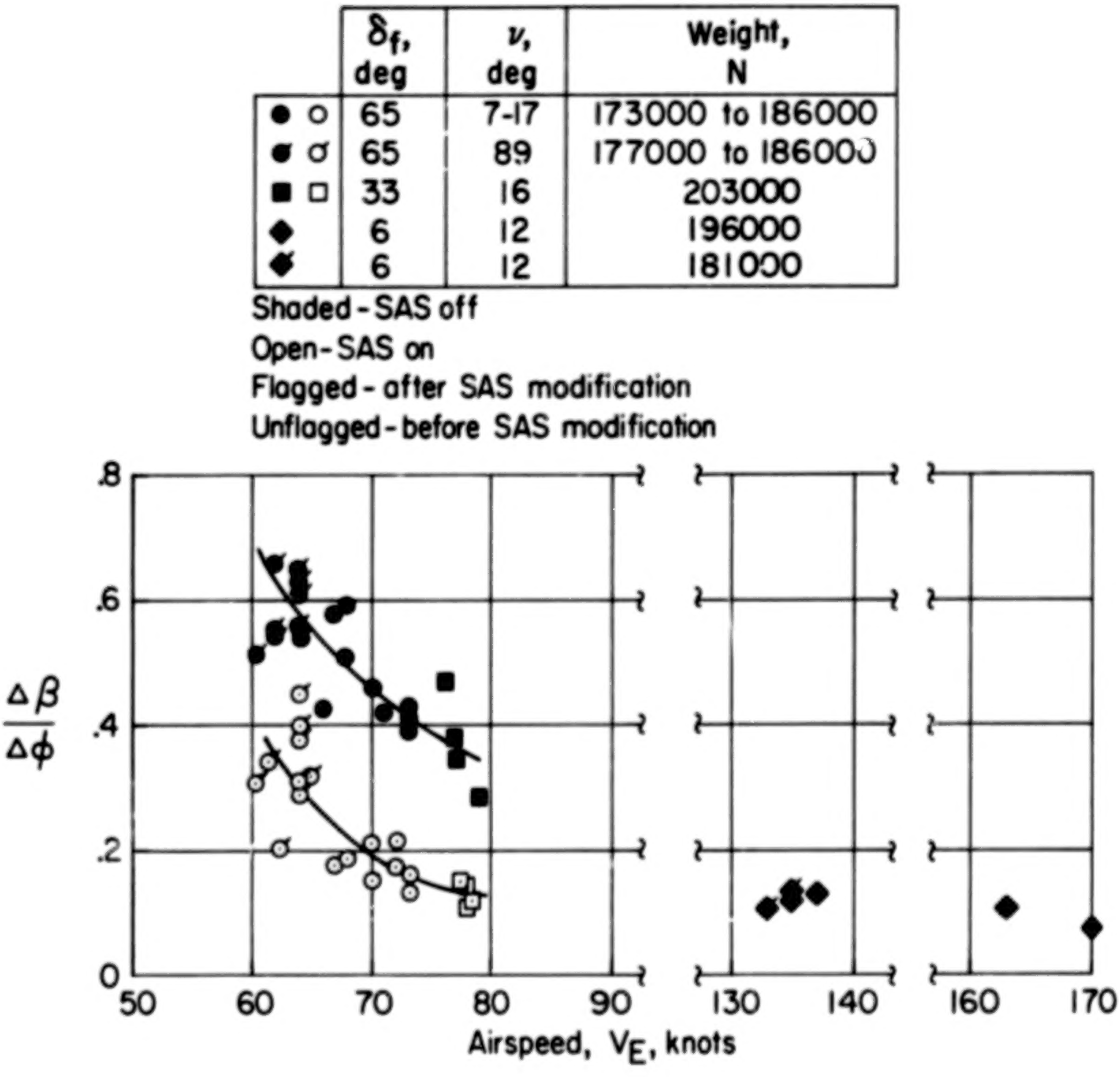

	δ_f, deg	ν, deg	Weight, N
● ○	65	7-17	173000 to 186000
● σ	65	89	177000 to 186000
■ □	33	16	203000
◆	6	12	196000
◆	6	12	181000

Shaded - SAS off
Open - SAS on
Flagged - after SAS modification
Unflagged - before SAS modification

Figure 63.– Turn coordination.

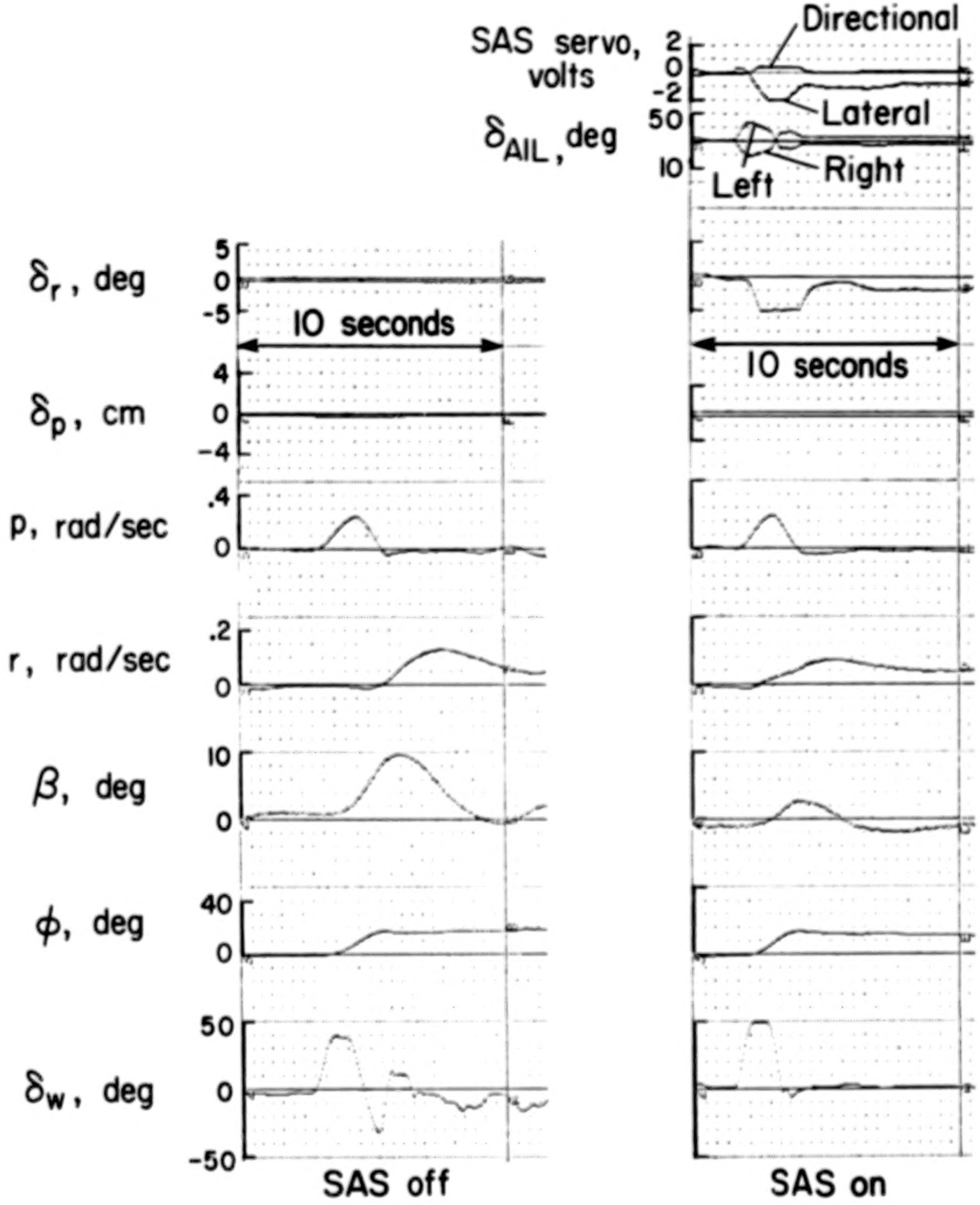

Figure 64.– Turn entry maneuvers – $\delta_f = 67°$, $V_E = 68$ knots.

1. Report No.
NASA TP-1254

2. Government Accession No.

3. Recipient's Catalog No.

4. Title and Subtitle
A FLIGHT INVESTIGATION OF THE STABILITY, CONTROL, AND HANDLING QUALITIES OF AN AUGMENTED JET FLAP STOL AIRPLANE

5. Report Date
June 1978

6. Performing Organization Code

7. Author(s)
Richard F. Vomaske,* Robert C. Innis,* Brian E. Swan,† and Seth W. Grossmith‡

8. Performing Organization Report No.
A-7246

9. Performing Organization Name and Address
*NASA, Ames Research Center, Moffett Field, Calif. 94035
†Canadian Armed Forces, Ottawa, Ontario K1A OK2
‡Canadian Department of Transport, Ottawa, Ontario K1A ON8

10. Work Unit No.
761-72-02

11. Contract or Grant No.

12. Sponsoring Agency Name and Address
National Aeronautics and Space Administration
Washington, D. C. 20546

13. Type of Report and Period Covered
Technical Paper

14. Sponsoring Agency Code

15. Supplementary Notes

16. Abstract

The stability, control, and handling qualities of an augmented jet flap STOL airplane are presented. The airplane is an extensively modified de Havilland "Buffalo" military transport. The modified airplane has two fan-jet engines which provide vectorable thrust and compressed air for the augmentor jet flap and Boundary-Layer Control (BLC). The augmentor and BLC air is cross ducted to minimize asymmetric moments produced when one engine is inoperative. The modifications incorporated in the airplane include a Stability Augmentation System (SAS), a powered elevator, and a powered lateral control system. The test gross weight of the airplane was between 165,000 and 209,000 N (37,000 and 47,000 lb).

Stability, control, and handling qualities are presented for the airspeed range of 40 to 180 knots. The lateral-directional handling qualities are considered satisfactory for the normal operating range of 65 to 160 knots airspeed when the SAS is functioning. With the SAS inoperative, poor turn coordination and spiral instability are primary deficiencies contributing to marginal handling qualities in the landing approach.

The powered elevator control system enhanced the controllability in pitch, particularly in the landing flare and stall recovery.

17. Key Words (Suggested by Author(s))
STOL
Augmented jet flap
Stability and control
Handling qualities
Stability augmentation

18. Distribution Statement
Unlimited

STAR Category – 08

19. Security Classif. (of this report)	20. Security Classif. (of this page)	21. No. of Pages	22. Price*
Unclassified	Unclassified	147	$6.00

*For sale by the National Technical Information Service, Springfield, Virginia 22161

NASA-Langley, 1978

90

50